TRPV4 IN THE CHOROID PLEXUS EPITHELIUM: PATHWAY ANALYSIS AND IMPLICATIONS FOR CEREBROSPINAL FLUID PRODUCTION

by

Daniel Preston

A Thesis

Submitted to the Faculty of Purdue University

In Partial Fulfillment of the Requirements for the degree of

Master of Science

Department of Biology at IUPUI

Indianapolis, Indiana

December 2019

THE PURDUE UNIVERSITY GRADUATE SCHOOL
STATEMENT OF COMMITTEE APPROVAL

Dr. Bonnie Blazer-Yost, Chair
Department of Biology

Dr. Teri Belecky-Adams
Department of Biology

Dr. Nick Berbari
Department of Biology

Dr. James Clack
Department of Biology, Indiana University-Purdue University Columbus

Approved by:
Dr. A.J. Baucum

To Stefanie, and to my Family, who have always supported me and will never read this thesis.

And to my Cat, Loki, who never failed to sleep on my mouse when I was trying to write.

ACKNOWLEDGMENTS

I would like to acknowledge my thesis committee for their support and guidance through the graduate program. In addition, I would like to thank Stefanie Simpson, Hillary Smith, Alex Hochstetler, Makenna Reed, Keith Gafunderi, Patrick Antonellis for their technical support, assistance with conducting experiments and contributions to data analysis.

TABLE OF CONTENTS

LIST OF TABLES 8
LIST OF FIGURES 9
LIST OF ABBREVIATIONS 11
ABSTRACT 13
CHAPTER 1. INTRODUCTION 14
1.1 Hydrocephalus 14
1.2 Treatment of Hydrocephalus 15
1.3 The Choroid Plexus 16
1.4 Transient Receptor Potential Vanilloid 4 17
1.5 The WPK Rat Model of Hydrocephalus 18
1.6 Porcine Choroid Plexus Cell Line 19
1.7 Chloride Transporters 19
1.8 Calcium-Activated Potassium Channels 20
1.9 Sodium-Potassium-Chloride and Potassium-Chloride Cotransporters 21
1.10 STE20/SPS1-Related Proline-Alanine-Rich Protein Kinase 22
1.11 Translational Potential 22
1.12 References 25
CHAPTER 2. ACTIVATION OF TRPV4 STIMULATES ION FLUX IN PCP-R CELLS 35
2.1 Preface 35
2.2 Activation of TRPV4 Stimulates Transepithelial Ion Flux in a Porcine CP Cell Line 36
2.3 Abstract 37
2.4 Introduction 37
2.5 Materials and Methods 39
2.6 Results 41
2.7 Discussion 43
2.8 Acknowledgements 48
2.9 Grants 48
2.10 Disclosures 48
2.11 References 70

CHAPTER 3. THE ROLE OF NKCC1 AND SPAK IN TRPV4-MEDIATED TRANSPORT 74
3.1 Preface ... 74
3.2 SPAK Inhibition Blocks TRPV4 Mediated Ion Flux in Choroid Plexus Epithelial Cells 74
3.3 Abstract ... 75
3.4 Introduction ... 75
3.5 Methods and Materials ... 78
3.6 Results ... 80
3.7 Discussion ... 82
3.8 Acknowledgments ... 86
3.9 Grants ... 86
3.10 Disclosures ... 86
3.11 References ... 105
CHAPTER 4. CHLORIDE CHANNELS IN CPE TRANSEPITHELIAL TRANSPORT ... 110
4.1 Introduction ... 110
4.2 Methods and Materials ... 112
4.3 Results ... 114
4.4 Discussion ... 116
4.5 References ... 143
CHAPTER 5. INFLAMMATORY EFFECTS ON TRPV4 IN THE CHOROID PLEXUS ... 147
5.1 Preface ... 147
5.2 Inflammatory Effects on TRPV4 in the Choroid Plexus ... 147
5.3 Abstract ... 148
5.4 Introduction ... 149
5.5 Materials and Methods ... 151
5.6 Results ... 154
5.7 Discussion ... 155
5.8 Acknowledgments ... 160
5.9 Grant Support ... 160
5.10 Disclosures ... 160
5.11 References ... 189
CHAPTER 6. SUMMARY ... 194

6.1 Summary 194
6.2 Addressing the PCP-R Cell Polarity 196

LIST OF TABLES

Table 2.1 Primer Pairs Used for RT-PCR with Corresponding Product Sizes (bp). 49

Table 3.1 *Sus Scrofa* Primers Used for RT-PCR with Corresponding Product Sizes (bp)..... 87

Table 4.1 *Sus Scrofa* Primers Used for RT-PCR with Corresponding Product Sizes (bp)..... 121

Table 5.1 Reported Cytokine Functions in the Inflammatory Pathway..... 161

Table 5.2 *Sus Scrofa* Primers Used for RT-PCR with Corresponding Product Sizes (bp)..... 162

LIST OF FIGURES

Figure 1.1 Ventricular Volumes of Treated vs Untreated WPK Rats..... 24
Figure 2.1 Development of Transepithelial Resistance of the PCP-R Cell Line..... 50
Figure 2.2 Effect of TRPV4 Agonist and Antagonists in the PCP-R Cells..... 52
Figure 2.3 Dose Response for TRPV4 Agonist GSK1016790A in PCP-R Cells..... 54
Figure 2.4 Dose Response for TRPV4 Antagonist RN1734 Pre-Treatment in PCP-R Cells..... 56
Figure 2.5 Reversibility of a TRPV4 Agonist Response by a TRPV4 Antagonist..... 58
Figure 2.6 Immunohistological Staining of Claudin 1 in the PCP-R Cell Line. 59
Figure 2.7 RT-PCR of Selected Ion Channels in the PCP-R Cell Line..... 60
Figure 2.8 Effect of BK Channel Inhibitor on TRPV4-Mediated Responses..... 61
Figure 2.9 Effect of SK Channel Inhibitor on TRPV4-Mediated Responses. 63
Figure 2.10 Effect of High/Low Doses of IK Inhibitor on TRPV4-Mediated Responses..... 65
Figure 2.11 Sidedness of IK Channel Inhibitor on TRPV4-Mediated Responses..... 67
Figure 2.12 Diagram of Selected Transporters in the Choroid Plexus Epithelia..... 69
Figure 3.1 RT-PCR in the PCP-R Cell Line..... 88
Figure 3.2 Effect of SPAK Inhibitor on TRPV4-Mediated Responses. 90
Figure 3.3 Effect of SPAK Inhibitor on TRPV4-Mediated Responses. 92
Figure 3.4 Effect of NKCC Inhibitor on TRPV4-Mediated Responses. 94
Figure 3.5 Sidedness of NKCC Inhibitor on TRPV4-Mediated Responses. 96
Figure 3.6 Sidedness of KCC Inhibitor on TRPV4-Mediated Responses..... 98
Figure 3.7 Effect of NKCC and KCC Inhibitors on TRPV4-Mediated Responses..... 100
Figure 3.8 Effect of NKCC Inhibitor on mRNA Transcription..... 102
Figure 3.9 Effect of SPAK Inhibitor on mRNA Transcription..... 104
Figure 4.1 RT-PCR in the PCP-R Cell Line..... 122
Figure 4.2 Effect of TMEM16A Inhibitor on TMEM16A-Mediated Responses..... 124
Figure 4.3 Effect of TMEM16A Inhibitor on TRPV4-Mediated Responses..... 126
Figure 4.4 Sidedness of TMEM16A Inhibitor on TRPV4-Mediated Responses. 128
Figure 4.5 Reversibility of a TRPV4 Agonist Response by a TMEM16A Inhibitor. 130

Figure 4.6 Effect of TRPV4 Inhibitor on TMEM16A-Mediated Responses..... 132
Figure 4.7 Effect of Low Dose Agonists on TMEM16A and TRPV4 Induced Responses..... 134
Figure 4.8 Effect of TMEM16A and TRPV4 Agonist on TMEM16A and TRV4 Responses... 136
Figure 4.9 Effect of CFTR Inhibitor on TRPV4-Mediated Responses. 138
Figure 4.10 Effect of VRAC Inhibitor on TRPV4-Mediated Responses. 140
Figure 4.11 Effect of Anion Exchange Inhibitor on TRPV4-Mediated Responses..... 142
Figure 5.1 RT-PCR in PCP-R Cells..... 164
Figure 5.2 Treatment of PCP-R Cells with IL-1β 24-hrs Prior to TRPV4 Agonist Addition. ... 166
Figure 5.3 Treatment of PCP-R Cells with TNF-α 24-hrs Prior to TRPV4 Agonist Addition. . 168
Figure 5.4 Treatment of PCP-R Cells with TGF-β1 24-hrs Prior to TRPV4 Agonist Addition. 170
Figure 5.5 Treatment of PCP-R Cells with IL-6 24-hrs Prior to TRPV4 Agonist Addition. 172
Figure 5.6 Treatment of PCP-R Cells with IL-10 24-hrs Prior to TRPV4 Agonist Addition. ... 174
Figure 5.7 Treatment of PCP-R Cells with IL-4 24-hrs Prior to TRPV4 Agonist Addition. 176
Figure 5.8 Treatment of PCP-R Cells with PDTC 10-min Prior to TRPV4 Agonist Addition.. 178
Figure 5.9 Treatment of PCP-R Cells with PDTC 24-hrs Prior to TRPV4 Agonist Addition. .. 180
Figure 5.10 Relative Fold Change in TRPV4 24-hrs Post Incubation with Specific Cytokines. 181
Figure 5.11 Treatment of PCP-R Cells with AA 24-hrs Prior to TRPV4 Agonist Addition..... 183
Figure 5.12 Dose Effect of AA on TRPV4-Mediated Transepithelial Ion Flux..... 184
Figure 5.13 AA Metabolite Treatment of PCP-R Cells Prior to TRPV4 Agonist Addition..... 186
Figure 5.14 Treatment of PCP-R Cells with 5,6-EET Prior to TRPV4 Agonist Addition. 188

LIST OF ABBREVIATIONS

CP: Choroid Plexus

CSF: Cerebrospinal Fluid

MKS3: Meckel Gruber Syndrome Type 3

TMEM67: Transmembrane Protein 67

Wpk: Wistar Polycystic Kidney

PKD: Polycystic Kidney Disease

PCP-R: Porcine Choroid Plexus-Riems

TRPV4: Transient Receptor Potential Vanilloid 4

NKCC1: $Na^+/K^+/2Cl^-$ Cotransporter

KCC: K^+/Cl^- Cotransporter

SK: Small Conductance K^+ Channel

IK: Intermediate Conductance K^+ Channel

BK: Large Conductance K^+ Channel

TER: Transepithelial Electrical Resistance

SCC: Short Circuit Current

TBI: Traumatic Brain Injury

NPH: Normal Pressure Hydrocephalus

PHHP: Post-Hemorrhagic Hydrocephalus of Prematurity

ETV: Endoscopic Third Ventriculostomy

CNS: Central Nervous System

RT-PCR: Reverse Transcriptase Polymerase Chain Reaction

qPCR: Quantitative Polymerase Chain Reaction

AE2: Anion Exchange Protein 2

NCBE: $Na^+/Cl^-/HCO^{3-}$ Dependent Exchange Protein

CaCC: Calcium Activated Chloride Channel

TMEM16A: Transmembrane Member 16

CFTR: Cystic Fibrosis Transmembrane Regulatory Protein

mRNA: Messenger RNA

SPAK: STE20/SPS1-Related Proline-Alanine-Rich Protein Kinase

WNK: With no lysine (K) Kinase

VRAC: Volume Regulated Anion Channel

RVD: Regulatory Volume Decrease

cAMP: Cyclic AMP

PKA: Protein Kinase A

AA: Arachidonic Acid

EET: Epoxyeicosatrienoic Acids

IL: Interleukin

TNF: Tumor Necrosis Factor

TGF: Transforming Growth Factor

TLR: Toll-like Receptor

CYP: Cytochrome P

LOX: Lipoxygenase

COX: Cyclooxygenase

HIBCPP: Human Choroid Plexus Papilloma

ABSTRACT

Hydrocephalus is a disease characterized by an increase in cerebrospinal fluid (CSF) in the ventricles of the brain. This manifests as a result of either overproduction or underabsorption of CSF leading to increases in pressure, swelling and loss of brain matter. Current treatments for this disease include surgical interventions via the introduction of shunts or endoscopic third ventriculostomy, both of which aim to redirect flow of CSF in to another cavity for absorption. Limited pharmacotherapies are available in the treatment of hydrocephalus, and there exists a clinical need for drug therapies, which can ameliorate the pathophysiology associated with hydrocephalus and ventriculomegaly. CSF is produced primarily by the choroid plexus (CP), found in the ventricles of the brain. Composed of a high resistance epithelium surrounding a capillary network, the CP epithelium acts as a barrier, regulating ion transport between the CSF and blood. Transient Receptor Potential Vanilloid-4 (TRPV4) is a nonselective Ca^{2+}-permeable cation channel expressed in the CP which is being investigated for its role in CSF production.

To study hydrocephalus, we utilize two model systems; the TMEM67$^{-/-}$ Wpk rat, and the PCP-R cell line. The Wpk rat model is used to study the effects of drug intervention on the development and progression of hydrocephalus. The PCP-R cell line is utilized for studies which aim to understand the mechanisms by which CSF is produced. Using Ussing chamber electrophysiology, we are able to study the role of specific channels, transporters and modulators in driving epithelial ion flux across the CP.

This research aims to establish a role for TRPV4 in production and regulation of CSF, and to interrogate a mechanism by which this ion transport occurs. The chapters that follow describe components of the pathway by which TRPV4 is activated and ion flux is stimulated.

CHAPTER 1. INTRODUCTION

1.1 Hydrocephalus

Hydrocephalus, colloquially known as "water on the brain" is a condition in which the cerebrospinal fluid (CSF) production, secretion, absorption and/or composition may be aberrant, and can manifest in one of several ways culminating with the enlargement of the cerebral ventricles. Communicating hydrocephalus is a state in which CSF is either overproduced, or underabsorbed (10,13,45). Alternatively, hydrocephalus can develop as a result of a blockage in the CSF circulatory pathways called non-communicating hydrocephalus. Non-communicating hydrocephalus typically occurs as a result of aqueductal stenosis, the blocking of the cerebral aqueducts (11,31). Various tumors including cerebral tumors, intraventricular tumors of the ependyma, or choroid plexus papilloma have all been shown to result in hydrocephalus. Additionally, genetic defects, intracranial hemorrhaging, inflammation due to chronic or acute infection, and head trauma can also lead to the development of hydrocephalus (31,53).

Hydrocephalus may occur at any age in individuals, with multiple unique etiologies contributing to the disease. In newborns, this causes the characteristic doming of the cranium when left untreated (10,45,84). In the elderly population, neurodegenerative disease has recently also been implicated in occurrences of hydrocephalus (11,84). In contrast to classical hydrocephalus, which is marked by increased pressure on the brain due to the accumulation of CSF in the ventricles, the disease may also manifest in the elderly population as normal pressure hydrocephalus (NPH) (84). Though not well understood, this form of hydrocephalus generally does not feature increased intracranial pressure, while still typically displaying enlarged cerebral ventricles. Recent literature, however, suggests that NPH may also display aberrant intracranial pressures. Rarely diagnosed, due to similarities with other neurodegenerative diseases, NPH is considered one of the more readily treated and reversible forms of hydrocephalus if identified early in its progression (84).

Hydrocephalus in the juvenile population occurs at a rate of approximately 1 in 1000 live births and is among the most severe forms of the disease (85,97). The most common cause of hydrocephalus in infants is a result of intraventricular hemorrhaging, resulting in the development

of post-hemorrhagic hydrocephalus of prematurity (PHHP) (28). In addition, genetic defects, spina bifida, and traumatic brain injury are among other causes that also lead to the accumulation of CSF in the ventricles, causing significant increases in intracranial hydrostatic pressure and resulting in loss of brain matter, neuronal cell death, cranial doming, and potentially death (85).

1.2 Treatment of Hydrocephalus

Surgical intervention is the most common treatment for hydrocephalus. Most common is shunt implantation, which redirects flow of CSF drainage in to an alternative body cavity. Additionally, endoscopic third ventriculostomy (ETV) is utilized in non-communicating hydrocephalus. By creating a small perforation in the third ventricle via an endoscope, the blockage can be bypassed allowing CSF to be redirected to an alternative cavity for reabsorption (54,97). Also in clinical trials is choroid plexus cauterization, which involves irreversible destruction of the main source of CSF production within the ventricles (54). Surgical interventions come with significant risk; shunt implantation, currently the most widely used treatment for hydrocephalus, often requires surgical revision to treat infections, blockages or juveniles outgrowing their shunts. The rate of revision is approximately 70% at one year post-implantation of the shunts in the pediatric population, with lower rates in the adult population (97).

ETVs and choroid plexus cauterization also come with considerable risk. In the case of ETVs, closure of the hole can occur, resulting in ETV failure and necessitating the implantation of a shunt to redirect CSF flow (54,97). Finally, choroid plexus cauterization is an irreversible procedure which results in destruction of the CSF-producing choroid plexus. This procedure also comes with a failure rate of 59% at 12 months (54,97). Failure is defined as either recurrence of symptomatic hydrocephalus, CSF infection, or significant intraoperative complication, including neurological defects and death. Furthermore, if successful, the long-term effects of this procedure on developing children is currently unknown. While more often performed in underdeveloped nations where access to surgical care for shunt revisions is less accessible, cauterization nevertheless is a relatively new procedure being established across the globe.

The risks and side effects of any of the surgical interventions highlight the need for non-invasive pharmacological alternatives to treat hydrocephalus. The studies in our laboratory are directed toward a better understanding of the process involved in CSF production and, consequently, an identification of potential drug targets.

1.3 The Choroid Plexus

The human brain weights approximately 1500 grams, yet while cushioned in the CSF, which provides neutral buoyancy, the net weight of the brain is only observed to be about 25 to 50 grams (11,14). CSF protects the brain from injury, by reducing the effective weight of the tissue (11,14). At any given time, the body only contains 150 ml of CSF, however the body produces roughly 500 ml of CSF daily, almost a 3-time turnover rate (11,15,53,101). The bulk of this CSF is produced by the choroid plexus (CP), a highly vascularized branching network of cells extending outward in to the cerebral ventricles (14,15,19,20,38,53,56,62,74,90,101). The choroid plexus is composed of a high-resistance monolayer epithelium surrounding a fenestrated capillary bed and is present in both lateral ventricles, as well as the third and fourth ventricles (14,15,19,20,53,56,62,74,90). Approximately 70-80% of the CSF is produced by the choroid plexus epithelium, with the remainder produced by the ependymal cells lining the ventricles, as well as cells lining the subarachnoid space (11,15,74). CSF is believed to play an integral role in the removal and clearance of waste products from the central nervous system (CNS) (16,27,38,80,103). This appears to be controlled primarily by the wake-sleep cycle, allowing for daily recycling of CSF, reducing the buildup of potentially toxic chemicals within the CNS (27).

CSF is produced by the flow of water and solutes from blood, via the choroid plexus epithelial cells, to the intraventricular space (11,15,18,69,71,74,90). Small ions, such as sodium, potassium, chloride and bicarbonate are transported across the epithelium via transport proteins and ion channels, representing both active and passive transport events. The presence of tight junctions restricts most solute movement and limit paracellular ion transport (39,56,75,77,92). Water moves via aquaporins in a transcellular fashion, as well as via paracellular tight junctional complexes (18,69,74). Differences in the composition of blood and CSF highlight the complex role of the choroid plexus in regulating and producing CSF (75,90). The CSF is hyperosmolar with regard to

blood, chloride increased in the CSF, while calcium and potassium are observed to be slightly higher in the plasma (75). Therefore, ion transporters located on the apical or basolateral membranes of the choroid plexus are potential targets for pharmacological regulation of ion flux and CSF production in hydrocephalic cases.

1.4 Transient Receptor Potential Vanilloid 4

Water movement and CSF production are driven by the transepithelial flow of ions from the blood to the CSF, which are transported via ion channels and transporters (67,76,86). One particular channel of interest is Transient Receptor Potential Vanilloid-4 (TRPV4). TRPV4 is a non-selective, calcium-permeable cation channel located on the apical membrane of the choroid plexus (67,68,76). TRPV4 is both mechano- and osmo-sensitive, allowing it to play a key role in many regulatory events among various cells, including Ca^{2+} homeostasis and regulatory volume decrease (RVD) (6,9,22,67,100).

TRPV4 can be activated by osmotic stress, pressure, changes in fluid flow, sheer shress, as well as chemical activators such as 4α-PDD, arachidonic acid metabolites, and synthetic compounds such as GSK1016790A (76,99,100). When activated, TRPV4 allows for movement of ions, including calcium, potassium and sodium, across the membrane of the cell (6,22,55,67,77,95). Influx of these ions into the cell results in stimulation of secondary proteins, notably calcium-activated potassium and calcium-activated chloride channels (6,55,57,58,76). When stimulated, these channels allow for additional movement of ions across the cell membranes. This transepithelial flow of ions may result in the movement of water and may ultimately contribute to the production of CSF.

In overventilated mice, TRPV4 inhibition prevented vascular leakage and lung inflammation (65). Additionally, following traumatic brain injury, TRPV4 expression was increased in rat hippocampus, dependent on the NKCC1 cotransporter (61). In mouse mammary cells, TRPV4 activation was shown to increase intracellular calcium, resulting in acute increases in transcellular conductance (77). This increase in conductance occurred in tandem with activation of the BK channel, a calcium activated cation channel. These pathways have multiple physiological effects,

suggesting TRPV4 TRPV4 therefore may act as a hub protein, integrating complex molecular signals to regulate ion flux across cells (22,76).

1.5 The WPK Rat Model of Hydrocephalus

To study the channels and pathways mentioned, we utilize an *in vitro* choroid plexus cell line model, as well as an *in vivo* Wpk rodent model. The WPK rat model is orthologous to Meckel-Gruber Type 3 syndrome (MKS3), a ciliopathy resulting in polycystic kidney disease as well as hydrocephalus (81,88). The WPK rat contains a single C to T point mutation in the TMEM67 gene on chromosome 5, resulting in a homozygous recessive phenotype which displays both severe polycystic kidney disease as well as a rapidly progressing hydrocephalus. The homozygous animals do not survive to weaning, providing a severe model analogous to neonatal hydrocephalus (81). The heterozygous mutants display a mild, asymmetrical hydrocephalus phenotype which is noticeably less severe than the homozygous mutants. This hydrocephalus progresses more slowly with the animals not exhibiting signs of distress until about one year of age (81). Interestingly, unlike the homozygous animals, the heterozygous population do not develop polycystic kidney disease. The heterozygous animals therefore appear to more closely mimic slowly progressing hydrocephalus typical of the geriatric population.

Preliminary animal studies with the Wpk rats have shown that inhibition of TRPV4 in the TMEM67$^{-/-}$ WPK rat model of hydrocephalus results in a reduction in ventricular volume (21,88). When treated with the TRPV4 inhibitor RN1734, the ventricular volumes of juvenile homozygous animals were shown to be similar to those of wild type animals treated with either RN1734 or vehicle, and significantly smaller than the ventricular volumes of vehicle treated homozygous animals (Figure 1.1). This difference in ventricular volume is defined as the change in ventricular volume from day 7 to day 15. These data suggest that TRPV4 may be an intriguing drug target to restrict production of CSF and ameliorate the pathophysiology associated with hydrocephalus.

1.6 **Porcine Choroid Plexus Cell Line**

The porcine choroid plexus-Riems (PCP-R) cell line was first described in 2012 by Schroten et al. (79). This *in vitro* model develops a high resistance monolayer, and expresses all proteins examined thus far which are seen in native CP tissue, with the exception of NCBE. The PCP-R cells grow as a polarized epithelium, allowing for the expression of transporters to specific membranes, which in the native tissue allows the CP to regulate ion flux across the epithelium and produce CSF (56,79). In our laboratory, we utilize the PCP-R cells for electrophysiological experiments as well as for studies utilizing immunofluorescence (IF), reverse-transcriptase based PCRs (RT-PCR), and quantitative PCR (qPCR). PCP-R cells are grown on permeable supports until confluent, ~10-11 days. Cells are then mounted in Ussing chambers, which are used to model the *in vivo* cell environments (76,86). These cells allow for studies related to the nature of transepithelial ion flux in the choroid plexus, through varied use of specific inhibitors, intracellular mediators such as cAMP, as well as modulation of the extracellular environment including temperature, fluid pressure, or ion gradients across the membrane (76,86). Short circuit current, a measure of net ion movement, and conductance, a measure of barrier permeability are recorded.

To elucidate a mechanism for TRPV4-mediated ion flux, we use inhibitors of various transporters, ion channels, kinases and other genes and observe their effects on transepithelial ion flux and conductance following activation of TRPV4 with its specific agonist GSK1016790A. These studies allow us to determine the role specific proteins play in the TRPV4 pathway, giving insight to the mechanism and providing new pharmacological targets for modulating TRPV4 activity.

1.7 **Chloride Transporters**

In the CP, [Cl^-] is exquisitely regulated via apically and basolaterally bound transporters and ion channels (14,15,19,20). The movement of Cl^- may be key to producing CSF; Cl^- must be actively transported against its ionic gradient via transcellular transport (14,19). Cl^- is thought to be transported down its osmotic gradient into the cell via the basolaterally localized Cl^-/HCO_3^- exchanger AE2 (Anion exchange protein 2, SLC4A2), resulting in net influx of Cl^- and efflux of HCO_3^- into the plasma (14,15,19). This influx of Cl^- appears to be driven by activity of the enzyme

carbonic anhydrase (19,20,74). Carbonic anhydrase is an enzyme found within the CP which converts intracellular CO_2 and water into HCO_3^- and free H^+. This conversion of CO_2 may in part be responsible for the influx of Cl^- necessary to drive fluid movement in a transcellular fashion (19). The resulting increase in intracellular [Cl^-] in turn drives the extrusion of Cl^- via apically localized transporters (14,15). In addition to AE2, NCBE (NBCn2, SLC4A10) is also responsible for Cl^-/HCO_3^- exchange, working in the opposite direction to AE2 (19,20). NCBE activity results in net influx of Na^+ and HCO_3^- from serum to the cytoplasm, coupled with Cl^- efflux in to the serum (19,20).

Calcium-activated chloride channels (CaCC's) are a group of proteins that are activated by increases in intracellular [Ca^{2+}] and respond by secreting Cl^- (66,72,93). This family of proteins is comprised primarily of the anoctamin family (17,66,72,93). The anoctamins consist of the TMEM16 genes, of which TMEM16A (ANO1) is a member. Originally identified in 2008, TMEM16A is an apically localized Cl^- channel, which, in intestinal and airway epithelia contribute to Cl^- conductances in a minor role (66). In isolated murine CP cells, TMEM16A was shown to contribute to Cl^- efflux induced by increases in intracellular [Ca^{2+}] (93).

The cystic fibrosis transmembrane regulatory protein (CFTR) is perhaps the most well-described chloride channel in transporting epithelia. Of the more than 2000 gene mutations described in the gene, more than 200 have been shown to cause a cystic fibrosis phenotype (17). Some controversy exists as to the role CFTR plays in Cl^- transport in the CP (44,51,52). Current consensus opinion is that CFTR mRNA is not present in the CP, and functional studies have demonstrated that CFTR does not contribute to Cl^- currents in the CP epithelium (19).

1.8 Calcium-Activated Potassium Channels

Calcium-activated potassium channels (K_{Ca}) are a group of proteins that are activated by increases in intracellular calcium (61,96,98). These include the large conductance (BK, K_{Ca}1.1, KCNMA1), intermediate conductance (IK, K_{Ca}3.1, KCNN4), and small conductance (SK1-3, K_{Ca} 2.1, 2.2, 2.3, KCNN1-3) potassium channels (1,7,8,30,59,71,87,96). Ca^{2+}-activated K^+ channels are widely expressed in epithelia, smooth muscle and neuronal tissues (1,4,7,8,30,41,59,71,87,96,98). These channels function to secrete K^+ in to the luminal space, contributing to polarization of membrane

potentials and limiting [Ca^{2+}] influx (1,7,8,30,41,59,96,98). The BK channel has been shown to form a Ca^{2+}-signaling complex with ryanodine receptors, resulting in arterial dilation and smooth muscle hyperpolarization (29). Additionally, apically localized BK channel can be activated by TRPV4 in mammary cells causing an increase in transcellular conductance (77). SK channels are typically expressed in the nervous system, where they contribute to hyperpolarization following action potentials (30,98). The IK channel is found in many epithelia, including surface skin cells, secretory gland epithelia, distal colon and rat choroid plexus (41,87,94). In arteriolar endothelial cells, the IK channel appears to contribute to hyperpolarization leading to a reduction in arterial tone and results in vasodilation (4).

1.9 Sodium-Potassium-Chloride and Potassium-Chloride Cotransporters

Recent published studies have suggested that the sodium-potassium-chloride cotransporters may also play a role in CSF production in the choroid plexus (25,39,42,49,50,63,102). The sodium-potassium-2 chloride (NKCC) cotransporter exists in humans in two forms; NKCC1 and NKCC2, encoded by SLC12A2 and SLC12A1, respectively (3,42). NKCC1 is typically found in the brain parenchyma, and specifically in the apical membrane of the choroid plexus, while NKCC2 is localized to the basolateral membrane of the thick ascending loop of Henle in the kidney (3,42,47,50). NKCC1 is more ubiquitously expressed throughout transporting epithelia while NKCC2 is thought to be kidney-specific (3,42,50). This transmembrane protein, when activated, transports two molecules of chloride for every one molecule of potassium and sodium.

Recently, it was suggested that alterations in osmotic concentrations can alter the direction of ion flux of NKCC, changing the driving forces from net influx to net efflux of ions (25,39). It has been suggested that this transporter may be an interesting target for CSF regulation (49). In the CP, it appears that NKCC may also be responsible for establishment of the electrochemical gradient, allowing for transepithelial ion flux and CSF secretion (8,25). Also of interest are the potassium chloride cotransporters (KCC1-4, SLC12A4-7) and the sodium-chloride cotransporter (NCC, SLC12A3). While not as well understood as the NKCCs, these proteins have been identified in the choroid plexus and may also contribute to fluid production (19,20,47,50,63,92,102). KCC4 is thought to be localized apically, while KCC3 is basolateral (15,19,20,48). Both KCCs in the CP appear to work in net efflux, driving Cl^- and K^+ efflux from the cytoplasm (15,19,20).

1.10 STE20/SPS1-Related Proline-Alanine-Rich Protein Kinase

TRPV4, NKCCs, and the KCCs are regulated by various intracellular mediators. Of particular interest is STE20/SPS1-related proline-alanine-rich protein kinase (SPAK). Evolutionarily redundant for OSR1, SPAK is a kinase which is phosphorylated by WNK (with no lysine, (K)) kinases, and in turn phosphorylates downstream targets (24,25,33-35,49,64,70,73,78). Called the WNK-SPAK/OSR1 pathway, this mechanism results in phosphorylation and activation of the NKCCs (2,3,24-26,32-35,37,43,46,47,64,73). This regulation of NKCC by SPAK may play a vital role in cell volume regulation and homeostasis (3,42,78). SPAK is also known to phosphorylate the NCC and the KCC cotransporters. Phosphorylation of NCC by SPAK results in activation, similar to NKCC, while phosphorylation of the KCCs by SPAK results in inhibition of the cotransporters (26,46,78). Anecdotal evidence exists to suggest that the WNK-SPAK/OSR1 pathway may also regulate TRPV4 activity. In human endothelial kidney (HEK-293) cells, WNK4 coexpression with TRPV4 resulted in downregulation of TRPV4 (32,36). Immunoprecipitation however was unable to show a direct effect of WNK4 on TRPV4, and the mechanism of regulation is of yet unknown.

1.11 Translational Potential

Hydrocephalus affects more than 6 million individuals worldwide, yet little is known about the mechanisms by which the disease develops. Currently, the only widely used treatments clinically are the insertion of shunts, which are prone to failure, particularly in the young (48). In some parts of the world with limited surgical availability, experimental treatments such as endoscopic third ventriculostomies and choroid plexus ablation are becoming more common (48,91). It is of great importance therefore to develop non-surgical treatments for hydrocephalus.

To develop better drug targets, more must be understood about the underlying mechanisms of CSF production by the choroid plexus. The focus of our research and in particular my project is to better understand the mechanisms responsible for production and regulation of CSF. Each of the

following chapters reflects different aspects of the projects to which I've contributed. Chapters 2 and 5 are published data, while chapters 3 and 4 detail studies that are being prepared for publication. Chapters 2, 3 and 5 each have a preface which outlines my unique contributions to the work, while chapter 4 is ongoing work in which I have been solely involved thus far.

Chapter 2 is a publication in which we characterized the PCP-R cell line, the basis for much of our mechanistic studies. This manuscript, titled "Activation of TRPV4 Stimulates Transepithelial Ion Flux in a Porcine Choroid Plexus Cell Line," was published in *American Journal of Physiology: Cell Physiology* in December 2018. The focus of this publication was to describe the interactions between TRPV4 and calcium activated potassium channels, and describe the role TRPV4 plays in stimulating transepithelial ion flux. Chapter 3 is a manuscript which is currently being prepared for publication, which attempts to elucidate the role of NKCC in the TRPV4 pathway and investigate the role SPAK plays in regulation of this pathway. Chapter 4 contains data pertaining to the role of calcium activated chloride channels in the TRPV4 mechanism and addresses the question of chloride regulation in the choroid plexus. Chapter 5 is a paper which was published in August 2019. This paper outlines the role of inflammatory mediators and cytokines play in modulating TRPV4 activity in the PCP-R cell line.

These studies contribute to establishing a mechanism of activation and regulation for TRPV4 in the choroid plexus. Taken together with the emerging animal data, these data demonstrate a role for TRPV4 in the development of hydrocephalus and offer a potential pharmacological target through which the production of CSF may be altered. Additionally, these studies contribute to an understanding of intracellular mechanisms by which various ions are regulated, leading to CSF production.

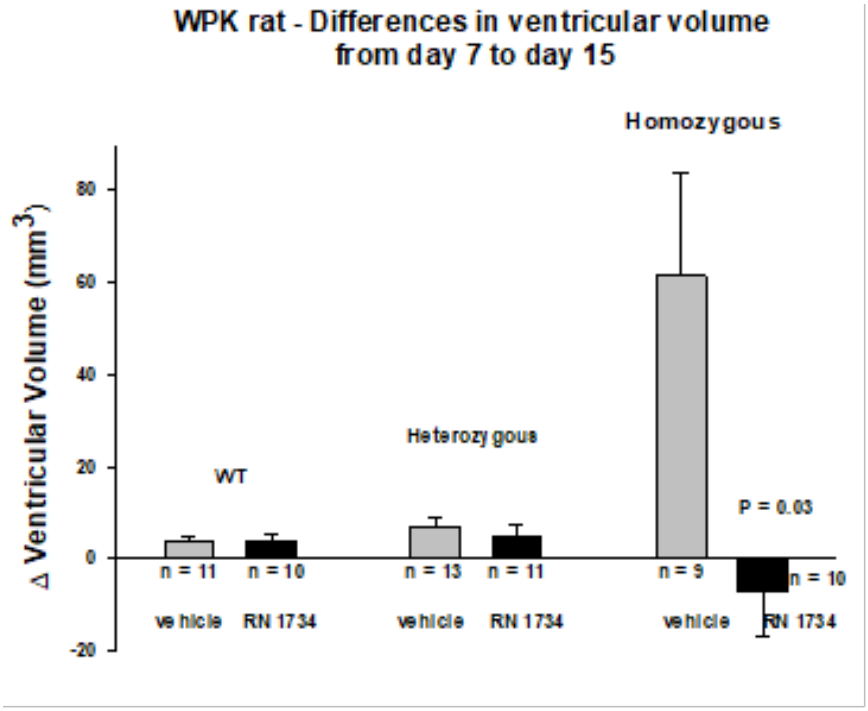

Figure 1.1 Ventricular Volumes of Treated vs Untreated WPK Rats.

Wild-type (WT), TMEM67(+/-), and TMEM67(-/-) pups were treated with 4 mg/kg body weight RN1734, a TRPV4 antagonist daily via i.p. injections from day 7 to 14. MRIs were taken on day 15. Hydrocephalus results in an increase in ventricular volume, shown from day 7 to 15 as Δ ventricular volume. This increase in ventricular volume was inhibited by drug treatment in homozygous rat pups ($p = 0.03$). Figure is unpublished data from the Blazer-Yost lab.

1.12 **References**

1. Adelman J, Maylie J, Sah P. Small-conductance Ca^{2+}-activated K^+ channels: Form and function. *Annual Review Of Physiology*, *74*(1), 245-269, 2012.
2. Alessi D, Zhang J, Khanna A, Hochdorfer T, Shang Y, Kahle K. The WNK-SPAK/OSR1 pathway: Master regulator of cation-chloride cotransporters. *Science Signaling* 7: 1-9, 2014.
3. Arroyo J, Kahle K, Gamba G. The SLC12 family of electroneutral cation-coupled chloride cotransporters. *Molecular Aspects of Medicine* 34: 288-298, 2013.
4. Bagher P, Beleznai T, Kansui Y, Mitchell R, Garland C, Dora K. Low intravascular pressure activates endothelial cell TRPV4 channels, local Ca^{2+} events, and IK_{Ca} channels, reducing arteriolar tone. *Proceedings Of The National Academy Of Sciences*, *109*(44), 18174-18179, 2012.
5. Banizs B, Pike M, Millican C, Ferguson W, Komlosi P, Sheetz J, Bell P, Schwiebert E, Yoder B. Dysfunctional cilia lead to altered ependyma and choroid plexus function, and result in the formation of hydrocephalus. *Development* 132: 5329-5339, 2005.
6. Baratchi S, Keov P, Darby W, Lai A, Khoshmanesh K, Thurgood P, Vahidi P, Ejendal K, McIntyre P. The TRPV4 Agonist GSK1016790A Regulates the Membrane Expression of TRPV4 Channels. *Frontiers in Pharmacology* 10, 2019.
7. Barmeyer C, Rahner C, Yang Y, Sigworth F, Binder H, Rajendran V. Cloning and identification of tissue-specific expression of KCNN4 splice variants in rat colon. *American Journal Of Physiology-Cell Physiology*, *299*(2), C251-C263, 2010.
8. Basalingappa K, Rajendran V, Wonderlin W. Characteristics of Kcnn4 channels in the apical membranes of an intestinal epithelial cell line. *American Journal Of Physiology-Gastrointestinal And Liver Physiology*, *301*(5), G905-G911, 2011.
9. Benfenati V, Caprini M, Dovizio M, Mylonakou M, Ferroni S, Ottersen O, Amiry-Moghaddam M. (2011). An aquaporin-4/transient receptor potential vanilloid 4 (AQP4/TRPV4) complex is essential for cell-volume control in astrocytes. *Proceedings Of The National Academy Of Sciences*, *108*(6), 2563-2568.
10. Bothwell S, Janigro D, Patabendige A. Cerebrospinal fluid dynamics and intracranial pressure elevation in neurological diseases. *Fluids and Barriers of the CNS* 16, 2019.

11. Bouzinova E, Praetorius J, Virkki L, Nielsen S, Boron W, Aalkjaer C. Na+-dependent HCO3− uptake into the rat choroid plexus epithelium is partially DIDS sensitive. *American Journal of Physiology-Cell Physiology* 289: C1448-C1456, 2005.
12. Brodbelt A, Stoodley M. CSF pathways: a review. *British Journal of Neurosurgery* 21: 510-520, 2007.
13. Brown P, Davies S, Speake T, Millar I. Molecular mechanisms of cerebrospinal fluid production. *Neuroscience* 129: 955-968, 2004.
14. Crossgrove J, Li G, Zheng W. The choroid plexus removes β-amyloid from brain cerebrospinal fluid. *Experimental Biology And Medicine*, *230*(10), 771-776, 2005.
15. Csanády L, Vergani P, Gadsby D. Structure, Gating, and Regulation of the CFTR Anion Channel. *Physiological Reviews* 99: 707-738, 2019.
16. Cserr H. Physiology of the choroid plexus. *Physiological Reviews*, *51*(2), 273-311, 1971.
17. Damkier H, Brown P, Praetorius J. Cerebrospinal Fluid Secretion by the Choroid Plexus. *Physiological Reviews* 93: 1847-1892, 2013.
18. Damkier H, Brown P, Praetorius J. Epithelial Pathways in Choroid Plexus Electrolyte Transport. *Physiology* 25: 239-249, 2010.
19. Danko C, Preston D, Simpson S, Blazer-Yost B. Effects of a TRPV4 antagonist on hydrocephalus in the Wpk rat model. Abstract *FASEB J* 31:1042.4, 2017.
20. Darby W, Grace M, Baratchi S, McIntyre P. Modulation of TRPV4 by diverse mechanisms. *The International Journal of Biochemistry & Cell Biology* 78: 217-228, 2016.
21. Deneka D, Sawicka M, Lam A, Paulino C, Dutzler R. Structure of a volume-regulated anion channel of the LRRC8 family. *Nature* 558: 254-259, 2018.
22. de los Heros P, Alessi D, Gourlay R, Campbell D, Deak M, Macartney T, Kahle K, Zhang J. The WNK-regulated SPAK/OSR1 kinases directly phosphorylate and inhibit the K+–Cl−co-transporters. *Biochemical Journal* 458: 559-573, 2014.
23. Delpire E, Gagnon K. Elusive role of the Na-K-2Cl cotransporter in the choroid plexus. *American Journal of Physiology-Cell Physiology* 316: C522-C524, 2019.
24. Delpire E, Gagnon K. SPAK and OSR1, key kinases involved in the regulation of chloride transport. *Acta Physiologica* 187: 103-113, 2006.

25. Ding F, O'Donnell J, Xu Q, Kang N, Goldman N, Nedergaard M. Changes in the composition of brain interstitial ions control the sleep-wake cycle. *Science* 352: 550-555, 2016.

26. Dorner R, Burton V, Allen M, Robinson S, Soares B. Preterm neuroimaging and neurodevelopmental outcome: a focus on intraventricular hemorrhage, post-hemorrhagic hydrocephalus, and associated brain injury. *Journal of Perinatology* 38: 1431-1443, 2018.

27. Earley S., Heppner T, Nelson M., Brayden J. TRPV4 forms a novel Ca^{2+} signaling complex with ryanodine receptors and BK_{Ca} channels. *Circulation Research*, *97*(12), 1270-1279, 2005.

28. Faber E, Sah P. FUNCTIONS OF SK CHANNELS IN CENTRAL NEURONS. *Clinical and Experimental Pharmacology and Physiology* 34: 1077-1083, 2007.

29. Filis A, Aghayev K, Vrionis F. Cerebrospinal Fluid and Hydrocephalus: Physiology, Diagnosis, and Treatment. *Cancer Control* 24: 6-8, 2017.

30. Fu Y, Subramanya A, Rozansky D, Cohen D. WNK kinases influence TRPV4 channel function and localization. *American Journal of Physiology-Renal Physiology* 290: F1305-F1314, 2006.

31. Gagnon K, Delpire E. Molecular Physiology of SPAK and OSR1: Two Ste20-Related Protein Kinases Regulating Ion Transport. *Physiological Reviews* 92: 1577-1617, 2012.

32. Gagnon K, England R, Delpire E. Characterization of SPAK and OSR1, Regulatory Kinases of the Na-K-2Cl Cotransporter. *Molecular and Cellular Biology* 26: 689-698, 2005.

33. Gagnon K, England R, Diehl L, Delpire E. Apoptosis-associated tyrosine kinase scaffolding of protein phosphatase 1 and SPAK reveals a novel pathway for Na-K-2C1 cotransporter regulation. *American Journal of Physiology-Cell Physiology* 292: C1809-C1815, 2007.

34. Gamba G. TRPV4: a new target for the hypertension-related kinases WNK1 and WNK4. *American Journal of Physiology-Renal Physiology* 290: F1303-F1304, 2006.

35. Geng Y, Hoke A, Delpire E. The Ste20 Kinases Ste20-related Proline-Alanine-rich Kinase and Oxidative-stress Response 1 Regulate NKCC1 Function in Sensory Neurons. *Journal of Biological Chemistry* 284: 14020-14028, 2009.

36. Ghersi-Egea J, Babikian A, Blondel S, Strazielle N. Changes in the cerebrospinal fluid circulatory system of the developing rat: quantitative volumetric analysis and effect on blood-CSF permeability interpretation. *Fluids And Barriers Of The CNS*, *12*(1), 8, 2015.

37. Gregoriades J, Madaris A, Alvarez F, Alvarez-Leefmans F. Genetic and pharmacological inactivation of apical Na+-K+-2Cl− cotransporter 1 in choroid plexus epithelial cells reveals the physiological function of the cotransporter. *American Journal of Physiology-Cell Physiology* 316: C525-C544, 2019.

38. Günzel D, Yu A. Claudins and the modulation of tight junction permeability. *Physiological Reviews*, *93*(2), 525-569, 2013.

39. Halm S, Liao T, and Halm D. Distinct K^+ conductive pathways are required for Cl^- and K^+ secretion across distal colonic epithelium. *American Journal Of Physiology-Cell Physiology*, *291*(4), C636-C648, 2006.

40. Hebert S, Mount D, Gamba G. Molecular physiology of cation-coupled Cl? cotransport: the SLC12 family. *European Journal of Physiology* 447: 580-593, 2004.

41. Hengl T, Kaneko H, Dauner K, Vocke K, Frings S, Mohrlen F. Molecular components of signal amplification in olfactory sensory cilia. *Proceedings of the National Academy of Sciences* 107: 6052-6057, 2010.

42. Hincke M, Nairn A, Staines W. Cystic Fibrosis Transmembrane Conductance Regulator Is Found Within Brain Ventricular Epithelium and Choroid Plexus. *Journal of Neurochemistry* 64: 1662-1668, 2002.

43. Kahle K, Ring A, Lifton R. Molecular Physiology of the WNK Kinases. *Annual Review of Physiology* 70: 329-355, 2008.

44. Kanaka C, Ohno K, Okabe A, Kuriyama K, Itoh T, Fukuda A, Sato K. The differential expression patterns of messenger RNAs encoding K-Cl cotransporters (KCC1,2) and Na-K-2Cl cotransporter (NKCC1) in the rat nervous system. *Neuroscience* 104: 933-946, 2001.

45. Karadsheh M, Byun N, Mount D, Delpire E. Localization of the kcc4 potassium–chloride cotransporter in the nervous system. *Neuroscience* 123: 381-391, 2004.

46. Karimy J, Zhang J, Kurland D, Theriault B, Duran D, Stokum J, Furey C, Zhou X, Mansuri M, Montejo J, Vera A, Diluna M, Delpire E, Alper S, Gunel M, Gerzanich V, Medzhitov R, Simard J, Kahle K. Inflammation-dependent cerebrospinal fluid hypersecretion by the choroid plexus epithelium in posthemorrhagic hydrocephalus. *Nature Medicine* 23: 997-1003, 2017.

47. Keep R, Xiang J, Betz A. Potassium cotransport at the rat choroid plexus. *American Journal of Physiology-Cell Physiology* 267: C1616-C1622, 1994.

48. Kibble J, Garner C, Colledge W, Brown S, Kajita H, Evans M, Brown P. Whole cell Cl- conductances in mouse choroid plexus epithelial cells do not require CFTR expression. *American Journal of Physiology-Cell Physiology* 272: C1899-C1907, 1997.

49. Kibble J, Trezise A, Brown P. Properties of the cAMP-activated Cl- current in choroid plexus epithelial cells isolated from the rat. *The Journal of Physiology* 496: 69-80, 1996.

50. Kousi M, Katsanis N. The Genetic Basis of Hydrocephalus. *Annual Review of Neuroscience* 39: 409-435, 2016.

51. Kulkarni A, Riva-Cambrin J, Rozzelle C, Naftel R, Alvey J, Reeder R, Holubkov R, Browd S, Cochrane D, Limbrick D, Simon T, Tamber M, Wellons J, Whitehead W, Kestle J. Endoscopic third ventriculostomy and choroid plexus cauterization in infant hydrocephalus: a prospective study by the Hydrocephalus Clinical Research Network. *Journal of Neurosurgery: Pediatrics* 21: 214-223, 2018.

52. Kumar H, Lee S, Kim K, Zeng X, Han I. TRPV4: a Sensor for Homeostasis and Pathological Events in the CNS. *Molecular Neurobiology* 55: 8695-8708, 2018.

53. Lauer A, Tenenbaum T, Schroten H, Schwerk C. The diverse cellular responses of the choroid plexus during infection of the central nervous system. *American Journal of Physiology-Cell Physiology* 314: C152-C165, 2018.

54. Lee E, Shin S, Chun J, Hyun S, Kim Y, Kang S. The modulation of TRPV4 channel activity through its Ser 824 residue phosphorylation by SGK1. *Animal Cells and Systems* 14: 99-114, 2010.

55. Liedtke W, Choe Y, Martí-Renom M, Bell A, Denis C, Šali A, Hudspeth A.J., Friedman J, Heller S. Vanilloid Receptor–Related Osmotically Activated Channel (VR-OAC), a candidate vertebrate osmoreceptor. *Cell*, *103*(3), 525-535, 2000.

56. Lin M, Jian M, Taylor M, Cioffi D, Yap F, Liedtke W, Townsley M. Functional Coupling of TRPV4, IK, and SK Channels Contributes to Ca^{2+}-Dependent Endothelial Injury in Rodent Lung. *Pulmonary Circulation* 5: 279-290, 2015.

57. Loo, D, Brown, P, Wright, E. Ca^{2+}-activated K^{+} currents in Necturus choroid plexus. *The Journal Of Membrane Biology*, *105*(3), 221-231, 1988.

58. Lu K, Huang T, Tsai Y, Yang Y. Transient receptor potential vanilloid type 4 channels mediate Na-K-Cl-co-transporter-induced brain edema after traumatic brain injury. *Journal of Neurochemistry* 140: 718-727, 2017.

59. Lun M, Monuki E, Lehtinen M. Development and functions of the choroid plexus–cerebrospinal fluid system. *Nature Reviews Neuroscience* 16: 445-457, 2015.

60. MacAulay N, Hamann S, Zeuthen T. Water transport in the brain: Role of cotransporters. *Neuroscience* 129: 1029-1042, 2004.

61. Mercier-Zuber A, O'Shaughnessy K. Role of SPAK and OSR1 signalling in the regulation of NaCl cotransporters. *Current Opinion in Nephrology and Hypertension* 20: 534-540, 2011.

62. Michalick L, Erfinanda L, Weichelt U, van der Giet M, Liedtke W, Kuebler W. Transient Receptor Potential Vanilloid 4 and Serum Glucocorticoid–regulated Kinase 1 Are Critical Mediators of Lung Injury in Overventilated Mice In Vivo. *Anesthesiology* 126: 300-311, 2017.

63. Namkung W, Phuan P, Verkman A. TMEM16A Inhibitors Reveal TMEM16A as a Minor Component of Calcium-activated Chloride Channel Conductance in Airway and Intestinal Epithelial Cells. *Journal of Biological Chemistry* 286: 2365-2374, 2010.

64. Narita K, Sasamoto S, Koizumi S, Okazaki S, Nakamura H, Inoue T, Takeda S. TRPV4 regulates the integrity of the blood-cerebrospinal fluid barrier and modulates transepithelial protein transport. *The FASEB Journal* 29: 2247-2259, 2015.

65. Nilius, B, Vriens, J, Prenen, J, Droogmans, G, Voets, T. TRPV4 calcium entry channel: a paradigm for gating diversity. *American Journal Of Physiology-Cell Physiology*, *286*(2), C195-C205, 2004.

66. Oshio K, Watanabe H, Song Y, Verkman A, Manley G. Reduced cerebrospinal fluid production and intracranial pressure in mice lacking choroid plexus water channel Aquaporin-1. *The FASEB Journal* 19: 76-78, 2005.

67. Park S, Ku S, Ji H, Choi J, Shin D. Ca^{2+} is a Regulator of the WNK/OSR1/NKCC Pathway in a Human Salivary Gland Cell Line. *The Korean Journal of Physiology & Pharmacology* 19: 249, 2015.

68. Pedarzani P, Stocker M. Molecular and cellular basis of small- and intermediate-conductance, calcium-activated potassium channel function in the brain. *Cellular and Molecular Life Sciences* 65: 3196-3217, 2008.

69. Pedemonte N, Galietta L. Structure and Function of TMEM16 Proteins (Anoctamins). *Physiological Reviews* 94: 419-459, 2014.

70. Piechotta K, Lu J, Delpire E. Cation Chloride Cotransporters Interact with the Stress-related Kinases Ste20-related Proline-Alanine-rich Kinase (SPAK) and Oxidative Stress Response 1 (OSR1). *Journal of Biological Chemistry* 277: 50812-50819, 2002.

71. Praetorius J, Damkier H. Transport across the choroid plexus epithelium. *American Journal of Physiology-Cell Physiology* 312: C673-C686, 2017.

72. Praetorius J, Nielsen S. Distribution of sodium transporters and aquaporin-1 in the human choroid plexus. *American Journal of Physiology-Cell Physiology* 291: C59-C67, 2006.

73. Preston D, Simpson S, Halm D, Hochstetler A, Schwerk C, Schroten H, Blazer-Yost B. Activation of TRPV4 stimulates transepithelial ion flux in a porcine choroid plexus cell line. *American Journal of Physiology-Cell Physiology* 315: C357-C366, 2018.

74. Reiter B, Kraft R, Günzel D, Zeissig S, Schulzke J, Fromm M, Harteneck C. TRPV4-mediated regulation of epithelial permeability. *The FASEB Journal* 20: 1802-1812, 2006.

75. Richardson C, Alessi D. The regulation of salt transport and blood pressure by the WNK-SPAK/OSR1 signalling pathway. *Journal of Cell Science* 121: 3293-3304, 2008.

76. Schroten H, Hanisch F, Quednau N, Stump C, Riebe R, Lenk M, Wolburg H, Tenenbaum T, Schwerk C. A Novel Porcine In Vitro Model of the Blood-Cerebrospinal Fluid Barrier with Strong Barrier Function. *PLoS ONE* 7: e39835, 2012.

77. Serot J, Zmudka J, Jouanny P. A possible role for CSF turnover and choroid plexus in the pathogenesis of late onset Alzheimer's disease. *Journal Of Alzheimer's Disease*, *30*(1), 17-26, 2-12.

78. Shim J, Territo P, Simpson S, Watson J, Jiang L, Riley A, McCarthy B, Persohn S, Fulkerson D, Blazer-Yost B. Hydrocephalus in a rat model of Meckel Gruber syndrome with a TMEM67 mutation. *Scientific Reports* 9, 2019.

79. Shin S, Lee E, Chun J, Hyun S, Kang S. Phosphorylation on TRPV4 Serine 824 Regulates Interaction with STIM1. *The Open Biochemistry Journal* 9: 24-33, 2015.

80. Shin S, Lee E, Hyun S, Chun J, Kim Y, Kang S. Phosphorylation on the Ser 824 residue of TRPV4 prefers to bind with F-actin than with microtubules to expand the cell surface area. *Cellular Signalling* 24: 641-651, 2012.

81. Shprecher D, Schwalb J, Kurlan R. Normal pressure hydrocephalus: Diagnosis and treatment. *Current Neurology and Neuroscience Reports* 8: 371-376, 2008.

82. Simon T, Riva-Cambrin J, Srivastava R, Bratton S, Dean J, Kestle J. Hospital care for children with hydrocephalus in the United States: utilization, charges, comorbidities, and deaths. *Journal of Neurosurgery: Pediatrics* 1: 131-137, 2008.

83. Simpson S, Preston D, Schwerk C, Schroten H, Blazer-Yost B. Cytokine and inflammatory mediator effects on TRPV4 function in choroid plexus epithelial cells. *American Journal of Physiology-Cell Physiology* (2019). doi: 10.1152/ajpcell.00205.2019 *IN PRESS*.

84. Singh S, O'Hara B, Talukder J, Rajendran V. Aldosterone induces active K^+ secretion by enhancing mucosal expression of Kcnn4c and Kcnna1 channels in rat distal colon. *American Journal Of Physiology-Cell Physiology*, *302*(9), C1353-C1360, 2012.

85. Smith H, Hochstetler A, Preston D, Blazer-Yost B. Preclinical testing of TRPV4 antagonists for the treatment of hydrocephalus. *FASEB* 708.4, 2019.

86. Smith U, Consugar M, Tee L, McKee B, Maina E, Whelan S, Morgan N, Goranson E, Gissen P, Lilliquist S, Aligianis I, Ward C, Pasha S, Punyashthiti R, Malik Sharif S, Batman P, Bennett C, Woods C, McKeown C, Bucourt M, Miller C, Cox P, AlGazali L, Trembath R, Torres V, Attie-Bitach T, Kelly D, Maher E, Gattone V, Harris P, Johnson C. The transmembrane protein meckelin (MKS3) is mutated in Meckel-Gruber syndrome and the wpk rat. *Nature Genetics* 38: 191-196, 2006.

87. Speake T, Whitwell C, Kajita H, Majid A, Brown P. Mechanisms of CSF secretion by the choroid plexus. *Microscopy Research and Technique* 52: 49-59, 2000.

88. Steffensen A, Oernbo E, Stoica A, Gerkau N, Barbuskaite D, Tritsaris K, Rose C, MacAulay N. Cotransporter-mediated water transport underlying cerebrospinal fluid formation. *Nature Communications* 9, 2018.

89. Steinemann A, Galm I, Chip S, Nitsch C, Maly I. Claudin-1, -2 and -3 are selectively expressed in the epithelia of the choroid plexus of the mouse from early development and into adulthood while claudin-5 is restricted to endothelial cells. *Frontiers In Neuroanatomy*, 10, 2016.

90. Takayama Y, Shibasaki K, Suzuki Y, Yamanaka A, Tominaga M. Modulation of water efflux through functional interaction between TRPV4 and TMEM16A/anoctamin 1. *The FASEB Journal* 28: 2238-2248, 2014.

91. Thompson-Vest N, Shimizu Y, Hunne B, Furness J. The distribution of intermediate-conductance, calcium-activated, potassium (IK) channels in epithelial cells. *Journal of Anatomy* 208: 219-229, 2006.

92. Toft-Bertelsen T, Larsen B, MacAulay N. Sensing and regulation of cell volume – we know so much and yet understand so little: TRPV4 as a sensor of volume changes but possibly without a volume-regulatory role?. *Channels* 12: 100-108, 2018.

93. Vergara C, Latorre R, Marrion N, Adelman J. Calcium-activated potassium channels. *Current Opinion In Neurobiology*, *8*(3), 321-329, 1998.

94. Vinchon M, Rekate H, Kulkarni A. Pediatric hydrocephalus outcomes: a review. *Fluids and Barriers of the CNS* 9, 2012.

95. Weatherall K, Goodchild S, Jane D, Marrion N. Small conductance calcium-activated potassium channels: From structure to function. *Progress In Neurobiology*, *91*(3), 242-255, 2010.

96. White J, Cibelli M, Urban L, Nilius B, McGeown J, Nagy I. TRPV4: Molecular Conductor of a Diverse Orchestra. *Physiological Reviews* 96: 911-973, 2016.

97. Willette R, Bao W, Nerurkar S, Yue T, Doe C, Stankus G, Turner G, Ju H, Thomas H, Fishman C, Sulpizio A, Behm D, Hoffman S, Lin Z, Lozinskaya I, Casillas L, Lin M, Trout R, Votta B, Thorneloe K, Lashinger E, Figueroa D, Marquis R, Xu X. Systemic activation of the transient receptor potential vanilloid subtype 4 channel causes endothelial failure and circulatory collapse: Part 2. *Journal Of Pharmacology And Experimental Therapeutics*, *326*(2), 443-452, 2008.

98. Wright E. Transport processes in the formation of the cerebrospinal fluid. *Reviews Of Physiology, Biochemistry And Pharmacology, 83*, 3-34, 1978.

99. Wu Q, Delpire E, Hebert S, Strange K. Functional demonstration of Na^+-K^+-$2Cl^-$ cotransporter activity in isolated, polarized choroid plexus cells. *American Journal Of Physiology-Cell Physiology*, *275*(6), C1565-C1572, 1998.

100. Xie L, Kang H, Xu Q, Chen M, Liao Y, Thiyagarajan M,)'Donnell J, Christensen D, Nicholson C, Iliff J, Takano T, Deane R, Nedergaard M. Sleep drives metabolite clearance from the adult brain. *Science*, *342*(6156), 373-377, 2013.

CHAPTER 2. ACTIVATION OF TRPV4 STIMULATES ION FLUX IN PCP-R CELLS

2.1 Preface

The journal article which immediately follows was accepted by *American Journal of Physiology: Cell Physiology* in May 2018. To this publication, I contributed electrophysiological experiments utilizing inhibitors of TRPV4 to determine efficacy of the inhibitors in our porcine choroid plexus cell line (Figures 2,4). These involved treating cultured cells with specific inhibitors of TRPV4, to show complete inhibition of transepithelial ion flux mediated by activation of TRPV4. Additionally, I conducted experiments demonstrating that use of inhibitors of several calcium-activated potassium channels were incapable of blocking the TRPV4-mediated ion flux. This included use of iberiotoxin to block the BK channel, as well as Apamin, Tamapin, Lei-Dab7, and Scyllatoxin to block the SK channels (Figures 8-9). This series of experiments showed that changes in short circuit currents observed upon activation of TRPV4 were not dependent on the large, or small conductance potassium channels.

My contributions further included design of all PCR primers utilized, as well as designing and performing all RT-PCR experiments. These experiments confirmed that mRNAs for the SK2 channel, as well as the IK channel were present in the PCP-R cell line, showing the ability of cells to transcribe these proteins. Additionally, we showed that TRPV4 was well expressed, an expected result from the activation of TRPV4, and that the BK channel was not expressed in our cell line, contradictory to the expression patterns in other tissues.

My final contributions to the paper involved drawing and designing a diagram of the choroid plexus epithelium (Figure 12). Additionally, I was involved in the manuscript preparation both prior to submission and during the review process, as well as preparing the primary figures for experiments I contributed towards. Additionally, I contributed to answering reviewers' questions and editing the manuscript accordingly following submission of the manuscript.

2.2 Activation of TRPV4 Stimulates Transepithelial Ion Flux in a Porcine CP Cell Line

Daniel Preston[1*], Stefanie Simpson[1*], Dan Halm[2], Alexandra Hochstetler[1], Christian Schwerk[3], Horst Schroten[3], Bonnie L. Blazer-Yost[1]

1. Department of Biology, Indiana University-Purdue University at Indianapolis, Indiana
2. Neuroscience, Cell Biology and Physiology, Wright State University, Dayton, Ohio
3. Mannheim Medical Faculty, University of Heidelberg, Childrens Hospital, Mannheim, Germany
* These authors contributed equally to the research

Running Title: The TRPV4 Hub Protein in Choroid Plexus

Corresponding Author
Bonnie L. Blazer-Yost
Indiana University-Purdue University Indianapolis
Biology Department, SL 358
723 West Michigan Street
Indianapolis, IN 46202
Tel: 317-278-1145; Fax: 317-274-2846
email: bblazer@iupui.edu

Keywords: Ca^{2+}-activated K^+ channels, epithelial conductance, blood-choroid plexus barrier, IK, TRAM34

D.P., S.S. and A.H. performed the electrophysiological experiments and calculated the results; D.P. conducted the RT-PCR experiments; S.S. performed the confocal imaging; D.H. provided intellectual input regarding the calculation and interpretation of conductance measurements; C.S. and H.S. provided the PCP-R cell line and advice regarding the culturing of the cells; B.B.Y. designed the experiments, approved the final data presentation and wrote the manuscript.

2.3 **Abstract**

The choroid plexus (CP) epithelium plays a major role in the production of cerebrospinal fluid (CSF). A polarized cell line, the porcine choroid plexus – Riems (PCP-R) line, that exhibits many of the characteristics of the native epithelium, was used to study the effect of activation of the transient receptor potential vanilloid 4 (TRPV4) cation channel found in the PCP-R cells as well as in the native epithelium. Ussing-style electrophysiological experiments showed that activation of TRPV4 with a specific agonist, GSK 1016790A, resulted in an immediate increase in both transepithelial ion flux and conductance. These changes were inhibited by either of two distinct antagonists, HC067047 or RN1734. The change in conductance was reversible and did not involve disruption of epithelial junctional complexes. Activation of TRPV4 results in Ca^{2+} influx, therefore, we examined whether the electrophysiological changes were the result of secondary activation of Ca^{2+}-sensitive channels. PCP-R cells contain two Ca^{2+}-activated K^+ channels, the small conductance (SK) 2 and the intermediate conductance (IK) channels. Based on inhibitor studies, the former is not involved in the TRPV4-mediated electrophysiological changes while one of the three isoforms of the IK channel (KCNN4c) may play a role in the apical secretion of K^+. Blocking the activity of this IK isoform with TRAM34 inhibited the TRPV4-mediated change in net transepithelial ion flux and the increased conductance. These studies implicate TRPV4 as a hub protein in the control of CSF production through stimulation by multiple effectors resulting in transepithelial ion and subsequent water movement.

2.4 **Introduction**

The choroid plexus (CP), formed by a tufted capillary surrounded by an epithelial monolayer, is thought to be responsible for the majority of cerebrospinal fluid (CSF) production. CSF cushions and protects the brain, substantially reducing the effective weight of the organ. CSF also serves as a medium to deliver nutrients, effectors and immune modulators as well as to remove toxins including β-amyloid (6, 22, 27, 36). In addition, CSF contributes to more subtle functions that are dependent on minor changes in electrolyte composition such as modulating sleep/wake cycles and neuronal excitability (10).

The CP is among the most secretory of the organ systems, with approximately 2 grams of tissue producing in excess of 0.5 liters of CSF per day in an adult human (7, 22, 34). The capillary bed that serves as the source of the major components of the CSF is lined with a fenestrated endothelium, therefore, producing a plasma filtrate based primarily on molecular size. The CP epithelium that surrounds the capillaries forms the blood-CSF barrier and is the basis for the selectivity that is responsible for the unique composition of the CSF by the regulated movement of electrolytes and water (7, 22, 34). Notably, in addition to a pH differential in which CSF is slightly more acidic (pH 7.27) compared to the interstitial fluid (pH 7.46), there are differences in electrolyte composition between the CSF and the plasma (22). Transporters and regulatory proteins present in the CP epithelial cells are responsible for creating and maintaining these crucial compositional differences. As recently reviewed (22), the major electrolyte transporters and aquaporins present in the CP have been elucidated, and their polarization within the epithelial membranes is well established. Other, less well-documented transporters remain to be identified. The effectors that control the expression and activation of these CP transport proteins remain largely unknown. Because the composition and volume of the CSF is not static but varies on a diurnal basis (10), understanding the complex mechanisms controlling the production of CSF is crucial for understanding critical brain functions in both health and disease.

Transient receptor potential vanilloid 4 (TRPV4) is one member of a family of mechano- and osmotic-sensitive channels found in multiple cell types, including the CP (16, 21, 33). When activated, TRPV4 acts as a non-specific cation channel that allows the influx of Ca^{2+} into cells. In several tissues, TRPV4 serves as a hub protein that coordinates multiple internal and external signals with the activation of electrolyte and water channels in a tissue-specific manner (9). TRPV4 has been shown to have direct effects on transport proteins in the brain including aquaporin-4 in astrocytes (5), and the Ca^{2+}-activated Cl^- channel, TMEM16A, in primary cultures of CP cells (30). In the hippocampus, TRPV4 was elevated 8 hours after traumatic brain injury and the increased expression was dependent on NKCC1 (18), a co-transporter which is also found in the apical membrane of native CP epithelia (35). Calcium influx through TRPV4 has also been shown to stimulate Ca^{2+}-sensitive K^+ channels in a tissue-specific manner. Ca^{2+}-sensitive K^+ channels fall into three categories: BK (big conductance; $K_{Ca}1.1$); IK (intermediate conductance; $K_{Ca}3.1$; KCNN4); or SK1, SK2, SK3 (small conductance; K_{Ca} 2.1, 2.2, 2.3) channels (28). In

endothelial cells of smaller resistance arteries and arterioles, low intraluminal pressure stimulates TRPV4 causing localized Ca^{2+} sparkletts which activate IK channels and reduce arteriole tone (2). In these resistance arteries, activation of the TRPV4 did not stimulate SK channels although the SK channel $K_{Ca}2.3$ is present in the endothelial cells. In freshly isolated cerebral myocytes, there are indications that TRPV4 forms a Ca^{2+} signaling complex with ryanodine receptors and BK channels that elicits smooth muscle hyper-polarization and arterial dilation (11). TRPV4 activation also resulted in the secondary activation of the BK channel in a high resistance mammary epithelial cell line (23). TRPV4 has been identified on the apical membrane of native CP epithelia (24, 30) and in primary CP cell lines (20, 30).

The complexity of the CP *in vivo* makes studying the regulation of electrolyte transporters challenging. Unfortunately, most *in vitro* primary cultures of CP epithelial cells exhibit a very low transepithelial electrical resistance (TER) that is inconsistent with the barrier function of these epithelia *in vivo*. In addition, a low transepithelial resistance poses technical difficulties when measuring permeability changes that may be part of an effector response. Continuous cell lines recently established in one of our laboratories (H.S. and C.S.) are, to our knowledge, the only lines described that exhibit a moderate to high TER (25, 26). The porcine choroid plexus – Riems (PCP-R) cell line expresses tight junction components, including claudin-1, claudin-3, ZO-1 and occludin, and develops a high transepithelial resistance when grown on permeable supports indicating the formation of a barrier epithelium (25). In the current studies, the PCP-R line was used to examine the physiological effects of TRPV4 stimulation on the permeability of the epithelial monolayer and on activation on electrogenic transepithelial ion flux.

2.5 **Materials and Methods**

Cell Culture: The PCP-R cell line was derived from primary cultures of porcine choroid plexus (25). PCP-R cells were grown in DMEM containing 4.5 g /L glucose, 3.7 g/L $NaHCO_3$, 24 mM HEPES, 10% fetal bovine serum, 100 U/ml penicillin, 100 mg/ml streptomycin and 5 µg/ml insulin. Cells were grown in a 75 cm^2 flask until confluent (typically 7-10 days). For electrophysiology experiments, cells were trypsinized and seeded onto a permeable, 0.4 µm pore diameter, filter support (EMD Millipore, Billerica, MA) at 50% confluent density in PCP-R media and placed

inside a 6-well plate (Corning, Corning, NY). The bottom of each well was bathed in 2 ml of PCP-R media, and 1.5 ml of the media containing cells was placed on the top of the filter. PCP-R media was replaced thrice weekly.

Electrophysiology: For electrophysiological analyses, PCP-R cells were cultured on 6-well, Transwell filters for 9-12 days. Ussing-style electrophysiological techniques were used to monitor TER/conductance as well as changes in electrogenic transepithelial ion flux. Filters were excised, mounted in Ussing chambers, and connected to a DVC-1000 Voltage/Current Clamp (World Precision Instruments) with voltage and current electrodes on either side of the membrane. Each half of the chamber contains a tapered fluid compartment with fittings for voltage electrodes (close to the epithelial membrane) and current electrodes (at the opposite end of the chamber). Each fluid chamber was water jacketed to maintain a constant temperature (37ºC). The cells were bathed in serum-free media. Media were circulated in the chambers and oxygenated by means of a 5% CO_2/O_2 gas lift. The spontaneous transepithelial potential difference was measured and clamped to zero, and the resultant short-circuit current (SCC) was monitored continuously as a measurement of net transepithelial ion flux. As per convention, a positive deflection in the SCC is either anion secretion (from blood to CSF) or cation absorption (CSF to blood) and a negative deflection indicates the opposite. TER is recorded every 200 seconds throughout each experiment by applying a 2 mV pulse and using the resulting deflection in the SCC to calculate the TER and conductance by Ohm's law. Cultures that showed basal TERs of less than 500 $\Omega.cm^2$ were not used. Conductances were also calculated from the change in SCC during the voltages pulses as $\Delta I/\Delta V$. In all cases, the graphs shown in each panel represent a series of control and experimental cultures that were grown and analyzed in parallel.

Immunostaining: PCP-R cells were grown to confluency on Transwell filters (9-12 days). Cells were treated with diluent or the TRPV4 agonist GSK101679A for 10 minutes and then immediately fixed with 4% paraformaldehyde in PBS. For immunohistochemistry, the fixed cells were washed and incubated overnight with anti-claudin-1 primary antibody (Abcam ab15098; 1:200 dilution) diluted in blocking solution (PBS, 1% goat serum, 1% BSA, 0.1% sodium azide) at 4°C. The cells were then washed and incubated with secondary antibody. The secondary antibody was Alexa Fluor dye-conjugated goat anti-rabbit (Jackson ImmunoResearch 111-545-

144, 1:1000 dilution in blocking solution). For nuclear staining DAPI (500 ng/ml; Sigma D9542) was used. Confocal images were taken on a Leica TCS SP8 (upright high-speed multiphoton and confocal imaging system).

RT-PCR: PCP-R cells were grown as a monolayer in a 75 cm^2 flask in PCP-R media until confluent. Total RNA was isolated using the RNeasy mini kit (Qiagen, Hilden, Germany), according to the manufacturer's supplementary protocol for animal cells grown in a monolayer. 5 µg of total RNA was transcribed to cDNA using the Superscript IV First-Strand Synthesis System (Invitrogen, Carlsbad, CA) according to the manufacturer's protocol using both random hexamers and oligo-dT primers. Specific primers were designed using Primer3Plus according to mRNA sequences obtained from Ensembl and verified using the NCBI database. cDNA was then used for PCR utilizing GoTaq Green Master Mix (Promega, Madison, WI) and 10 µM forward and reverse primers (IDT, Coralville, IA) (Table 3.1) and the products separated on a gradient agarose gel to determine optimum annealing temperatures. A second PCR was carried out using only optimum annealing temperatures for each primer pair. Electrophoresis was carried out on a 1.5% agarose gel stained with ethidium bromide utilizing flanking 1 kb and 100 bp ladders and visualized under UV light using a ChemiDoc XRS imager (Bio-Rad, Hercules, CA). The primers used are shown in Table 3.1.

Statistics: All results shown are displayed as mean ± S.E.M. for the number of experiments indicated on the graphs. Indicated plot points on all figures were compared using Two-tailed Students *t-test*. P-values less than 0.02 were considered significant. All statistical analyses were performed using SigmaPlot 13.0.

2.6 **Results**

The PCP-R cell line develops a high resistance monolayer when grown on permeable supports with optimal resistances occurring 9-12 days post seeding (Figure 3.1). Addition of the TRPV4 agonist GSK1016790A to PCP-R cells causes an increase in transepithelial conductance indicating an increased permeability across the epithelial monolayer (Figure 3.2, top). Concurrently with the initiation of the conductance change is a stimulation of short circuit current (SCC) indicating net

electrogenic transepithelial ion flux composed of anion absorption (CSF to blood) and/or cation secretion (blood to CSF) (Figure 3.2, bottom). Although the conductance remains elevated, the net electrolyte flux returns to a level that is statistically equal to the basal level within 20-30 minutes after agonist addition. A 10 minute pre-treatment with either of two structurally unrelated TRPV4 antagonists, HC067047 or RN1734, completely blocked the increased permeability of the monolayer as well as the electrogenic ion flux (Figure 3.2). To determine the maximal concentration of the agonist which did not result in an irreversible change in conductance and ion flux, a dose response was performed using concentrations of 0.1, 1, 3, 5, and 10 nM GSK1016790A (Figure 3.3). When the TER of the epithelial monolayer falls below 100 Ω*cm^2 or the conductance rises higher than 10 mS/cm^2 it is observed that the TER will continue to fall to unmeasureable levels and the experiment using this culture has to be discarded (data not shown).

A limited dose response was also performed for the TRPV4 antagonist RN1734 at concentrations of 5, 25, and 50 μM in order to determine the maximal inhibitory concentration (Figure 3.4). Interestingly, the agonist-induced conductance responses are immediately reversible upon the addition of a TRPV4 antagonist. This reversal is accompanied by a statistically significant change in the electrogenic flux (Figure 3.5).

To visualize how the TRPV4 agonist was affecting the junctional complexes, PCP-R cells grown on Transwell filter supports were treated with GSK1016790A or diluent for 10 minutes before fixation and staining with anti-claudin-1 antibody (Figure 3.6). During the incubations, the Ca^{2+} concentration was maintained by the use of serum-free media because changes in extracellular Ca^{2+} have profound effects on tight junctions and epithelial conductance (13,19). The untreated, agonist treated, and negative control (no primary antibody) cells were grown in the same 6-well Transwell plate and were treated, fixed, stained and imaged in parallel. No obvious difference was observed between the junctional complexes in any of the monolayers examined; rather all junctional complexes remained intact.

Stimulation of TRPV4 causes an influx of Ca^{2+} which is postulated to secondarily stimulate Ca^{2+}-activated channels. Therefore primers were designed to determine the presence of Ca^{2+}-activated K^+ channels in the PCP-R cell line. When negative results were obtained, a second primer pair

was designed to confirm the results (Table 3.1). The only Ca^{2+}-sensitive K^+ channels found in the PCP-R cell line were the intermediate conductance (IK; $K_{Ca}3.1$) and the small conductance (SK) 2 channels (Figure 3.7). As expected, TRPV4 is endogenously expressed in the cell line (Figure 3.7).

The RT-PCR results were followed by electrophysiological experiments. As expected from the PCR results, iberiotoxin, an inhibitor of big conductance potassium channels (BK; $K_{Ca}1.1$) had no effect on the TRPV4-stimulated conductance change or transepithelial ion flux (Figure 3.8). Unexpectedly, apamin, a pan-SK channel blocker, was also without effect on TRPV4-mediated ion flux or conductance changes (Figure 3.9). A similar lack of effect on either electrophysiological parameter was noted after pre-incubation with the more SK2-specific inhibitors tamapin, Lei-Dab, or scyllatoxin (data not shown).

Pre-treatment with low dose (1 μM) TRAM 34, an inhibitor of two of the three isoforms of IK, also termed Kcnn4, had no effect on the subsequent response to TRPV4 agonist. However, increasing the TRAM 34 concentration to 50 μM resulted in an inhibition of both the increased conductance and short-circuit current (Figure 3.10). If a moderately high dose of TRAM 34 (25 μM) was added to the apical bathing media during the pre-incubation, the response to the TRPV4 agonist was completely inhibited; conversely if the same concentration was added only to the media bathing the serosal face of the tissue, there was a reduced inhibition of the ion flux accompanied by a substantial, but not complete, inhibition of the increased conductance (Figure 3.11).

2.7 **Discussion**

Choroid plexus cell line models should be expected to have a phenotype characteristic of epithelia that maintain controlled movement of electrolytes and fluid. In the initial description of the PCP-R cell line, the cultures developed a transepithelial resistance of 300-600 $\Omega.cm^2$ after 6 days of culture on permeable supports depending on seeding density (25). In the current studies, additional days in culture resulted in monolayers that exhibited even tighter epithelia, more suitable for electrophysiological experiments.

In preliminary studies, TRPV4 antagonists decrease hydrocephalic development in a genetic rat model of the disease suggesting a role for TRPV4 in CSF secretion (8). As in the native CP (33), the PCP-R cells contain TRPV4 which can be activated by a specific TRPV4 agonist. The electrophysiological changes elicited by the TRPV4 agonist are inhibited by two structurally distinct and specific antagonists which underscores the specificity of the response.

The rapid and substantial increase in transepithelial conductance elicited in response to the TRPV4 agonist was unexpected and indicates a large change in transcellular permeability. The conductance plateaus at a high level indicating that the permeability remains increased even though the electrogenic ion flux returns toward basal levels by 20-25 minutes. Similar large conductance changes have previously been described in colonic epithelia, another epithelium capable of large secretory fluxes, after stimulation with prostaglandins (15). In the PCP-R cells, both the increased permeability and stimulated ion flux are immediately reversible by TRPV4 antagonists even after the initiation of a response.

TRPV4 has been previously reported to regulate the integrity of the blood-CSF barrier (20). However, these studies are difficult to compare to the current experiments because the starting resistances of the primary cultures used were low (50-70 $\Omega.cm^2$) and treatment with 10 nM GSK1016970A caused a disintegration of the cell junctions within 10-20 minutes. Activation of TRPV4 by the phorbol ester 4α-PDD (4α-phorbol-12,13-didecanoate) also caused a decrease in transepithelial resistance (increased conductance) in a mammary epithelial cell line similar to the change seen in the PCP-R cells (23). In the latter phase of mammary cell response there was down-regulation of junctional claudins and frequent large breaks in the tight junction strands.

A dose response using the TRPV4 agonist GSK1016790A in the PCP-R cell line indicated that while 5 and 10 nM elicited stronger responses, treatment of PCP-R cells with 3 nM GSK1016970A caused no overt changes in the cell junctions and did not cause an irreversible disruption of the epithelial structure in confluent monolayers. To mimic a physiologically relevant response, 3 nM agonist was used in the majority of the experiments.

A dose response was performed using the TRPV4 antagonist RN1734, at concentrations of 5, 25 and 50 μM, clearly indicating that while concentrations of both 25 and 50 μM caused complete inhibition of the change in conductance, 50 μM had the more complete inhibition of the change in SCC with no adverse effects on cellular viability as measured by TER (conductance).

Claudin-1, endogenously present in both native CP (12, 14, 29) and the PCP-R cell line (25 and Figure 3.2), is considered a barrier claudin important for maintenance of transepithelial permeability (14). The immunolocalization of claudin-1 did not change after stimulation with GSK1016970A, a finding which is consistent with the rapid reversal of the TRPV4 agonist-mediated response by antagonist. Both findings suggest that, under our experimental conditions, the junctional complexes are not irreparably broken.

Taken together, our results are consistent with a change in transepithelial permeability that does not involve the breakdown of tight junctions, the dissociation of the epithelial cells, or a decrease in claudin-1 expression in the tight junctions. The reasons for the difference between the current studies and the previous reports showing a breakdown of junctional complexes is unknown but the agonist concentration may play a role. Over-activation of TRPV4 by exogenous agonists does have pathological consequences. For example, i.v. administration of GSK1016790A caused circulatory collapse in mice, rats and dogs due to endothelial barrier function failure (33). While the current studies did not explore the long term effects on the junctional complexes, it is important to consider the normal *in vivo* role of TRPV4. It is unlikely that the endogenous regulation of the channel will lead to catastrophic breakdown of tight junctions. GSK1016970A has been shown to have nanomolar potency with EC_{50}s between 1-5 nM in human, dog and bovine cellular assays and EC_{50}s of 10-18.5 nM in rodents (33). The PCP-R cells are exquisitely sensitive to the agonist with ~50% of cultures resulting in an irreversible change in conductance at both 5 and 10 nM. The maximum agonist concentration that does not result in an irreversible change in resistance/conductance appears to be 3 nM and we have chosen, therefore, not to use higher concentrations in the majority of the experiments.

When examining the transepithelial ion fluxes using short-circuit current electrophysiology, the initial direction of the TRPV4-mediated ion flux is consistent with anion absorption and/or cation

secretion. Given that the CP is, on a per gram basis, one of the most secretory epithelia in the body, it is likely that cation secretion accounts for the majority of the electrolyte flux within the first few minutes. Thereafter the net transport indicated by the SCC plateaus briefly and then reverses indicating a complex mixture of net electrogenic fluxes.

Although Na^+ secretion cannot be discounted, amiloride, an inhibitor of the epithelial Na^+ channel found in many high-resistance epithelia, did not block the TRPV4-mediated flux (data not shown). The role of other Na^+ transporters was not examined in these studies. TRPV4 is a cation channel that, when activated, transports Ca^{2+} into cells. The most likely candidate for the cation secretion was postulated to be K^+ channels, specifically Ca^{2+}-activated K^+ channels. The importance of Ca^{2+}-activated K^+ channels in CP epithelia has been recognized for over three decades (17) but the identification has remained elusive. RT-PCR of the PCP-R cells indicated the presence of SK2 and IK but not SK1 SK3, or BK. In agreement with these data an inhibitor of BK (iberiotoxin) did not block the TRPV4-stimulated changes in transepithelial ion flux or conductance in the PCP-R cell line. While the SK channels are differentially sensitive to apamin, 100 nM of this bee venom should have blocked the all three channels (32). However, pretreatment with apamin did not block the TRPV4-mediated ion flux or conductance change. Likewise, preincubation with tamapin, Lei-Dab7 or scyllatoxin, relatively specific inhibitors of SK2 (1, 32) did not inhibit GSK1016790A-stimulated electrogenic ion flux or conductance (data not shown). Thus, although SK2 appears to be present in the cell line, it is not involved in TRPV4 agonist-stimulated ion flux or conductance changes.

IK, also known as KCNN4, has recently been shown to have 3 isoforms in the rat. KCNN4a-specific transcripts were found in smooth muscle while KCNN4b and KCNN4c were expressed in epithelial cells (3). Interestingly, these latter two isoforms show a divergence in TRAM34 sensitivity as well as epithelial cell polarity. In intestinal cells, the IC_{50} for the inhibitory effect of TRAM34 on the KCNN4b isoform was in the sub-micromolar range while the IC_{50} for the KCNN4c isoform was approximately an order of magnitude higher in the low micromolar range (3, 4, 15). The KCNN4b isoform was localized to the basolateral membrane of intestinal cells where it was involved in K^+ absorption while the KCNN4c isoform was localized to the apical membrane where it is involved in K^+ secretion (4, 15, 28).

Low dose (1 μM) TRAM34 did not affect TRPV4-stimulated ion flux or conductance while 50 μM completely inhibited both parameters. These data are consistent with the involvement of the Kcnn4c isoform of the IK channel. A moderately high dose of TRAM34 (25 μM) completely inhibited TRPV4-mediated ion flux and conductance changes when added to the apical bathing media indicating an apical localization of this isoform as found in previous studies (4, 15, 28). However, addition of the same concentration of the inhibitor to the serosal bathing media partially inhibited TRPV4-mediated ion flux and substantially, but not completely, blocked the increase in conductance. These data indicate a relatively complex inhibitor effect that could be due to transepithelial permeability of the TRAM34 or to off-target effects of the inhibitor. In immune cells, micromolar concentration of TRAM-34 reduced lysophosphatidylcholine induced increases in intracellular calcium by inhibiting non-selective cation channels (24). Similar effects on non-selective cation channels, including TRPV4, cannot be ruled out in the current experiments. Figure 3.12 contains a diagram of the choroid plexus and the hypothesized placement of the IK channel based on the current studies. Additional experiments will be necessary to clarify additional components that are likely to be contributing to the electrophysiological responses.

In the 1980's, a series of elegant electrophysiological experiments by Wright and colleagues in *Necturus* CP showed that the apical membrane accounted for more than 90% of the K^+ conductance of the epithelial cells and suggested the presence of an apical Ca^{2+}-activated K^+ channel (17, 37) . Our current studies are in agreement with this early work and suggest that the apical Ca^{2+}-activated K^+ channel is the KCNN4c isoform of IK.

In summary, we have shown that activation of TRPV4 stimulates a striking change in transepithelial permeability accompanied by a transepithelial ion flux. The effect of the TRPV4 agonist appears to be specific because the effect is blocked by two chemically distinct antagonists. The lack of permeability change after antagonist pre-incubation further indicates that the agonist is not having a nonspecific effect on the epithelial cell junctions. Agents that block the increase in conductance also block the electrogenic transepithelial ion flux. We hypothesize that the transepithelial ion flux is due to cation secretion because a preliminary study has indicated that TRPV4 antagonists are effective in decreasing the hydrocephalus in a model of the communicating form of the disease (8), thus suggesting that electrolyte flux into the CP is an integral component

of the response. A substantial portion of the transepithelial ion flux due to stimulation of a Ca^{2+}-activated K^+ channel, IK. The decreased sensitivity and the apical localization of the TRAM34 effect in the CP cells indicates that the form of IK found in the CP is KCNN4c. However, the sustained conductance change suggests that the response to TRPV4 stimulation is complex, likely involving electrogenic and electroneutral transporters. Further experimentation will be necessary to determine the exact nature of the osmolyte permeability and which transport effects are primary and which are secondary.

2.8 **Acknowledgements**

The authors would like to thank Dr. Nicolas Berbari for help in designing the RT-PCR primers.

2.9 **Grants**

These studies were supported by a Hydrocephalus Association/ Team Hydro Innovator Award; pilot funding from the Indiana University Collaborative Research Grant Funds of the Office of the Vice President for Research; and a Project Development Team within the ICTSI NIH/NCRR grant # ULITR001108.

2.10 **Disclosures**

None.

Table 2.1 Primer Pairs Used for RT-PCR with Corresponding Product Sizes (bp).

To confirm the presence or absence of the gene of interest for the K^+ channels, two different primer pairs were used. *Gapdh* was used as a positive control in all RT-PCR experiments.

Sus Scrofa gene	Protein	Primer Sequences 5' - 3'		Product Size (bp)
		Forward Primer	Reverse Primer	
Kcnn1	SK1	GGAAGAGGAAGAAGATGAGGAA	GAGAGGAAAGTGATGGAGATGA	801
	SK1	CTTCAGCATCTCCTCCTGGATC	TGGATGGCTTGGAGGAACTTAC	432
Kcnn2	SK2	AGAACCAGAATATCGGCTACAA	TAAAAGCATGACTCTGGCAATC	488
	SK2	TCTGATTGCCAGAGTCATGCTT	CACGTGCTTTTCTGCTTTGGTA	418
Kcnn3	SK3	AACACACAAAGCTGCTAAAGAA	TCTGGAGTGGGGAGTTTTATTT	466
	SK3	GGCGAGTACAAGTTCTTCTGGA	TAGCTTGCAGGAACTTCCTCTG	685
Kcnn4	IK	CTGGTTTGTGGCCAAGTTGTAC	TCCTACGCGTGTGTTTGTAGAA	419
	IK	ATCAGCATTTCCACGTTCTTGC	TCCTACGCGTGTGTTTGTAGAA	799
Kcnma1	BK	ACTTGGAAGGAGTCTCAAATGA	ATCTGATCATTGCCAGGGATTA	445
	BK	TTACTGCAAGGCCTGTCATGAT	AAGGTCCGTATCAGGGTAAGGA	990
Trpv4	TRPV4	AGATTGGGATCTTTCAGCACAT	AGCAAGTAGACCAGCAGGAAAC	724
Gapdh	GAPDH	TTTTAACTCTGGCAAAGTGGAC	CATTGTCGTACCAGGAAATGAG	884

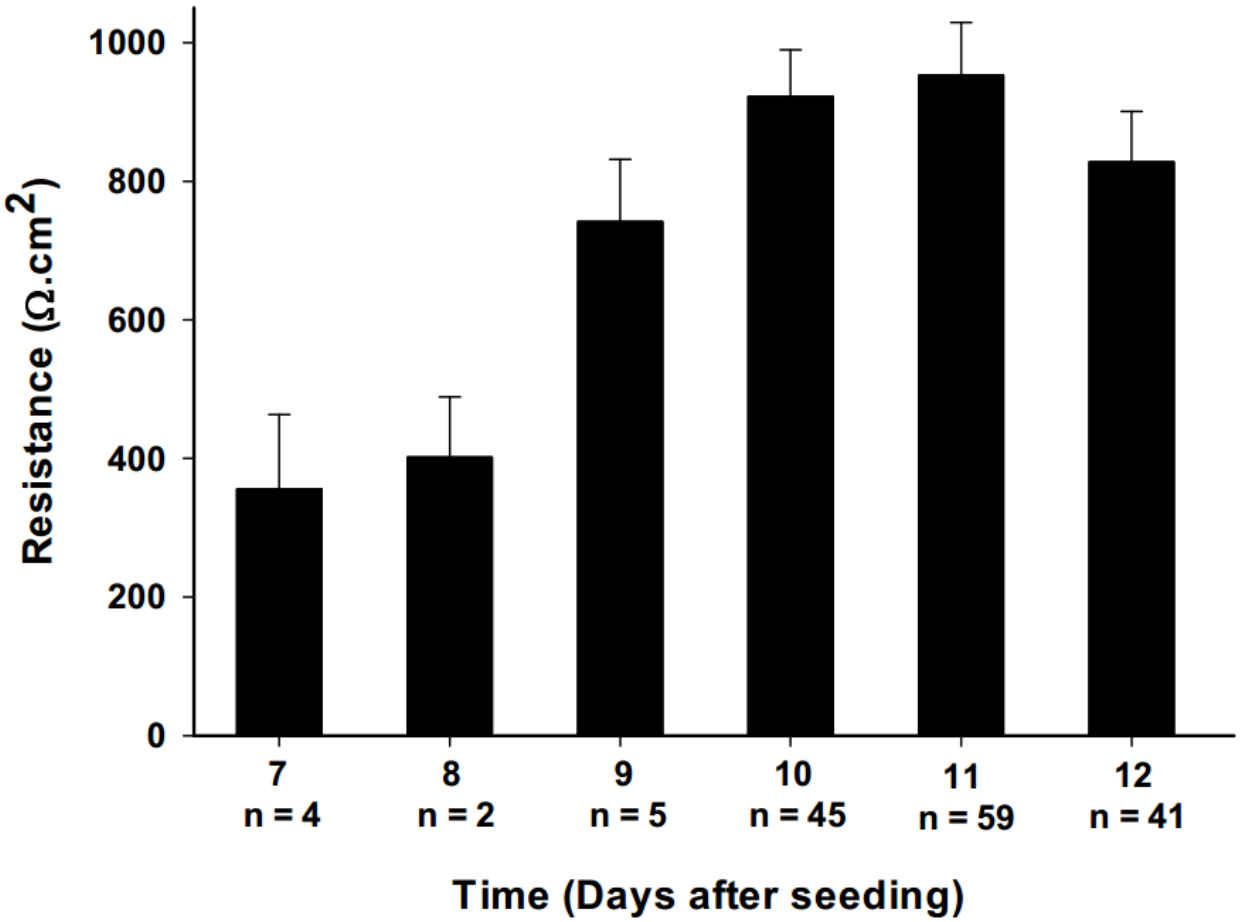

Figure 2.1 Development of Transepithelial Resistance of the PCP-R Cell Line.

Development of transepithelial resistance of the PCP-R cell line after seeding on Transwell supports. The bars are a composite of control values from multiple electrophysiological experiments conducted over a two-year period. In each case the resistance was measured just before the addition of an electrolyte transport effector, i.e., after the cells were mounted in the Ussing chambers and allowed to reach a stable baseline current. The bars represent the mean ±S.E.M. for the number of experiments listed.

Figure 2.2: Effect of TRPV4 agonist and antagonists on transepithelial conductance and electrogenic ion flux in the PCP-R cell line. RN1734 or HC067047, specific TRPV4 antagonists were added to the PCP-R cultures indicated by the open circles and grey squares at time T = -10 minutes. At time 0, the TRPV4 agonist GSK 1016790A was added to all cultures. The symbols represent the means $\pm$ S.E.M. for the number of experiments indicated on the graphs. SCC = short-circuit current. * indicates statistically significant differences between the two conditions ($p < 0.02$) as measured by Students *t-test*, paired data.

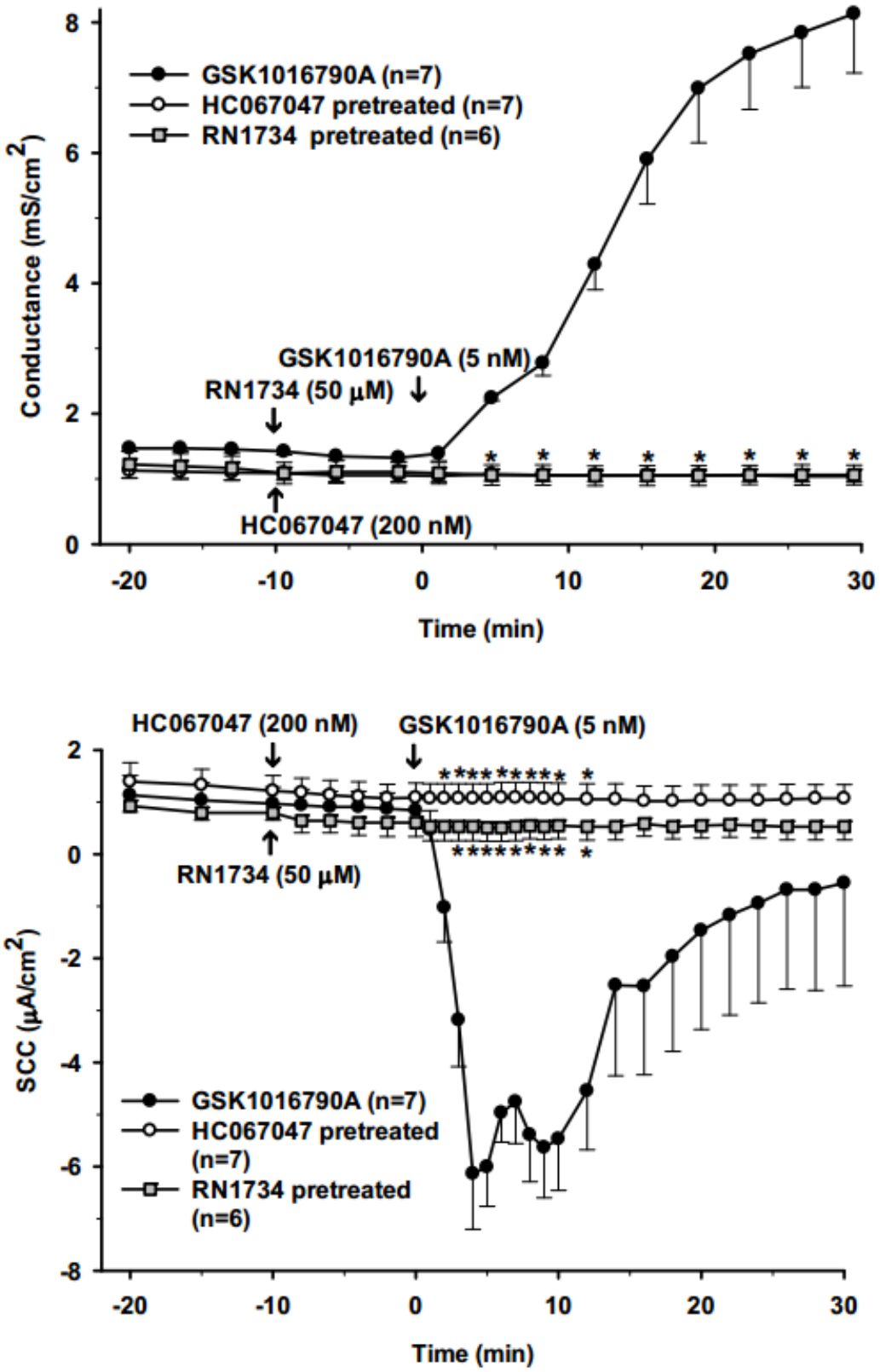

Figure 2.2 Effect of TRPV4 Agonist and Antagonists in the PCP-R Cells.

Figure 2.3: Dose response for the TRPV4 agonist GSK1016790A effect on transepithelial conductance and ion movement in the PCP-R cell line. Concentrations of 0.1, 1, 3, 5, and 10 nM GSK1016790A were added to the PCP-R cultures at T = 0 minutes. Cell cultures whose resistance drops below 100 Ω*cm^2 or the conductance rises higher than 10 mS/cm^2 were considered irreversibly altered by the agonist and were not included. The same experimental data were used for both graphs. Delta (Δ) SCC is defined as the difference in SCC between the value just before agonist addition and the value at the point of the maximal response The symbols represent the means + S.E.M. for the number of experiments indicated on the graphs. SCC = short-circuit current.

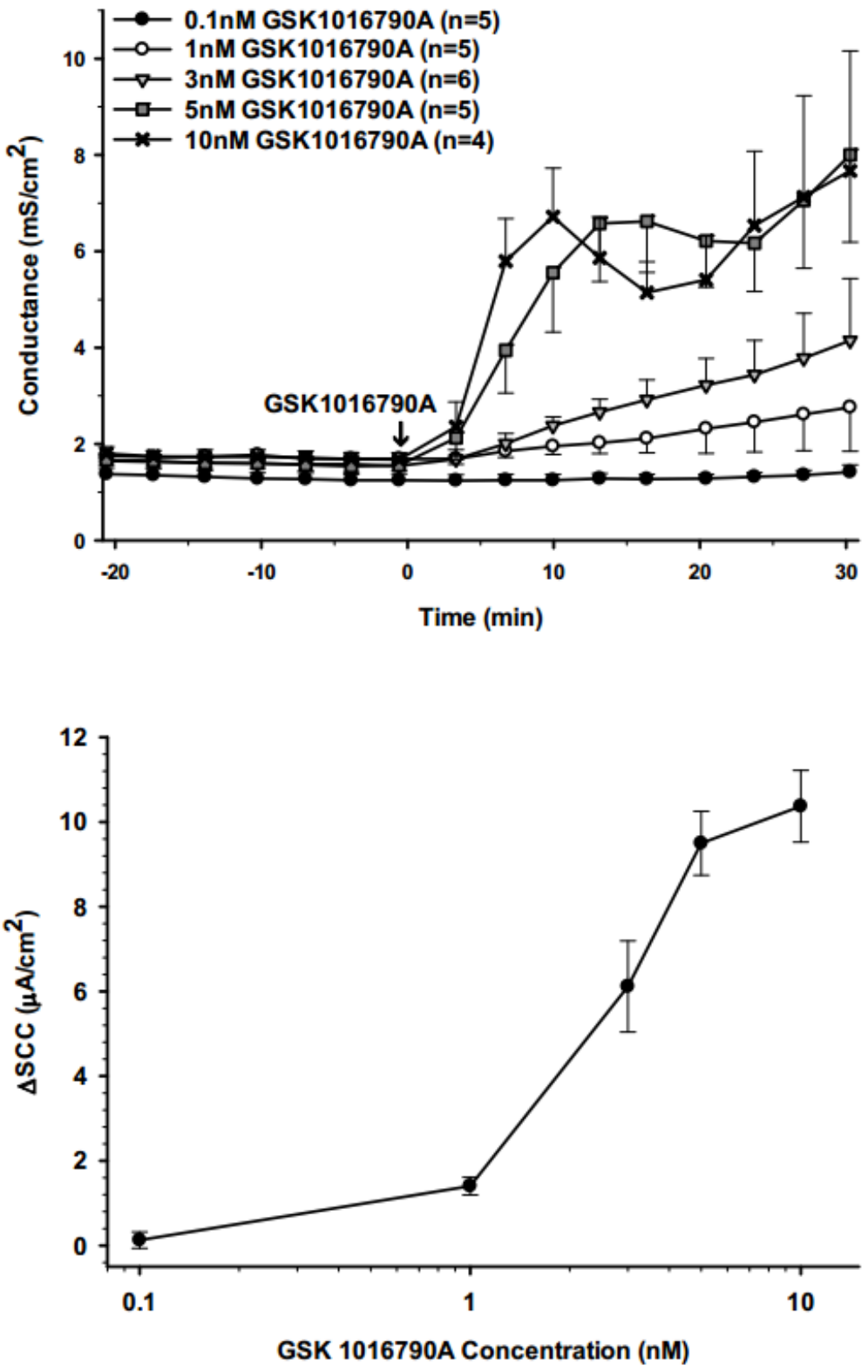

Figure 2.3 Dose Response for TRPV4 Agonist GSK1016790A in PCP-R Cells.

Figure 2.4: Dose response for the TRPV4 antagonist RN1734 pre-treatment in the PCP-R cell line. Concentrations of 5, 25, and 50 μM RN1734 were added to the PCP-R cultures at T = -10 minutes. At time 0, the TRPV4 agonist GSK1016790A was added to all cultures. The symbols represent the means + S.E.M. for the number of experiments indicated on the graphs. SCC = short-circuit current.

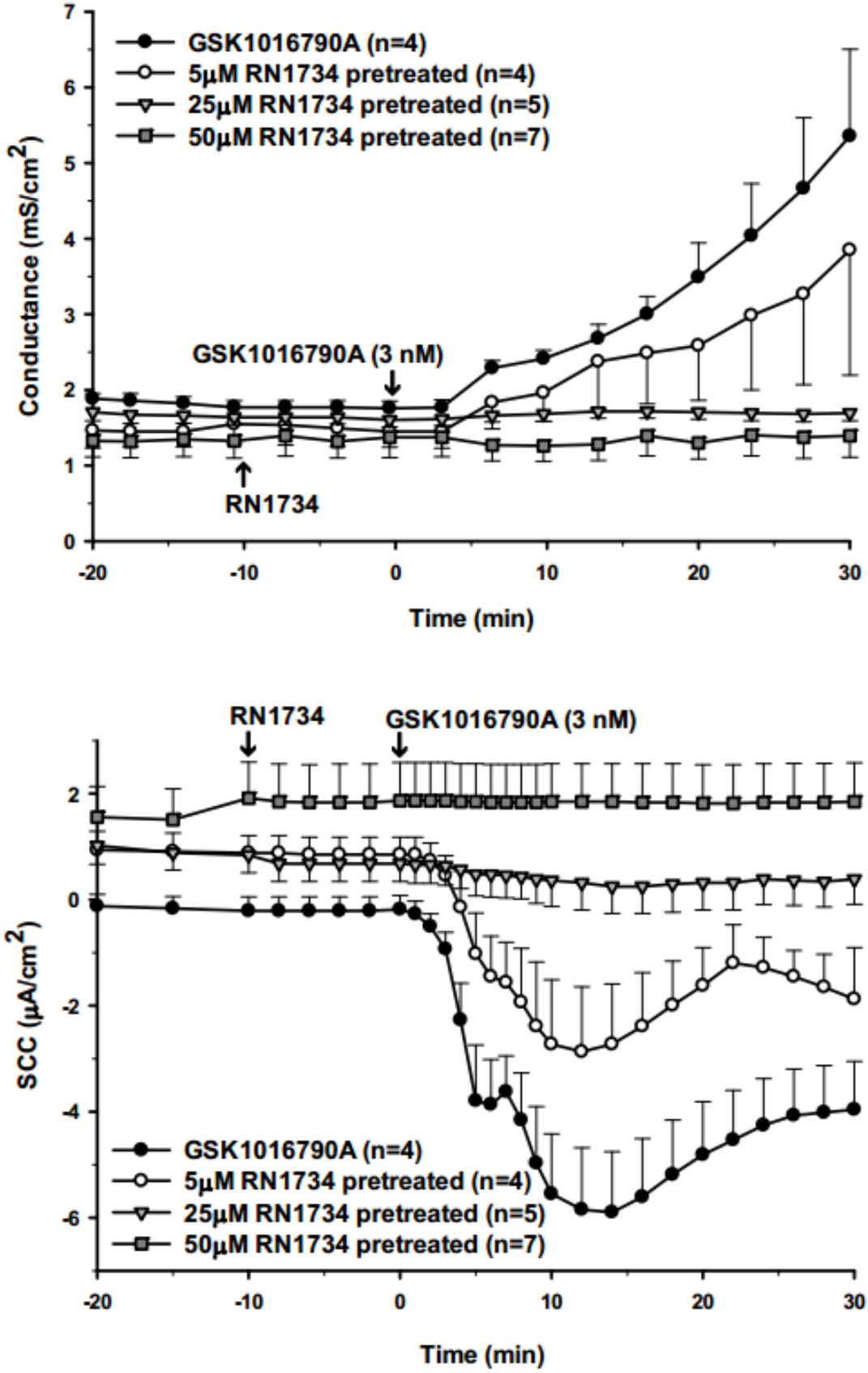

Figure 2.4 Dose Response for TRPV4 Antagonist RN1734 Pre-Treatment in PCP-R Cells.

Figure 2.5: Reversibility of a TRPV4 agonist response by a TRPV4 antagonist. At time 0 the TRPV4 agonist GSK1016790A was added to all culture. RN 1734, a TRPV4 antagonist, was added to the cultures indicated by the open circles 15 minutes after the addition of the agonist. The symbols represent the means $\pm$ S.E.M. for the number of experiments indicated on the graphs. SCC = short-circuit current. * indicates statistically significant differences between the two conditions as measured by a 2-tailed Student's t-test ($p < 0.02$).

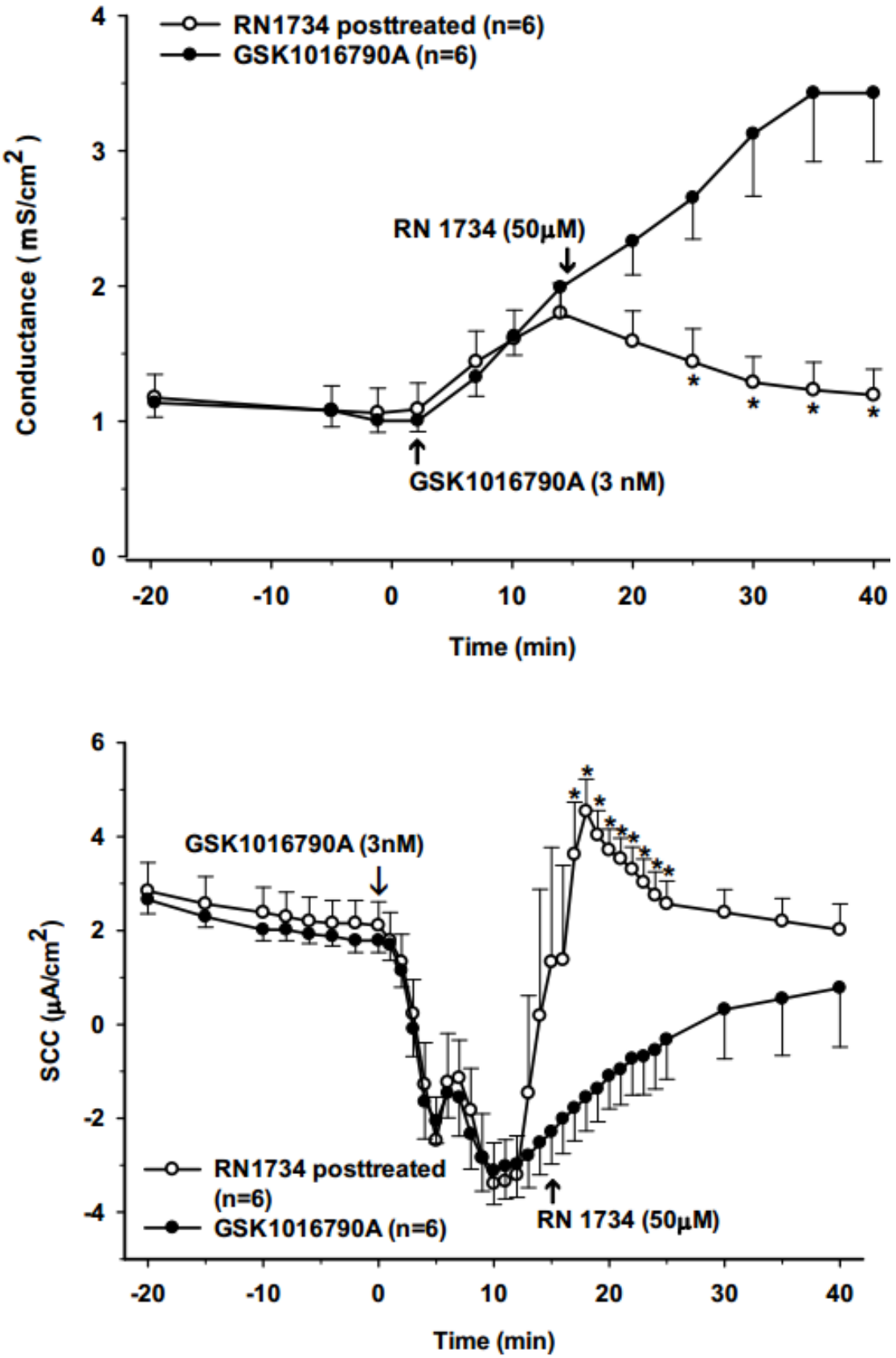

Figure 2.5 Reversibility of a TRPV4 Agonist Response by a TRPV4 Antagonist.

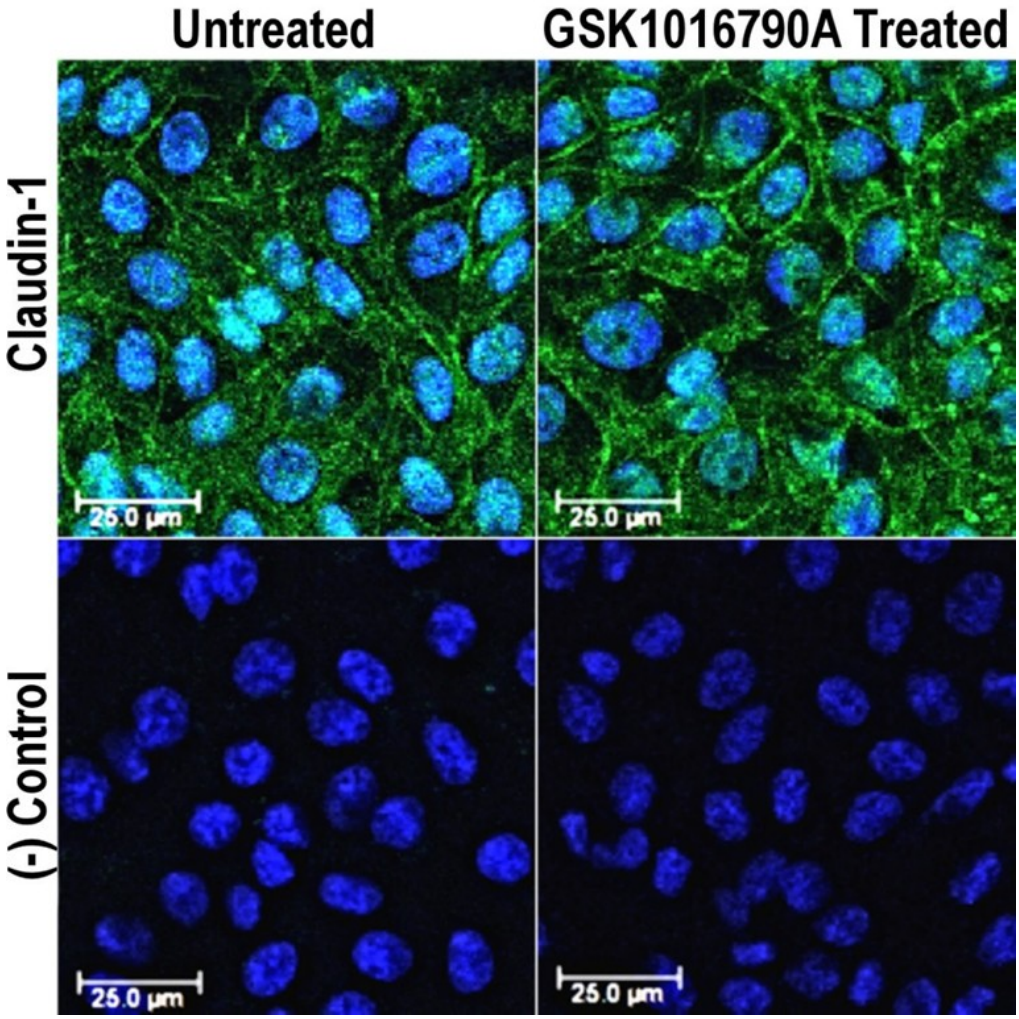

Figure 2.6 Immunohistological Staining of Claudin 1 in the PCP-R Cell Line.

Cells were stained with DAPI (blue) to visualize nuclei and anti-claudin-1 antibody (green) to show the presence of tight junctions. Treated cells were pre-incubated with TRPV4 agonist, GSK1016790A (3nM), for 10 minutes before fixation and staining. Negative control cells were stained with DAPI and secondary antibody only. This figure is representative of 4 independently conducted experiments. Scale bars represent 25µm.

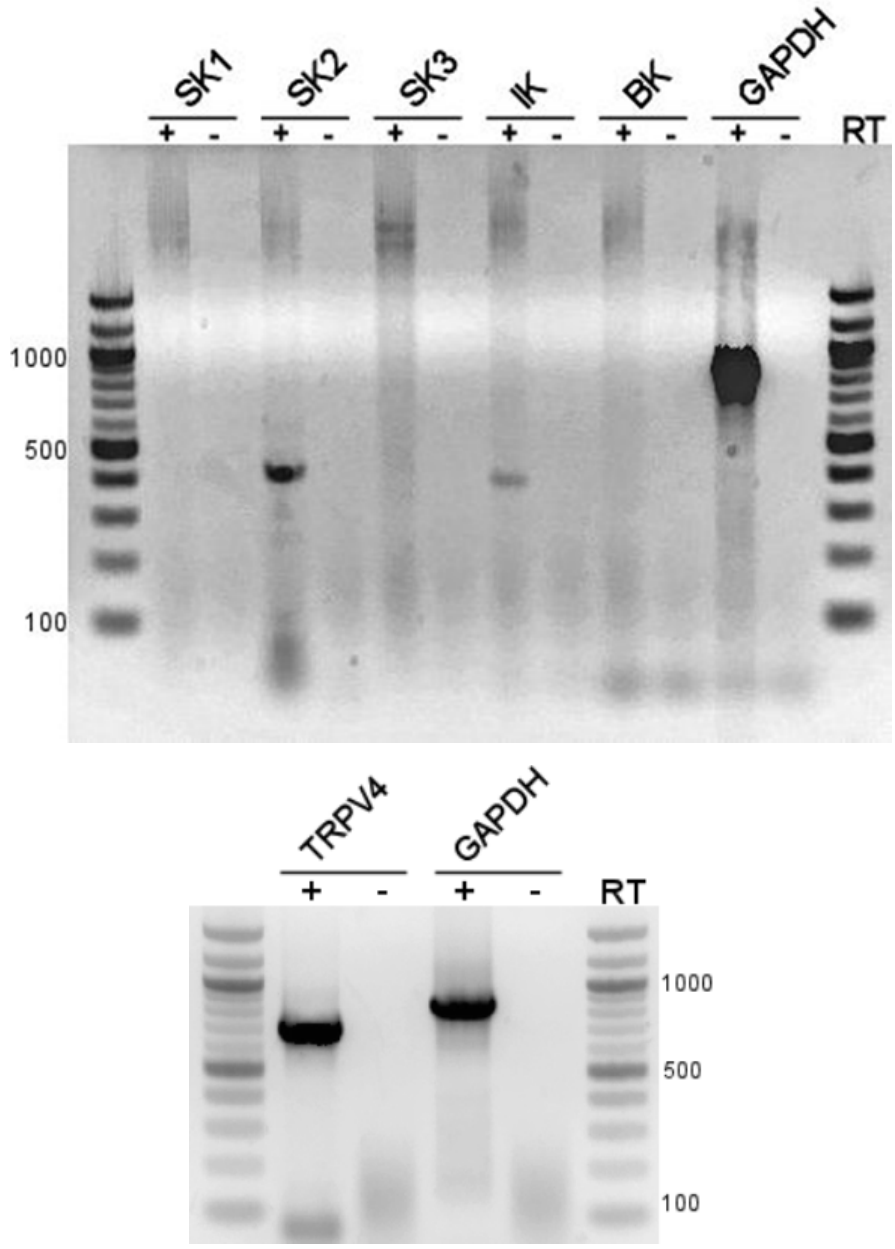

Figure 2.7 RT-PCR of Selected Ion Channels in the PCP-R Cell Line.

Left hand gel shows the results of RT-PCR of Ca^{2+}-activated K^+ channels. The gel shows expression of only SK2 and IK among the calcium activated potassium channels. SK1, SK3 and BK were all notably absent. The second gel shows expression of TRPV4 For any channels not present, additional primer sets were utilized to confirm absence of the cDNA. SK = small conductance K^+ channel; IK = intermediate conductance K^+ channel; BK = big conductance K^+ channel; TRPV4 = transient receptor potential vanilloid 4; GAPDH = glyceraldehyde 3-phosphate dehydrogenase

Figure 2.8: Effect of pre-treatment with a BK channel inhibitor on TRPV4 agonist stimulated increases in transepithelial conductance and ion transport. Iberiotoxin, an inhibitor of big conductance potassium (BK) channel was added to the PCP-R cultures indicated by the open circles at time T = -10 minutes. At time 0, the TRPV4 agonist GSK 1016790A was added to all cultures. The symbols represent the means $\pm$ S.E.M. for the number of experiments indicated on the graphs. SCC = short-circuit current.

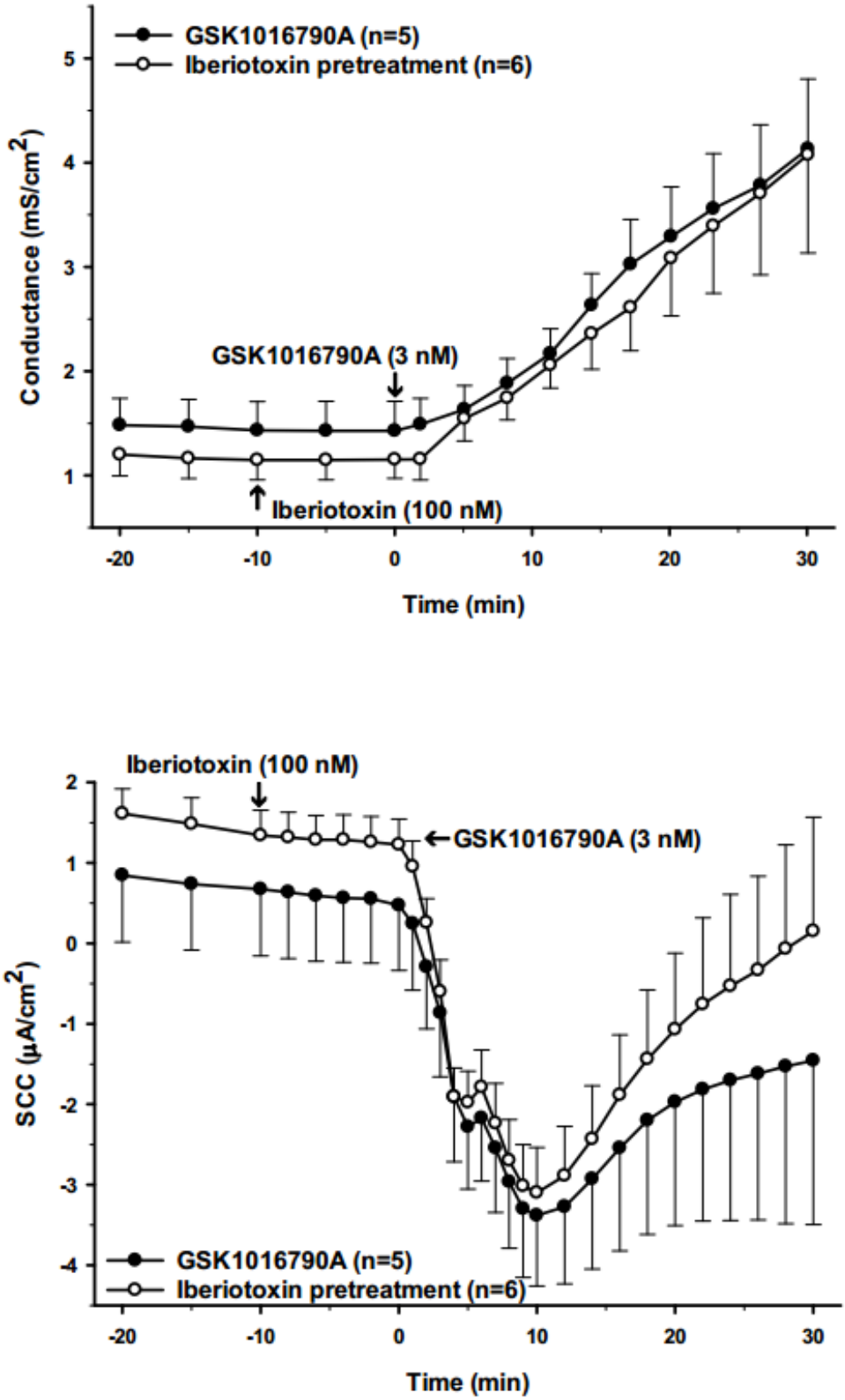

Figure 2.8 Effect of BK Channel Inhibitor on TRPV4-Mediated Responses.

Figure 2.9: Effect of pre-treatment with an inhibitor of SK channels on TRPV4 agonist stimulated increases in transepithelial conductance and ion transport. Apamin, an inhibitor of small conductance potassium (SK) channels, was added to the PCP-R cultures indicated by the open circles at time T = -10 minutes. At time 0, the TRPV4 agonist GSK 1016790A was added to all cultures. The symbols represent the means $\pm$ S.E.M. for the number of experiments indicated on the graphs. SCC = short-circuit current.

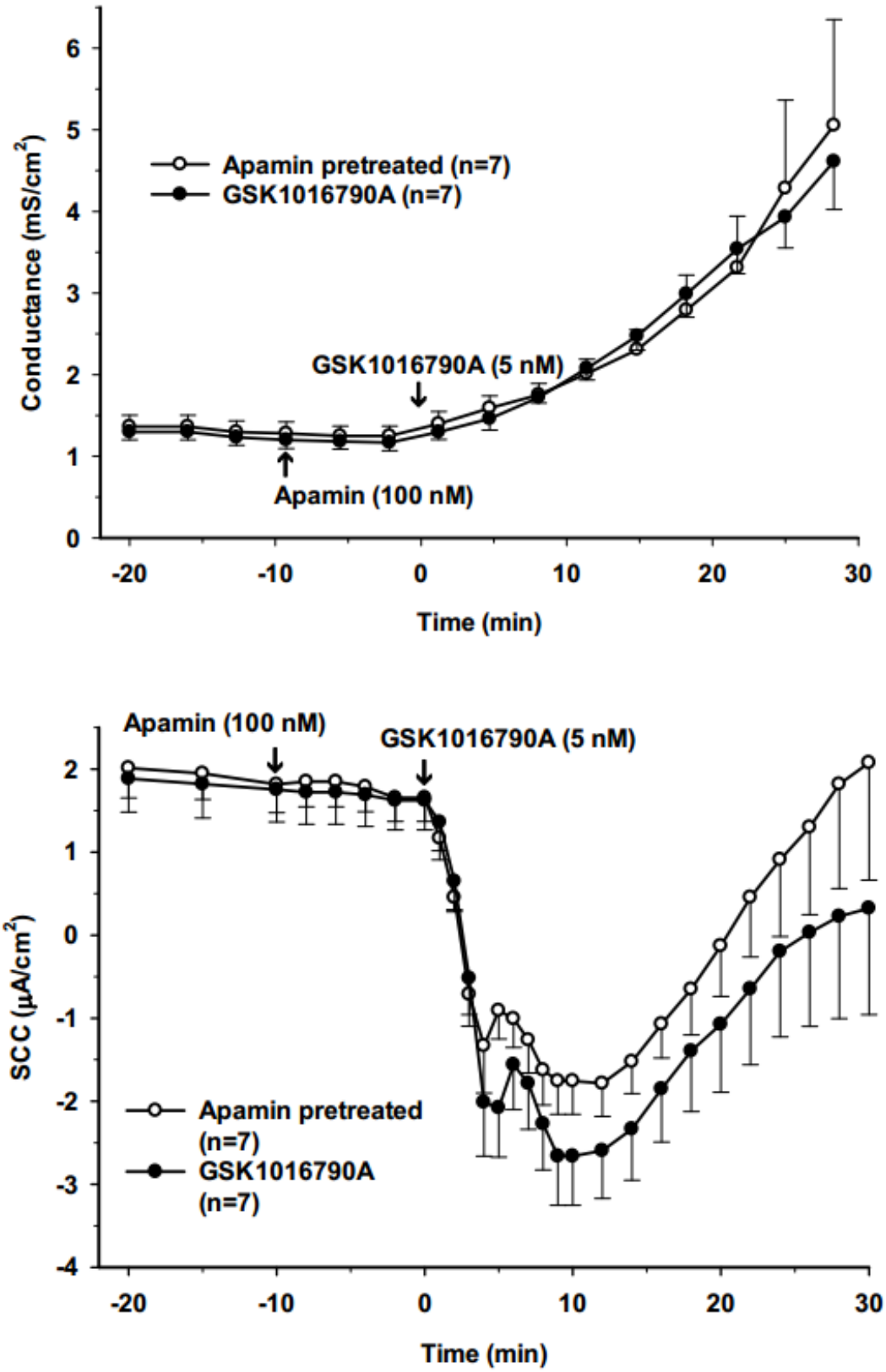

Figure 2.9 Effect of SK Channel Inhibitor on TRPV4-Mediated Responses.

Figure 2.10: Effect of pre-treatment with high and low doses of an IK channel inhibitor on TRPV4 agonist stimulated increases in transepithelial conductance and ion transport. TRAM34, an inhibitor of intermediate conductance potassium (IK) channels, was added bilaterally to the PCP-R cultures indicated by the open circles or inverted triangles at time T = -10 minutes. At time 0, the TRPV4 agonist GSK 1016790A was added to all cultures. The symbols represent the means $\pm$ S.E.M. for the number of experiments indicated on the graphs. SCC = short-circuit current. The positive control data (GSK1016790A only) shown in this figure are the same data that are shown in figure 11. * indicates statistically significant differences between the experimental and control (solid circles) groups ($p < 0.02$) as measured by Students *t-test*, paired data. τ indicates statistically significant differences between the two experimental (open circles and inverted triangles) groups ($p < 0.02$) as measured by Students *t-test*, paired data.

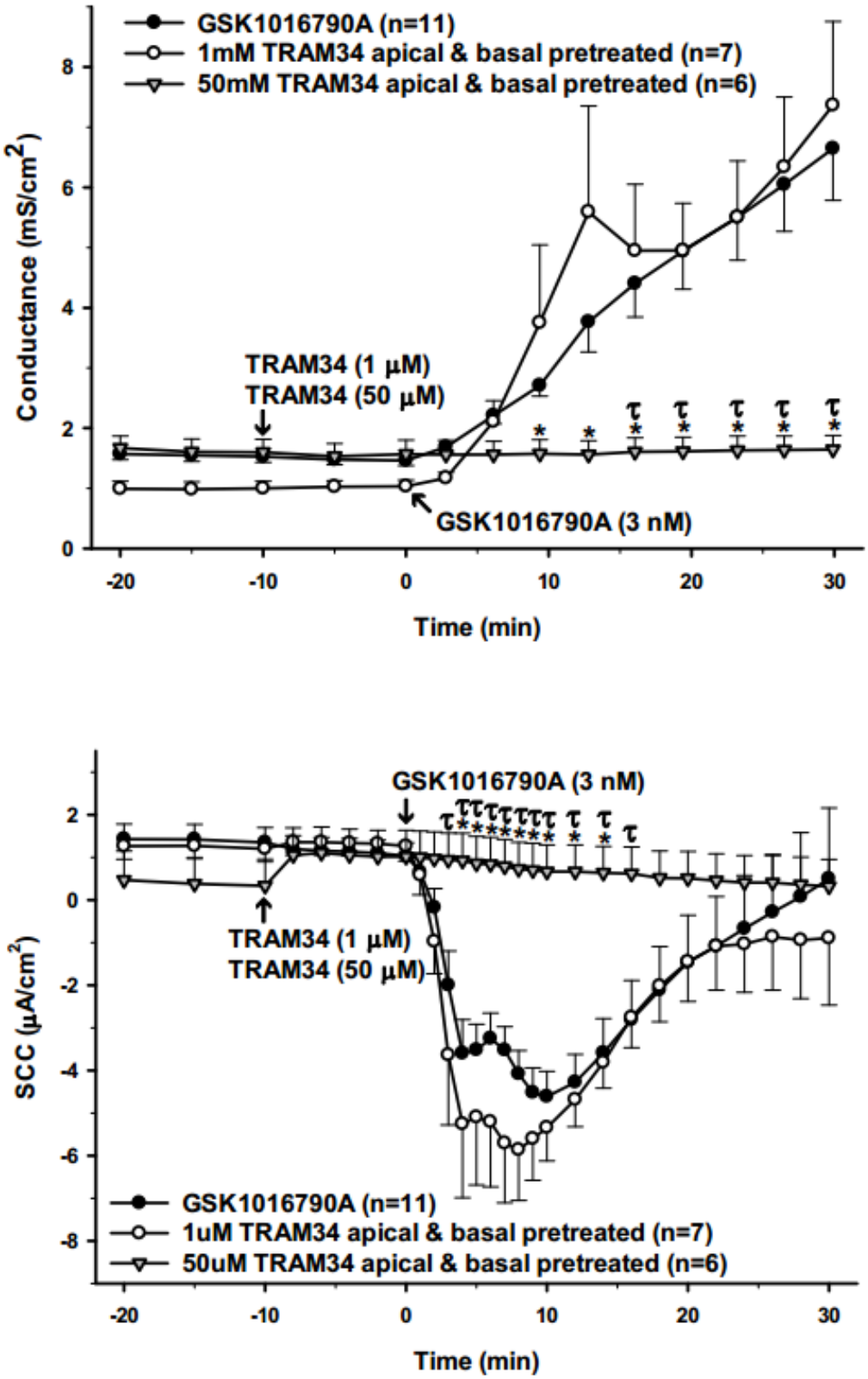

Figure 2.10 Effect of High/Low Doses of IK Inhibitor on TRPV4-Mediated Responses.

Figure 2.11: Sidedness of the effect of an inhibitor of IK channels on TRPV4 agonist stimulated increases in transepithelial conductance and ion transport. TRAM34, an inhibitor of intermediate conductance potassium (IK) channels, was added to either the serosal or apical bathing media of the PCP-R cultures indicated by the open circles or inverted triangles at time T = -10 minutes. At time 0, the TRPV4 agonist GSK 1016790A was added to all cultures. The symbols represent the means $\pm$ S.E.M. for the number of experiments indicated on the graphs. SCC = short-circuit current. The positive control data (GSK1016790A only) shown in this figure are the same data that are shown in figure 10. * indicates statistically significant differences between the experimental and control (solid circles) groups ($p < 0.02$) as measured by Students *t-test*, paired data. τ indicates statistically significant differences between the two experimental (open circles and inverted triangles) groups ($p < 0.02$) as measured by Students *t-test*, paired data.

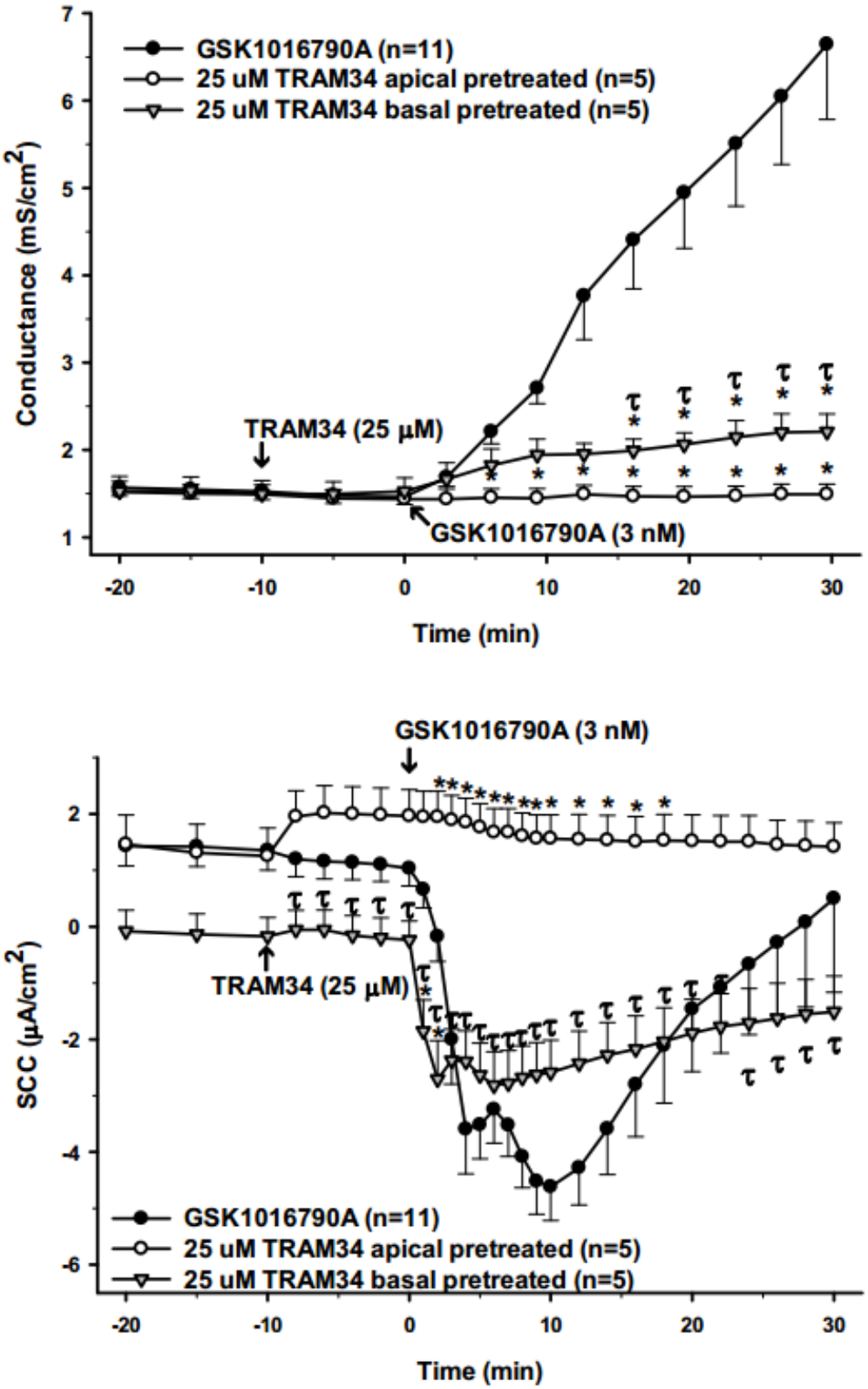

Figure 2.11 Sidedness of IK Channel Inhibitor on TRPV4-Mediated Responses.

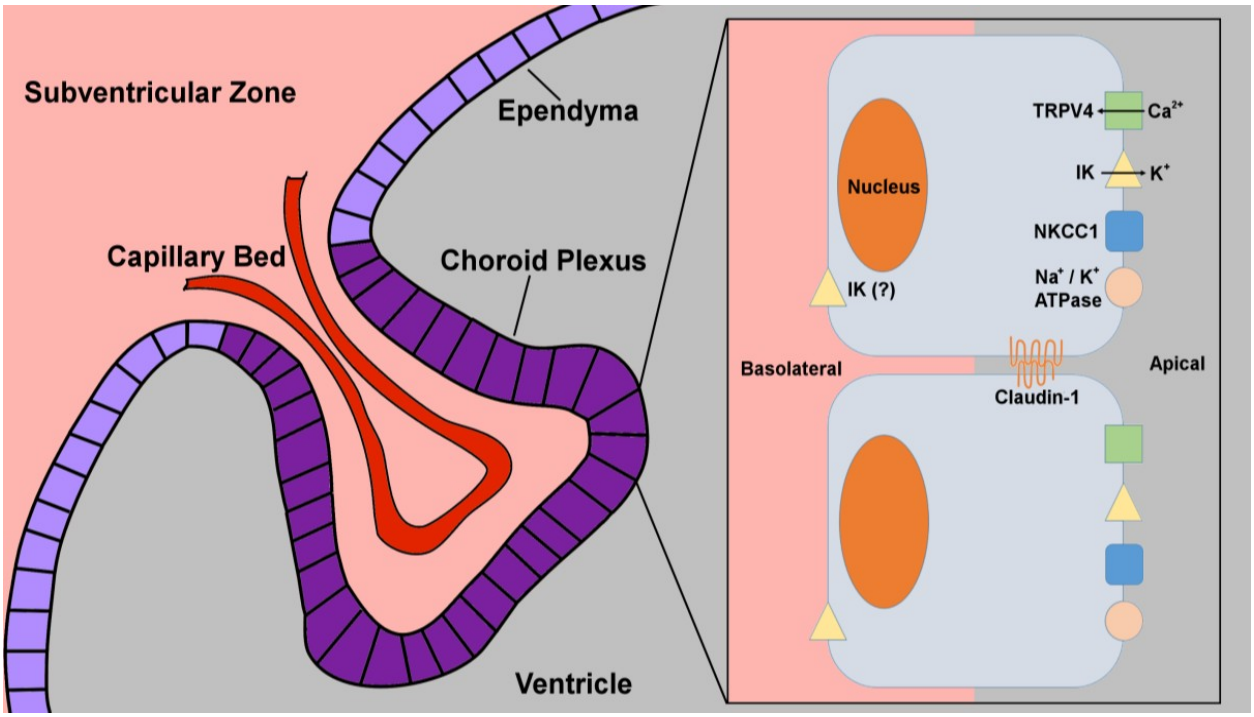

Figure 2.12 Diagram of Selected Transporters in the Choroid Plexus Epithelia.

The left hand side of the diagram illustrates that the choroid plexus within the ventricle is continuous with the ependymal cells. Choroid plexus cells (dark purple) are increased in size compared to ependymal cells (light purple). On the right-hand part of the diagram, individual choroid plexus cells are shown as polarized with transporters on both the apical and basolateral membranes, and connected by tight junctional proteins.

2.11 **References**

1. Adelman, J., Maylie, J., and Sah, P. (2012). Small-conductance Ca^{2+}-activated K^+ channels: Form and function. *Annual Review Of Physiology*, *74*(1), 245-269.
2. Bagher, P., Beleznai, T., Kansui, Y., Mitchell, R., Garland, C., and Dora, K. (2012). Low intravascular pressure activates endothelial cell TRPV4 channels, local Ca^{2+} events, and IK_{Ca} channels, reducing arteriolar tone. *Proceedings Of The National Academy Of Sciences*, *109*(44), 18174-18179.
3. Barmeyer, C., Rahner, C., Yang, Y., Sigworth, F., Binder, H., and Rajendran, V. (2010). Cloning and identification of tissue-specific expression of KCNN4 splice variants in rat colon. *American Journal Of Physiology-Cell Physiology*, *299*(2), C251-C263.
4. Basalingappa, K., Rajendran, V., and Wonderlin, W. (2011). Characteristics of Kcnn4 channels in the apical membranes of an intestinal epithelial cell line. *American Journal Of Physiology-Gastrointestinal And Liver Physiology*, *301*(5), G905-G911.
5. Benfenati, V., Caprini, M., Dovizio, M., Mylonakou, M., Ferroni, S., Ottersen, O., and Amiry-Moghaddam, M. (2011). An aquaporin-4/transient receptor potential vanilloid 4 (AQP4/TRPV4) complex is essential for cell-volume control in astrocytes. *Proceedings Of The National Academy Of Sciences*, *108*(6), 2563-2568.
6. Crossgrove, J., Li, G., and Zheng, W. (2005). The choroid plexus removes β-amyloid from brain cerebrospinal fluid. *Experimental Biology And Medicine*, *230*(10), 771-776.
7. Cserr, H. (1971). Physiology of the choroid plexus. *Physiological Reviews*, *51*(2), 273-311.
8. Danko, C., Preston, D., Simpson, S., and Blazer-Yost, B. (2017) Effects of a TRPV4 antagonist on hydrocephalus in the Wpk rat model. Abstract *FASEB J* 31:1042.4.
9. Darby, W., Grace, M., Baratchi, S., and McIntyre, P. (2016). Modulation of TRPV4 by diverse mechanisms. *The International Journal Of Biochemistry & Cell Biology*, *78*, 217-228.
10. Ding, F., O'Donnell, J., Xu, Q., Kang, N., Goldman, N., and Nedergaard, M. (2016). Changes in the composition of brain interstitial ions control the sleep-wake cycle. *Science*, *352*(6285), 550-555.
11. Earley, S., Heppner, T., Nelson, M., and Brayden, J. (2005). TRPV4 forms a novel Ca^{2+} signaling complex with ryanodine receptors and BK_{Ca} channels. *Circulation Research*, *97*(12), 1270-1279.

12. Ghersi-Egea, J., Babikian, A., Blondel, S., and Strazielle, N. (2015). Changes in the cerebrospinal fluid circulatory system of the developing rat: quantitative volumetric analysis and effect on blood-CSF permeability interpretation. *Fluids And Barriers Of The CNS*, *12*(1), 8.

13. Gonzalez-Mariscal, L., Contreras, R., Bolivar, J., Ponce, A., Chavez De Ramirez, B., and Cereijido, M. (1990). Role of calcium in tight junction formation between epithelial cells. *American Journal Of Physiology-Cell Physiology*, *259*(6), C978-C986.

14. Günzel, D., and Yu, A. (2013). Claudins and the modulation of tight junction permeability. *Physiological Reviews*, *93*(2), 525-569.

15. Halm, S., Liao, T., and Halm, D. (2006). Distinct K^+ conductive pathways are required for Cl^- and K^+ secretion across distal colonic epithelium. *American Journal Of Physiology-Cell Physiology*, *291*(4), C636-C648.

16. Liedtke, W., Choe, Y., Martí-Renom, M., Bell, A., Denis, C., and Šali, A. et al. (2000). Vanilloid Receptor–Related Osmotically Activated Channel (VR-OAC), a candidate vertebrate osmoreceptor. *Cell*, *103*(3), 525-535.

17. Loo, D., Brown, P., and Wright, E. (1988). Ca^{2+}-activated K^+ currents in Necturus choroid plexus. *The Journal Of Membrane Biology*, *105*(3), 221-231.

18. Lu, K., Huang, T., Tsai, Y., and Yang, Y. (2017). Transient receptor potential vanilloid type 4 channels mediate Na-K-Cl-co-transporter-induced brain edema after traumatic brain injury. *Journal Of Neurochemistry*, *140*(5), 718-727.

19. Ma, T., Hoa, N., Tran, D., Merryfield, M., Nguyen, D., and Tarnawski, A. (2000). Mechanism of extracellular calcium regulation of intestinal epithelial tight junction barrier: Role of cytoskeletal involvement. *Gastroenterology*, *118*(4), A1268.

20. Narita, K., Sasamoto, S., Koizumi, S., Okazaki, S., Nakamura, H., Inoue, T., and Takeda, S. (2015). TRPV4 regulates the integrity of the blood-cerebrospinal fluid barrier and modulates transepithelial protein transport. *The FASEB Journal*, *29*(6), 2247-2259.

21. Nilius, B., Vriens, J., Prenen, J., Droogmans, G., and Voets, T. (2004). TRPV4 calcium entry channel: a paradigm for gating diversity. *American Journal Of Physiology-Cell Physiology*, *286*(2), C195-C205.

22. Praetorius, J., and Damkier, H. (2017). Transport across the choroid plexus epithelium. *American Journal Of Physiology-Cell Physiology*, *312*(6), C673-C686.

23. Reiter, B., Kraft, R., Günzel, D., Zeissig, S., Schulzke, J., Fromm, M., and Harteneck, C. (2006). TRPV4-mediated regulation of epithelial permeability. *The FASEB Journal*, *20*(11), 1802-1812.

24. Schilling, T., and Eder, C. (2007). TRAM-34 inhibits nonselective cation channels. *Pflügers Archiv - European Journal Of Physiology*, *454*(4), 559-563.

25. Schroten, M., Hanisch, F., Quednau, N., Stump, C., Riebe, R., and Lenk, M. et al. (2012). A novel porcine in vitro model of the blood-cerebrospinal fluid barrier with strong barrier function. *Plos ONE*, *7*(6), e39835.

26. Schwerk, C., Papandreou, T., Schuhmann, D., Nickol, L., Borkowski, J., and Steinmann, U. et al. (2012). Polar invasion and translocation of *Neisseria meningitidis* and *Streptococcus suis* in a novel human model of the blood-cerebrospinal fluid barrier. *Plos ONE*, *7*(1), e30069.

27. Serot, J., Zmudka, J., and Jouanny, P. (2012). A possible role for CSF turnover and choroid plexus in the pathogenesis of late onset Alzheimer's disease. *Journal Of Alzheimer's Disease*, *30*(1), 17-26.

28. Singh, S., O'Hara, B., Talukder, J., and Rajendran, V. (2012). Aldosterone induces active K^+ secretion by enhancing mucosal expression of Kcnn4c and Kcnna1 channels in rat distal colon. *American Journal Of Physiology-Cell Physiology*, *302*(9), C1353-C1360.

29. Steinemann, A., Galm, I., Chip, S., Nitsch, C., and Maly, I. (2016). Claudin-1, -2 and -3 are selectively expressed in the epithelia of the choroid plexus of the mouse from early development and into adulthood while claudin-5 is restricted to endothelial cells. *Frontiers In Neuroanatomy*, *10*.

30. Takayama, Y., Shibasaki, K., Suzuki, Y., Yamanaka, A., and Tominaga, M. (2014). Modulation of water efflux through functional interaction between TRPV4 and TMEM16A/anoctamin 1. *The FASEB Journal*, *28*(5), 2238-2248.

31. Vergara, C., Latorre, R., Marrion, N., and Adelman, J. (1998). Calcium-activated potassium channels. *Current Opinion In Neurobiology*, *8*(3), 321-329.

32. Weatherall, K., Goodchild, S., Jane, D., and Marrion, N. (2010). Small conductance calcium-activated potassium channels: From structure to function. *Progress In Neurobiology*, *91*(3), 242-255.

33. Willette, R., Bao, W., Nerurkar, S., Yue, T., Doe, C., and Stankus, G. et al. (2008). Systemic activation of the transient receptor potential vanilloid subtype 4 channel causes endothelial failure and circulatory collapse: Part 2. *Journal Of Pharmacology And Experimental Therapeutics*, *326*(2), 443-452.

34. Wright, E. (1978). Transport processes in the formation of the cerebrospinal fluid. *Reviews Of Physiology, Biochemistry And Pharmacology, 83*, 3-34.

35. Wu, Q., Delpire, E., Hebert, S., and Strange, K. (1998). Functional demonstration of Na^+-K^+-$2Cl^-$ cotransporter activity in isolated, polarized choroid plexus cells. *American Journal Of Physiology-Cell Physiology*, *275*(6), C1565-C1572.

36. Xie, L., Kang, H., Xu, Q., Chen, M., Liao, Y., and Thiyagarajan, M. et al. (2013). Sleep drives metabolite clearance from the adult brain. *Science*, *342*(6156), 373-377.

37. Zeuthen, T., & Wright, E. (1981). Epithelial potassium transport: Tracer and electrophysiological studies in choroid plexus. *The Journal Of Membrane Biology*, *60*(2), 105-128.

CHAPTER 3. THE ROLE OF NKCC1 AND SPAK IN TRPV4-MEDIATED TRANSPORT

3.1 Preface

The journal article that follows is being prepared for the *American Journal of Physiology: Cell Physiology* and therefore follows the style of that journal. As first author, my contributions include drafting the manuscript, designing and conducting experiments conducted including electrophysiological experiments, RT-PCR and qPCR experiments. I analyzed the subsequent data, and produced the figures for publication. Exceptions to this included the contributions of Stefanie Simpson and Keith Gafunderi. Stefanie Simpson contributed the rafoxanide experiment to inhibit SPAK, as well as the final formatting for all electrophysiology figures. Keith Gafunderi contributed to conducting RT-PCR and qPCR experiments and assisted with preparation of RNA from experimental samples for PCR experiments.

3.2 SPAK Inhibition Blocks TRPV4 Mediated Ion Flux in Choroid Plexus Epithelial Cells

Daniel Preston[1], Stefanie Simpson[1], Makenna Reed[1], Keith Gafunderi[1], and Bonnie Blazer-Yost[1]

1. Department of Biology, Indiana University-Purdue University at Indianapolis, Indiana

Running Title: SPAK and TRPV4 in the Choroid Plexus

Corresponding Author
Bonnie L. Blazer-Yost
Indiana University-Purdue University Indianapolis
Biology Department, SL 358
723 West Michigan Street
Indianapolis, IN 46202
Tel: 317-278-1145; Fax: 317-274-2846
email: bblazer@iupui.edu

Keywords: NKCC1, WNK, Blood-CSF Barrier

D.P., S.S. and B.B.Y. designed the experiments. D.P., S.S., M.R., and K.G. conducted the experiments. D.P., S.S., and M.R. analyzed data and prepared figures. D.P., S.S., M.R., and B.B.Y. interpreted the results of experiments. D.P. drafted the manuscript. D.P., S.S., M.R., K.G., and B.B.Y. edited, revised, and approved final manuscript.

3.3 **Abstract**

Cerebrospinal fluid (CSF) is produced primarily by the choroid plexus (CP), a network of secretory epithelial cells surrounding a fenestrated capillary bed. The CP establishes a barrier between the blood and CSF, maintaining a gradient which allows for secretion of ions and fluid, thus producing CSF. Transient Receptor Potential Vanilloid-4 (TRPV4) is a non-selective cation channel which has been shown to stimulate transepithelial ion flux in CP cells. Using the porcine choroid plexus -Riems (PCP-R) cell line, we have investigated the role of the Na^+-K^+-$2Cl^-$ (NKCC1) cotransporter in TRPV4-mediated electrogenic ion flux. The acute changes in short circuit current (SCC) as well as transepithelial conductance stimulated in response to TRPV4 activation were not affected by bumetanide, a specific inhibitor of NKCC1. Prolonged inhibition of NKCC1 also resulted in no significant changes to the transcription of TRPV4 or STE20/SPS1-related proline/alanine rich kinase (SPAK), a regulatory kinase known to phosphorylate and activate NKCC1. However, inhibition of SPAK with the specific inhibitor, STOCK2S-26016, inhibited both the transepithelial ion flux and barrier permeability changes associated with TRPV4 stimulation. Finally, extended 24 hour inhibition of SPAK resulted in increased transcription of TRPV4. These studies suggest that TRPV4 may be regulated via SPAK but independent of the established NKCC1 mechanism of homeostatic and volume regulation.

3.4 **Introduction**

The choroid plexus (CP) is thought to be the primary tissue responsible for the production of cerebrospinal fluid (CSF) in the brain. Located in the lateral, third, and fourth ventricles, the CP consists of a branching network of epithelial cells surrounding a fenestrated capillary bed (6-8,29,33,40,46). CP epithelial cells are responsible for regulating the movement of water and small

molecules through the use of ion channels, transporters and aquaporins, resulting in the production of 500 to 600 ml of CSF per day in adult humans (5,29,46). Evidence suggests that up to 80% of CSF is produced by the CP (4,5,40). The remainder is thought to be produced by the ependymal epithelial cells lining the ventricles, which are contiguous with the CP epithelia, in addition to cells lining the subarachnoid space (4,46). CSF is responsible for cushioning the brain and protecting it from injury by reducing the effective weight of the tissue from 1500 grams to approximately 50 grams, by virtue of buoyancy (4,5,46). Additionally, it is thought to play a key role in waste and toxin clearance from the central nervous system, tightly controlled by the sleep-wake cycle (13). However, little is understood about the control mechanisms by which the CSF is produced, absorbed and regulated.

It has been previously demonstrated that Transient Receptor Potential Vanilloid-4 (TRPV4) may play a role in the transepithelial movement of ions across the blood-CP barrier, thereby altering the production of CSF (41,45). TRPV4 is a nonselective cation channel, which has been shown to transport small ions including sodium, potassium and calcium (3,28,30,36,42,48). TRPV4 is widely expressed in lung and gut epithelia, as well as in the kidney and various brain regions, including the hippocampus, dorsal root ganglion, neurons, and the CP (9,28,36,42,48). Localized on the apical membrane of CP epithelial cells, TRPV4 is a mechano- and osmo-sensitive hub protein that may act to direct ion transport events responsible for the regulation of CSF production (36,41).

A potential link between TRPV4 and the electroneutral Na^+-K^+-$2Cl^-$ cotransporter (NKCC) has been explored previously in the hippocampus in brain edema following traumatic brain injury (TBI). In this study, it was shown that NKCC1 is necessary for TRPV4 activation in the hippocampus, which leads to activation of the MAPK signaling cascade (32). Belonging to the SLC12 family of cotransporters, NKCC is expressed as either NKCC1 or NKCC2. NKCC2, encoded by the gene SLC12A1, is localized primarily in the thick ascending limb of renal tubules and is thought to be kidney specific (2,21). NKCC1 is more widely expressed in transporting polarized epithelia and is typically found localized to the basolateral membrane (2,21,26). In the CP, however, NKCC1 has been identified as being on the apical membrane (20,27,34,39,47). Several studies have demonstrated that NKCC1 is one of the transporters responsible for

establishing the electrochemical gradient across the CP and for maintaining the driving forces necessary for CSF secretion (8,11). Interestingly, Gregoriades et al. showed that the net direction of NKCC1 transport in the CP may be either inward or outward, depending on the intracellular concentrations of Na^+, K^+, and Cl^- and the kinetics of this reversal were demonstrated by Delpire and Gagnon (11,20). This suggests that NKCC1 is capable of responding to a variety of physiological conditions and thusly directing the net flow of ions across the CP epithelia. The SLC12 family also contain the four potassium-chloride cotransporters (KCC1-4). These cotransporters are thought to work exclusively in the net efflux direction and have been identified on both the apical and basal membranes of secretory epithelia (5,7).

Ste20/SPS1-related proline/alanine rich kinase (SPAK) is responsible for modulation of various biological processes (12). SPAK is an evolutionarily redundant kinase for OSR1, which also acts through a mechanism called the WNK-SPAK/OSR1 pathway. WNK kinases have been demonstrated to phosphorylate and activate SPAK, which in turn is responsible for phosphorylation and activation of downstream targets. One such target is NKCC1 which, when phosphorylated, results in activation of the cotransporter (1,2,10-12,15-17,19-23,26,35,37,38,43). As the movement of ions via NKCC1 also allows for the transepithelial movement of water, this regulation of NKCC1 may play a significant role in cell volume homeostasis (2,21). Additionally, the WNK-SPAK/OSR1 pathway also regulates the KCCs via phosphorylation (12,23). However, in contrast to the NKCCs, phosphorylation of the KCCs by the WNK-SPAK/OSR1 pathway results in inhibition (12,22,23,43). Studies have shown that TRPV4 may be regulated in part by WNK4 (18). However, thus far, no interactions have been proven between TRPV4 and SPAK.

The porcine choroid plexus -Riems (PCP-R) cell line has previously been utilized as an *in vitro* model of CP function and expresses a variety of ion channels and transporters found in *in vivo* (41,44,45). Exhibiting many distinct characteristics of CP epithelium, the PCP-R cell line consists of a high resistance monolayer epithelium and expression of tight junctional proteins, including claudins and occludins. We have previously used this model to study the role of TRPV4 in transepithelial ion transport across the CP (41,45).

In this study, we investigate the interactions between TRPV4, NKCC1, and the regulatory WNK kinase, SPAK, in the PCP-R cell line. From these studies, we hope to establish a better understanding of the role of TRPV4 in CSF regulation and the mechanisms behind it.

3.5 Methods and Materials

Cell Culture: PCP-R cells were seeded on 6-well cluster plates containing 0.4 μM filter diameter polycarbonate permeable bottom supports (Corning Life Sciences, Lowell, MA; #3412) for approximately 10-12 days, until cell cultures achieved a transepithelial resistance (TER) >500 Ωcm^2. Cultures below 500 Ωcm^2 were not considered high resistance and were not used for experiments. Additionally, cultures whose TERs dropped below 100 Ωcm^2 during the time course of the experiments were also not used, due to irreversible changes in the tight junctions. PCP-R cell cultures were grown using DMEM (Gibco, Gaithersburg, MD; #12100-046), with 4.5 g/L glucose, 3.7 g/L $NaHCO_3$, 24 mM HEPES, 10% fetal bovine serum (Atlanta Biologicals, Flowery Branch, GA), 100 U/ml penicillin, 100 mg/ml streptomycin, and 5 μg/ml insulin. Cells were bathed in 2 ml of the PCP-R media apically (filter top) and 3 ml basolaterally (filter bottom). PCP-R media was replaced 3 times weekly.

Electrophysiology: For electrophysiological experiments, PCP-R cells were grown on transwell plates until confluent (10-12 days), excised and subsequently mounted in Ussing chambers connected to a DVC-1000 Voltage/Current clamp (World Precision Instruments, Sarasota, FL) with voltage and current electrodes attached on either side of the membrane. Each side of the chamber was bathed in 10 ml of serum free media at 37°C. Media-containing chambers were water jacketed to maintain a constant physiological temperature of 37°C. A 5% CO_2/95% O_2 gas lift circulated media through chambers and oxygenated the chamber-mounted cells. The spontaneous transepithelial potential difference was clamped to zero, and cells were allowed to equilibrate for at least 20 minutes. Experimental compounds were added to the apical and/or basal media, and the resulting short circuit current (SCC) was recorded as a measurement of net transepithelial ion movement. By convention, a positive deflection of the SCC represents either anion secretion (blood to CSF directed movement) or cation absorption (CSF to blood), while the opposite is true for a negative deflection. Additionally, a 2 mV pulse was applied every 180 seconds, and the resulting change in SCC was recorded. This change in SCC was used to calculate transepithelial

resistance (TER) using Ohm's Law, and the resulting TER values were converted to transepithelial conductance by calculating the inverse of the TER. The transepithelial conductance is an indication of net ion movement and barrier permeability in cells. A low conductance (<2 mS/cm^2) represents low net ion movement and a tight barrier. Any increase in the transepithelial conductance is observed to be an increase in the transepithelial ion movement and/or increased cellular permeability. For all electrophysiological experiments, both the control and experimental groups were analyzed simultaneously, as represented in the graphs.

Reverse Transcriptase (RT)-PCR: PCP-R cells were grown to confluence on transwells. The monolayers were washed twice with cold 1X PBS, and total cell RNA was collected utilizing the Monarch Total RNA Miniprep Kit (New England Biolabs, #T2010S) using the manufacturer's directions for cultured mammalian cells. RNA concentration was measured using an ND2000 Nanodrop (Fisher Scientific, Waltham, MA). Approximately 100 ng of total RNA was reverse transcribed into cDNA using the Monarch LunaScript RT SuperMix Kit (New England Biolabs; #E3010L), along with corresponding No-template and -RT controls, according to the manufacturer's directions. *Sus Scrofa e*xon mRNA sequences for each gene were obtained using Ensembl, and primer pairs for each were designed using Primer3Plus. Approximately 500 ng of template cDNA was combined with the forward and reverse primers (IDT, Coralville, IA), as well as GoTaq Green Master Mix (Promega Corporation, Madison, WI; #M7122). Reactions were run as a gradient to determine optimum annealing temperature for each primer pair, and products were separated on a 1.5% agarose gel with ethidium bromide. Flanking 100 bp ladders were used as molecular weight markers, and gels were imaged using a ChemiDoc XRS imager (Bio-Rad, Hercules, CA). Single band amplicons of the correct molecular weight were sequenced (Eton Biosciences, Union, NJ) and the correct products were validated using NCBI and Ensembl BLAST.

Quantitative (q)PCR: PCP-R cells were grown as previously described until confluent. 24 hours prior to mRNA collection, experimental cells were treated with specific compounds both apically and basolaterally and allowed to incubate overnight. Cells were washed twice with cold 1x PBS, and total RNA was collected using the Monarch Total RNA Miniprep Kit (New England Biolabs) according to the manufacturer's directions for cells cultured in a monolayer. The resulting purified RNA concentration was measured using an ND2000 Nanodrop (Fisher Scientific, Waltham, MA).

100 ng of total RNA was reverse transcribed into cDNA using the Monarch LunaScript RT SuperMix Kit (New England Biolabs). The cDNA was then diluted 1:10 with nuclease-free water (New England Biolabs). qPCR was performed using a LightCycler 480 Instrument II real-time PCR system (Roche LifeScience, Penzberg, Germany), utilzing LightCycler 480 SYBR Green I Master Mix (Roche LifeScience, #04707516001). qPCR cycle conditions were 95°C for 5 minutes; followed by 45 cycles of 95°C for 10 seconds, 60°C for 10 seconds, and 72°C for 10 seconds. Data are displayed as relative fold change in expression using the $2^{-\Delta\ \Delta CT}$ method (31), relative to the calibrator housekeeping genes GAPDH and Rps18. Data are shown as fold change of TRPV4 or NKCC1 in treated cell cultures relative to the normalized controls.

Statistics: Statistics were calculated using Two-tailed Students t-test in Sigma Plot 13. $p < 0.05$ is considered significant. Students t-test was used to compare experimental groups to the control as indicated by the symbols defined in the figure legends.

3.6 **Results**

Three sets of redundant primer pairs per gene were utilized to determine the presence of specific genes of interest in the PCP-R cell line using RT-PCR (Table 1). Single band amplicons were sequenced to confirm the correct mRNA had been amplified. mRNA encoding for NKCC1 was identified in the PCP-R cells, as well as mRNA for all four KCC cotransporters (KCC1-4) (Figure 1). NKCC2 is typically thought to be a kidney-specific isoform, primarily found in the thick ascending limb, while NKCC1 is expressed in nearly all secretory cell types. All 4 KCCs have been identified in various parts of the central nervous system, with KCC2 thought to be responsible for maintaining low Cl- in neurons (25,50). Additionally, STK39 mRNA, which encodes for SPAK was shown to be present in the PCP-R cells. As previously demonstrated, TRPV4 mRNA is also shown to be expressed in the PCP-R cell line. GAPDH was used as an internal positive control.

Ussing chamber electrophysiology was used to measure net changes in transepithelial ion flux as well as barrier permeability. As previously demonstrated, addition of the TRPV4 agonist GSK1016790A stimulates a multiphasic change in SCC, accompanied by an increase in transepithelial conductance (41,45). The negative change in SCC is representative of a net

electrogenic transepithelial ion transport, which is consistent with either anion absorption and/or cation secretion. The positive change in transepithelial conductance is consistent with an increase in barrier permeability (41,45). For each subsequent figure, experiments were conducted with paired controls, which utilized a vehicle for the pre-incubated effector and the TRPV4 agonist GSK1016790A. In each experiment, the TRPV4 agonist was added at time point T = 0 for all cultures. For experimental cultures, cells were pre-treated with specific inhibitors or modulators 10 minutes prior to the addition of the TRPV4 agonist.

Several studies have shown the kinase SPAK to phosphorylate and activate the NKCC cotransporters, as well as phosphorylating and inhibiting the KCC channels (1,2,10-12,15-17,19-21,23,26,35,37,38,43). Therefore, it is heavily involved in the regulation of ion transport and could potentially be involved in TRPV4-mediated transport. Pretreatment of the PCP-R cells with a SPAK/OSR1 inhibitor, rafoxanide, prior to stimulating TRPV4 with its agonist resulted in a significant inhibition of the change in basal transepithelial ion flux. Interestingly, the change in cellular permeability showed a rapid increase immediately following the addition of the SPAK/OSR1 inhibitor. This increase was statistically significant immediately following inhibition of the kinases and remained significantly higher than the control experiment conductance until approximately 5 minutes post-addition of the TRPV4 agonist (Figure 2). A second, more specific inhibitor of the WNK-SPAK pathway, STOCK2S 26016, was utilized at 10 μM to inhibit the kinase. Following pretreatment with STOCK2S, both the SCC and conductance changes normally observed upon addition of the TRPV4 agonist were substantially inhibited. However, in these experiments, no initial increase in transepithelial conductance was observed upon SPAK inhibition alone (Figure 3).

Pretreatment of the PCP-R cells with 100 μM bumetanide, a specific inhibitor of NKCC, on both the apical and basolateral membranes 10 minutes prior to the addition of the TRPV4 agonist resulted in a statistically significant inhibition of the TRPV4-mediated ion flux during the second phase (T = 10-20) of the agonist-induced SCC change (Figure 4). In the CP, NKCC1 has been identified on the apical membrane. To determine whether the bumetanide effect was restricted to a single membrane, cells were treated on either the apical or the basolateral membranes. When

added to only one membrane, 100 μM bumetanide was observed to have no effect on the TRPV4 agonist-stimulated transepithelial ion flux or permeability changes (Figure 5).

As the KCC ion channels are regulated by the WNK-SPAK/OSR1 pathway similar to the NKCCs, we also investigated whether the KCCs are involved in the TRPV4-mediated pathway (12,23). Therefore, PCP-R cells were pretreated with 25 μM R-(+)-DIOA, a nonspecific inhibitor of the KCC cotransporters, either on the apical or basolateral membrane. However, treatment with the KCC inhibitor had no effect on either the SCC or transepithelial conductance following addition of the TRPV4 agonist (Figure 6).

To determine if NKCC and the KCCs acted in concert relative to each other for regulation of intracellular [Cl^-], cells were co-incubated with a cocktail containing 100 μM bumetanide and 25 μM R-(+)-DIOA added to both sides of the membrane. No effects on TRPV4-mediated transepithelial ion flux nor permeability changes were observed following treatment with the TRPV4 agonist (Figure 7).

To determine whether NKCC1 or SPAK inhibition had an effect on gene expression, cultures were incubated for 24 hours with 100 μM bumetanide or 10 μM STOCK2S, and mRNA was collected for qPCR analysis. The expression of TRPV4, NKCC1 and SPAK mRNA were observed relative to their respective expression in parallel control cultures incubated with vehicle only. Incubation with bumetanide had no significant effect on mRNA expression of TRPV4, NKCC1 or SPAK (Figure 8). 24 hour incubation with the SPAK inhibitor STOCK2S resulted in a net 2-fold decrease in NKCC1 and SPAK mRNA expression, while no changes in TRPV4 mRNA were observed (Figure 9).

3.7 **Discussion**

NKCC1 is ubiquitously expressed in many secretory epithelia and is thought to be involved in the maintenance of cell volume and homeostasis (2,21). In most tissues, it is localized to the basolateral membrane (2,21). However, in the CP is has been demonstrated that NKCC1 localizes to the apical membrane in CP, a somewhat curious finding (20,34,47). The apical localization of NKCC1 has been a cause of significant controversy for several years, with two arguments typically presented.

If NKCC1 operates in net efflux mode (not generally found in other tissues), it contributes to the production of CSF via the movement of ions from the intracellular space to the intraventricular space (11,20,47). Alternatively, if NKCC1 operates in net influx on the apical membrane, then it is assumed to contribute to reabsorption of ions into the intracellular space of CP cells, maintaining cell volume and homeostasis (2,11,20,21). Evidence exists to support both hypotheses, and a rationale has been proposed that suggests NKCC1 is capable of reversing its directionality based upon cellular physiological needs as well as on ion gradients of which TRPV4 is capable of creating (11,20).

In addition to NKCC1, all four KCC cotransporters have been identified in different regions of the central nervous system (24,25,50). Previous reports have suggested that KCC4 and KCC3 may be expressed on the apical and basolateral membranes of the CP epithelia, respectively (7,8,25). In this tissue, these ion channels are thought to be involved in chloride efflux from the cell; with KCC4 contributing to chloride efflux into the CSF, and KCC3 contributing to chloride efflux into the blood (7,8,40). Additionally, it has been shown that KCC1 is also present in the CP cells, although its localization has not been resolved (24,49).

Following collection of mRNA from cultured PCP-R cells, RT-PCR showed clear expression of NKCC1 and all four KCC variants. This was somewhat surprising, as KCC2 has not previously been identified in CP. In mouse choroid plexus, Kanaka et al. showed an absence of KCC2 mRNA, while KCC1, KCC3 and KCC4 have all been identified in both mouse and rat CP (7,8,24,25,49). This channel's presence in porcine CP epithelia, but absence in rodent CP epithelia may suggests species-specific differences in gene regulation.

In regards to the interactions between NKCC1 and TRPV4, the relationship has remained elusive for a number of years. One study suggests that TRPV4 is responsible for mediating brain edema induced by NKCC1 following traumatic brain injury (TBI) (32). In this study, it was found that treatment with bumetanide in TBI-induced brain edema resulted in a reversal of the upregulation of TRPV4 expression in the hippocampus following TBI. On the other hand, treatment with the TRPV4 inhibitor RN1734 was ineffective towards the expression of NKCC1 following TBI. This suggests that NKCC1 regulates TRPV4 expression in the hippocampus. In our experiments,

inhibition of NKCC1 with a high dose of bumetanide resulted in a statistically significant inhibition of some components ofthe TRPV4-mediated ion flux. However, 100 μM bumetanide was shown to have no effect on the resulting increase in transepithelial conductance, which remained high in both the experimental and control groups. We then sought to determine whether this effect was observed on either the apical or basolateral membrane alone. Treatment with 100 μM bumetanide on only one side of the membrane, however, resulted in no changes to the resulting electrogenic ion flux or conductance.

To ascertain a role for the KCC cotransporters in TRPV4-mediated flux. R-(+)-DIOA, a nonspecific pan-KCC inhibitor was used at 25 μM, with no effect observed on either the TRPV4 agonist-stimulated SCC or conductance changes. This was not entirely unexpected, as the KCCs are localized to both membranes, with transport resulting in net efflux of Cl^- and K^+. Finally, to ascertain whether the KCCs acted in concert with NKCC1, we co-incubated cells with both 100 μM bumetanide and 25 μM R-(+)-DIOA. Again, as with previous experiments, no effects were observed. These data suggest that while NKCC1 and the KCCs may play a role in CP epithelial cell homeostasis, it appears they do not in fact regulate TRPV4 activity.

SPAK has been demonstrated to phosphorylate and activate NKCC1, as well as to phosphorylate and inhibit the KCCs (12,34,43). Thus far, no direct link between SPAK and TRPV4 has been shown. However, anecdotal evidence exists suggesting a role for SPAK in regulating TRPV4 activity. In the HEK-293 cells, WNK4 expression has been shown to downregulate TRPV4 function (14,18). WNK kinases regulate SPAK and the redundant kinase OSR1 upstream, which suggests a signaling cascade which may perturb TRPV4 function. To address this, we inhibited the WNK pathway in PCP-R cells with the SPAK/OSR1 inhibitor, rafoxanide. Upon stimulation of TRPV4 with its agonist, we observed a near-complete inhibition of the TRPV4-mediated ion flux in the SPAK-inhibited cultures. Interestingly, initial treatment with rafoxanide also resulted in an immediate and sustained increase in the conductance, suggesting the WNK pathway plays a role in basal ion permeability and cell volume homeostasis, likely through an ion transporter it regulates. This change in cellular permeability, upon addition of the TRPV4 agonist closely mimicked that of the control experiments. A second, more specific inhibitor of the WNK-SPAK activation pathway, STOCK2S-26016, was employed to confirm this result in regards to SPAK.

From this, we found no initial conductance increase was observed in the PCP-R cells when SPAK phosphorylation was inhibited as compared to inhibition of both SPAK and OSR1. Contradictory to the previous result, specific inhibition of SPAK resulted in inhibition of not only the TRPV4-mediated change in transepithelial ion flux, but also of the change in cellular permeability. These data suggest a regulatory role for SPAK in the TRPV4 pathway with TRPV4-mediated activity dependent on the kinase, although the mechanism of this regulation is currently unknown. Taken together with the bumetanide results, it appears that the regulatory role of SPAK occurs independently of NKCC1 activation, as direct inhibition of NKCC1 did not inhibit TRPV4-stimulated permeability nor transepithelial ion flux changes to the same degree observed with SPAK inhibition.

Previously, bumetanide-induced inhibition of NKCC1 has not to our knowledge been demonstrated to effect gene regulation. Following prolonged exposure of the PCP-R cells to bumetanide, we have shown that NKCC1 inhibition does not affect the transcription of TRPV4, NKCC1 or SPAK. This suggests that a compensatory feedback mechanism does not exist at the transcription level in the cells in response to aberrantly regulated NKCC1. Transcription of the same genes in PCP-R cells were observed following SPAK inhibition with STOCK2S for 24 hours in order to determine the effect on gene regulation. Interestingly, NKCC1 expression decreased 4-fold following 24 hour inhibition of SPAK. This suggests that SPAK is necessary for both transcription and activation of NKCC1, albeit through an unknown mechanism. Additionally, TRPV4 mRNA expression was observed to increase 2-fold, while SPAK mRNA expression did not appear to change in response to prolonged SPAK inhibition. These data appear to contradict the electrophysiological results, suggesting that the inhibition of SPAK actually results in more TRPV4. A simple explanation may, however, answer this question. If SPAK inhibition over an extended period results in inhibited TRPV4, there may exist a feedback mechanism by which TRPV4 is overexpressed to compensate for inactive TRPV4 at the apical membrane.

In summary, inhibition of NKCC1 with bumetanide resulted in moderate inhibition of TRPV4-mediated transepithelial ion fluxes but did not inhibit increases in conductance associated with TRPV4 activation. Our studies show that inhibition of the KCCs had no effect on either TRPV4-mediatedion transport or conductance changes. Additionally, co-incubation with inhibitors of both

NKCCs and the KCCs resulted in no inhibition of TRPV4-mediated activity. We found, however, that inhibition of SPAK resulted in inhibition of both the transepithelial ion flux and permeability changes associated with activation of TRPV4. Previous data from our laboratory has established that transepithelial ion flux and alterations in cellular permeability in CP epithelia are carefully regulated via TRPV4. However, we now have shown that SPAK appears to be a significant regulator of the TRPV4-mediated ion flux pathway. Although, unexpectedly, this regulation appears to be not through regulation of NKCC1. Future experimentation will be necessary to elucidate the regulatory role of SPAK for TRPV4 activation and begin to organize the molecular orchestra responsible for the production of CSF.

3.8 **Acknowledgments**

We would like to thank Dr. Nick Berbari and Patrick Antonellis for their invaluable support in optimizing the qPCR experiments and interpreting preliminary data.

3.9 **Grants**

This research was supported by the United States Department of Defense Investigator Initiated Research Award W81XWH-16-PRMRP-IIRA (BBY).

3.10 **Disclosures**

None.

Table 3.1 *Sus Scrofa* Primers Used for RT-PCR with Corresponding Product Sizes (bp).

Three different primer sets were generated and tested for each gene. Primers included in this table were utilized for Figure 1. GAPDH was used as a positive control.

Sus Scrofa gene	Protein	Primer Sequences 5' - 3'		Product Size (bp)
		Forward Primer	Reverse Primer	
TRPV4	TRPV4	AGATTGGGATCTTTCAGCACAT	AGCAAGTAGACCAGCAGGAAAC	724
Stk39	SPAK	TAGCAACAGGGGGTGATGTTAC	CTCTTTGGGCTATGTCTGGTGT	432
SLC12A2	NKCC1	ATTTTCGCGAGGAAGAGACCTT	TGCACTCACAAGGGATGCTAAT	428
SLC12A4	KCC1	TGTACCACCTACGTCTTGAAGC	GCACTTCCAGGAACTCCATGTA	495
SLC12A5	KCC2	CTGGCTTACCTTTTCCCAGCTA	TTGGTCAGATAGGAGCTCCAGA	485
SLC12A6	KCC3	AGGCAGAGAACATCACTGAAGG	ATACCACCAACACCATGAGGAC	498
SLC12A7	KCC4	TTACATGATATCGCGGTCCCTG	CAAAATACGGGTCACAGGAGGA	494
Gapdh	GAPDH	TTTTAACTCTGGCAAAGTGGAC	CATTGTCGTACCAGGAAATGAG	884

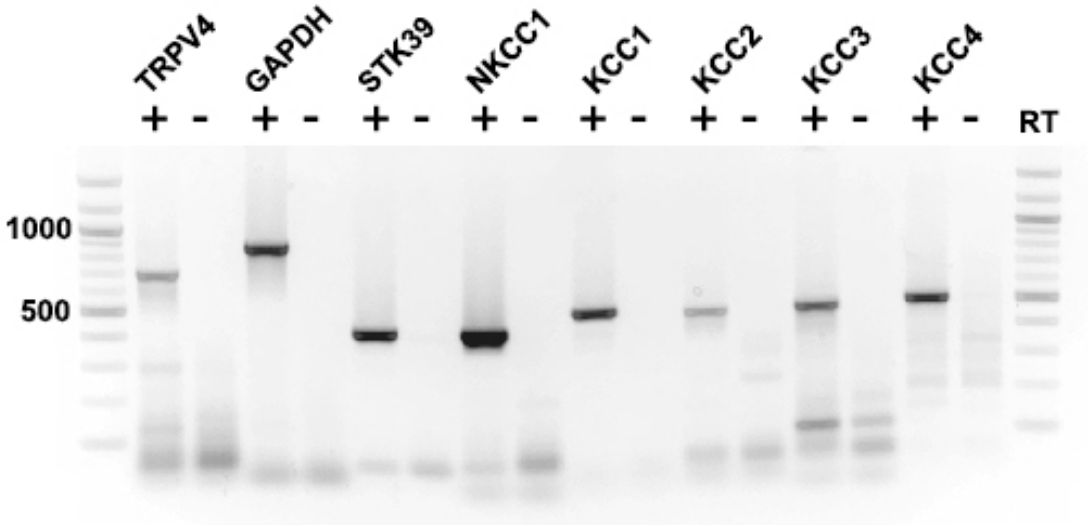

Figure 3.1 RT-PCR in the PCP-R Cell Line.

RT-PCR in the PCP-R cell line. mRNA for NKCC1, KCC1-4, TRPV4, and STK39 are present in the PCP-R cell line. GAPDH was used as a positive control. 100 bp flanking ladders were used. RT = Reverse transcriptase. Lanes denoted as (+) or (-) RT identify the presence or absence of reverse transcriptase in the PCR mixture.

Figure 3.2: Pre-treatment of PCP-R cells with a SPAK inhibitor prior to addition of a TRPV4 agonist. Net changes in transepithelial ion flux and conductance were measured. Rafoxanide (10 μM) was added both apically and basolaterally at T = -10 minutes. The TRPV4 agonist GSK1016790A was added to the basolateral side of the membrane in all cultures at T = 0 minutes. Pre-incubation with Rafoxanide is represented by white open circles. The GSK-treated positive controls are denoted by black filled circles. Circles represent mean values, and error bars represent +/- SEM for the *n* indicated. SCC = short circuit current. * = $p < 0.05$ against control experiments.

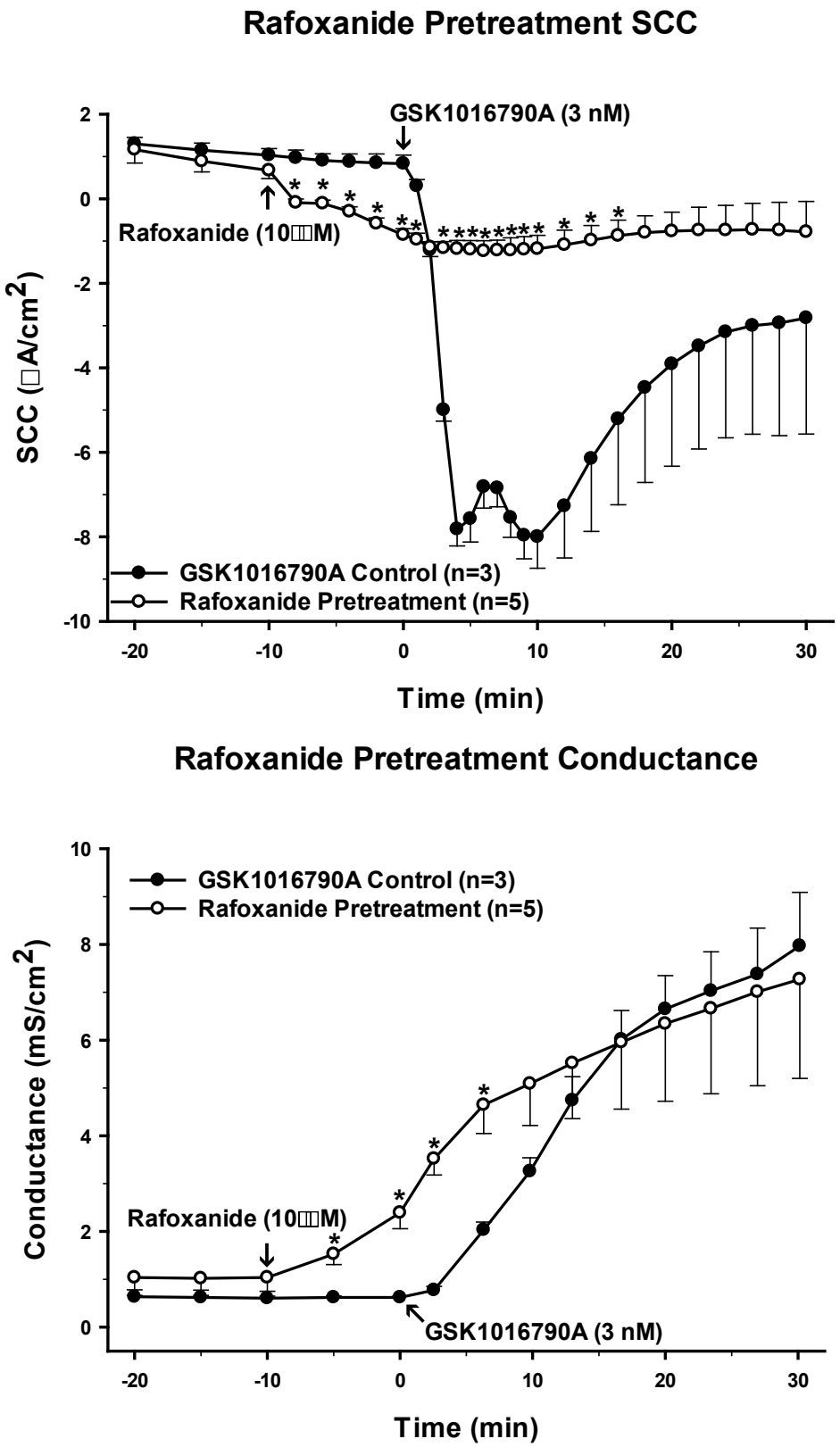

Figure 3.2 Effect of SPAK Inhibitor on TRPV4-Mediated Responses.

Figure 3.3: Pre-treatment of PCP-R cells with a SPAK inhibitor prior to addition of a TRPV4 agonist. Net changes in transepithelial ion flux and conductance were measured. STOCK2S 26016 (10 μM) was added both apically and basolaterally at T = -10 minutes. The TRPV4 agonist GSK1016790A was added to the basolateral side of the membrane in all cultures at T = 0 minutes. Pre-incubation with STOCK2S 26016 is represented by white open circles. The GSK-treated positive controls are denoted by black filled circles. Circles represent mean values, and error bars represent +/- SEM for the *n* indicated. SCC = short circuit current. * = $p < 0.05$ against control experiments.

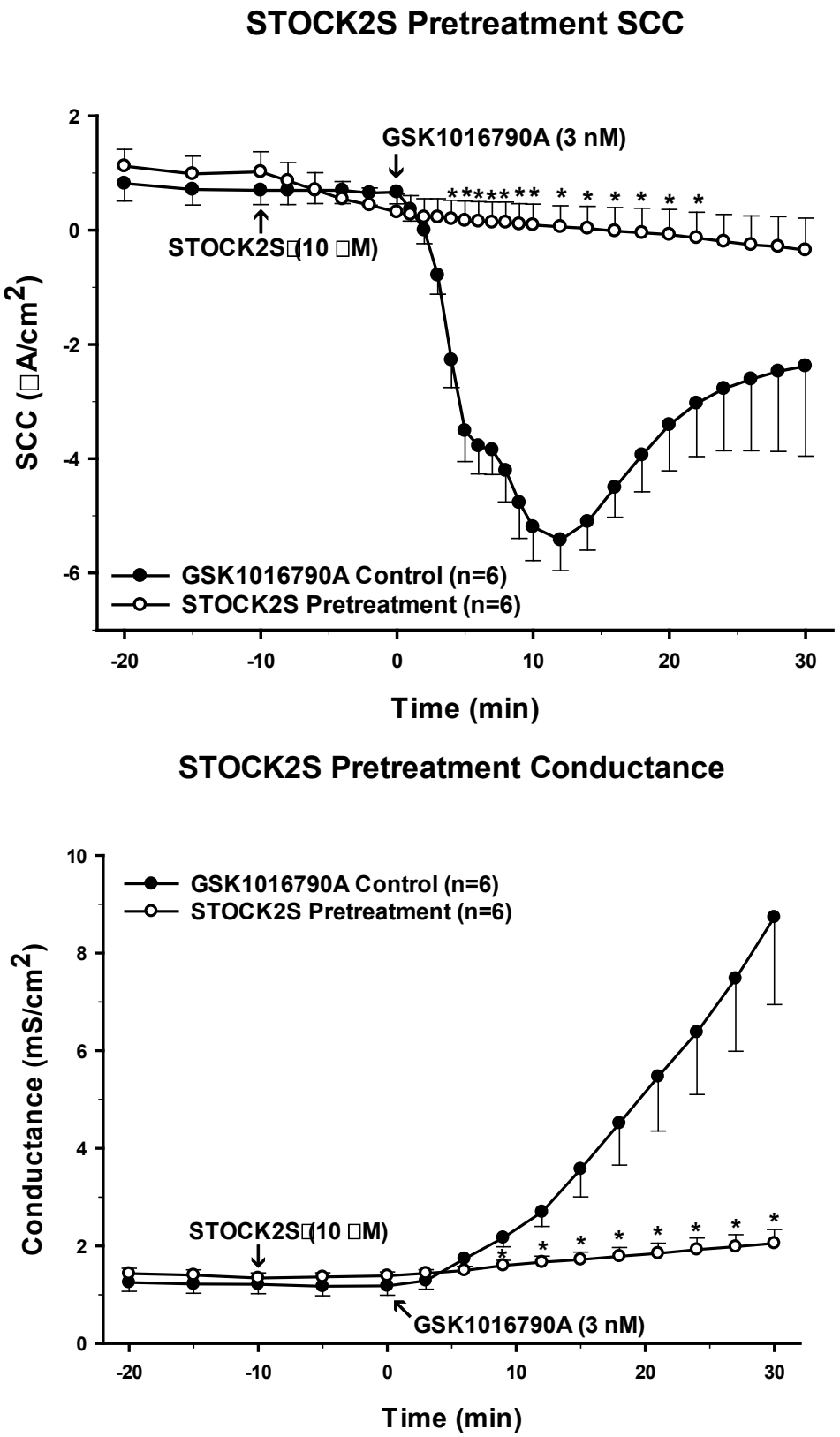

Figure 3.3 Effect of SPAK Inhibitor on TRPV4-Mediated Responses.

Figure 3.4: Pre-treatment of PCP-R cells with an NKCC inhibitor prior to addition of a TRPV4 agonist. Net changes in transepithelial ion flux and conductance were measured. Bumetanide (100 μM) was added simultaneously to both the apical and basal surfaces at T = -10 minutes. The TRPV4 agonist GSK1016790A was added to the basolateral side of the membrane in all cultures at T = 0 minutes. Pre-incubation with Bumetanide is represented by white open circles. The GSK controls are denoted by black filled circles. Circles represent mean values, and error bars represent +/- SEM for the *n* indicated. SCC = short circuit current. * = $p < 0.05$ against control experiments.

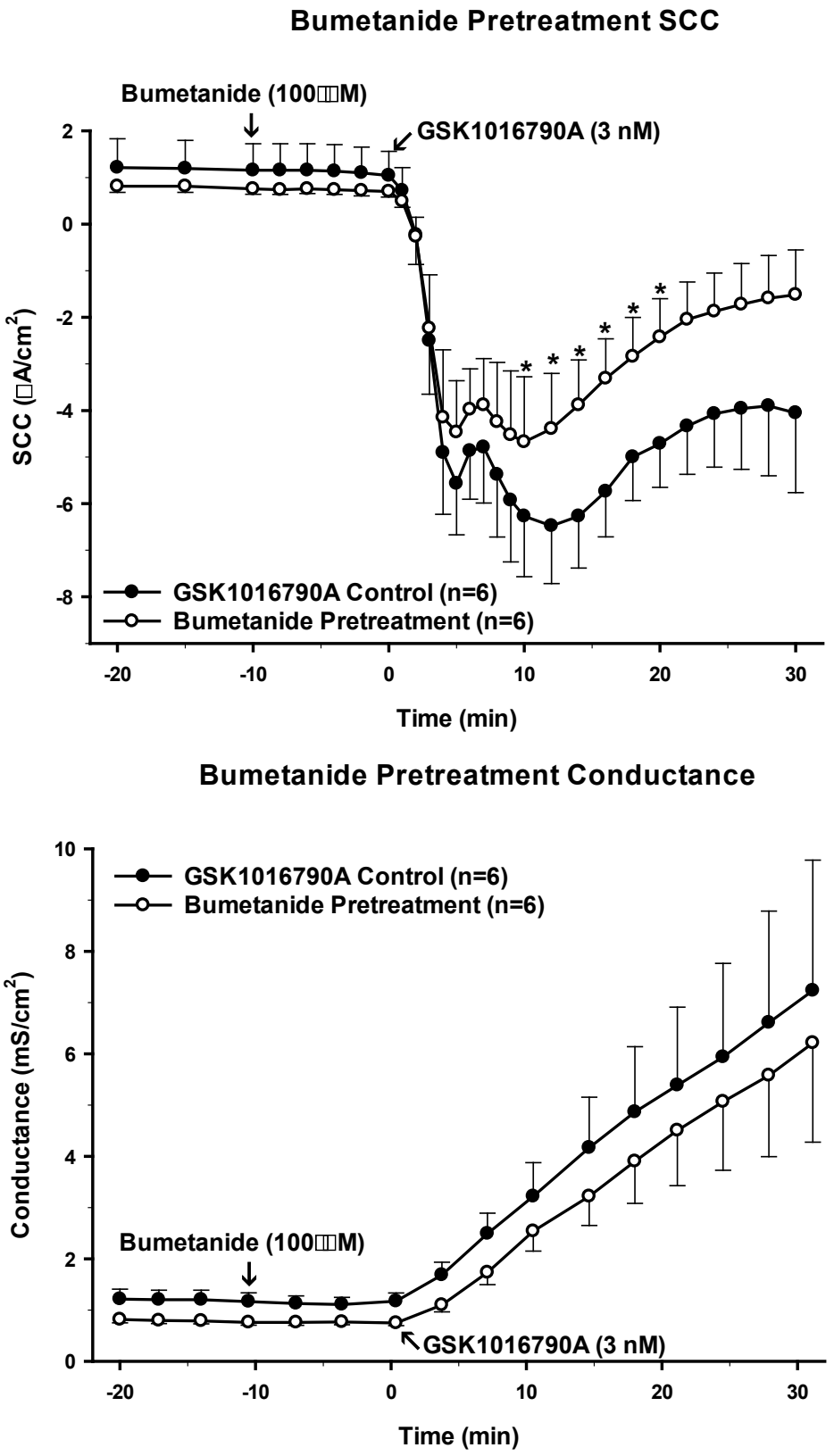

Figure 3.4 Effect of NKCC Inhibitor on TRPV4-Mediated Responses.

Figure 3.5: Pre-treatment of PCP-R cells with an NKCC inhibitor prior to addition of a TRPV4 agonist. Net changes in transepithelial ion flux and conductance were measured. Bumetanide (100 μM) was added either apically or basolaterally at T = -10 minutes. The TRPV4 agonist GSK1016790A was added to the basolateral side of the membrane in all cultures at T = 0 minutes. Pre-incubation with Bumetanide to the apical or basolateral surfaces is represented by white open circles, or grey filled circles, respectively. The GSK-treated positive controls are denoted by black filled circles. Circles represent mean values, and error bars represent +/- SEM for the *n* indicated. SCC = short circuit current. * = $p < 0.05$ against control experiments.

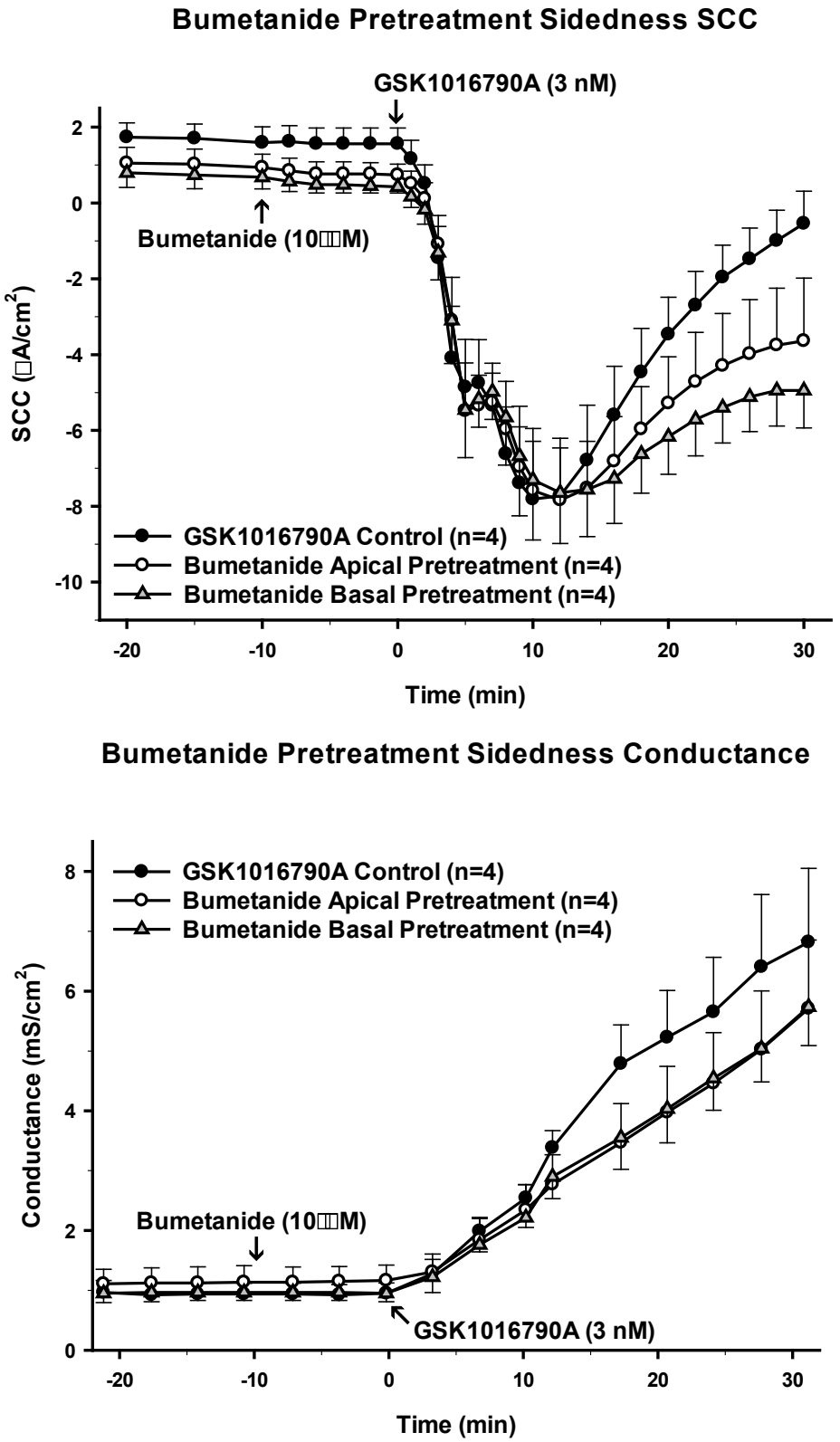

Figure 3.5 Sidedness of NKCC Inhibitor on TRPV4-Mediated Responses.

Figure 3.6: Pre-treatment of PCP-R cells with a KCC inhibitor prior to addition of a TRPV4 agonist. Net changes in transepithelial ion flux and conductance were measured. R-(+)-DIOA (25 μM) was added either apically or basolaterally at T = -10 minutes. The TRPV4 agonist GSK1016790A was added to the basolateral side of the membrane in all cultures at T = 0 minutes. Pre-incubation with R-(+)-DIOA apically or basolaterally is represented by white open circles, or grey filled triangles, respectively. The GSK-treated positive controls are denoted by black filled circles. Circles represent mean values, and error bars represent +/- SEM for the *n* indicated. SCC = short circuit current. * = $p < 0.05$ against control experiments.

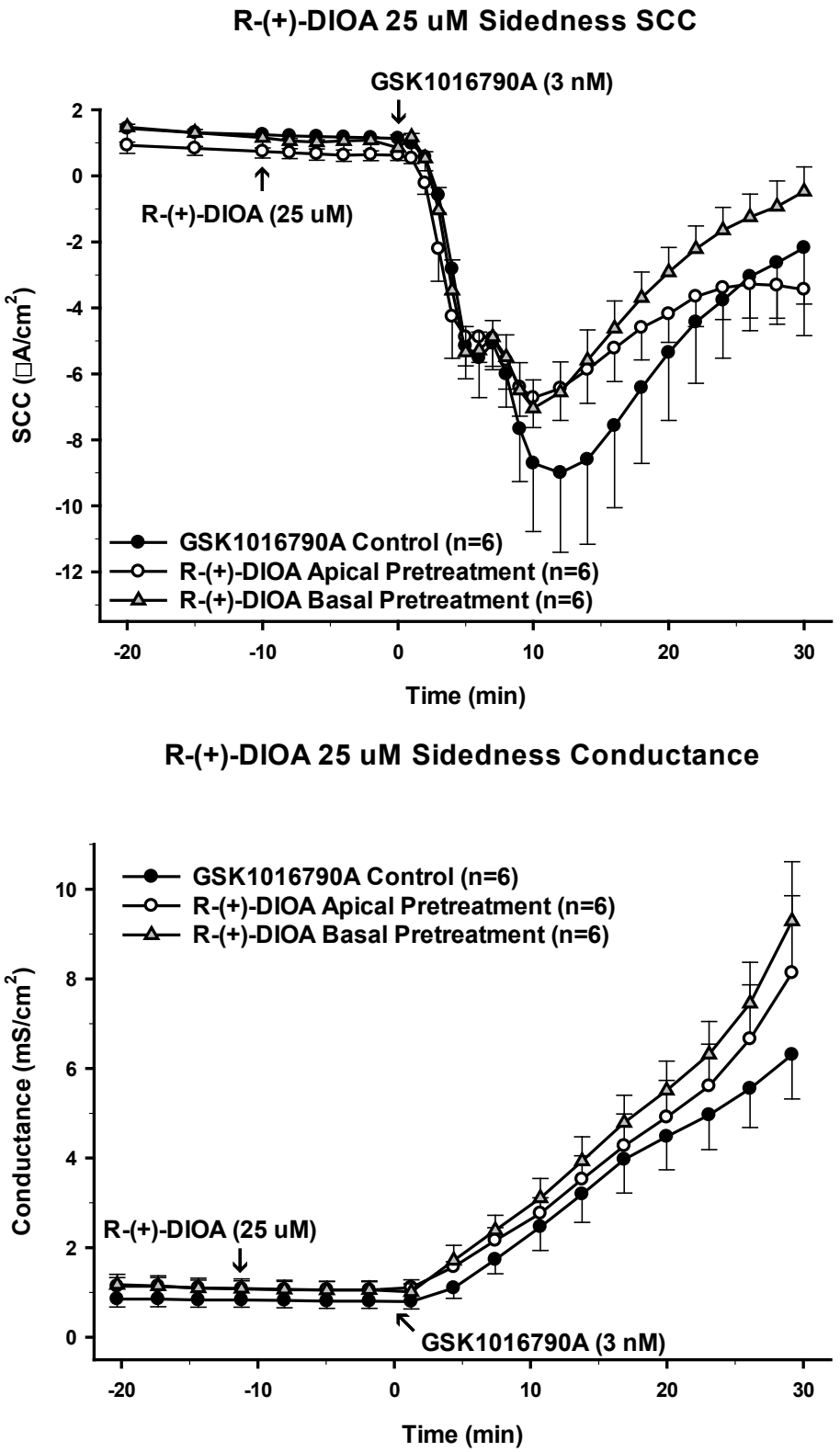

Figure 3.6 Sidedness of KCC Inhibitor on TRPV4-Mediated Responses.

Figure 3.7: Pre-treatment of PCP-R cells with an NKCC and KCC inhibitor cocktail prior to addition of a TRPV4 agonist. Net changes in transepithelial ion flux and conductance were measured. A bumetanide (100 μM) and R-(+)-DIOA (25 μM) cocktail was added both apically and basolaterally at T = -10 minutes. The TRPV4 agonist GSK1016790A was added to the basolateral side of the membrane in all cultures at T = 0 minutes. Pre-incubation with the bumetanide and R-(+)-DIOA cocktail is represented by white open circles. The GSK-treated positive controls are denoted by black filled circles. Circles represent mean values, and error bars represent +/- SEM for the *n* indicated. SCC = short circuit current. * = $p < 0.05$ against control experiments.

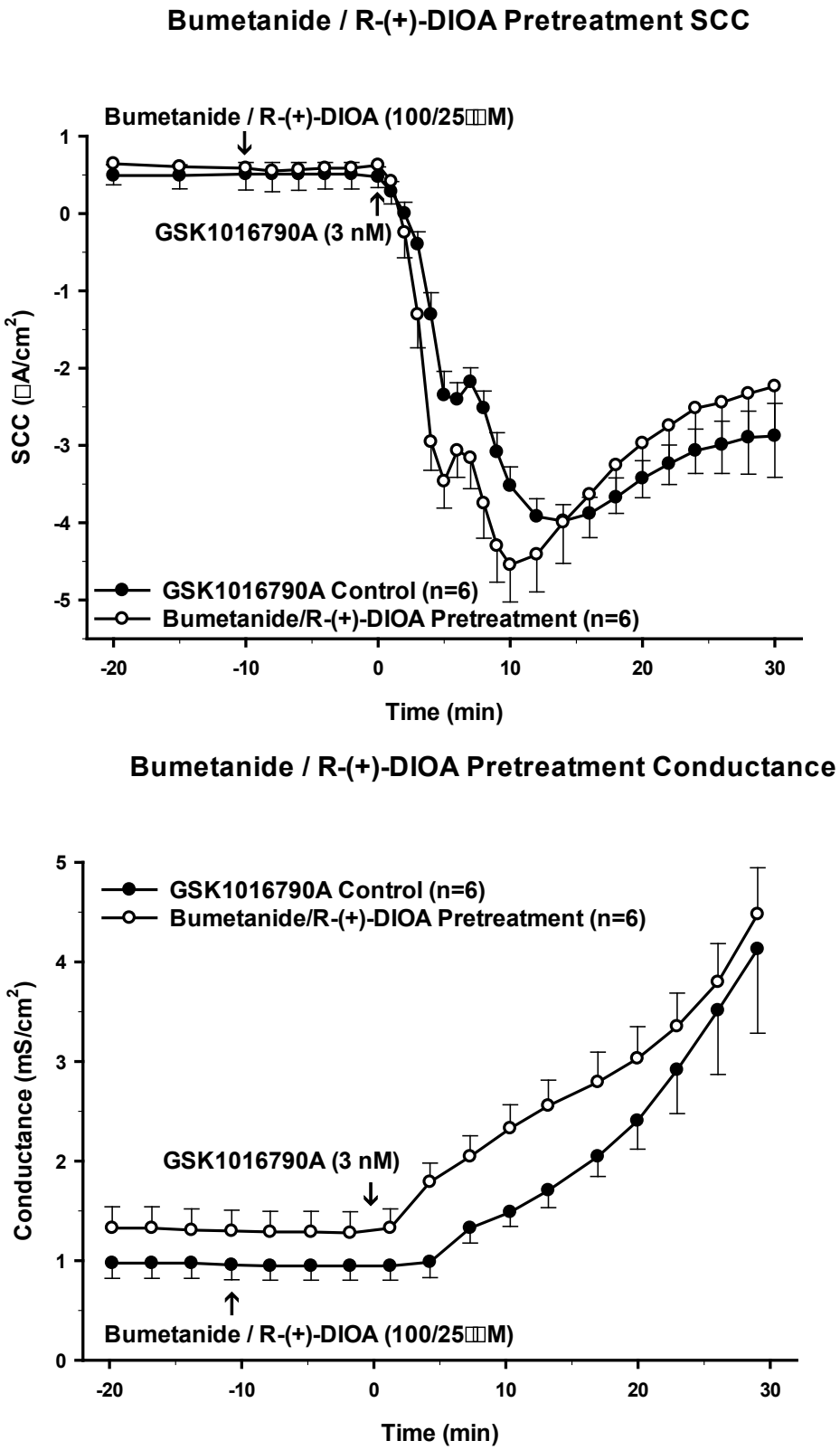

Figure 3.7 Effect of NKCC and KCC Inhibitors on TRPV4-Mediated Responses.

Figure 3.8: Relative fold change of mRNAs in PCP-R cells 24 hours post-incubation with a specific inhibitor of NKCC. Bumetanide (100 μM) was added both apically and basolaterally to individual experimental wells (n=6 for each inhibitor). The fold change in TRPV4, NKCC or SPAK in bumetanide-treated cultures are shown relative to normalized controls (n=6). GAPDH and RPS18 were used as housekeeping genes to calculate the $2^{-\Delta\Delta CT}$ fold change in each gene. Individual points shown are the minimum and maximum fold change values. Boxes represent +/- SEM for the experiments indicated, and the line within each box represents the mean value for those experiments.

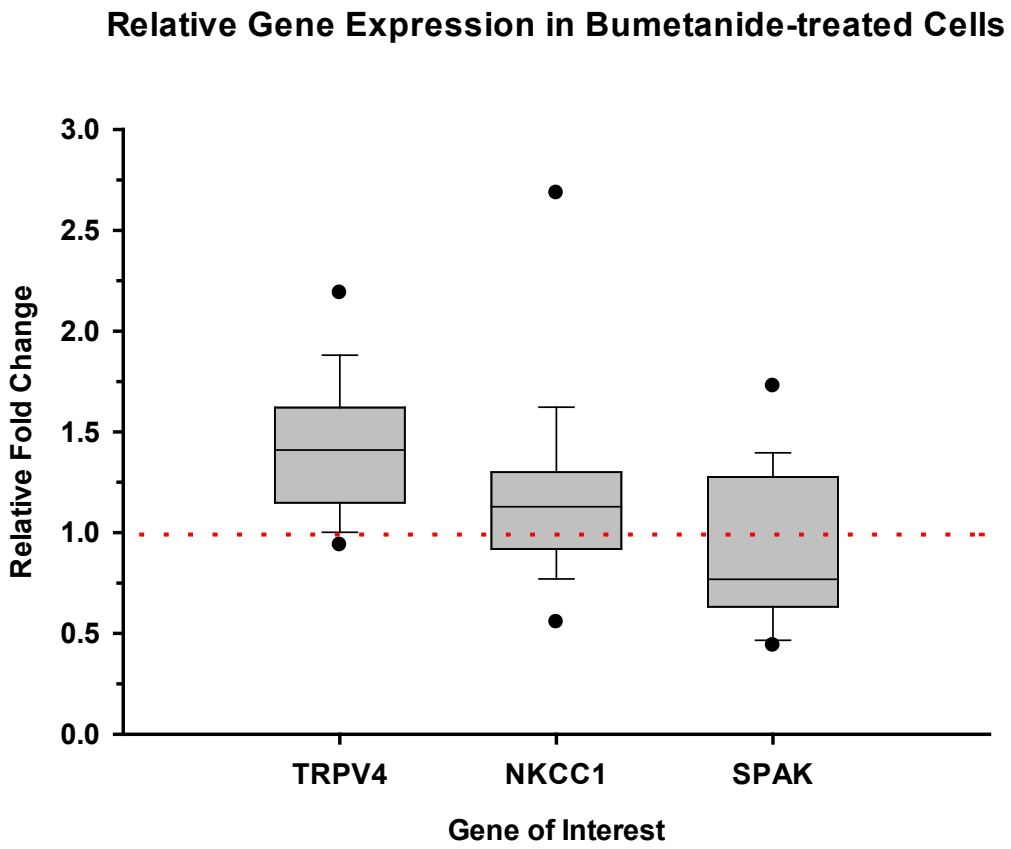

Figure 3.8 Effect of NKCC Inhibitor on mRNA Transcription.

Relative fold change of mRNAs in PCP-R cells 24 hours post-incubation with a specific inhibitor of NKCC. Bumetanide (100 μM) was added both apically and basolaterally to individual experimental wells (n=6 for each inhibitor). The fold change in TRPV4, NKCC or SPAK in bumetanide-treated cultures are shown relative to normalized controls (n=6). GAPDH and RPS18 were used as housekeeping genes to calculate the $2^{-\Delta\Delta CT}$ fold change in each gene. Individual points shown are the minimum and maximum fold change values. Boxes represent +/- SEM for the experiments indicated, and the line within each box represents the mean value for those experiments.

Figure 3.9: Relative fold change of mRNAs in PCP-R cells 24 hours post-incubation with a specific inhibitor of SPAK. STOCK2S 26016 (1 μM) was added both apically and basolaterally to individual experimental wells (n=6 for each inhibitor). The fold change in TRPV4, NKCC or SPAK are shown relative to normalized controls (n=6). GAPDH and RPS18 were used as housekeeping genes to calculate the $2^{-\Delta\Delta CT}$ fold change in each gene. Individual points shown are the minimum and maximum fold change values. Boxes represent +/- SEM for the experiments indicated, and the line within each box represents the mean value for those experiments.

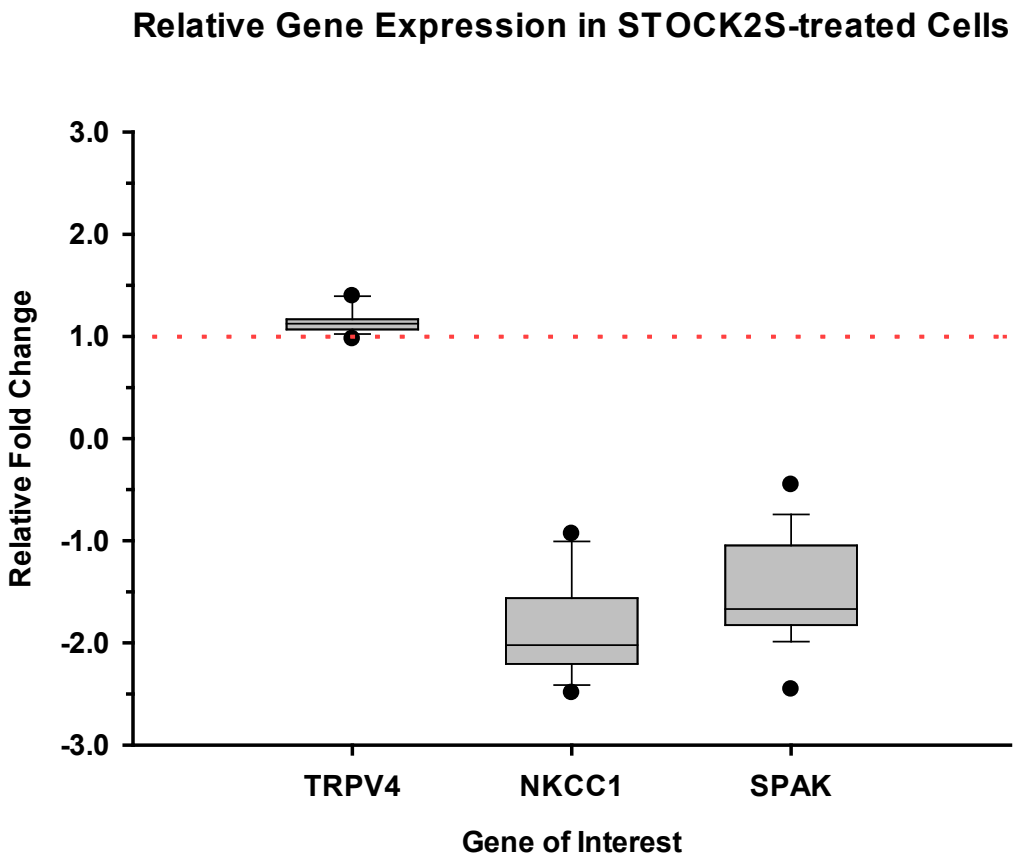

Figure 3.9 Effect of SPAK Inhibitor on mRNA Transcription.

3.11 **References**

1. Alessi D, Zhang J, Khanna A, Hochdorfer T, Shang Y, Kahle K. The WNK-SPAK/OSR1 pathway: Master regulator of cation-chloride cotransporters. *Science Signaling* 7: 1-9, 2014.
2. Arroyo J, Kahle K, Gamba G. The SLC12 family of electroneutral cation-coupled chloride cotransporters. *Molecular Aspects of Medicine* 34: 288-298, 2013.
3. Baratchi S, Keov P, Darby W, Lai A, Khoshmanesh K, Thurgood P, Vahidi P, Ejendal K, McIntyre P. The TRPV4 Agonist GSK1016790A Regulates the Membrane Expression of TRPV4 Channels. *Frontiers in Pharmacology* 10, 2019.
4. Bothwell S, Janigro D, Patabendige A. Cerebrospinal fluid dynamics and intracranial pressure elevation in neurological diseases. *Fluids and Barriers of the CNS* 16, 2019.
5. Brodbelt A, Stoodley M. CSF pathways: a review. *British Journal of Neurosurgery* 21: 510-520, 2007.
6. Brown P, Davies S, Speake T, Millar I. Molecular mechanisms of cerebrospinal fluid production. *Neuroscience* 129: 955-968, 2004.
7. Damkier H, Brown P, Praetorius J. Epithelial Pathways in Choroid Plexus Electrolyte Transport. *Physiology* 25: 239-249, 2010.
8. Damkier H, Brown P, Praetorius J. Cerebrospinal Fluid Secretion by the Choroid Plexus. *Physiological Reviews* 93: 1847-1892, 2013.
9. Darby W, Grace M, Baratchi S, McIntyre P. Modulation of TRPV4 by diverse mechanisms. *The International Journal of Biochemistry & Cell Biology* 78: 217-228, 2016.
10. de los Heros P, Alessi D, Gourlay R, Campbell D, Deak M, Macartney T, Kahle K, Zhang J. The WNK-regulated SPAK/OSR1 kinases directly phosphorylate and inhibit the K+–Cl−co-transporters. *Biochemical Journal* 458: 559-573, 2014.
11. Delpire E, Gagnon K. Elusive role of the Na-K-2Cl cotransporter in the choroid plexus. *American Journal of Physiology-Cell Physiology* 316: C522-C524, 2019.
12. Delpire E, Gagnon K. SPAK and OSR1, key kinases involved in the regulation of chloride transport. *Acta Physiologica* 187: 103-113, 2006.
13. Ding F, O'Donnell J, Xu Q, Kang N, Goldman N, Nedergaard M. Changes in the composition of brain interstitial ions control the sleep-wake cycle. *Science* 352: 550-555, 2016.

14. Fu Y, Subramanya A, Rozansky D, Cohen D. WNK kinases influence TRPV4 channel function and localization. *American Journal of Physiology-Renal Physiology* 290: F1305-F1314, 2006.
15. Gagnon K, England R, Delpire E. Characterization of SPAK and OSR1, Regulatory Kinases of the Na-K-2Cl Cotransporter. *Molecular and Cellular Biology* 26: 689-698, 2005.
16. Gagnon K, England R, Diehl L, Delpire E. Apoptosis-associated tyrosine kinase scaffolding of protein phosphatase 1 and SPAK reveals a novel pathway for Na-K-2C1 cotransporter regulation. *American Journal of Physiology-Cell Physiology* 292: C1809-C1815, 2007.
17. Gagnon K, Delpire E. Molecular Physiology of SPAK and OSR1: Two Ste20-Related Protein Kinases Regulating Ion Transport. *Physiological Reviews* 92: 1577-1617, 2012.
18. Gamba G. TRPV4: a new target for the hypertension-related kinases WNK1 and WNK4. *American Journal of Physiology-Renal Physiology* 290: F1303-F1304, 2006.
19. Geng Y, Hoke A, Delpire E. The Ste20 Kinases Ste20-related Proline-Alanine-rich Kinase and Oxidative-stress Response 1 Regulate NKCC1 Function in Sensory Neurons. *Journal of Biological Chemistry* 284: 14020-14028, 2009.
20. Gregoriades J, Madaris A, Alvarez F, Alvarez-Leefmans F. Genetic and pharmacological inactivation of apical Na+-K+-2Cl− cotransporter 1 in choroid plexus epithelial cells reveals the physiological function of the cotransporter. *American Journal of Physiology-Cell Physiology* 316: C525-C544, 2019.
21. Hebert S, Mount D, Gamba G. Molecular physiology of cation-coupled Cl? cotransport: the SLC12 family. *European Journal of Physiology* 447: 580-593, 2004.
22. Hengl T, Kaneko H, Dauner K, Vocke K, Frings S, Mohrlen F. Molecular components of signal amplification in olfactory sensory cilia. *Proceedings of the National Academy of Sciences* 107: 6052-6057, 2010.
23. Kahle K, Ring A, Lifton R. Molecular Physiology of the WNK Kinases. *Annual Review of Physiology* 70: 329-355, 2008.
24. Kanaka C, Ohno K, Okabe A, Kuriyama K, Itoh T, Fukuda A, Sato K. The differential expression patterns of messenger RNAs encoding K-Cl cotransporters (KCC1,2) and Na-K-2Cl cotransporter (NKCC1) in the rat nervous system. *Neuroscience* 104: 933-946, 2001.
25. Karadsheh M, Byun N, Mount D, Delpire E. Localization of the kcc4 potassium–chloride cotransporter in the nervous system. *Neuroscience* 123: 381-391, 2004.

26. Karimy J, Zhang J, Kurland D, Theriault B, Duran D, Stokum J, Furey C, Zhou X, Mansuri M, Montejo J, Vera A, Diluna M, Delpire E, Alper S, Gunel M, Gerzanich V, Medzhitov R, Simard J, Kahle K. Inflammation-dependent cerebrospinal fluid hypersecretion by the choroid plexus epithelium in posthemorrhagic hydrocephalus. *Nature Medicine* 23: 997-1003, 2017.
27. Keep R, Xiang J, Betz A. Potassium cotransport at the rat choroid plexus. *American Journal of Physiology-Cell Physiology* 267: C1616-C1622, 1994.
28. Kumar H, Lee S, Kim K, Zeng X, Han I. TRPV4: a Sensor for Homeostasis and Pathological Events in the CNS. *Molecular Neurobiology* 55: 8695-8708, 2018.
29. Lauer A, Tenenbaum T, Schroten H, Schwerk C. The diverse cellular responses of the choroid plexus during infection of the central nervous system. *American Journal of Physiology-Cell Physiology* 314: C152-C165, 2018.
30. Lee E, Shin S, Chun J, Hyun S, Kim Y, Kang S. The modulation of TRPV4 channel activity through its Ser 824 residue phosphorylation by SGK1. *Animal Cells and Systems* 14: 99-114, 2010.
31. Livak K, Schmittgen T. Analysis of Relative Gene Expression Data Using Real-Time Quantitative PCR and the $2^{-\Delta\Delta CT}$ Method. *Methods* 25: 402-408, 2001.
32. Lu K, Huang T, Tsai Y, Yang Y. Transient receptor potential vanilloid type 4 channels mediate Na-K-Cl-co-transporter-induced brain edema after traumatic brain injury. *Journal of Neurochemistry* 140: 718-727, 2017.
33. Lun M, Monuki E, Lehtinen M. Development and functions of the choroid plexus–cerebrospinal fluid system. *Nature Reviews Neuroscience* 16: 445-457, 2015.
34. MacAulay N, Hamann S, Zeuthen T. Water transport in the brain: Role of cotransporters. *Neuroscience* 129: 1029-1042, 2004.
35. Mercier-Zuber A, O'Shaughnessy K. Role of SPAK and OSR1 signalling in the regulation of NaCl cotransporters. *Current Opinion in Nephrology and Hypertension* 20: 534-540, 2011.
36. Narita K, Sasamoto S, Koizumi S, Okazaki S, Nakamura H, Inoue T, Takeda S. TRPV4 regulates the integrity of the blood-cerebrospinal fluid barrier and modulates transepithelial protein transport. *The FASEB Journal* 29: 2247-2259, 2015.

37. Park S, Ku S, Ji H, Choi J, Shin D. Ca^{2+} is a Regulator of the WNK/OSR1/NKCC Pathway in a Human Salivary Gland Cell Line. *The Korean Journal of Physiology & Pharmacology* 19: 249, 2015.
38. Piechotta K, Lu J, Delpire E. Cation Chloride Cotransporters Interact with the Stress-related Kinases Ste20-related Proline-Alanine-rich Kinase (SPAK) and Oxidative Stress Response 1 (OSR1). *Journal of Biological Chemistry* 277: 50812-50819, 2002.
39. Praetorius J, Nielsen S. Distribution of sodium transporters and aquaporin-1 in the human choroid plexus. *American Journal of Physiology-Cell Physiology* 291: C59-C67, 2006.
40. Praetorius J, Damkier H. Transport across the choroid plexus epithelium. *American Journal of Physiology-Cell Physiology* 312: C673-C686, 2017.
41. Preston D, Simpson S, Halm D, Hochstetler A, Schwerk C, Schroten H, Blazer-Yost B. Activation of TRPV4 stimulates transepithelial ion flux in a porcine choroid plexus cell line. *American Journal of Physiology-Cell Physiology* 315: C357-C366, 2018.
42. Reiter B, Kraft R, Günzel D, Zeissig S, Schulzke J, Fromm M, Harteneck C. TRPV4-mediated regulation of epithelial permeability. *The FASEB Journal* 20: 1802-1812, 2006.
43. Richardson C, Alessi D. The regulation of salt transport and blood pressure by the WNK-SPAK/OSR1 signalling pathway. *Journal of Cell Science* 121: 3293-3304, 2008.
44. Schroten H, Hanisch F, Quednau N, Stump C, Riebe R, Lenk M, Wolburg H, Tenenbaum T, Schwerk C. A Novel Porcine In Vitro Model of the Blood-Cerebrospinal Fluid Barrier with Strong Barrier Function. *PLoS ONE* 7: e39835, 2012.
45. Simpson S, Preston D, Schwerk C, Schroten H, Blazer-Yost B. Cytokine and inflammatory mediator effects on TRPV4 function in choroid plexus epithelial cells. *American Journal of Physiology-Cell Physiology* (2019). doi: 10.1152/ajpcell.00205.2019 *IN PRESS*.
46. Speake T, Whitwell C, Kajita H, Majid A, Brown P. Mechanisms of CSF secretion by the choroid plexus. *Microscopy Research and Technique* 52: 49-59, 2000.
47. Steffensen A, Oernbo E, Stoica A, Gerkau N, Barbuskaite D, Tritsaris K, Rose C, MacAulay N. Cotransporter-mediated water transport underlying cerebrospinal fluid formation. *Nature Communications* 9, 2018.
48. Toft-Bertelsen T, Larsen B, MacAulay N. Sensing and regulation of cell volume – we know so much and yet understand so little: TRPV4 as a sensor of volume changes but possibly without a volume-regulatory role?. *Channels* 12: 100-108, 2018.

49. White J, Cibelli M, Urban L, Nilius B, McGeown J, Nagy I. TRPV4: Molecular Conductor of a Diverse Orchestra. *Physiological Reviews* 96: 911-973, 2016.
50. Yan Y, Dalmasso G, Thi Thu Nguyen H, Obertone T, Sitaraman S, Merlin D. Ste20-Related Proline/Alanine-Rich Kinase (SPAK) Regulated Transcriptionally by Hyperosmolarity Is Involved in Intestinal Barrier Function. *PLoS ONE* 4: e5049, 2009.

CHAPTER 4. CHLORIDE CHANNELS IN CPE TRANSEPITHELIAL TRANSPORT

4.1 Introduction

Transcellular transport of ions forms the basis of CSF production, and several chloride channels have been described for their roles in Cl^- movement across the choroid plexus (CP) epithelium (1-5,8-13,20,22,25,27,33,34,36,39). Perhaps the best described transporter of Cl^- in the CP is the Na-K-2Cl cotransporter (NKCC). First described in the kidney, and encoded by the SLC12A genes, NKCC couples the movement of sodium and potassium to the movement of 2 chloride ions, in unidirectional fashion (4,5,10-13,17,22,36). In the CP, NKCC1 (SLC12A2) has been shown to be reversible, such that the direction of movement can be either net influx, or net efflux, depending on the intracellular [Cl^-] (12,16). In addition to NKCC, the potassium chloride cotransporters (KCC1-4) have also been shown to transport Cl^- in the CP (4,5,10,11,21). The KCCs have been described on both the apical and basolateral membranes of the CP, and operate in the net efflux direction, driving Cl^- and potassium out of the cell to either the blood or luminal surfaces. The roles of NKCC and the KCCs in transepithelial transport are described more fully in chapter 3.

Anion exchange protein 2 (AE2, SLC4A2) and the sodium-driven chloride bicarbonate exchanger (NCBE, NBCn2, SLC4A10) are both chloride-bicarbonate exchangers in the CP, and both have been described exclusively on the basolateral membrane of the epithelium (2-5,8,10,11,19,25,33,34,36,37). AE2 is thought to be the primary basolateral loader of Cl^- in to the CP, which is then passed through the apical membrane by Cl^- extruders (2,4,5). In other tissues such as renal tubules and epithelia of the gastrointestinal tract, AE2 is similarly expressed on the basolateral surface and plays a key role in basal loading of Cl^- ions in to transporting epithelia (2,11). AE2 operates at the basal surface by exchanging extracellular Cl^- for intracellular HCO_3^- (2,10,11). In contrast to AE2, NCBE is the primary basal loader of HCO_3^- in the CP (3,10,11). NCBE works in an opposite manner to AE2, extruding Cl^- in exchange for extracellular HCO_3^- and Na^+. These channels are important for two distinct cellular processes. AE2, as previously mentioned, loads Cl^- in the extracellular space, to be secreted at the apical surface into the intraventricular space. NCBE operates primarily in maintenance of intracellular pH, by increasing intracellular HCO_3^- and acidifying the cytoplasm (11). NCBE also contributes to epithelial

transport of ions, albeit in a manner opposite to AE2, allowing for transepithelial transport of HCO_3^- to be extruded on the apical surface by the sodium bicarbonate cotransporter (NBCe2, SLC4A5), an electroneutral transporter of HCO_3^- and Na^+ (7,11,34). Interestingly, both AE2 and NCBE have been described as being DIDS sensitive, an important consideration for their apparently opposite roles in Cl^-/HCO_3^- exchange (1,3).

Several channels exist on the apical surface of CP cells which are capable of extruding Cl^- loaded by AE2 on the basolateral surface. Previously, a channel known as the voltage regulated anion channel (VRAC) was shown to be a minor contributor to Cl^- movement across the apical surface (11). Recently, VRAC was identified as the leucine-rich repeat-containing protein 8 (LRRC8) (13,15,26,38,40,42). VRAC is a key player in the maintenance of cell volume regulation and responds to intracellular swelling by driving water and K^+ efflux to reduce intracellular volumes (13,15,38). VRAC appears to be ubiquitously expressed in mammalian cells, contributing to regulatory volume decrease (RVD) across all cell types (10,13).

CFTR has been identified as the primary protein dysregulated in cystic fibrosis. More than 2000 mutations have been described in the CFTR gene, more than 200 of which results in a cystic fibrosis phenotype, with a deletion at phenylalanine 508, ΔF508 being the most common contributor to cystic fibrosis (6). Localized to the apical surface in all cell types in which it is expressed, CFTR is regulated by cyclic AMP (cAMP)-dependent protein kinase A (PKA) phosphorylation (6,18,23). Conflicting reports question the presence of CFTR in the CP, and some controversy exists regarding its expression. In 1995, Hincke et al showed by western blot and immunolocalization studies that CFTR was found in rat CP (18). However, in 1996 and 1997, several studies demonstrated that CFTR mRNA was not present in rat CP by RT-PCR and *in-situ* hybridization studies (10,23,24). Current opinions are that CFTR is likely not expressed in most mammalian CP and is not likely involved in transepithelial transport of Cl^- (10,23).

Ca^{2+}-activated Cl^- channels (CaCC's) are channels which respond to increases in intracellular $[Ca^{2+}]$ by extruding Cl^- (6,31,32,39,41). CaCC's are comprised primarily of the anoctamin family of channels, which includes the transmembrane member 16 (TMEM16A-K) genes (6,18,32). TMEM16A is a Ca^{2+}-activated Cl^- channel that was initially identified in 2008 (41). TMEM16A

is thought to be localized to the apical membrane and acts as a Cl^- extruder (39). In airway and intestinal epithelium, TMEM16A is thought to contribute a minor part to Cl^- conductance (28). In mandibular acinar cells, TMEM16A was immunolocalized to the apical membrane, demonstrating that CaCC's exist on the apical surface as Cl^- extruders (31). Largely ignored in the CP, one study demonstrated that TMEM16A was natively expressed in the CP of mice and contributed to Cl^- efflux from the epithelium (38).

The role of TRPV4 in Cl^- transport has not been well studied. As a non-selective Ca^{2+} permeable cation channel, TRPV4 is capable of increasing intracellular [Ca^{2+}] (27,29,35). This increase in [Ca^{2+}] may activate CaCC's, and stimulate the transport of Cl^- in the CP. Additionally, TRPV4 has been shown to be regulated by WNK4 activity, which responds to increases in intracellular [Cl^-] (14). This suggests that TRPV4 may be involved in evoking and integrating various molecular signals responsible for efflux of Cl^- in the CP (39). Here we describe the interaction between TRPV4 and TMEM16A, responsible for mediating transepithelial ion flux at the CP. These interactions appear not to be mediated by activity of basal Cl^- loaders AE2 and NCBE, CFTR, or VRAC.

4.2 **Methods and Materials**

Cell Culture: PCP-R cells were seeded on 6-well cluster plates containing 0.4 µM filter diameter polycarbonate permeable bottom supports (Corning Life Sciences, Lowell, MA; #3412) for approximately 10-12 days, until cell cultures achieved a transepithelial resistance (TER) >500 Ωcm^2. Cultures below 500 Ωcm^2 were not considered high resistance and were not used for experiments. Additionally, cultures whose TERs dropped below 100 Ωcm^2 during the time course of the experiments were also not used, due to irreversible changes in the tight junctions. PCP-R cell cultures were grown using DMEM (Gibco, Gaithersburg, MD; #12100-046), with 4.5 g/L glucose, 3.7 g/L $NaHCO_3$, 24 mM HEPES, 10% fetal bovine serum (Atlanta Biologicals, Flowery Branch, GA), 100 U/ml penicillin, 100 mg/ml streptomycin, and 5 µg/ml insulin. Cells were bathed in 2 ml of the PCP-R media apically (filter top) and 3 ml basolaterally (filter bottom). PCP-R media was replaced 3 times weekly.

Electrophysiology: For electrophysiological analysis, PCP-R cells were grown on transwell plates until confluent (10-12 days), excised and subsequently mounted in Ussing chambers connected to a DVC-1000 Voltage/Current clamp (World Precision Instruments, Sarasota, FL) with voltage and current electrodes attached on either side of the membrane. Each side of the chamber was bathed in 10 ml of serum free media at 37°C. Media-containing chambers were water jacketed to maintain a constant physiological temperature of 37°C. A 5% CO_2/95% O_2 gas lift circulated media through chambers and oxygenated the chamber-mounted cells. The spontaneous transepithelial potential difference was clamped to zero, and cells were allowed to equilibrate for at least 20 minutes. Experimental compounds were added to the apical and/or basal media, and the resulting short circuit current (SCC) was recorded as a measurement of net transepithelial ion movement. By convention, a positive deflection of the SCC represents either anion secretion (blood to CSF directed movement) or cation absorption (CSF to blood), while the opposite is true for a negative deflection. Additionally, a 2 mV pulse was applied every 180 seconds, and the resulting change in SCC was recorded. This change in SCC was used to calculate transepithelial resistance (TER) using Ohm's Law, and the resulting TER values were converted to transepithelial conductance by calculating the inverse of the TER. The transepithelial conductance is an indication of net ion movement and barrier permeability in cells. A low conductance (<2 mS/cm^2) represents low net ion movement and a tight barrier. Any increase in the transepithelial conductance is observed to be an increase in the transepithelial ion movement and/or increased cellular permeability. For all electrophysiological experiments, both the control and experimental groups were analyzed simultaneously, as represented in the graphs.

Reverse Transcriptase (RT)-PCR: PCP-R cells were grown to confluence on transwells. Cell monolayers were washed twice with cold 1X PBS, and total cell RNA was isolated utilizing the Monarch Total RNA Miniprep Kit (New England Biolabs, #T2010S) according to the manufacturer's directions for cultured mammalian cells. RNA concentration was measured using an ND2000 Nanodrop (Fisher Scientific, Waltham, MA). Approximately 100 ng of total RNA was reverse transcribed into cDNA using the Monarch LunaScript RT SuperMix Kit (New England Biolabs; #E3010L), along with corresponding No-template and -RT controls, according to the manufacturer's directions. *Sus Scrofa e*xon mRNA sequences for each gene were obtained using Ensembl, and primer pairs for each were designed using Primer3Plus. Approximately 500 ng of

template cDNA was combined with the forward and reverse primers (IDT, Coralville, IA), as well as GoTaq Green Master Mix (Promega Corporation, Madison, WI; #M7122). Reactions were run as a gradient to determine optimum annealing temperature for each primer pair, and products were separated on a 1.5% agarose gel with ethidium bromide. Flanking 100 bp ladders were used as molecular weight markers, and gels were imaged using a ChemiDoc XRS imager (Bio-Rad, Hercules, CA). Single band amplicons of the predicted molecular weight were sequenced (Eton Biosciences, Union, NJ) and the correct products were validated using NCBI and Ensembl BLAST.

Statistics: Statistics were calculated using Two-tailed Students t-test in Sigma Plot 13. $p < 0.05$ is considered significant. Student's t-test was used to compare experimental groups to the control as indicated by the symbols defined in the figure legends.

4.3 **Results**

We used three sets of redundant primer pairs for each gene of interest to determine its presence in the PCP-R cells and sequenced the resulting single band amplicons to confirm correct gene amplification (Table 1). mRNA encoding for TMEM16A and CFTR, both Ca^{2+}-activated Cl^- channels was identified (Figure 1). The presence of CFTR mRNA is somewhat surprising, given the body of literature suggesting CFTR is absent in other mammalian cells.

We used Ussing chamber electrophysiology to record net electrogenic changes in transepithelial ion flux and barrier permeability. By convention, a negative change in SCC is representative of net transepithelial ion transport consistent with anion absorption (CSF to blood) or cation secretion (blood to CSF). An increase in conductance is consistent with an increase in barrier permeability of the cells. For each figure, experiments were conducted with paired controls which utilize an agonist of either TMEM16A or TRPV4. In each experiment, the control agonist was added at time T = 0. In experimental cultures, cells were pretreated with specific inhibitors, modulators or agonists 10 minutes prior to or following the addition of the control agonist.

Pre-treatment of PCP-R cell cultures with 10 µM T16Ainh-A01, a specific inhibitor of TMEM16A on both the apical and basolateral membranes 10 minutes prior to the addition of the TMEM16A

agonist 1.5 μM EACT resulted in a statistically significant inhibition of TMEM16A-mediated ion flux and conductance changes (Figure 2). This stimulator/inhibitor pairing substantiates the specificity of the response for TMEM16A.

To investigate whether TMEM16A plays a role in TRPV4-mediated ion flux, PCP-R cells were pretreated with 10 μM T16Ainh-A01 on both the apical and basolateral membranes 10 minutes prior to addition of the TRPV4 agonist GSK1016790A (3 nM) on the basolateral membrane. Pretreatment with T16Ainh-A01 resulted in inhibition of TRPV4-stimulated ion flux, as well as an inhibition of the TRPV4-stimulated conductance chances (Figure 3). To determine if this effect was restricted to one side of the membrane, cultures were treated on either the apical or basolateral sides with 10 μM T16Ainh-A01 prior to the addition of 3 nM GSK1016790A. Inhibition of TMEM16A on the apical surface resulted in greater inhibition of the TRPV4-mediated SCC responses than did inhibition of TMEM16A on the basal surface. However, both were found to result in statistically significant inhibition of the TRPV4 response. Interestingly, pretreatment on either membrane resulted in complete inhibition of the conductance increases observed upon TRPV4 activation (Figure 4).

To determine if the TRPV4-induced SCC and conductance changes could be reversed, we first treated cells with 3 nM GSK1016790A for 10 minutes followed by treatment with 10 μM T16Ainh-A01. Inhibition of TMEM16A following activation of TRPV4 resulted in a reversal of the TRPV4-induced SCC changes, while the increase in conductance was only shown to plateau rather than reverse (Figure 5).

Next we attempted to determine if TRPV4 and TMEM16A were co-dependent for activation. Previously we had determined that inhibition of TMEM16A was capable of inhibiting the TRPV4 response (Figures 3,4,5). To determine the reciprocal nature, we pretreated cells with 50 μM RN1734, a specific TRPV4 inhibitor, prior to addition of the TMEM16A agonist EACT (1.5 μM). Similar to inhibition of the TRPV4 response via inhibition of TMEM16A, we observed that the TMEM16A-induced SCC and conductance changes were blocked by inhibiting TRPV4 (Figure 6).

To further elucidate the complex interactions between TMEM16A and TRPV4, we pretreated cells with low dose (300 pM) GSK1016790A, followed by low dose EACT (1.5 μM). Independently, GSK1016790A and EACT were not capable of stimulating SCC or conductance changes. However, when cells initially treated with GSK were followed with low dose EACT, a small decrease in SCC was observed, with no changes in conductance being noted (Figure 7). To determine whether TMEM16A played a role in the multiphasic SCC response induced by TRPV4 activation, we initially treated PCP-R cells with 1.5 μM EACT. These cells were then treated with 300 pM GSK1016790A. Interestingly, following activation of TMEM16A, a monophasic SCC response was observed upon activation of TRPV4. It was also observed that upon addition of GSK1016790A, only a moderate increase in conductance was observed (Figure 8).

We next investigated whether other apical Cl^- channels played a role in the TRPV4 pathway. To determine the role of CFTR, cells were pretreated with the specific inhibitor CFTRinh172 (50 μM) both apically and basolaterally, followed by 3 nM GSK1016790A. No significant effects on SCC or conductance were observed in response to CFTR inhibition (Figure 9). Similarly, apical and basal pretreatment with a VRAC inhibitor, DCPIB (1 μM) resulted in no significant effects on the TRPV4-stimulated responses.

Finally, to determine the role of basolateral Cl^-/HCO_3^- exchangers in the TRPV4 mechanism, cells were pretreated with 10 μM DIDS, an inhibitor of both AE2 and NCBE prior to addition of 3 nM GSK1016790A. No effects on the TRPV4-mediated SCC and conductance changes were observed when pretreated with DIDS relative to the GSK controls (Figure 10).

4.4 **Discussion**

Chloride is thought to be the major anion regulated for cell volume regulation and homeostasis in most mammalian cell types (10,11,33). To accomplish this, several well described Cl^- channels and transporters maintain exquisite control over intracellular [Cl^-], adjusting intracellular concentrations to match physiological needs (4,5,10,11,27,33). In the choroid plexus, CSF is produced by transepithelial movement of ions and other small molecules from the serum to the intraventricular space which drives movement of water (11,33). Paramount to this is the movement

of Cl^-, which is introduced to the cytoplasm primarily by basal Cl^-/HCO_3^- exchangers such as AE2 (1,2,10). From there, Cl^- is extruded from the cell via apically bound transporters (4,5,10). A gradient of [Cl^-] exists across the CP, with plasma [Cl^-] reported at approximately 106 mM, and CSF [Cl^-] at 130 mM, requiring specific transporters to move Cl^- against a transepithelial chemical gradient (10).

Previous reports have described the roles of NKCC1 and KCC4 in apical Cl^- transport out of CP cells (4,5,10,11). In addition to transepithelial movement, several channels and transporters exist with the primary role of maintaining intracellular pH and homeostasis by way of exchanging extracellular HCO_3^- in the blood for cytoplasmic Cl^-, thus acidifying the cytoplasm. In the CP, NCBE appears to be the primary basolateral transporter responsible for this exchange (11). On the apical surface, NKCC1 also plays a role in cell homeostasis (11,12,16). This transporter appears to be reversible, such that the direction of flow can operate in net influx to transport Cl^-, Na^+ and K^+ back into the cell, depending primarily on the intracellular [Cl^-]. KCC3 and KCC4 are K^+/Cl^- cotransporters located on the basal and apical surfaces, respectively (4,5,10,20). These transporters appear to primarily be responsible for extrusion of Cl^- on either surface in maintenance of the [Cl^-] gradient across the CP (4,5,10).

A body of literature exists describing the role of NKCC1 in CP-dependent CSF production and transepithelial transport (4,5,10,12,16). In chapter 3, we describe the role of NKCC1 in the PCP-R cells and demonstrated that NKCC1 appears to play a minor role in TRPV4-mediated electrogenic ion flux across the CP. However, other Cl^- channels responsible for secretion have not been well described in the CP, nor their roles in CSF production elucidated. TMEM16A, a Ca^{2+}-activated Cl^- channel is one such protein. Increases in intracellular Ca^{2+} stimulate the excitation of TMEM16A, causing secretion of Cl^- in to the lumen (32). Activation of TRPV4 results in increases in intracellular Ca^{2+} and may be capable of activating TMEM16A.

To characterize the Cl^- channels and transporters in the CP, we first performed RT-PCR identifying mRNAs encoding for TMEM16A and CFTR. CFTR, a key Cl^- extruder in other epithelia such as lung and kidney, appears not to be present in the CP according to several reports (10,23,24). (10,23,24). The expression of CFTR in the PCP-R cells is therefore a somewhat curious finding.

In chapter 3, we identified the mRNAs encoding for NKCC1, as well as KCC3 and KCC4, both of which have been previously described in the CP. These results are consistent with previous reports showing expression of a variety of Cl^- channels, transporters and exchangers in the CP (4,5,10).

The role of CaCC's in CSF production remains elusive. In airway and intestinal epithelia, TMEM16A was shown to contribute to CaCC-dependent currents (28). Interestingly, in the same study TMEM16A was also shown in salivary gland epithelia to be responsible for nearly all of the CaCC-dependent current. Conversely, little is known about TMEM16A and its expression in the CP or any role it may play in CSF production. 1.5 μM EACT, an activator of TMEM16A evoked an initial decrease in SCC consistent with either anion absorption or cation secretion, followed by an increase in SCC, indicative of the reverse. This change in SCC was mitigated by pretreatment with 10 μM T16AinhA01, a TMEM16A-specific inhibitor.

Previously, it has been demonstrated that TRPV4 activation with GSK1016790A (3 nM) results in a multiphasic transepithelial ion flux response along with an acute increase in conductance (35). Pretreatment with the TMEM16A inhibitor substantially blocked this TRPV4-mediated SCC and conductance change, suggesting a functional interaction between the two channels. Addition of the TMEM16A inhibitor to either the apical or serosal media resulted in significant inhibition of the resulting SCC changes elicited by TRPV4 activation, although this effect was more pronounced on the apical surface. Interestingly, addition of the inhibitor to either side had the same inhibitory effect on the conductance changes, substantially blocking any TRPV4-mediated increases in SCC. Somewhat unexpectedly, the conductance increase observed upon activation of TMEM16A is smaller than the conductance changes observed upon activation of TRPV4, suggesting that TRPV4 plays a larger role in maintenance of cell permeability.

In chapter 2, we showed that the TRPV4-mediated SCC and conductance changes could be reversed and returned to baseline upon addition of the TRPV4 inhibitor RN1734. Addition of the TMEM16A inhibitor to TRPV4 agonist treated cultures had a similar effect on the SCC changes; upon addition of the TMEM16A inhibitor, the initial SCC decrease acutely returned to baseline. However, unlike the previous studies, the TMEM16A inhibitor was not able to reverse the

conductance increase, instead resulting in plateauing of the conductance. To further explore the relationship, cells were pretreated with the TRPV4 inhibitor RN1734 (50 μM), followed by the TMEM16A activator EACT (1.5 μM). Here, inhibition of TRPV4 was able to completely block both the SCC and conductance changes caused by TMEM16A activation. These data suggest a complicated interaction between TMEM16A and TRPV4 by which the channels are reciprocally dependent upon each other for activation; inhibition of either blocks channel activation of the other.

In the PCP-R cells, TRPV4-mediated changes in the SCC are not observable when treated with GSK1016790A below 1 μM (35). Therefore, to further interrogate the complex interactions between TMEM16A and TRPV4, cells were treated initially with the TRPV4 agonist at a sub micromolar concentration (300 pM), followed by a concentration of the TMEM16A agonist (150 nM) which also does not elicit a SCC response. The combined effect of low-dose stimulation of both TRPV4 and TMEM16A resulted in a small but measurable decrease in SCC, while resulting in no net conductance changes. When stimulated with 1.5 μM EACT, followed by 300 pM GSK1016790A, a complex SCC response was observed. An initial acute decrease in SCC, followed by a return to baseline was observed, typical of TMEM16A activation. However, upon addition of GSK1016790A at 300 pM, a biphasic SCC response was observed, instead of the typical multiphasic SCC response observed upon activation of TRPV4 with 3 nM GSK1016790A. These data together further suggest a complex interaction between TMEM16A and TRPV4 in which each channel responds to the other's activation.

While mRNA encoding CFTR was identified in the PCP-R cells, it is not believed to play a role in transepithelial flux of ions in the CP. When pretreated with CFTRinh172, no inhibition of GSK1016790A-induced electrogenic ion flux or conductance was observed. These data therefore suggest that CFTR is not responsible for anion currents in the CP.

The voltage regulated anion channel VRAC thought to be a significant contributor to Cl^- currents in the CP was recently identified as LRRC8 (13,15,25,38,40). This channel is thought to play a role in cell volume regulation, primarily through regulatory volume decrease (13,15,26,38,40,42). To investigate whether VRAC contributes to TRPV4-stimulated electrogenic ion flux, cells were pretreated with 1 μM DCPIB, a specific inhibitor of VRAC. Inhibition of VRAC did not alter the

TRPV4-induced changes in SCC or conductance, suggesting that VRAC is not involved in TRPV4-mediated ion flux.

Transepithelial ion flux is dependent on activity of channels on both the apical and basolateral surfaces of the CP (9,10,32,34). On the basolateral membrane, the DIDS-sensitive Cl^-/HCO_3^- exchanger AE2 is believed to be the primary loader of Cl^- in to the cytoplasm from the serum, secreting HCO_3^- in to the plasma in exchange for extracellular Cl^- (2,4,5,25,33,37). Operating in reverse to AE2, NCBE is a DIDS-sensitive Cl^-/HCO_3^- exchanger that has the added benefit of absorbing plasma Na^+ into the cell along with HCO_3^- (3,10). To determine whether either of these exchangers are involved in TRPV4-mediated ion flux at the basolateral surface, cells were treated with 10 μM DIDS, followed by 3 nM GSK1016790A. No effect on either the SCC or the transepithelial conductance was observed, suggesting that AE2 and NCBE are not likely involved in the TRPV4 pathway of ion flux.

In summary, we have demonstrated that TMEM16A activation is dependent on TRPV4 activity. In addition, TRPV4 activation is also dependent on TMEM16A activity, suggesting a reciprocal interaction. Stimulation of either channel was blocked by inhibition of the other, and it was shown that TRPV4-induced currents were reversible upon inhibition of TMEM16A. Our studies further demonstrated that while many canonical CP Cl^- transporters are present in the PCP-R cell line, only TMEM16A appears to be significantly involved in the TRPV4 pathway of transepithelial ion flux. CFTR appears not to play a significant role in TRPV4-evoked electrogenic ion flux, nor does VRAC. Additionally, we demonstrated that inhibition of basal Cl^- transport did not have a significant effect on TRPV4-mediated transport. These data suggest a complex interaction between TMEM16A and TRPV4 which deserves further investigation. If in fact TRPV4 acts a hub protein to integrate complex molecular signals to stimulate CSF production, TMEM16A may be an intriguing point of regulation worthy of additional studies.

Table 4.1 *Sus Scrofa* Primers Used for RT-PCR with Corresponding Product Sizes (bp).

Three different primer sets were generated and tested for each gene. Primers included in this table were utilized for Figure 1. GAPDH was used as a positive control.

Sus Scrofa gene	Protein	Primer Sequences 5' - 3'		Product Size (bp)
		Forward Primer	Reverse Primer	
Ano1	TMEM16A	CTCACCAAGATCGAGGTTCCAA	GGGGTGTAGGAATTCACGAACT	95
CFTR	CFTR	AAAGCATTCACCGAAAGACAGC	GGTTGACATAGGGGCTTGAAGA	548
Gapdh	GAPDH	TTTTAACTCTGGCAAAGTGGAC	CATTGTCGTACCAGGAAATGAG	884

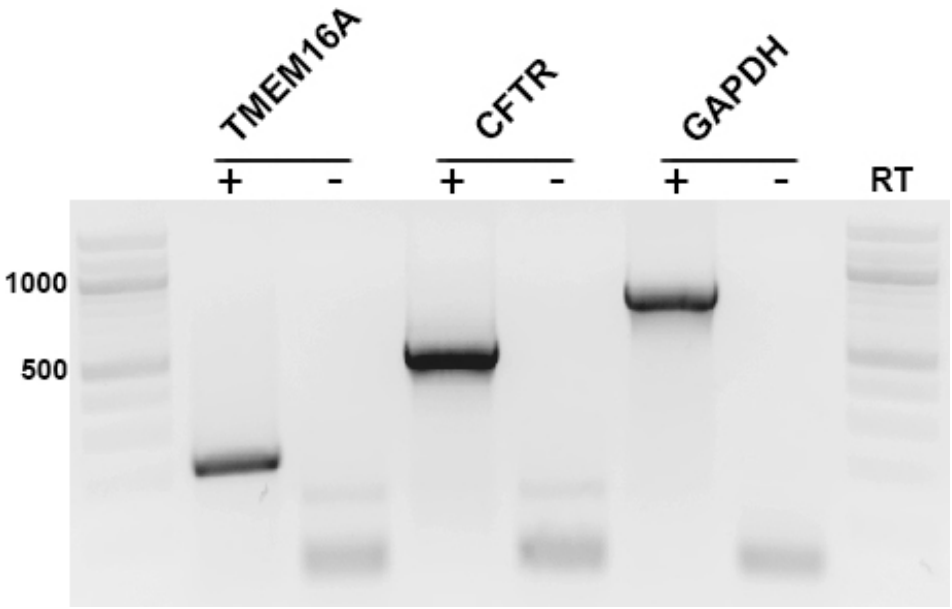

Figure 4.1 RT-PCR in the PCP-R Cell Line.

mRNA for TRPV4, TMEM16A, and CFTR are present in the PCP-R cell line. GAPDH was used as a positive control. 100 bp flanking ladders were used. RT = Reverse transcriptase. Lanes denoted as (+) or (-) RT identify the presence or absence of reverse transcriptase in the PCR mixture.

Figure 4.2: Pre-treatment of PCP-R cells with a TMEM16A inhibitor prior to addition of a TMEM16A agonist. Net changes in transepithelial ion flux and conductance were measured. T16Ainh-A01 (10 μM) was added to both the apical and basolateral surfaces at T = -10 minutes. The TMEM16A agonist EACT (1.5 μM) was added to both the apical and basolateral sides of the membrane in all cultures at T = 0 minutes. Pre-incubation with T16Ainh-A01 is represented by white open circles. The EACT-treated positive controls are denoted by black filled circles. Circles represent mean values, and error bars represent +/- SEM for the *n* indicated. SCC = short circuit current. * = $p < 0.05$ against control experiments.

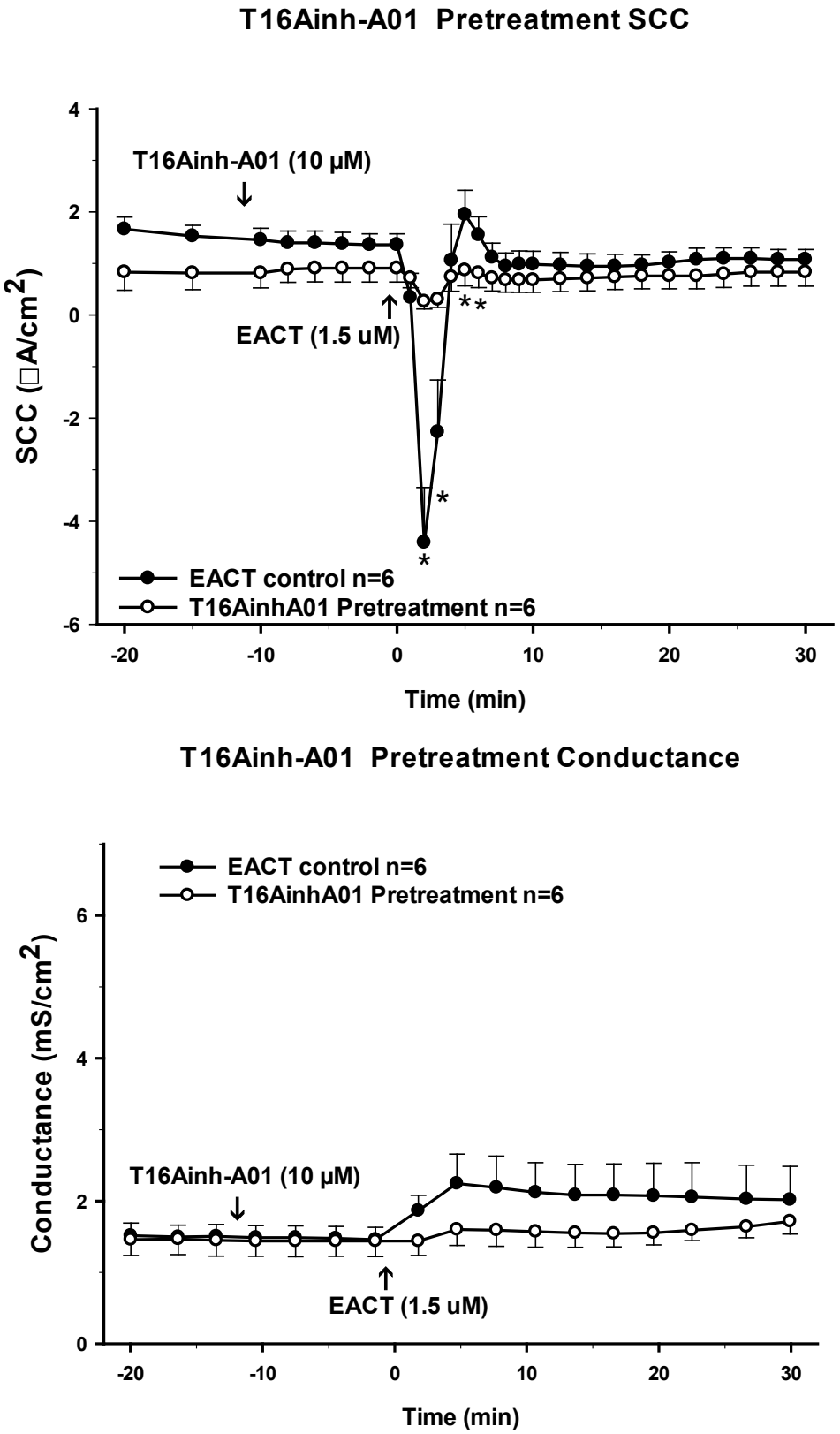

Figure 4.2 Effect of TMEM16A Inhibitor on TMEM16A-Mediated Responses.

Figure 4.3: Pre-treatment of PCP-R cells with a TMEM16A inhibitor prior to addition of a TRPV4 agonist. Net changes in transepithelial ion flux and conductance were measured. T16Ainh-A01 (10 μM) was added to both the apical and basolateral surfaces at T = -10 minutes. The TRPV4 agonist GSK1016790A (3 nM) was added to both the apical and basolateral sides of the membrane in all cultures at T = 0 minutes. Pre-incubation with T16Ainh-A01 is represented by white open circles. GSK-treated positive controls are denoted by black filled circles. Circles represent mean values, and error bars represent +/- SEM for the *n* indicated. SCC = short circuit current. * = $p < 0.05$ against control experiments.

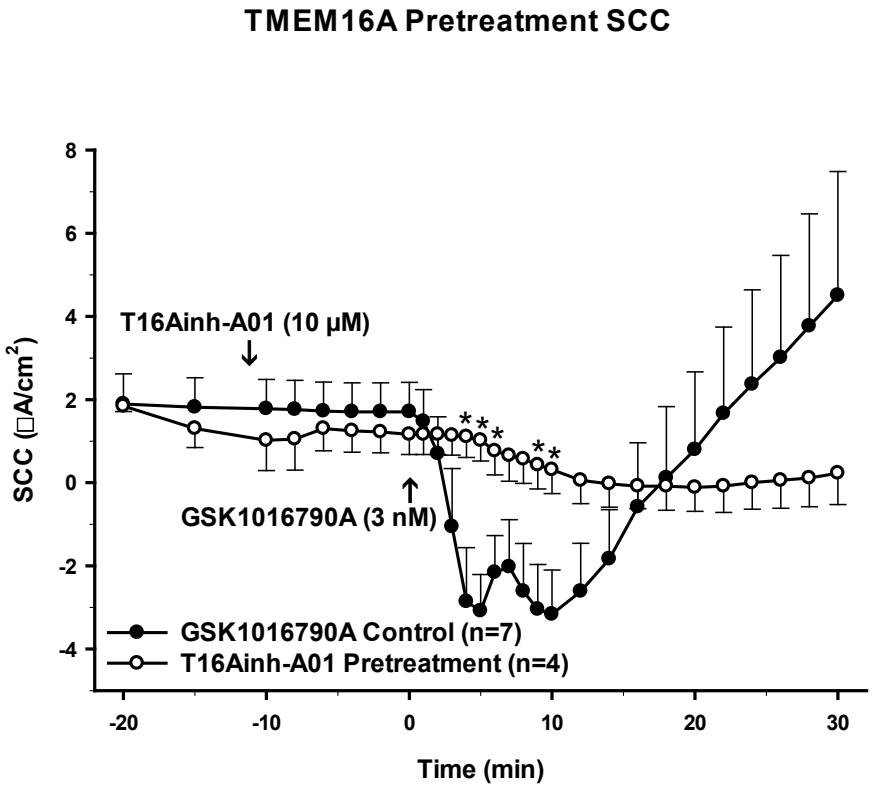

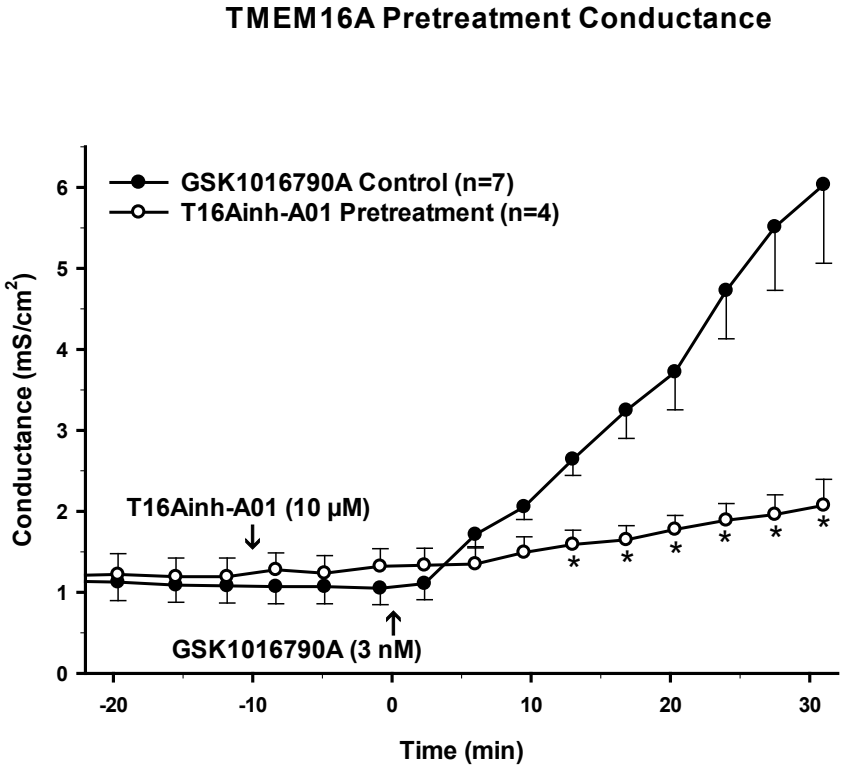

Figure 4.3 Effect of TMEM16A Inhibitor on TRPV4-Mediated Responses.

Figure 4.4: Sidedness of a TMEM16A inhibitor prior to addition of a TRPV4 agonist. Net changes in transepithelial ion flux and conductance were measured. T16AinhA01 (10 μM) was added either apically or basolaterally at T = -10 minutes. The TRPV4 agonist GSK1016790A (3 nM) was added to the basolateral side of the membrane in all cultures at T = 0 minutes. Pre-incubation with T16Ainh-A01 either apically, or basolaterally is represented by white open circles or grey filled triangles, respectively. The GSK-treated positive controls are denoted by black filled circles. Circles represent mean values, and error bars represent +/- SEM for the *n* indicated. SCC = short circuit current. * = $p < 0.05$ against control experiments.

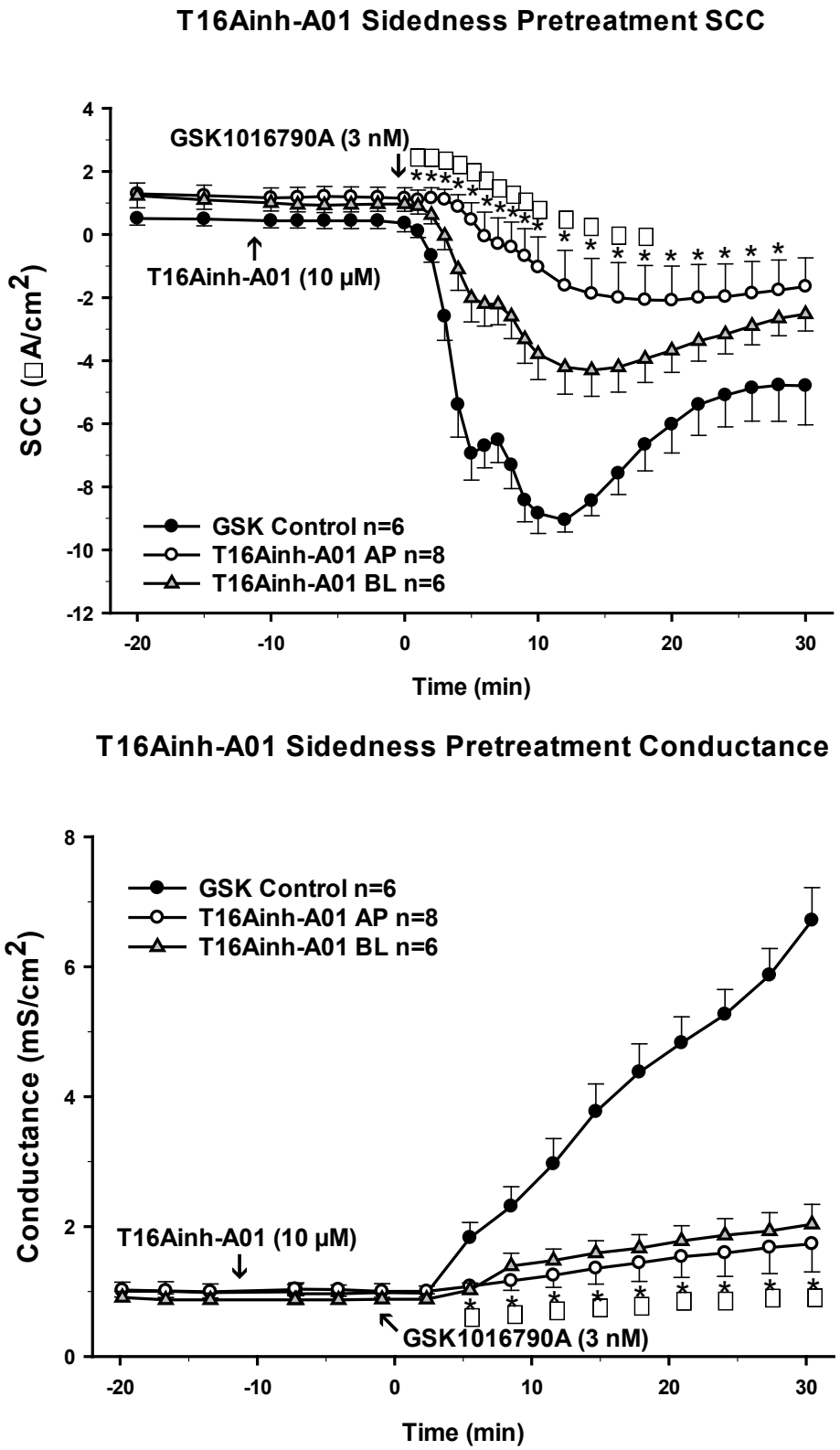

Figure 4.4 Sidedness of TMEM16A Inhibitor on TRPV4-Mediated Responses.

Figure 4.5: Reversibility of a TRPV4 agonist response by a TMEM16A antagonist. Net changes in transepithelial ion flux and conductance were measured. The TRPV4 agonist GSK1016790A (3 nM) was added to the basolateral surface of all cultures at T = 0 minutes. T16Ainh-A01 (10 μM) was added both apically and basolaterally at T = 10 minutes. Post-treatment with T16Ainh-A01 is represented by white open circles. The GSK-treated positive controls are denoted by black filled circles. Circles represent mean values, and error bars represent +/- SEM for the *n* indicated. SCC = short circuit current. * = $p < 0.05$ against control experiments.

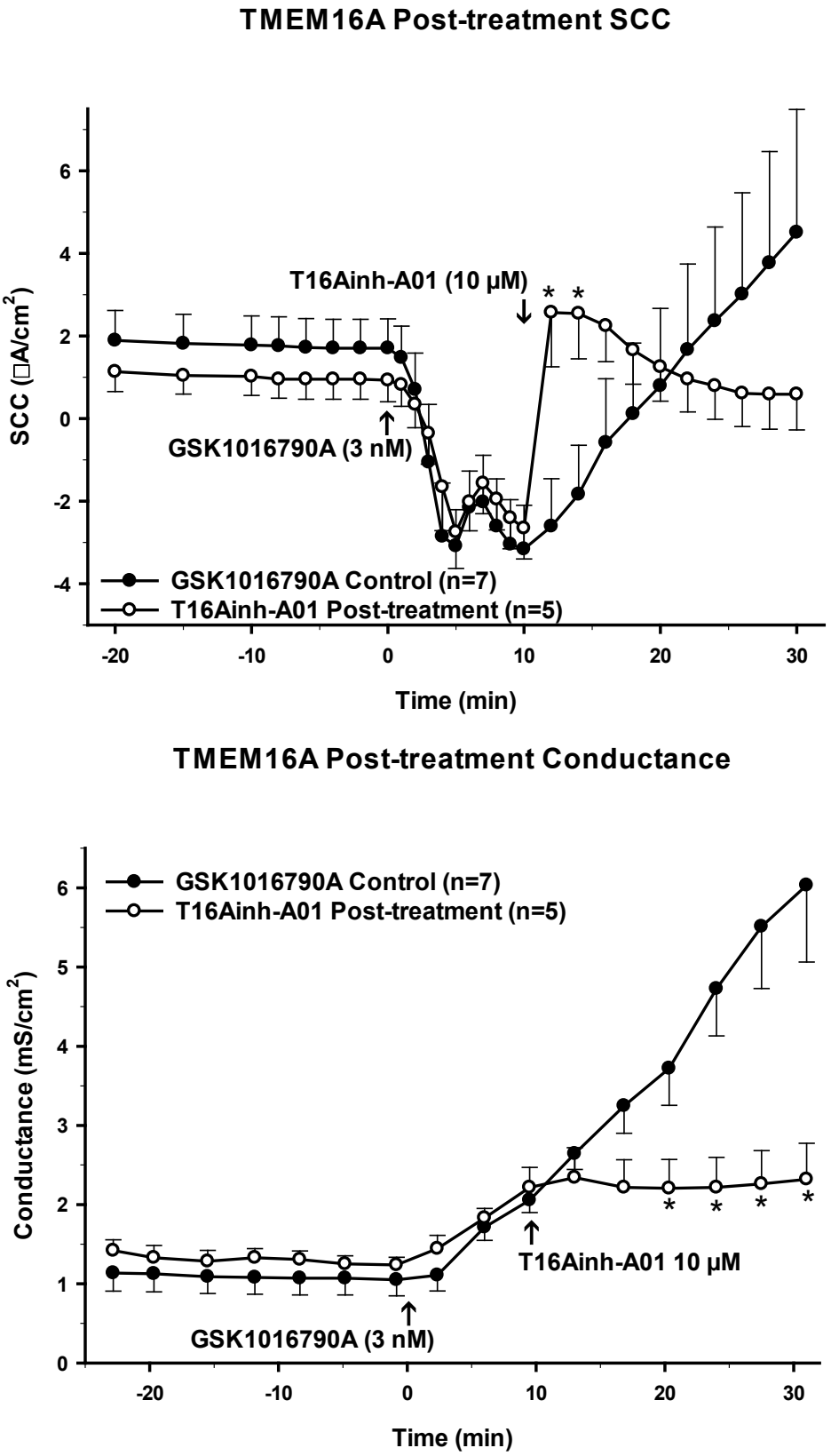

Figure 4.5 Reversibility of a TRPV4 Agonist Response by a TMEM16A Inhibitor.

Figure 4.6: Pre-treatment of PCP-R cells with a TRPV4 inhibitor prior to addition of a TMEM16A agonist. Net changes in transepithelial ion flux and conductance were measured. RN1734 (50 μM) was added to both the apical and basolateral surfaces at T = -10 minutes. The TMEM16A agonist EACT (1.5 μM) was added to both the apical and basolateral sides of the membrane in all cultures at T = 0 minutes. Pre-incubation with RN1734 is represented by white open circles. The EACT-treated positive controls are denoted by black filled circles. Circles represent mean values, and error bars represent +/- SEM for the *n* indicated. SCC = short circuit current. * = $p < 0.05$ against control experiments.

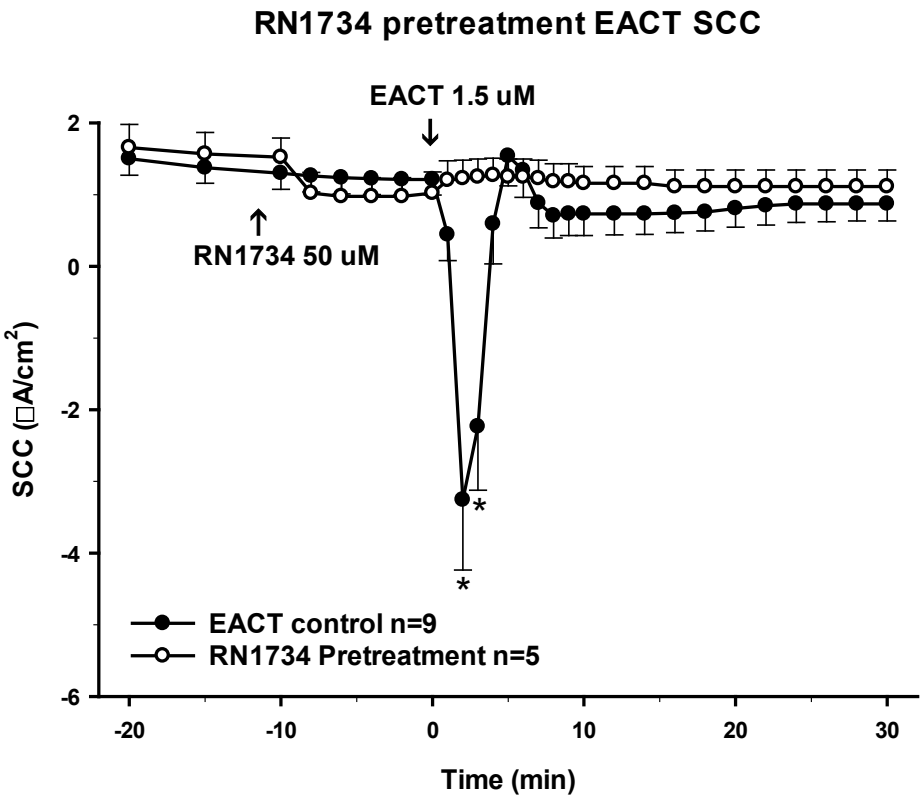

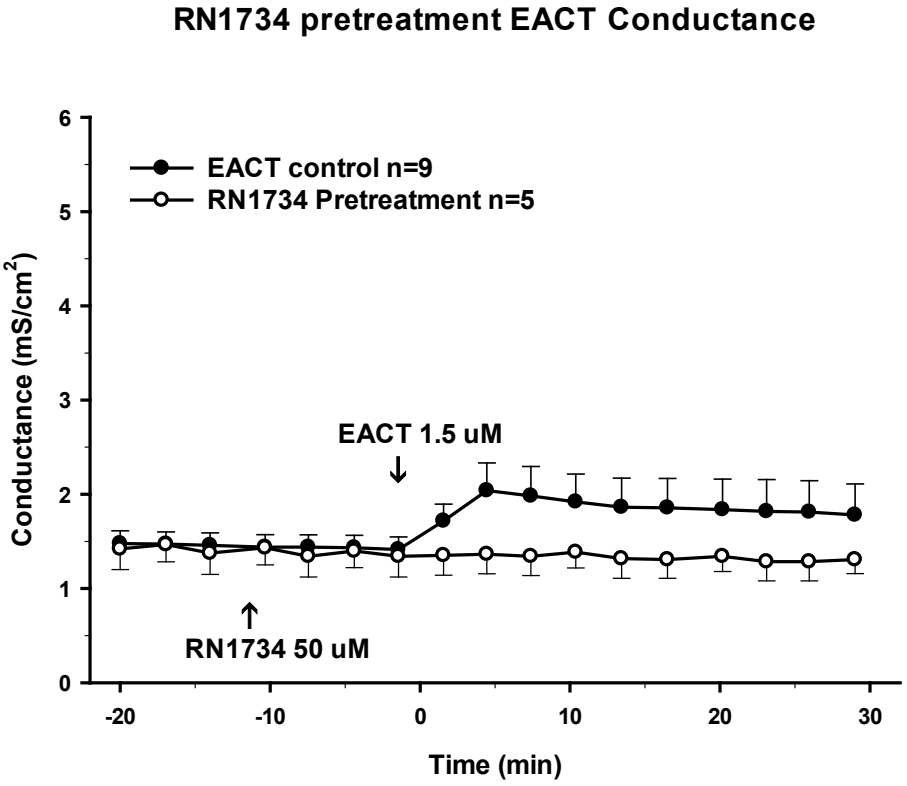

Figure 4.6 Effect of TRPV4 Inhibitor on TMEM16A-Mediated Responses.

Figure 4.7: Pre-treatment of PCP-R cells with a TRPV4 agonist prior to addition of a TMEM16A agonist. Net changes in transepithelial ion flux and conductance were measured. GSK1016790A (300 pM) was added to the basolateral surfaces of experimental and TRPV4 control cultures at T = -10 minutes. The TMEM16A agonist EACT (1.5 μM) was added to both the apical and basolateral sides of the membrane in experimental cultures and TMEM16A control cultures at T = 0 minutes. Pre-incubation with GSK1016790A prior to addition of EACT is represented by white open circles. The GSK-treated controls are denoted by black filled circles. The EACT controls are denoted by grey filled triangles. Circles represent mean values, and error bars represent +/- SEM for the *n* indicated. SCC = short circuit current. * = $p < 0.05$ against control experiments.

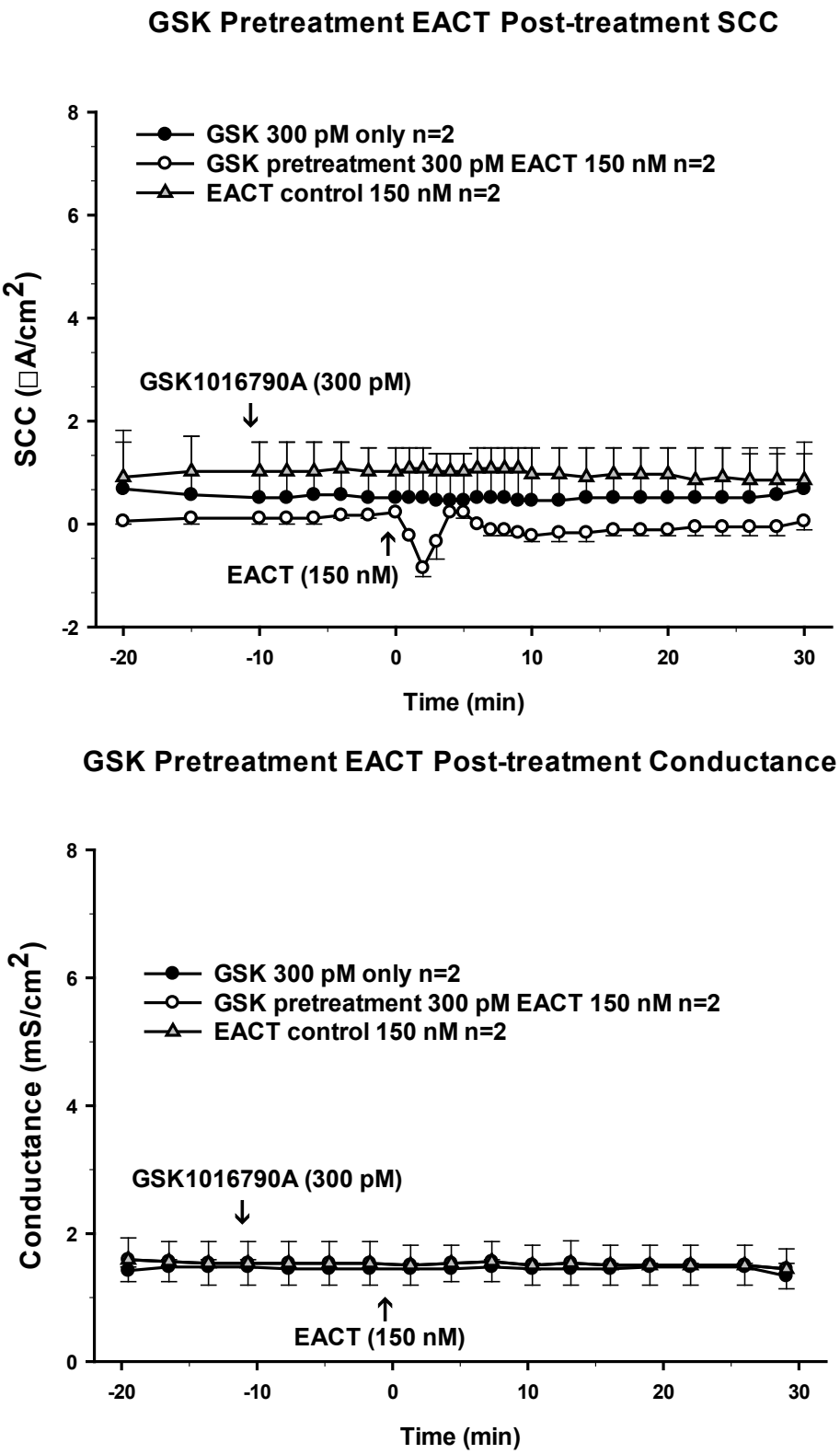

Figure 4.7 Effect of Low Dose Agonists on TMEM16A and TRPV4 Induced Responses.

Figure 4.8: Pre-treatment of PCP-R cells with a TMEM16A agonist prior to addition of a TRPV4 agonist. Net changes in transepithelial ion flux and conductance were measured. EACT (10 μM) was added to both the apical and basolateral surfaces at T = -10 minutes. The TRPV4 agonist GSK1016790A (300 pM) was added to both the apical and basolateral sides of the membrane in all cultures at T = 0 minutes. Pre-incubation with EACT is represented by white open circles. The GSK-treated controls are denoted by black filled circles. Circles represent mean values, and error bars represent +/- SEM for the *n* indicated. SCC = short circuit current. * = $p < 0.05$ against control experiments.

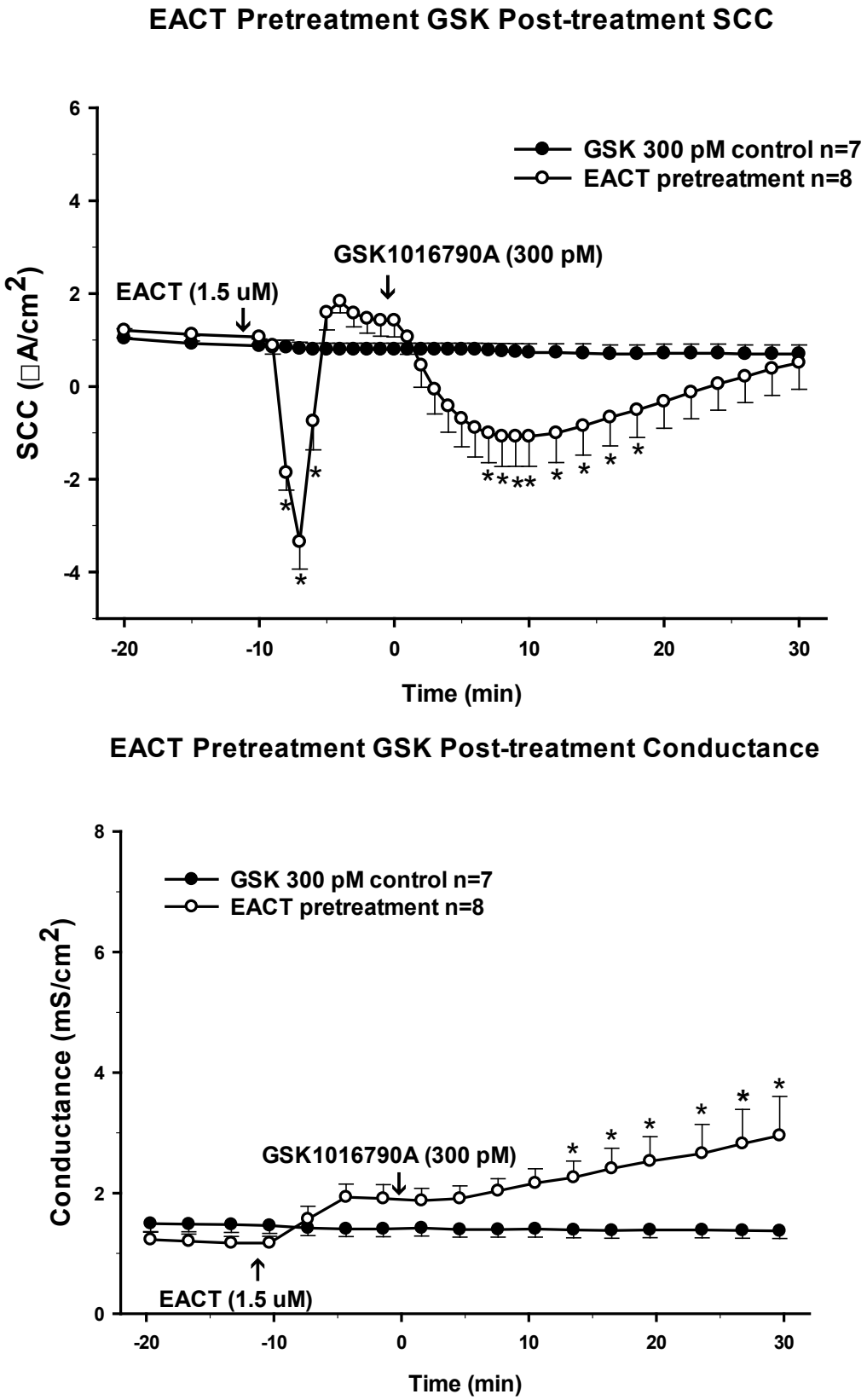

Figure 4.8 Effect of TMEM16A and TRPV4 Agonist on TMEM16A and TRV4 Responses.

Figure 4.9: Pre-treatment of PCP-R cells with a CFTR inhibitor prior to addition of a TRPV4 agonist. Net changes in transepithelial ion flux and conductance were measured. CFTRinh172 (50 μM) was added to both the apical and basolateral surfaces at T = -10 minutes. The TRPV4 agonist GSK1016790A (3 nM) was added to both the apical and basolateral sides of the membrane in all cultures at T = 0 minutes. Pre-incubation with CFTRinh172 is represented by white open circles. The GSK controls are denoted by black filled circles. Circles represent mean values, and error bars represent +/- SEM for the *n* indicated. SCC = short circuit current. * = $p < 0.05$ against control experiments.

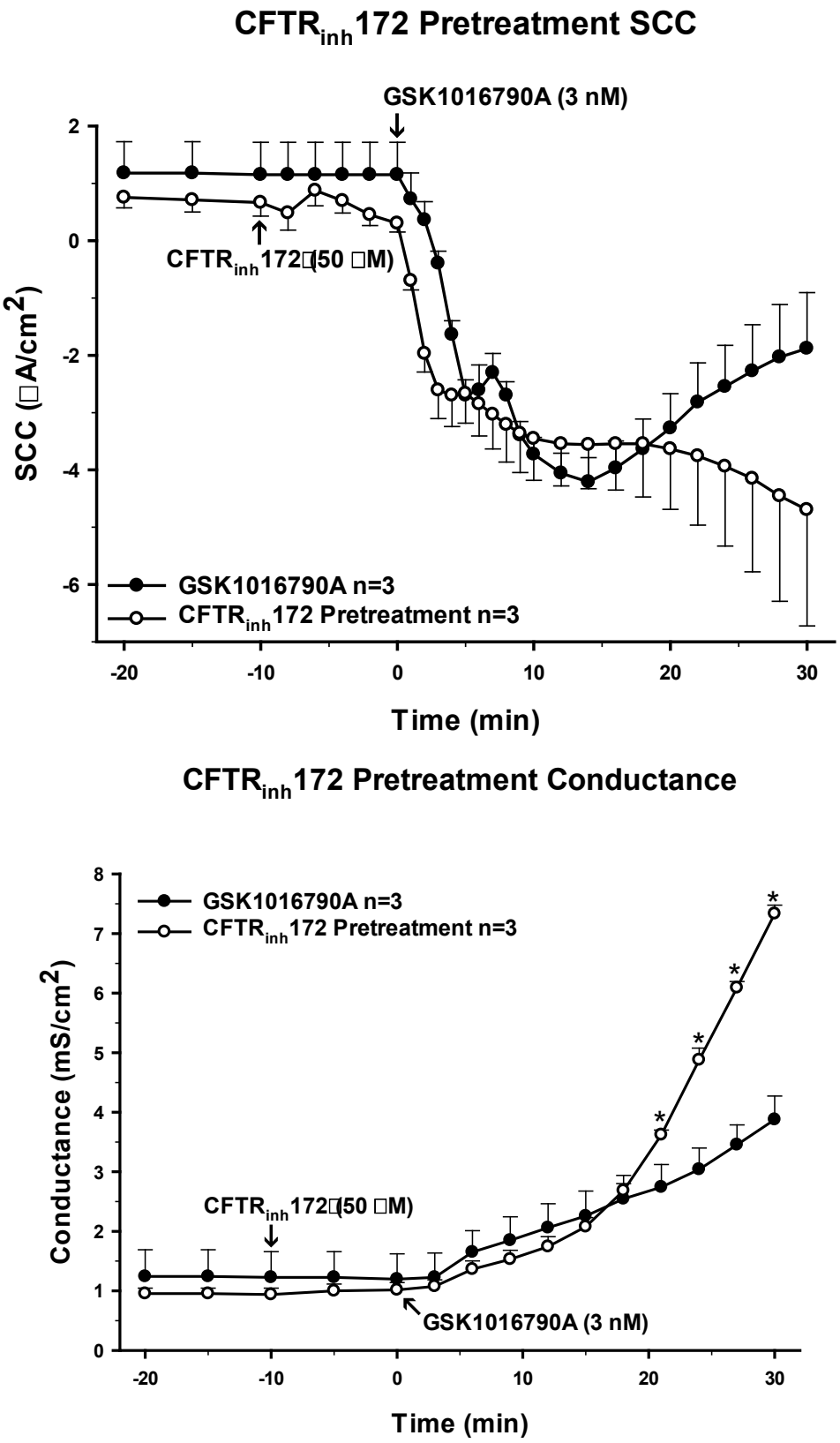

Figure 4.9 Effect of CFTR Inhibitor on TRPV4-Mediated Responses.

Figure 4.10: Pre-treatment of PCP-R cells with a VRAC inhibitor prior to addition of a TRPV4 agonist. Net changes in transepithelial ion flux and conductance were measured. DCPIB (1 μM) was added to both the apical and basolateral surfaces at T = -10 minutes. The TRPV4 agonist GSK1016790A (3 nM) was added to both the apical and basolateral sides of the membrane in all cultures at T = 0 minutes. Pre-incubation with DCPIB is represented by white open circles. The GSK controls are denoted by black filled circles. Circles represent mean values, and error bars represent +/- SEM for the *n* indicated. SCC = short circuit current. * = $p < 0.05$ against control experiments.

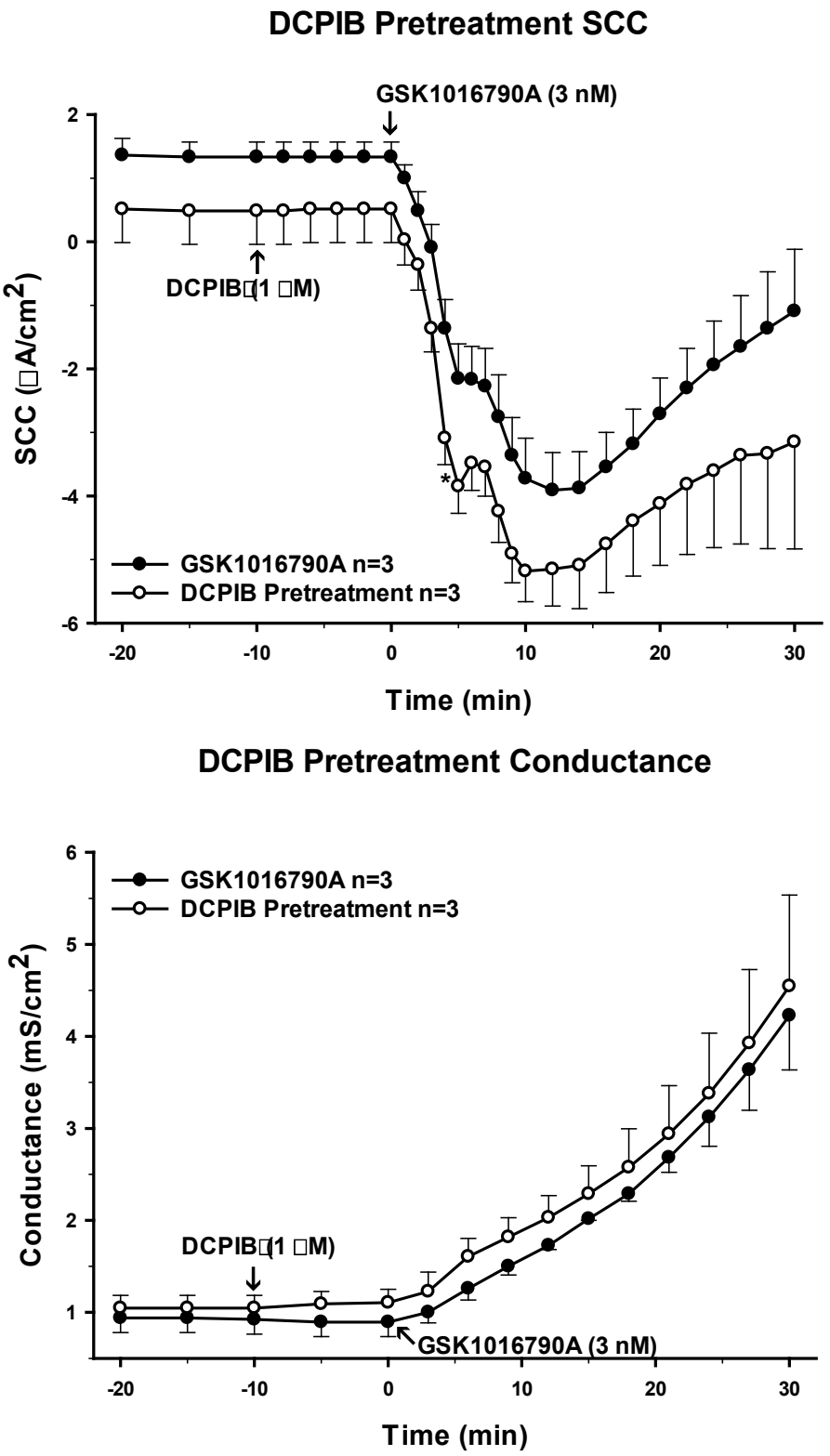

Figure 4.10 Effect of VRAC Inhibitor on TRPV4-Mediated Responses.

Figure 4.11: Pre-treatment of PCP-R cells with a Cl^-/HCO_3^- exchange inhibitor prior to addition of a TRPV4 agonist. Net changes in transepithelial ion flux and conductance were measured. DIDS (10 μM) was added to both the apical and basolateral surfaces at T = -10 minutes. The TRPV4 agonist GSK1016790A (3 nM) was added to both the apical and basolateral sides of the membrane in all cultures at T = 0 minutes. Pre-incubation with DIDS is represented by white open circles. The GSK controls are denoted by black filled circles. Circles represent mean values, and error bars represent +/- SEM for the *n* indicated. SCC = short circuit current. * = $p < 0.05$ against control experiments.

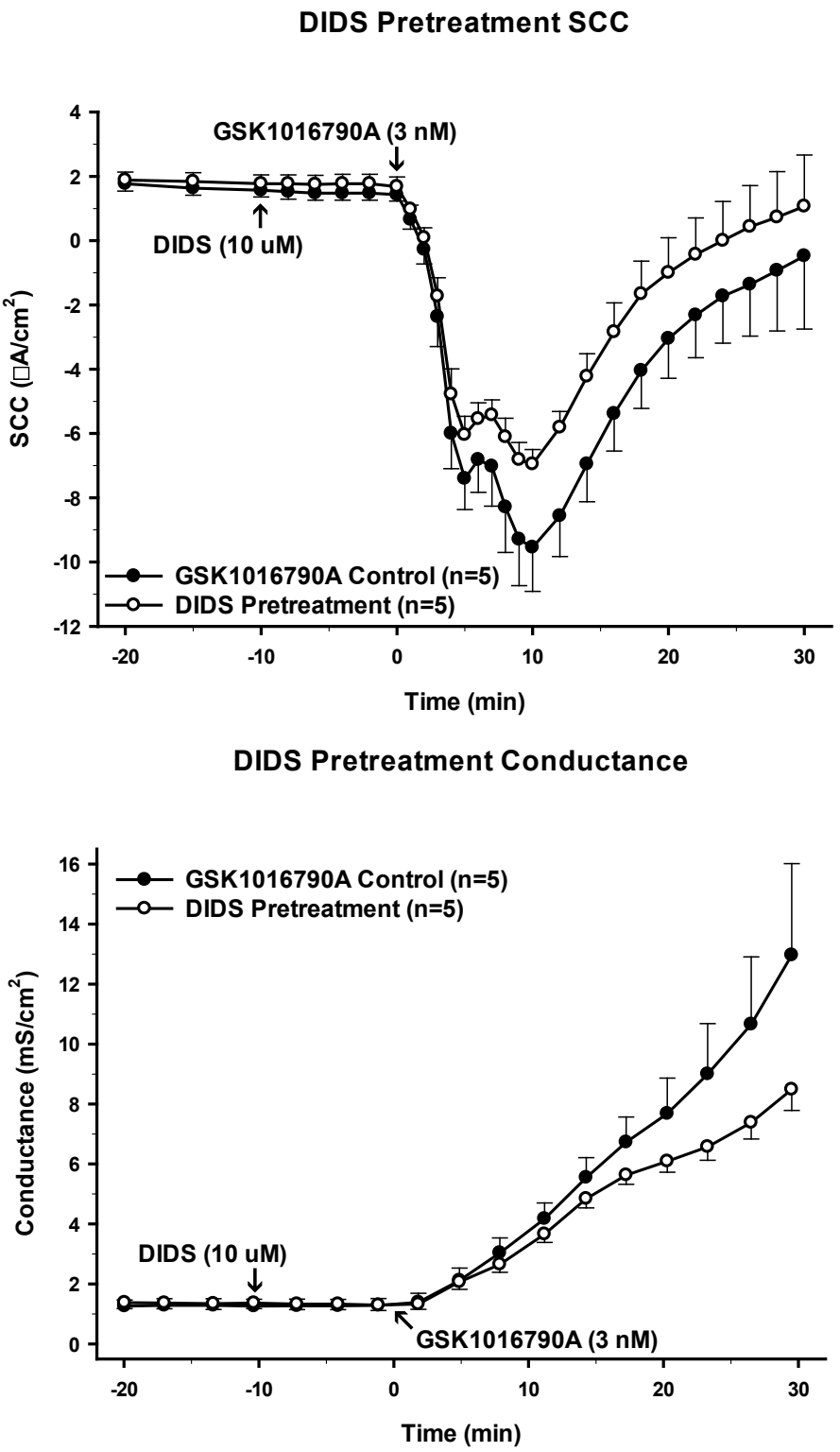

Figure 4.11 Effect of Anion Exchange Inhibitor on TRPV4-Mediated Responses.

4.5 References

1. Alper S, Stuart-Tilley A, Biemesderfer D, Shmukler B, Brown D. Immunolocalization of AE2 anion exchanger in rat kidney. *American Journal of Physiology-Renal Physiology* 273: F601-F614, 1997.
2. Alper S, Stuart-Tilley A, Simmons C, Brown D, Drenckhahn D. The fodrin-ankyrin cytoskeleton of choroid plexus preferentially colocalizes with apical Na+K(+)-ATPase rather than with basolateral anion exchanger AE2. *Journal of Clinical Investigation* 93: 1430-1438, 1994.
3. Bouzinova E, Praetorius J, Virkki L, Nielsen S, Boron W, Aalkjaer C. Na+-dependent HCO3− uptake into the rat choroid plexus epithelium is partially DIDS sensitive. *American Journal of Physiology-Cell Physiology* 289: C1448-C1456, 2005.
4. Brodbelt A, Stoodley M. CSF pathways: a review. *British Journal of Neurosurgery* 21: 510-520, 2007.
5. Brown P, Davies S, Speake T, Millar I. Molecular mechanisms of cerebrospinal fluid production. *Neuroscience* 129: 955-968, 2004.
6. Csanády L, Vergani P, Gadsby D. Structure, Gating, and Regulation of the CFTR Anion Channel. *Physiological Reviews* 99: 707-738, 2019.
7. Christensen H, Barbuskaite D, Rojek A, Malte H, Christensen I, Füchtbauer A, Füchtbauer E, Wang T, Praetorius J, Damkier H. The choroid plexus sodium-bicarbonate cotransporter NBCe2 regulates mouse cerebrospinal fluid pH. *The Journal of Physiology* 596: 4709-4728, 2018.
8. Christensen I, Gyldenholm T, Damkier H, Praetorius J. Polarization of membrane associated proteins in the choroid plexus epithelium from normal and slc4a10 knockout mice. *Frontiers in Physiology* 4: 1-15, 2013.
9. Cserr H. Physiology of the choroid plexus. *Physiological Reviews*, *51*(2), 273-311, 1971.
10. Damkier H, Brown P, Praetorius J. Cerebrospinal Fluid Secretion by the Choroid Plexus. *Physiological Reviews* 93: 1847-1892, 2013.
11. Damkier H, Brown P, Praetorius J. Epithelial Pathways in Choroid Plexus Electrolyte Transport. *Physiology* 25: 239-249, 2010.
12. Delpire E, Gagnon K. Elusive role of the Na-K-2Cl cotransporter in the choroid plexus. *American Journal of Physiology-Cell Physiology* 316: C522-C524, 2019.

13. Deneka D, Sawicka M, Lam A, Paulino C, Dutzler R. Structure of a volume-regulated anion channel of the LRRC8 family. *Nature* 558: 254-259, 2018.
14. Fu Y, Subramanya A, Rozansky D, Cohen D. WNK kinases influence TRPV4 channel function and localization. *American Journal of Physiology-Renal Physiology* 290: F1305-F1314, 2006.
15. Gaitán-Peñas H, Gradogna A, Laparra-Cuervo L, Solsona C, Fernández-Dueñas V, Barrallo-Gimeno A, Ciruela F, Lakadamyali M, Pusch M, Estévez R. Investigation of LRRC8-Mediated Volume-Regulated Anion Currents in Xenopus Oocytes. *Biophysical Journal* 111: 1429-1443, 2016.
16. Gregoriades J, Madaris A, Alvarez F, Alvarez-Leefmans F. Genetic and pharmacological inactivation of apical Na+-K+-2Cl− cotransporter 1 in choroid plexus epithelial cells reveals the physiological function of the cotransporter. *American Journal of Physiology-Cell Physiology* 316: C525-C544, 2019.
17. Hebert S, Mount D, Gamba G. Molecular physiology of cation-coupled Cl? cotransport: the SLC12 family. *European Journal of Physiology* 447: 580-593, 2004.
18. Hincke M, Nairn A, Staines W. Cystic Fibrosis Transmembrane Conductance Regulator Is Found Within Brain Ventricular Epithelium and Choroid Plexus. *Journal of Neurochemistry* 64: 1662-1668, 2002.
19. Hübner C, Hentschke M, Jacobs S, Hermans-Borgmeyer I. Expression of the sodium-driven chloride bicarbonate exchanger NCBE during prenatal mouse development. *Gene Expression Patterns* 5: 219-223, 2004.
20. Millar I, Bruce J, Brown P. Ion channel diversity, channel expression and function in the choroid plexuses. *Cerebrospinal Fluid Research* 4: 8, 2007.
21. Karadsheh M, Byun N, Mount D, Delpire E. Localization of the kcc4 potassium–chloride cotransporter in the nervous system. *Neuroscience* 123: 381-391, 2004.
22. Keep R, Xiang J, Betz A. Potassium cotransport at the rat choroid plexus. *American Journal of Physiology-Cell Physiology* 267: C1616-C1622, 1994.
23. Kibble J, Garner C, Colledge W, Brown S, Kajita H, Evans M, Brown P. Whole cell Cl- conductances in mouse choroid plexus epithelial cells do not require CFTR expression. *American Journal of Physiology-Cell Physiology* 272: C1899-C1907, 1997.
24. Kibble J, Trezise A, Brown P. Properties of the cAMP-activated Cl- current in choroid plexus epithelial cells isolated from the rat. *The Journal of Physiology* 496: 69-80, 1996.

25. Lindsey A, Schneider K, Simmons D, Baron R, Lee B, Kopito R. Functional expression and subcellular localization of an anion exchanger cloned from choroid plexus. *Proceedings of the National Academy of Sciences* 87: 5278-5282, 1990.
26. Lutter D, Ullrich F, Lueck J, Kempa S, Jentsch T. Selective transport of neurotransmitters and –modulators by distinct volume-regulated LRRC8 anion channels. *Journal of Cell Science* (2017). doi: 10.1242/jcs.196253.
27. Millar I, Bruce J, Brown P. Ion channel diversity, channel expression and function in the choroid plexuses. *Cerebrospinal Fluid Research* 4: 8, 2007.
28. Namkung W, Phuan P, Verkman A. TMEM16A Inhibitors Reveal TMEM16A as a Minor Component of Calcium-activated Chloride Channel Conductance in Airway and Intestinal Epithelial Cells. *Journal of Biological Chemistry* 286: 2365-2374, 2010.
29. Narita K, Sasamoto S, Koizumi S, Okazaki S, Nakamura H, Inoue T, Takeda S. TRPV4 regulates the integrity of the blood-cerebrospinal fluid barrier and modulates transepithelial protein transport. *The FASEB Journal* 29: 2247-2259, 2015.
30. Nilius, B, Vriens, J, Prenen, J, Droogmans, G, Voets, T. TRPV4 calcium entry channel: a paradigm for gating diversity. *American Journal Of Physiology-Cell Physiology*, *286*(2), C195-C205, 2004.
31. Ousingsawat J, Martins J, Schreiber R, Rock J, Harfe B, Kunzelmann K. Loss of TMEM16A Causes a Defect in Epithelial Ca2+-dependent Chloride Transport. *Journal of Biological Chemistry* 284: 28698-28703, 2009.
32. Pedemonte N, Galietta L. Structure and Function of TMEM16 Proteins (Anoctamins). *Physiological Reviews* 94: 419-459, 2014.
33. Praetorius J, Damkier H. Transport across the choroid plexus epithelium. *American Journal of Physiology-Cell Physiology* 312: C673-C686, 2017.
34. Praetorius J, Nejsum L, Nielsen S. A SCL4A10 gene product maps selectively to the basolateral plasma membrane of choroid plexus epithelial cells. *American Journal of Physiology-Cell Physiology* 286: C601-C610, 2004.
35. Preston D, Simpson S, Halm D, Hochstetler A, Schwerk C, Schroten H, Blazer-Yost B. Activation of TRPV4 stimulates transepithelial ion flux in a porcine choroid plexus cell line. *American Journal of Physiology-Cell Physiology* 315: C357-C366, 2018.

36. Speake T, Whitwell C, Kajita H, Majid A, Brown P. Mechanisms of CSF secretion by the choroid plexus. *Microscopy Research and Technique* 52: 49-59, 2000.
37. Stuart-Tilley A, Sardet C, Pouyssegur J, Schwartz M, Brown D, Alper S. Immunolocalization of anion exchanger AE2 and cation exchanger NHE-1 in distinct adjacent cells of gastric mucosa. *American Journal of Physiology-Cell Physiology* 266: C559-C568, 1994.
38. Syeda R, Qiu Z, Dubin A, Murthy S, Florendo M, Mason D, Mathur J, Cahalan S, Peters E, Montal M, Patapoutian A. LRRC8 Proteins Form Volume-Regulated Anion Channels that Sense Ionic Strength. *Cell* 164: 499-511, 2016.
39. Takayama Y, Shibasaki K, Suzuki Y, Yamanaka A, Tominaga M. Modulation of water efflux through functional interaction between TRPV4 and TMEM16A/anoctamin 1. *The FASEB Journal* 28: 2238-2248, 2014.
40. Voss F, Ullrich F, Munch J, Lazarow K, Lutter D, Mah N, Andrade-Navarro M, von Kries J, Stauber T, Jentsch T. Identification of LRRC8 Heteromers as an Essential Component of the Volume-Regulated Anion Channel VRAC. *Science* 344: 634-638, 2014.
41. Yang Y, Cho H, Koo J, Tak M, Cho Y, Shim W, Park S, Lee J, Lee B, Kim B, Raouf R, Shin Y, Oh U. TMEM16A confers receptor-activated calcium-dependent chloride conductance. *Nature* 455: 1210-1215, 2008.
42. Zhang Y, Zhang H, Feustel P, Kimelberg H. DCPIB, a specific inhibitor of volume regulated anion channels (VRACs), reduces infarct size in MCAo and the release of glutamate in the ischemic cortical penumbra. *Experimental Neurology* 210: 514-520, 2008.

CHAPTER 5. INFLAMMATORY EFFECTS ON TRPV4 IN THE CHOROID PLEXUS

5.1 Preface

This publication was accepted by the *American Journal of Physiology: Cell Physiology* in August 2019. For this article, I was the second author. My contributions to this publication included conducting RT-PCR experiments to look at the expression of mRNAs for several cytokine receptors, as well as preparation of figures associated with the RT-PCR experiments (Figure 1). Additionally, I designed qPCR experiments to look at the expression of TRPV4 mRNA in cells treated with various cytokines. These experiments demonstrated that overnight incubation with the cytokines had no significant effect on the expression of TRPV4 mRNA in the choroid plexus cell line. I was also involved in editing and proofing of the manuscript, as well as responding to reviewers' comments, and tasked with conducting additional experiments requested of the reviewer. This included validation of the RT-PCR primers by sequencing the amplicons to demonstrate that the correct mRNAs had been amplified.

5.2 Inflammatory Effects on TRPV4 in the Choroid Plexus

Stefanie Simpson[1], Daniel Preston[1], Christian Schwerk[2], Horst Schroten[2], and Bonnie Blazer-Yost [1]

1. Department of Biology, Indiana University-Purdue University at Indianapolis, Indiana
2. Mannheim Medical Faculty, University of Heidelberg, Children's Hospital, Mannheim, Germany

Running Title: Inflammation and TRPV4 in the Choroid Plexus

Corresponding Author
Bonnie L. Blazer-Yost
Indiana University-Purdue University Indianapolis
Biology Department, SL 358

723 West Michigan Street
Indianapolis, IN 46202
Tel: 317-278-1145; Fax: 317-274-2846
email: bblazer@iupui.edu

Keywords: arachidonic acid, blood-choroid plexus barrier, epoxyeicosatrienoic acid, NF-κB

Abbreviations:

CP – Choroid Plexus

CSF – Cerebrospinal Fluid

PCP-R – Porcine Choroid Plexus-Reims

TRPV4 – Transient Receptor Potential Vanilloid 4

IL – Interleukin

TNF – Tumor Necrosis Factor

TGF – Transforming Growth Factor

AA – Arachidonic Acid

EET – Epoxyeicosatrienoic acids

PKD – Polycystic Kidney Disease

CYP – Cytochrome P450 Epoxygenase

ALOX – Lipoxygenase

COX – Cyclooxygenase

SCC – Short Circuit Current

S. S. and B. B. Y. designed the experiments. C.S. and H.S. provided the PCP-R cell line. S. S. and D. P. conducted the experiments, analyzed data, and prepared figures. S. S., D. P., and B. B. Y. interpreted the results of experiments. S.S. drafted the manuscript. S. S., D. P., C.S., H.S., and B. B. Y. edited, revised, and approved final manuscript.

5.3 **Abstract**

The choroid plexus (CP), composed of capillaries surrounded by a barrier epithelium, is the main producer of cerebrospinal fluid (CSF). The CP epithelium regulates the transport of ions and water between the blood and the ventricles, contributing to CSF production and composition. Several

studies suggest a connection between the cation channel Transient Receptor Potential Vanilloid-4 (TRPV4) and transepithelial ion movement. TRPV4 is a non-selective, calcium permeable cation channel present in CP epithelia reported to be activated by cytokines and inflammatory mediators. Utilizing the PCP-R (porcine choroid plexus- Riems) cell line, we investigated the effects of various cytokines and inflammatory mediators on TRPV4-mediated activity. Select pro-inflammatory cytokines (TNF-α, IL-1β, TGF-β1) had inhibitory effects on TRPV4-stimulated transepithelial ion flux and permeability changes whereas anti-inflammatory cytokines (IL-10, IL-4, IL-6) had none. Quantitative mRNA analysis showed that these cytokines had no effect on TRPV4 transcription levels. Inhibition of the transcription factor NF-κB, involved in the production and regulation of several inflammatory cytokines, inhibited TRPV4-mediated activity, suggesting a link between TRPV4 and cytokine production. Contrary to published studies, the pro-inflammatory mediator arachidonic acid (AA) had inhibitory rather than stimulatory effects on TRPV4-mediated responses. However, inhibition of AA metabolism also caused inhibitory effects on TRPV4, suggesting a complex interaction of AA and its metabolites in the regulation of TRPV4 activity. Together these data imply that TRPV4 activity is involved in the inflammatory response; it is negatively affected by pro-inflammatory mediators. Furthermore, arachidonic acid metabolites, but not arachidonic acid itself, are positive regulators of TRPV4.

5.4 **Introduction**

Neurological and neurodegenerative conditions in the brain can result in an increase in the release of inflammatory mediators into the injured areas. These conditions can include head trauma, intracranial hemorrhage, infection, brain tumor, genetic defect or neurodegenerative disease (11, 13, 16, 18, 20, 21, 27, 29, 45, 46). In many of these cases, the development of transient or chronic enlargement of the brain ventricles and an increase in pressure due to the accumulation of cerebrospinal fluid (CSF) occurs. This accrual of fluid could be caused by increases in inflammation affecting the production and/or absorption of the CSF.

The main production of CSF comes from the choroid plexus (CP), present in the lateral, third, and fourth ventricles (10). Composed of a barrier epithelium that surrounds a network of capillaries, the CP epithelial cells regulate the transport of ions and water between the ventricles and capillaries via electrolyte transporters, thus controlling the production and composition of CSF. Aberrant

regulation of these transporters could be a causative agent leading to the emergence of fluid/electrolyte imbalances in the brain.

Previous data suggest a link between transepithelial ion movement and the cation channel, Transient Receptor Potential Vanilloid-4 (TRPV4) (29, 37, 44). This ion channel is found in choroid plexus epithelium (10, 37). TRPV4 is a mechano-, osmo-, and temperature-sensitive, non-selective, calcium-permeable cation channel that can serve as a hub protein for the activation of other transporters (26, 32, 37, 42). For example, in the porcine choroid plexus cell line – Riems (PCP-R), TRPV4 activation can lead to an influx of calcium into the cells, which subsequently stimulates calcium activated ion channels, such as the intermediate conductance potassium channels (37). Once these channels are activated, there is the potential for significant ion flux across the epithelia, resulting in compensatory water movement and a change in CSF production. TRPV4 can also be modulated through a number of stimuli, including chemical activators, such as cytokines and inflammatory mediators (26, 32, 37, 42). Indeed, it has been established that the inflammatory lipid endocannabinoid anandamide (AEA) and its metabolites, including arachidonic acid (AA), are capable of activating the channel (32). In addition, cytochrome P450 epoxygenases, cyclooxygenases, and lipoxygenases can metabolize AA into both inflammatory and anti-inflammatory factors epoxyeicosatrienoic acids (EETs), prostaglandins, and hydroperoxides, respectively, which are also believed to stimulate TRPV4 activity (32, 33).

Microglia, the macrophage-like cells of the central nervous system (CNS), can be triggered to release pro-inflammatory cytokines in response to abnormal protein accumulation or neuronal injury from chemical or physical means (7, 50). It is possible that such inflammation is associated with increases in CSF production associated with neurological disease (4, 17, 18, 35, 46). Summarized in Table 1, pro-inflammatory cytokines found upregulated in neurodegenerative states include interleukin (IL)-1β and tumor necrosis factor (TNF)-α. IL-10 and IL-4 are well-documented anti-inflammatory cytokines also found in various neurological diseases. TGF-β and IL-6 have both been implicated in pro- as well as anti-inflammatory effects (2, 7, 8, 14, 15, 24, 38, 41, 48). These cytokines can, therefore, potentially play a role in altering TRPV4 activity.

As an *in vitro* model, the PCP-R cell line can be utilized as a surrogate for *in vivo* CP tissue. This cell line exhibits many of the characteristics of the native epithelium including the formation of a barrier epithelial monolayer, expression of tight junctional proteins claudins 1 and 3, zona occludins-1 and occludin as well as the polarization of transporters and channels similar to those found *in vivo* (37, 39). A previous study has used this line to monitor changes in transepithelial ion flux and barrier permeability in response to factors that modulate choroid plexus electrolyte transporters in vivo (37). The polarity and barrier function exhibited by this cell line allows for experimentation modeling changes in the barrier function of choroid plexus *in vivo* (37, 39). Using a TRPV4 agonist, GSK1016790A, we are able to stimulate TRPV4 activation and observe changes in ion flux and transepithelial conductance in the presence of various cytokines and inflammatory mediators.

In this paper, we show that specific cytokines and inflammatory mediators can alter the function of TRPV4 in PCP-R cell epithelia. This provides more insight into the role of the cation channel in neuro-inflammatory states and suggesting this hub protein as a potential effector in CSF production.

5.5 **Materials and Methods**

Cell Culture: PCP-R cells were grown on 0.4 µm pore diameter filters inserts (MilliporeSigma, Burlington, MA; #PIHP03050) until the cultures developed a high transepithelial electrical resistance (TER) (10-12 days) (37). Only cultures with resistances above 500 Ωcm^2 were utilized. During experimental protocols that result in a change in resistance, cells that drop below 100 Ωcm^2 were also removed from analysis as their junctional complexes appear irreversibly altered. Cells were fed three times weekly with DMEM media (Gibco, Gaithersburg, MD; #12100-046) containing 4.5 g/L glucose, 3.7 g/L $NaHCO_3$, 5.71 g/L HEPES, 10% fetal bovine serum (Atlanta Biologicals, Flowery Branch, GA), 100 U/mL penicillin, 100 mg/mL streptomycin, and 5 µg/ml insulin. Each plate contained 6 filters in 6 different wells. Filtered inserts were bathed in 2 mL feeding media on the basolateral (bottom) side of the membrane and 1.5 mL feeding media on the apical (top) side of the membrane.

Reverse Transcriptase (RT)-PCR: For the RT-PCR, cells were grown in 75 cm^2 flasks until confluent. The monolayers were trypsinized, collected, and RNA from the cells extracted following the manufacturer's instructions for the New Monarch Total RNA Miniprep Kit (New England BioLabs Inc., Ipswich, MA; #T2010S). No template controls and cDNA were prepared by following manufacturer's protocol for the New England BioLabs LunaScript RT SuperMix Kit (#E3010S). Three primer sets for each gene were generated using Primer3Plus with mRNA sequences and tested on a temperature gradient. Only those primers used in the final images were included in Table 4.1. Sus scrofa mRNA sequences were obtained from Ensembl and additionally confirmed with sequences from the NCBI database. Forward and reverse primers (IDT) were combined with cDNA (approximately 500 ng) and GoTaq Green Master Mix (Promega Corporation, Madison, WI; #M7122) to perform gradients of PCR to determine the optimal annealing temperature. PCR products were then run on 1.5% agarose gels with ethidium bromide and 100bp flanking ladders. Gels were imaged using a ChemiDoc XRS imager (Bio-Rad, Hercules, CA). Following confirmation of single band amplification, PCR products were Sanger sequenced by Eton Bioscience (Union, NJ). Amplicons were confirmed to be the predicted transcript for each gene, validated using NCBI BLAST.

Quantitative (q) PCR: Choroid plexus cells were grown on 0.4 µM polycarbonate filtered inserts (MilliporeSigma) until confluent (10-12 days). 24 hours prior to use, experimental cells were treated with specific cytokines and allowed to incubate overnight. Cells were washed with cold 1X PBS twice, and total RNA was isolated using the Monarch Total RNA Miniprep Kit (New England Biolabs) according to the manufacturer's instructions for cultured cells. Purified RNA concentration was measured using an ND2000 NanoDrop (Fisher Scientific, Waltham, MA). Approximately 100 ng of total RNA was reverse transcribed into cDNA using the Monarch LunaScript RT SuperMix Kit (New England Biolabs). cDNA was diluted 1:10 with Nuclease-Free water (New England Biolabs). qPCR was carried out on a LightCycler 480 Instrument II real-time PCR system (Roche LifeScience, Penzberg, Germany), using LightCycler 480 SYBR Green I Master Mix (Roche LifeScience, #04707516001). qPCR cycle conditions were 95°C for 5 minutes; followed by 45 cycles of 95°C for 10 seconds, 60°C for 10 seconds, and 72°C for 10 seconds. Data are presented as relative expression fold change using the $2^{-\Delta\ \Delta CT}$ method (28) relative to the

calibrator housekeeping genes GAPDH and Rps18. Data are shown as fold change of TRPV4 in treated cells relative to the normalized controls.

Electrophysiology: Electrophysiological measurements were conducted by excising and mounting confluent (10-12 days) PCP-R cells grown on filter inserts in Ussing chambers which are attached to a DVC-1000 Voltage/Current Clamp (World Precision Instruments, Sarasota, FL) using voltage and current electrodes. To each side of the chamber, 10 mL of 37˚C serum-free media was added. The chambers were water jacketed to allow the cells and media to be kept at a consistent physiological temperature (37˚C). Furthermore, the media was continuously oxygenated and circulated by bubbling 5% CO_2/95% O_2 directly into the media. Following clamping of the spontaneous transepithelial potential difference to zero for an equilibration period of at least 30 minutes, experimental compounds were added to the apical and/or basolateral membranes by means of the serum-free media and the cultures were monitored for changes in short circuit current (SCC) and transepithelial resistance (TER). SCC is a measure of net transepithelial ion flux; a positive deflection indicates either anion absorption or cation secretion and a negative deflection indicates the reverse. TER is a measure of changes in epithelial barrier function and was measured every 200 seconds through a 2mV pulse. The instantaneous change in SCC from the pulse was used to calculate TERs by means of Ohm's Law. These resistance calculations were converted to conductance by taking the inverse of the resistances. Conductance is a measure of transepithelial permeability. These parameters provided real time information about transepithelial ion flux in response to modulators of ion channels or intracellular signaling molecules. In each experiment, the cells were pre-incubated on both basolateral and apical sides with the experimental compounds for either 10 or 20 minutes or 24 hours prior to addition of TRPV4 agonist GSK1016790A as indicated on the figures. In all experiments, control and effector-treated samples were grown and analyzed in parallel cultures.

Statistics: Statistics were performed using Two-tailed Students t-test in Sigma Plot 13. $p < 0.05$ is considered significant. Students t-test was used to compare experimental groups to the control group as well as the experimental groups to each other as indicated by the symbols defined in the figure legends.

5.6 **Results**

The PCP-R cell line develops a high resistance monolayer when grown on permeable supports with optimal resistances occurring 9-12 days post seeding (Figure 3.1). Addition of the TRPV4 agonist GSK1016790A to PCP-R cells causes an increase in transepithelial conductance indicating an increased permeability across the epithelial monolayer (Figure 3.2, top). Concurrently with the initiation of the conductance change is a stimulation of short circuit current (SCC) indicating net electrogenic transepithelial ion flux composed of anion absorption (CSF to blood) and/or cation secretion (blood to CSF) (Figure 3.2, bottom). Although the conductance remains elevated, the net electrolyte flux returns to a level that is statistically equal to the basal level within 20-30 minutes after agonist addition. A 10 minute pre-treatment with either of two structurally unrelated TRPV4 antagonists, HC067047 or RN1734, completely blocked the increased permeability of the monolayer as well as the electrogenic ion flux (Figure 3.2). To determine the maximal concentration of the agonist which did not result in an irreversible change in conductance and ion flux, a dose response was performed using concentrations of 0.1, 1, 3, 5, and 10 nM GSK1016790A (Figure 3.3). When the TER of the epithelial monolayer falls below 100 Ω*cm^2 or the conductance rises higher than 10 mS/cm^2 it is observed that the TER will continue to fall to unmeasureable levels and the experiment using this culture has to be discarded (data not shown).

A limited dose response was also performed for the TRPV4 antagonist RN1734 at concentrations of 5, 25, and 50 μM in order to determine the maximal inhibitory concentration (Figure 3.4). Interestingly, the agonist-induced conductance responses are immediately reversible upon the addition of a TRPV4 antagonist. This reversal is accompanied by a statistically significant change in the electrogenic flux (Figure 3.5).

To visualize how the TRPV4 agonist was affecting the junctional complexes, PCP-R cells grown on Transwell filter supports were treated with GSK1016790A or diluent for 10 minutes before fixation and staining with anti-claudin-1 antibody (Figure 3.6). During the incubations, the Ca^{2+} concentration was maintained by the use of serum-free media because changes in extracellular Ca^{2+} have profound effects on tight junctions and epithelial conductance (13,19). The untreated, agonist treated, and negative control (no primary antibody) cells were grown in the same 6-well Transwell plate and were treated, fixed, stained and imaged in parallel. No obvious difference

was observed between the junctional complexes in any of the monolayers examined; rather all junctional complexes remained intact.

Stimulation of TRPV4 causes an influx of Ca^{2+} which is postulated to secondarily stimulate Ca^{2+}-activated channels. Therefore primers were designed to determine the presence of Ca^{2+}-activated K^+ channels in the PCP-R cell line. When negative results were obtained, a second primer pair was designed to confirm the results (Table 3.1). The only Ca^{2+}-sensitive K^+ channels found in the PCP-R cell line were the intermediate conductance (IK; $K_{Ca}3.1$) and the small conductance (SK) 2 channels (Figure 3.7). As expected, TRPV4 is endogenously expressed in the cell line (Figure 3.7).

The RT-PCR results were followed by electrophysiological experiments. As expected from the PCR results, iberiotoxin, an inhibitor of big conductance potassium channels (BK; $K_{Ca}1.1$) had no effect on the TRPV4-stimulated conductance change or transepithelial ion flux (Figure 3.8). Unexpectedly, apamin, a pan-SK channel blocker, was also without effect on TRPV4-mediated ion flux or conductance changes (Figure 3.9). A similar lack of effect on either electrophysiological parameter was noted after pre-incubation with the more SK2-specific inhibitors tamapin, Lei-Dab, or scyllatoxin (data not shown).
Pre-treatment with low dose (1 μM) TRAM 34, an inhibitor of two of the three isoforms of IK, also termed Kcnn4, had no effect on the subsequent response to TRPV4 agonist. However, increasing the TRAM 34 concentration to 50 μM resulted in an inhibition of both the increased conductance and short-circuit current (Figure 3.10). If a moderately high dose of TRAM 34 (25 μM) was added to the apical bathing media during the pre-incubation, the response to the TRPV4 agonist was completely inhibited; conversely if the same concentration was added only to the media bathing the serosal face of the tissue, there was a reduced inhibition of the ion flux accompanied by a substantial, but not complete, inhibition of the increased conductance (Figure 3.11).

5.7 **Discussion**

TLRs are found on microglia, astrocytes, and other immune cells and are well known for playing a key role in the initiation of innate immunity in response to PAMPs and DAMPs. The TLRs not

only play a major role in a cell's ability to respond to inflammatory reactions, but they also enable the cells to contribute to the inflammation. When the TLRs detect PAMPs or DAMPs, this can cause a cascade of events leading to activation of transcription factors NF-κB and AP-1 and subsequent cytokine production (6, 34). In particular, TLR4 is best known for producing key pro- and anti-inflammatory cytokines, such as TNF-α, IL-6, and IL-10, and is most often associated with inflammation (6, 34). It is also of interest that expression levels of TLRs have been found to change during aging (34). Specifically, pro-inflammatory cytokine production increases while secretion of anti-inflammatory cytokines decreases. TLRs have been associated with age-related inflammatory neurodegenerative diseases, such as ischemic stroke, Alzheimer's disease, and multiple sclerosis (34).

The PCP-R cell line contains mRNA for the receptors of most cytokines tested, except for IL-10, and all 10 of the known porcine TLRs. This indicates that CP cells have the potential to respond to cytokines and inflammatory signals as well as produce several different cytokines, which would be secreted into the CSF. While we did not explore cytokine production in these studies, it is likely that autocrine or paracrine cytokines will have effects on CSF production by the CP cells.

In studies using lung and endothelial tissue, TRPV4 antagonists have been found to reduce pulmonary edema and protect against sepsis, respectively. In both studies, TRPV4 inhibition was also found to decrease inflammation and cytokine production (3, 9). This would suggest that TRPV4 acts in a pro-inflammatory manner. To confirm this in the brain, we looked at various types of cytokines, including pro-inflammatory, anti-inflammatory, and paradoxical pro- and anti-inflammatory cytokines. Indeed, long-term (24 hours) incubation with the pro-inflammatory cytokines had significant effects on TRPV4 activity. However, the responses seen with the two prominent pro-inflammatory cytokines were not the same. Furthermore, the paradoxical cytokines, TGF-β1 and IL-6, had varying effects with TGF-β1 causing strikingly similar results as IL-1β while IL-6 had no significant effect.

The exact nature of the electrophysiological response to TRPV4 agonists is undoubtedly complex. We have previously shown that a component of the response is due to potassium secretion via the intermediate conductance (IK) channel (37). However, the complex nature of the SCC response,

as well as the differential effects of cytokines on this response, strongly suggests a multitude of intersecting ion fluxes. SCC is a measure of net transepithelial ion movements. Although the current returns to "baseline" about 30 minutes after treatment with a TRPV4 agonist, the sustained high conductance suggests a continued transepithelial ion flux with anions and cations moving in opposite directions, resulting in an electroneutral short circuit current, or net zero electrogenic flux. The cytokines that have an effect on net ion fluxes appear to be doing so by altering different components of the complex response.

While it cannot be assumed that all pro-inflammatory pathways cause an attenuation or inhibition of the response, it is most likely, based upon our observations, that TGF-β1 is acting in a pro-inflammatory manner while IL-6 is acting in an anti-inflammatory manner in the CP cells. Together, these data imply that pro-inflammatory cytokines diminish TRPV4 function. While upstream activators, TNF-α and IL-1β, required 24 hours to mediate a measurable effect on the PCP-R cells, the finding that short-term inhibition of the pro-inflammatory transcription factor NF-κB caused a potentiation of TRPV4-mediated ion flux and permeability changes cannot be easily explained. This may indicate a preexisting tone of NF-κB activation in the PCP-R cells. The inhibition of this baseline activity may cause an increase in barrier permeability as ions are more easily able to move across the membrane. After 24 hours of inhibition, the basal conductance is substantially higher than the control, which further suggests underlying NF-κB activity. However, the attenuated response upon TRPV4 stimulation suggests that NF-κB activation, and possibly its downstream inflammatory effectors, can be considered contributors to TRPV4-mediated ion flux and permeability changes.

Effects seen after long-term cytokine incubations raised the question of whether the changes in TRPV4-mediated activity were due to an alteration of the transcription of TRPV4. However there were no statistical differences in the quantitative PCR of TRPV4 in response to 24-hour cytokine incubations indicating that the cytokines are having an effect on the downstream targets of the ion channel.

Several publications have reported that AA and its metabolites are able to cause a substantial elevation of $[Ca^{2+}]_i$ by activating TRPV4 with concentrations as low as 3 μM AA (5, 31, 47).

Specifically, these studies also cite EETs as the predominant activator of the cation channel (5, 7, 32, 47). However, it has also been reported that endogenous levels of AA can differ depending on the tissue type, with physiological concentrations varying from 2 to 16 μM. In pancreatic islet cells, the concentration was found to be as high as 75 μM (31). Based on previous studies, we hypothesized that TRPV4 activity would be potentiated after pre-incubation with either physiological concentrations of AA or its metabolites. Surprisingly, concentrations of AA comparable to previous publications (10 μM) failed to potentiate TRPV4-mediated activity. Rather, AA (up to 100 μM) caused an inhibition of the TRPV4-mediated response to transepithelial ion flux and cell permeability in a dose-dependent manner. AA inhibition of TRPV4-mediated ion flux in the PCP-R cells suggests a cell-type specific effect on TRPV4. Taken together with our cytokine data, in which selective pro-inflammatory cytokines down regulate TRPV4-mediated activity, this would imply that inflammation acts to decrease TRPV4 function.

There is controversy concerning which isoform of EET is responsible for activating TRPV4 (12). It is possible that different isoforms of EET affect TRPV4 in a cell-specific manner. While 5,6-EET is most often considered to be the activating isoform in other cell types, this does not appear to be the case when added exogenously in CP cells. It is possible that the 5,6-EET is only effective when produced inside the cells. However, it is unknown whether the PCP-R cell line is able to produce EETs. The production of EETs occurs when AA is metabolized by the enzymes cytochrome P450 epoxygenase, of which there are multiple isoforms (40). Currently, only two of these enzymes have been sequenced in pigs, *Cyp2c42* and *Cyp2e1*, neither of which were present in the cells. However, there are several other isoforms still untested, including those most associated with EET production, *Cyp2c8*, *Cyp2c9*, *Cyp2c19* and *Cyp2j2* (40). Therefore, these data cannot lead to the conclusion that there are no cytochrome P450 epoxygenases present. Furthermore, the dramatic inhibitory effects of the SKF-525A CYP450 inhibitor imply that endogenous EET production may activate TRPV4 in these cells. It is possible that a different EET isoform other than 5,6-EET is affecting TRPV4 in the CP or that the production occurs within a membrane limited compartment that is closely linked to the channel.

We determined the potential effects of the other AA metabolites in the CP cells. Both isoforms of cyclooxygenase were present in the PCP-R cells, therefore the cells are able to produce

prostaglandins, prostacyclin, and thromboxane A2 (36). However, inhibition of both COX1 and COX2 with the NSAID Indomethacin did not alter the effects of TRPV4 activation in the cells. Thus, these metabolites likely do not play a role in TRPV4-mediated pathways.

The lipoxygenase (LOX) pathway contains seven known gene isomers: *Aloxe*3, *-5*, *-5ap, -12, -12b, -15,* and *-15b* (30). Of the enzymes, ALOX12B, -E3, and -15B are found in the skin and other epithelial cells and ALOX5, -12, and -15 are located primarily in immune cells. Many of the isomers have been reported in different forms of cancers, but all of them can be involved in inflammation (30). Of the four sequenced porcine isomers, only ALOX15 and ALOX15B were found in our cell line. Interestingly, ALOX15 is considered one of the isoforms that can be partially controlled by cytokines. Anti-inflammatory cytokines, such as IL-4 and IL-13, have the potential to increase expression of this gene, which can then decrease production of pro-inflammatory cytokines, such as IL-12 (30). The isoform has also been associated with maintaining dermal integrity through anti-inflammatory suppression of inflammation in the skin (19). On the other hand, ALOX15 is also capable of increasing pro-inflammatory matrix metalloproteinase (MMP) expression and contributing to arthritic disease progression (49, 53). Once again, this leads to the question of whether TRPV4 is part of a pro- or anti-inflammatory process. Less is known about the ALOX15B isoform, but it has been implicated in decreasing epithelial barrier permeability (30). Thus, increases in this isoform could contribute to increases in transepithelial ion flux and conductance in the CP tissue.

As previously stated, inhibiting cyclooxygenases alone does not affect the cellular response to TRPV4 agonists. However, when both cyclooxygenases and lipoxygenases are inhibited, there is a partial inhibition of the TRPV4-mediated response. As shown above, inhibiting the CYP450s and subsequent EET production results in complete inhibition of the TRPV4-mediated response. Thus, the interaction between the AA metabolites and TRPV4 is complicated and may involve both positive and negative effectors produced in a stimulus dependent manner. Future experiments will investigate how these metabolites interact with the channel.

In summary, TRPV4-mediated transepithelial ion flux and increases in conductance are negatively affected by pro-inflammatory cytokines and mediators. We also found that, in contrast to

previously reported studies, arachidonic acid does not increase TRPV4-related activity. Rather, when added to choroid plexus cells, arachidonic acid diminished TRPV4-mediated transepithelial ion flux and changes in permeability. Finally, we confirmed that in the choroid plexus, inhibition of EET production causes a complete inhibition of TRPV4-mediated transepithelial ion flux and cellular permeability changes. Therefore, in the choroid plexus, TRPV4 regulation by inflammatory mediators is complex, consistent with the role of this channel as a hub protein which can integrate multiple extracellular signals and subsequently mediate a multiphasic change in transepithelial ion transport.

5.8 **Acknowledgments**

We would like to thank Nicolas Berbari and Patrick Antonellis for their input in optimizing and troubleshooting our qPCR assay methods.

5.9 **Grant Support**

This research was supported by the Indiana Clinical and Translational Sciences Institute Predoctoral Award UL1TR001108 (SS) and the United States Department of Defense Investigator Initiated Research Award W81XWH-16-PRMRP-IIRA (BBY).

5.10 **Disclosures**

None.

Table 5.1 Reported Cytokine Functions in the Inflammatory Pathway.

Inflammation Pathway	Cytokines	References
Pro-inflammatory	IL-1β, TNF-α	2, 7, 15, 41, 48
Anti-inflammatory	IL-10, IL-4	15, 41, 48
Pro- and Anti-Inflammatory	TGF-β, IL-6	2, 7, 8, 14, 15, 24, 38, 41, 48

Table 5.2 *Sus Scrofa* Primers Used for RT-PCR with Corresponding Product Sizes (bp).

Three different primer sets were generated and tested for each gene. Primers included in this table were utilized for Figures 1A, B, and C. GAPDH was used as a positive control.

Sus Scrofa gene	Protein	Primer Sequences 5' - 3'		Product Size (bp)
		Forward Primer	Reverse Primer	
Il1r1	IL1R1	TTACACAGAGACTACCGGTTGC	CAGTTTTATCACCCGGGAGACA	263
Il1r2	IL1R2	AAATGATTCCACGACCATCCCA	TCCCAAAACCAGGATGATGAGG	874
Tnfrsf1a	TNFRSF1A	GAAACAGGACACCATCTGCAAC	AAGCTAAGCCAACGAAGAGGAA	218
Tgfbr1	TGFBR1	GAGACAGGCCATTTGTATGTGC	TAAATCTCTGCCTCACGGAACC	520
Tgfbr2	TGFBR2	GGAAGCTGATGGAGTTCAGTGA	TCTCTGTCTTCCAGGAGGCATA	252
Tgfbr3	TGFBR3	ATATTCACCACAAGCCTGTCGT	ATACTCCTTTCGGGCCCAATTT	224
Il6r	IL6R	AAGATTCTGCGTCGGTACCATT	TGTTGCTGACATCATAAGGGCT	312
Il10ra	IL10RA	GGATGAAGTGACTCTGACGGTT	GCTTCACCCTGACACACAATTC	257
Il4r	IL4R	AGAGCTACCTGTACTCGGAACT	CCCTTTGTCTTCCTCCTCTTCC	695
Tlr1	TLR1	TGTCCCACAACAAGTTGGAGAA	TTGTGGGAAACTGAACACCTCA	650
Tlr2	TLR2	TCCCAAATCTGCGAATCCTGAA	ATGCAACCTCCGGACTGTTAAT	512
Tlr3	TLR3	CGATGACCTCCCGGCAAATATA	GAGATTTTCCAGTTGGAGCTGC	382
Tlr4	TLR4	TTCTCTCCTGCCTGAGATCTGA	ACTCCAGGTAGGTATTCCTGCT	555
Tlr5	TLR5	TCCTGTGGTCTCTCTGATGCTA	GGGTTCATACACTTCCCCCAAT	284
Tlr6	TLR6	AGACAATCTTGTGCCATCCCAT	GGCCCTTGAGTGAGTTCCAATA	409
Tlr7	TLR7	GACACTAAAGACCCAGCAGTGA	CTGAAGGGGCTTCTCAAGGAAT	297
Tlr8	TLR8	CTGAGGCAGAACAGGATTTCCT	TTCATCACCCAGTCTGTGACAG	542
Tlr9	TLR9	GCCTACGAACTCTCAACCTCAA	GGAAGTTCTCACTCAGGTCCAG	696
Tlr10	TLR10	TCAGGTGCTTGCCCAGAAATAT	TCTTGCCAGGATCAGAGTTTCC	717
Cyp2c42	CYP2C42	TCCTGTCTGCTTCTCCTTTCAC	GGGAGCACAGTCCAGGATAAAA	489
Cyp2e1	CYP2E1	TCGAGATTTCACTGACACCCTG	GTTAAAGTGCTGCAAGATGGCA	592
Alox5	5-LOX	TGACAGTGGATGAAGAACTGGG	TGTTTTTGCCGTGTTTCCAGTT	259
Alox12b	12R-LOX	ACACCATCCAGATCAACAGCAT	CCAGAGGACCAATAGGACGATG	602
Alox15	12/15-LOX	CAGGAGGATGAACTCTTTGGCT	TCGAATATACCTCCGTCCGAGA	578
Alox15b	15-LOX2	GCGAAATGCTGAGTTCTCCATC	CAGGGTGGAATAGTTCAGCTGT	283
Cox1	COX1	TCACCCGCAATACTATGAGCTC	TGTGTGATAGGGAGGAGGACAT	510
Cox2	COX2	CCCTTTCCAACTAGGCTTCCAA	TAGTCGTCCTGGGATAGCATCT	529
Gapdh	GAPDH	TTTTAACTCTGGCAAAGTGGAC	CATTGTCGTACCAGGAAATGAG	884

Figure 5.1: RT-PCR in PCP-R cells. A) mRNA for the various cytokine receptors. All were present except for the second isoform of the IL-1 receptors (*Il1r2*) and the IL-10 receptor (*Il10ra*). B) mRNA for porcine Toll-like receptors (TLR) 1-10 is present in the PCP-R cell line. C) RT-PCR results for various enzymes capable of arachidonic acid (AA) metabolism. Cytochrome P(CYP)450 epoxygenases, *Cyp2c42* and *Cyp2e1*, are both absent. mRNA for lipoxygenase (*Alox*)15 and *Alox15b* are present whereas *Alox5* and *Alox12* are absent. Cyclooxygenase (*Cox*) 1 and 2 are both present. *Gapdh* was utilized as positive controls for each gel. Band product sizes can be found in Table 2. Ladder = 100 bp. T = Template. Lanes denoted (+) or (-) "T" signifies addition or no addition of template control. D) Diagram of AA metabolism via the three different pathways, pathway inhibitors, and subsequent metabolites.

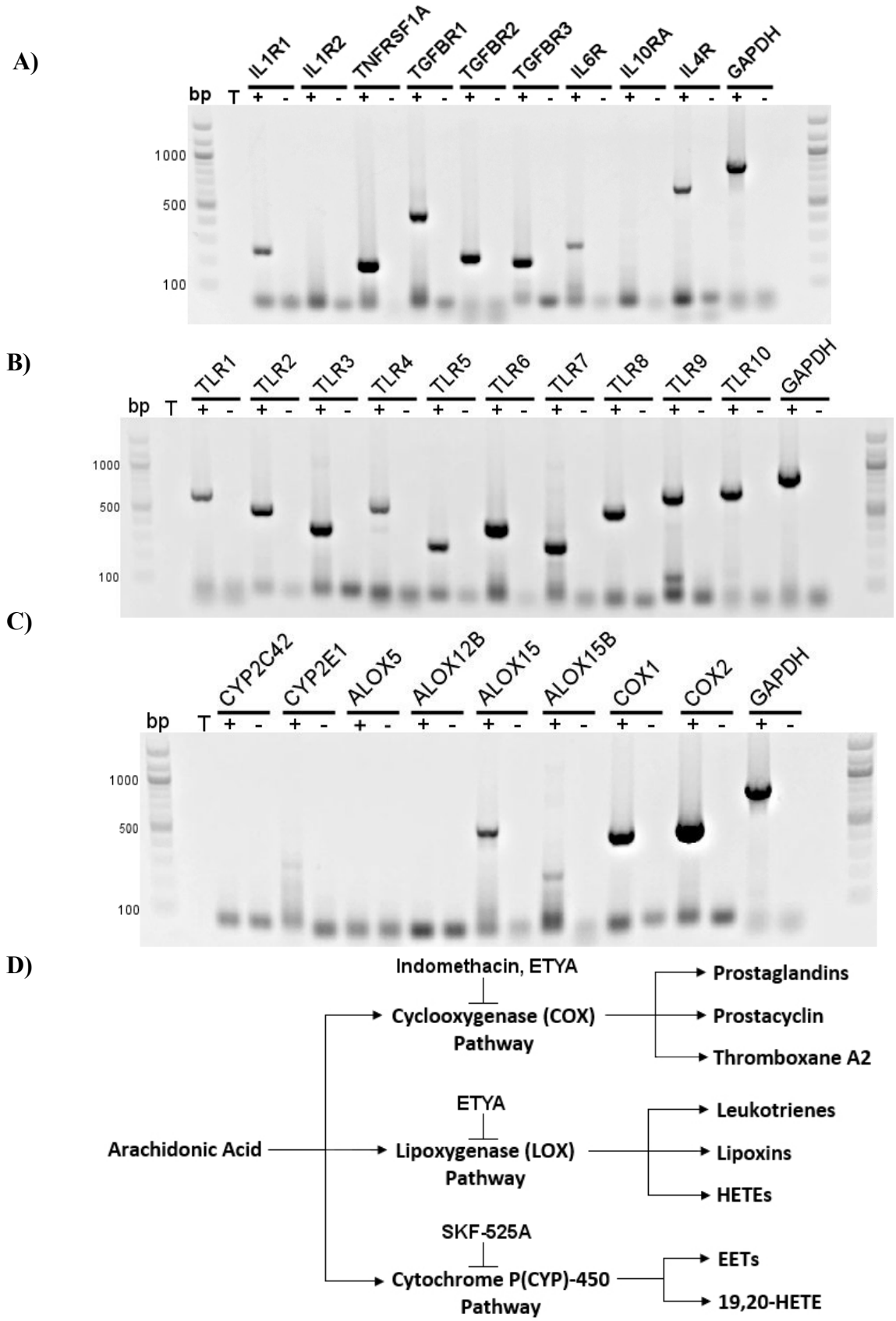

Figure 5.1 RT-PCR in PCP-R Cells.

Figure 5.2: Pre-treatment of PCP-R cells with pro-inflammatory cytokine IL-1β for 24-hours prior to TRPV4 agonist addition. Effect on transepithelial ion flux and conductance was measured. IL-1β (10 ng/mL in PBS) was added to the PCP-R media on both basolateral and apical sides of the membrane at T = -24 hours (not shown). TRPV4 agonist GSK1016790A was added to basolateral side of the membrane only at T = 0 minutes. 24-hour incubation with IL-1β is signified by white circles. GSK1016790A control is signified by black circles. Circles signify mean values and bars signify ±S.E.M. for number of experiments indicated. SCC = short circuit current. * = $p < 0.05$ against control.

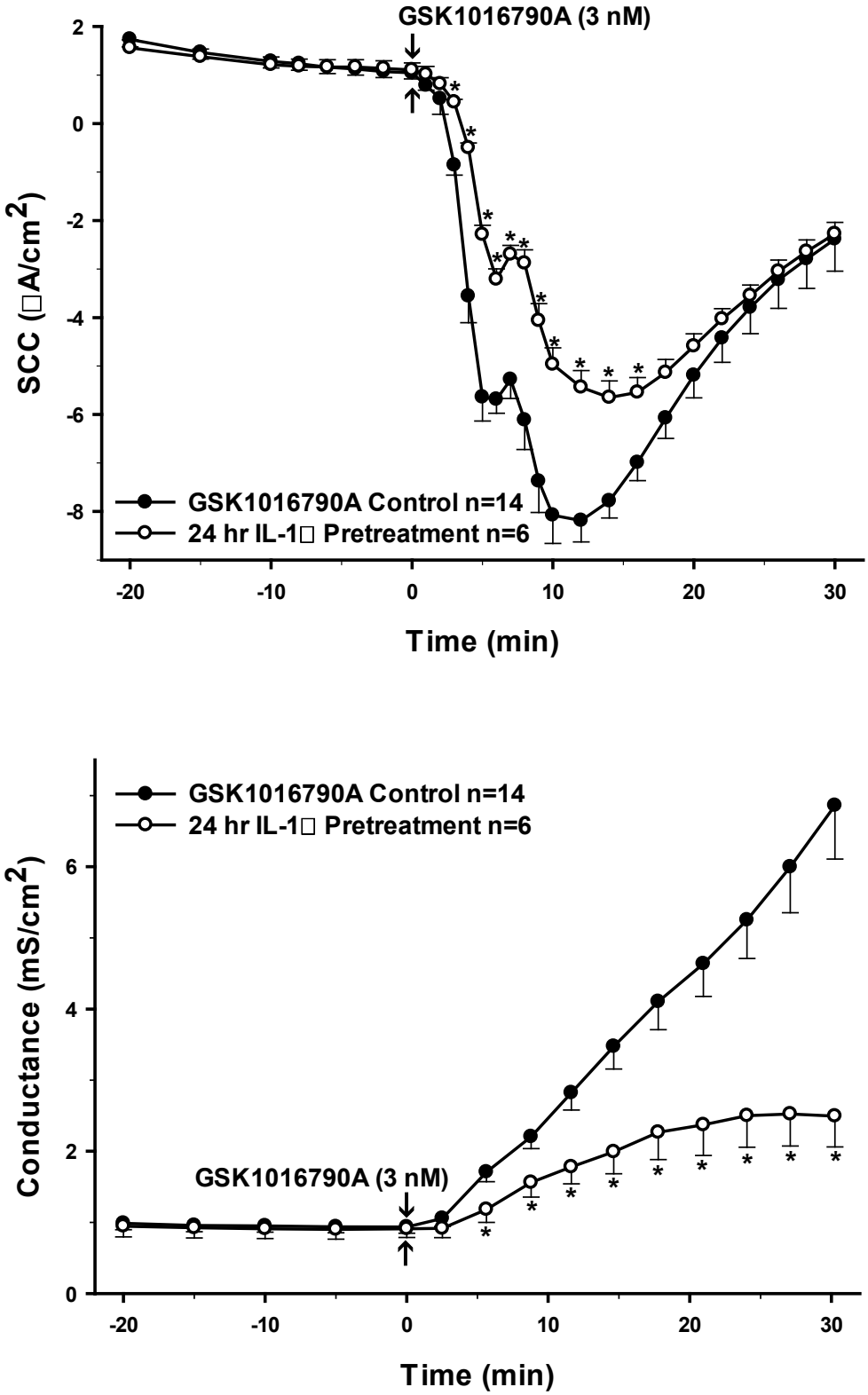

Figure 5.2 Treatment of PCP-R Cells with IL-1β 24-hrs Prior to TRPV4 Agonist Addition.

Figure 5.3: Pre-treatment of PCP-R cells with pro-inflammatory cytokine TNF-α for 24-hours prior to TRPV4 agonist addition. Effect on transepithelial ion flux and conductance was measured. TNF-α (0.15 ng/mL in deionized water) was added to the PCP-R media on both basolateral and apical sides of the membrane at T = -24 hours (not shown). TRPV4 agonist GSK1016790A was added to basolateral side of the membrane only at T = 0 minutes. 24-hour incubation with TNF-α is signified by white circles. GSK1016790A control is signified by black circles. Circles signify mean values and bars signify ±S.E.M. for number of experiments indicated. SCC = short circuit current. * = $p < 0.05$ against control.

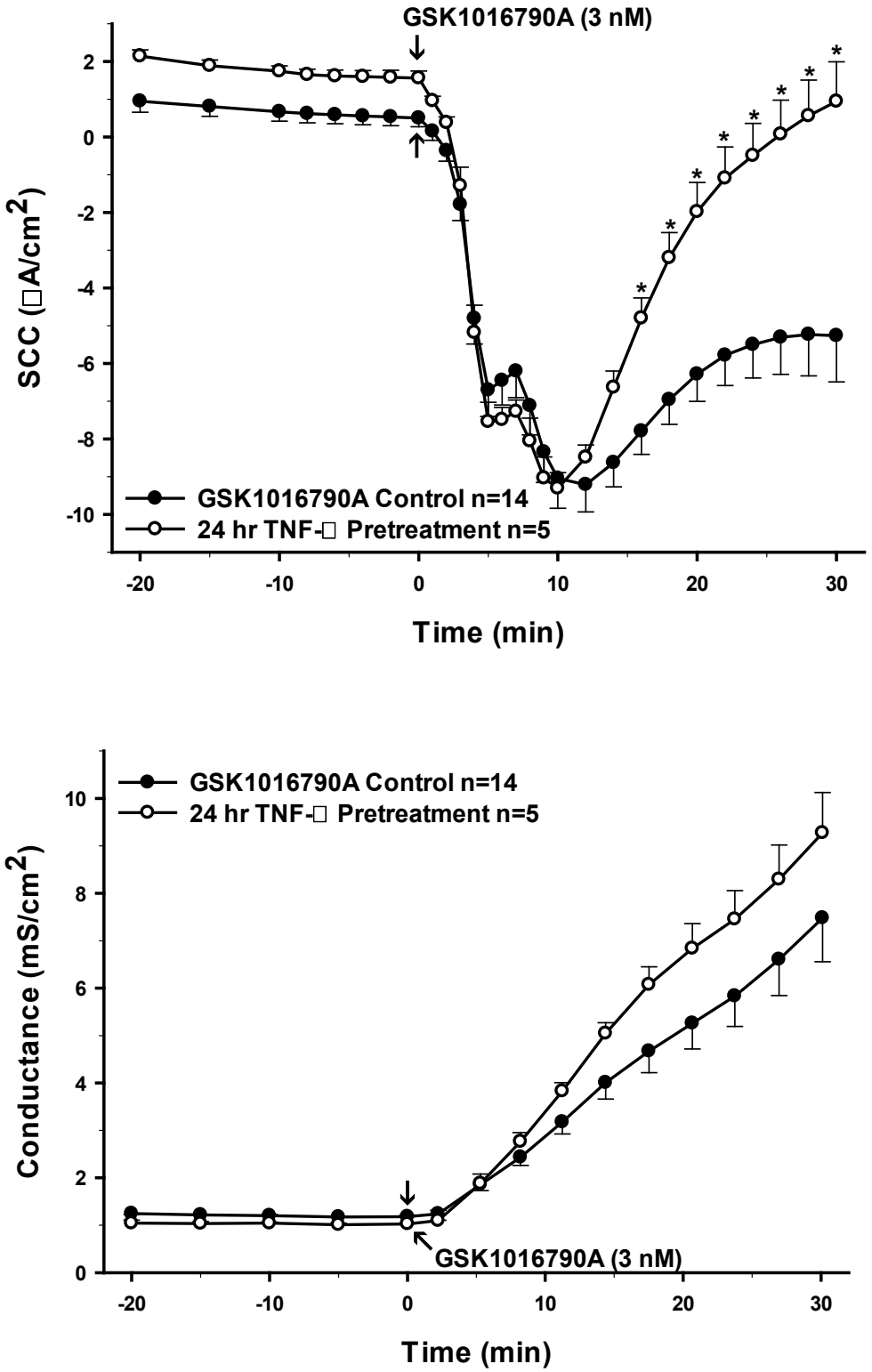

Figure 5.3 Treatment of PCP-R Cells with TNF-α 24-hrs Prior to TRPV4 Agonist Addition.

Figure 5.4: Pre-treatment of PCP-R cells with pro- and anti-inflammatory cytokine TGF-β1 for 24-hours prior to TRPV4 agonist addition. Effect on transepithelial ion flux and conductance was measured. TGF-β1 (2 ng/mL in 4 mM HCl) was added to the PCP-R media on both basolateral and apical sides of the membrane at T = -24 hours (not shown). TRPV4 agonist GSK1016790A was added to basolateral side of the membrane only at T = 0 minutes. 24-hour incubation with TGF-β1 is signified by white circles. GSK1016790A control is signified by black circles. Circles signify mean values and bars signify ±S.E.M. for number of experiments indicated. SCC = short circuit current. * = $p < 0.05$ against control.

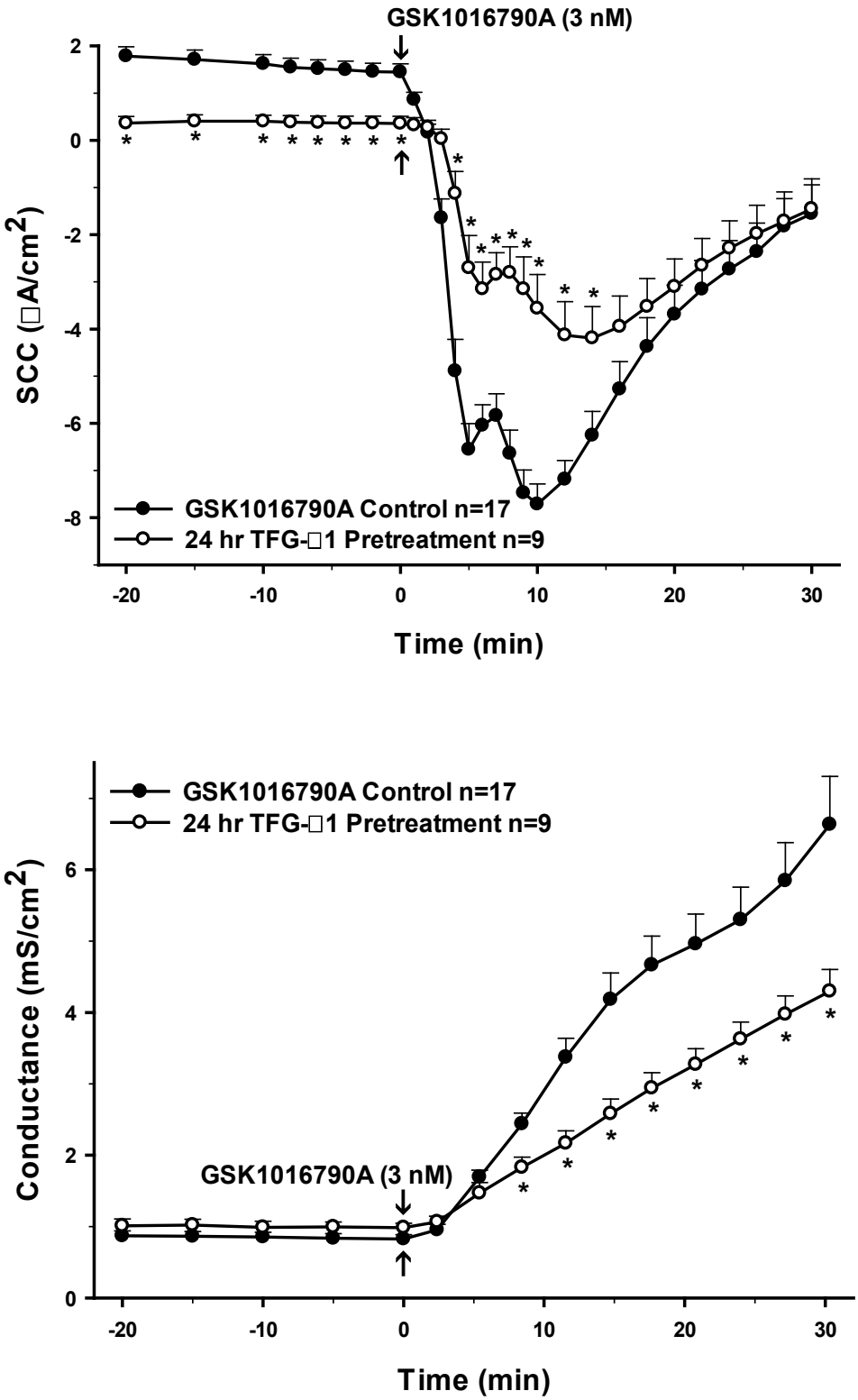

Figure 5.4 Treatment of PCP-R Cells with TGF-β1 24-hrs Prior to TRPV4 Agonist Addition.

Figure 5.5: Pre-treatment of PCP-R cells with anti-inflammatory cytokine IL-6 for 24-hours prior to TRPV4 agonist addition. Effect on transepithelial ion flux and conductance was measured. IL-6 (10 ng/mL in 4 mM HCl) was added to the PCP-R media on both basolateral and apical sides of the membrane at T = -24 hours (not shown). TRPV4 agonist GSK1016790A was added to basolateral side of the membrane only at T = 0 minutes. 24-hour incubation with IL-6 is signified by white circles. GSK1016790A control is signified by black circles. Circles signify mean values and bars signify ±S.E.M. for number of experiments indicated. SCC = short circuit current.

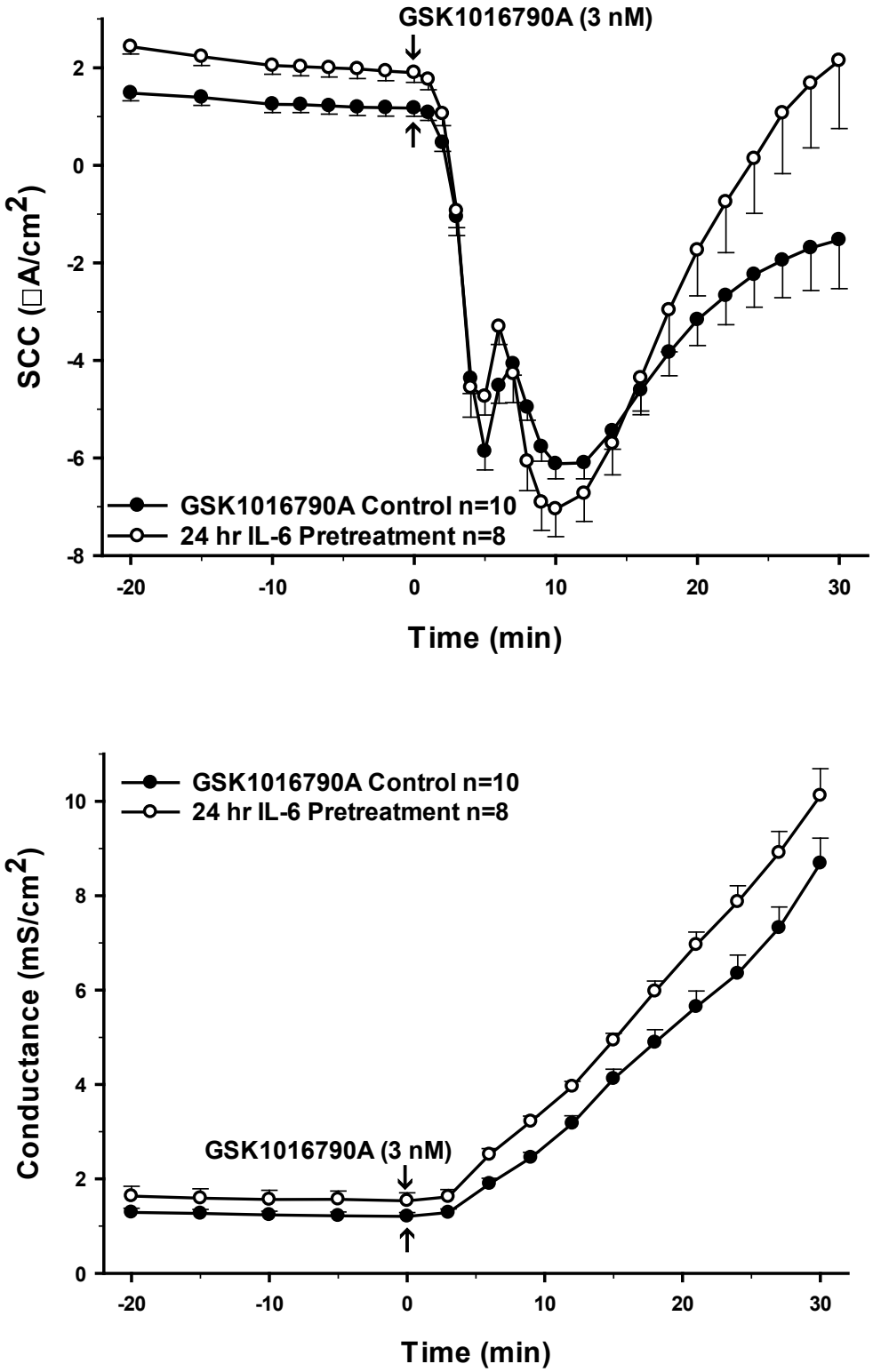

Figure 5.5 Treatment of PCP-R Cells with IL-6 24-hrs Prior to TRPV4 Agonist Addition.

Figure 5.6: Pre-treatment of PCP-R cells with anti-inflammatory cytokine IL-10 for 24-hours prior to TRPV4 agonist addition. Effect on transepithelial ion flux and conductance was measured. IL-10 (5 ng/mL in PBS) was added to the PCP-R media on both basolateral and apical sides of the membrane at T = -24 hours (not shown). TRPV4 agonist GSK1016790A was added to basolateral side of the membrane only at T = 0 minutes. 24-hour incubation with IL-10 is signified by white circles. GSK1016790A control is signified by black circles. Circles signify mean values and bars signify ±S.E.M. for number of experiments indicated. SCC = short circuit current.

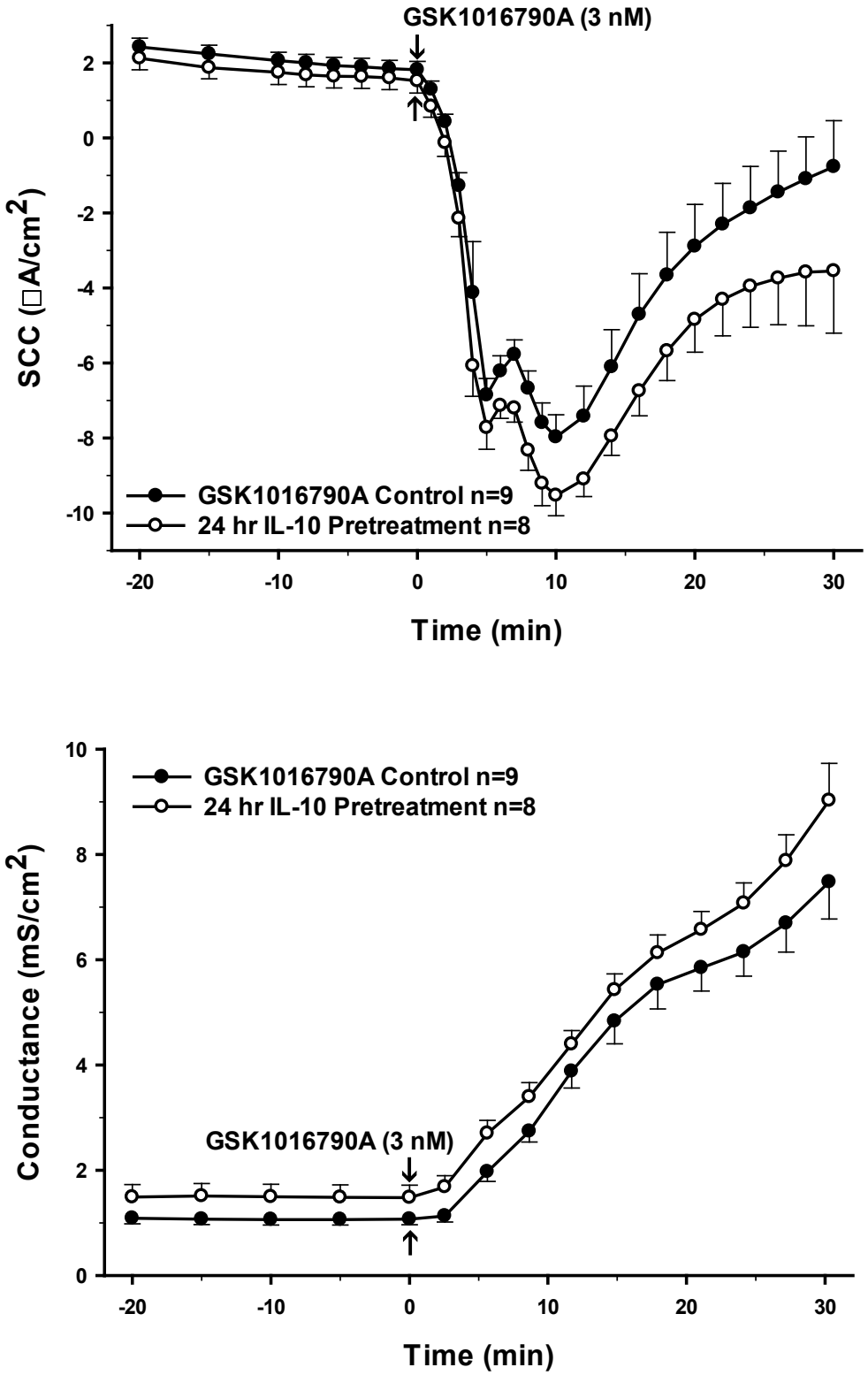

Figure 5.6 Treatment of PCP-R Cells with IL-10 24-hrs Prior to TRPV4 Agonist Addition.

Figure 5.7: Pre-treatment of PCP-R cells with pro- and anti-inflammatory cytokine IL-4 for 24-hours prior to TRPV4 agonist addition. Effect on transepithelial ion flux and conductance was measured. IL-4 (20 ng/mL in PBS) was added to the PCP-R media on both basolateral and apical sides of the membrane at T = -24 hours (not shown). TRPV4 agonist GSK1016790A was added to basolateral side of the membrane only at T = 0 minutes. 24-hour incubation with IL-4 is signified by white circles. GSK1016790A control is signified by black circles. Circles signify mean values and bars signify ±S.E.M. for number of experiments indicated. SCC = short circuit current.

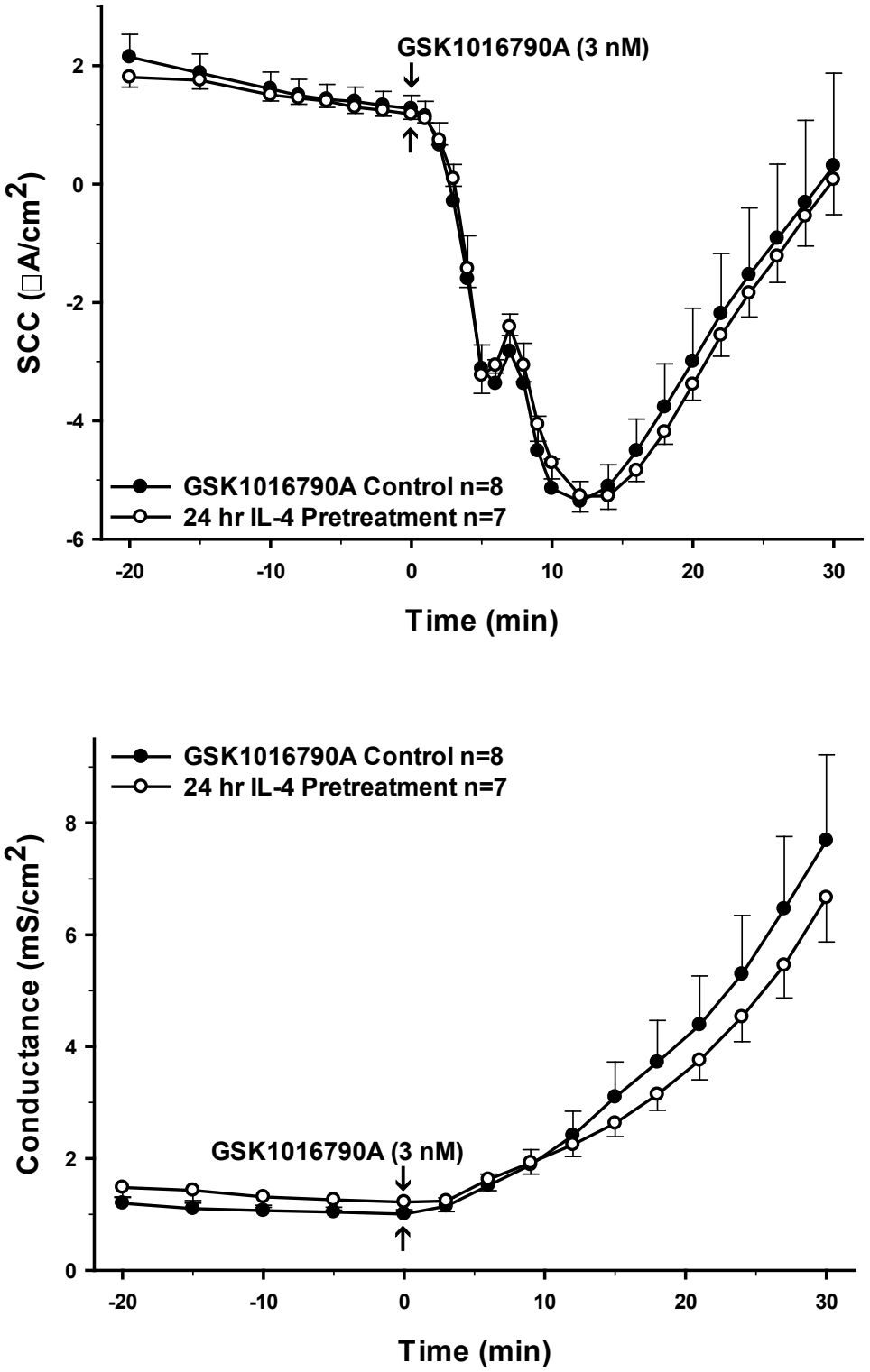

Figure 5.7 Treatment of PCP-R Cells with IL-4 24-hrs Prior to TRPV4 Agonist Addition.

Figure 5.8: Pre-treatment of PCP-R cells with NF-κB inhibitor PDTC for 10 minutes prior to TRPV4 agonist addition. Effect on transepithelial ion flux and conductance was measured. PDTC (10 μM in DMSO) was added to the PCP-R media on both basolateral and apical sides of the membrane at T = -10 minutes. TRPV4 agonist GSK1016790A was added to basolateral side of the membrane only at T = 0 minutes. 10-minute incubation with PDTC is signified by white circles. GSK1016790A control is signified by black circles. Circles signify mean values and bars signify ±S.E.M. for number of experiments indicated. SCC = short circuit current. * = $p < 0.05$ against control.

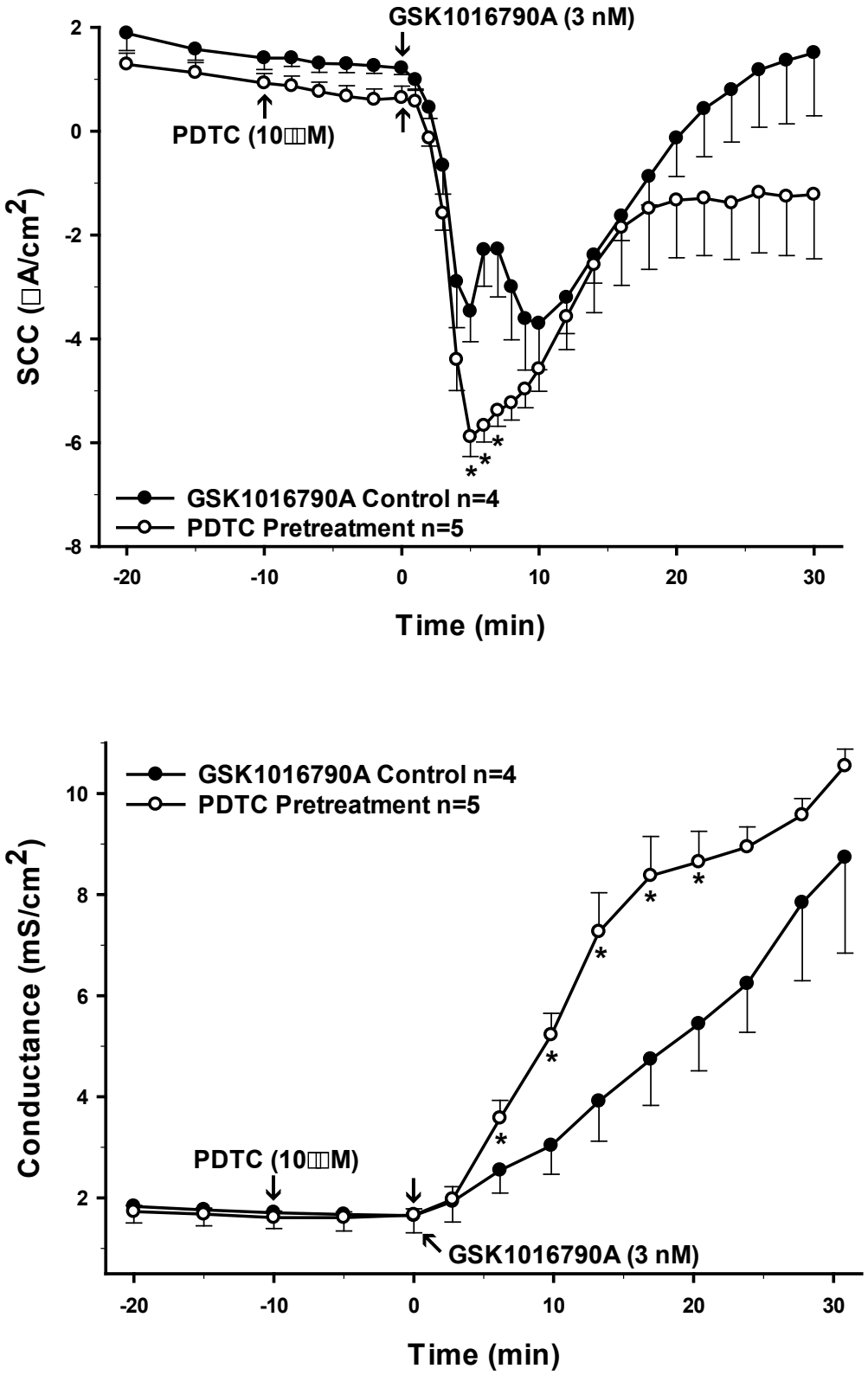

Figure 5.8 Treatment of PCP-R Cells with PDTC 10-min Prior to TRPV4 Agonist Addition.

Figure 5.9: Pre-treatment of PCP-R cells with NF-κB inhibitor PDTC for 24-hours prior to TRPV4 agonist addition. Effect on transepithelial ion flux and conductance was measured. PDTC (10 μM in DMSO) was added to the PCP-R media on both basolateral and apical sides of the membrane at T = -24 hours (not shown). TRPV4 agonist GSK1016790A was added to basolateral side of the membrane only at T = 0 minutes. 24-hour incubation with PDTC is signified by white circles. GSK1016790A control is signified by black circles. Circles signify mean values and bars signify ±S.E.M. for number of experiments indicated. SCC = short circuit current. * = $p < 0.05$ against control.

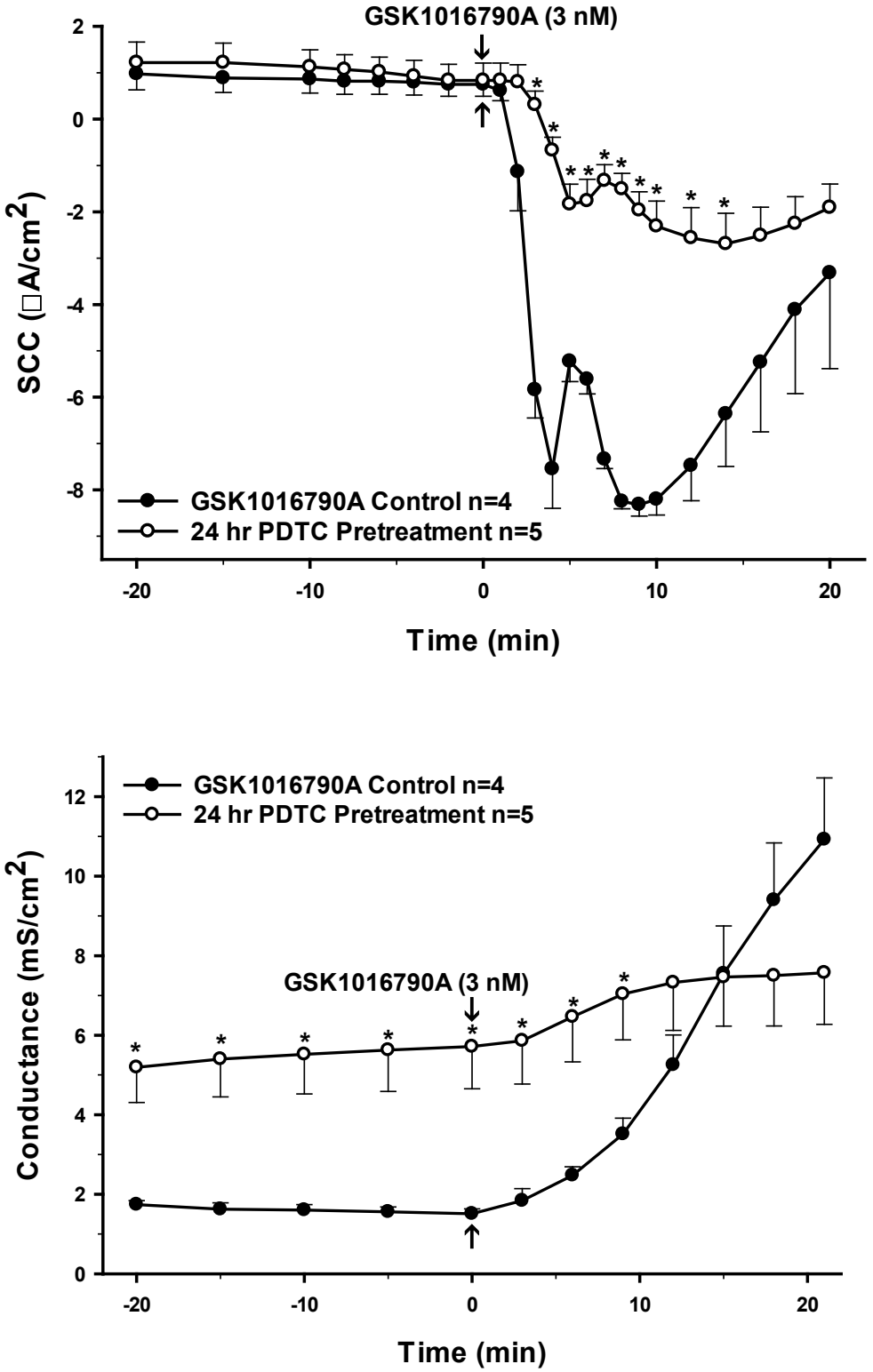

Figure 5.9 Treatment of PCP-R Cells with PDTC 24-hrs Prior to TRPV4 Agonist Addition.

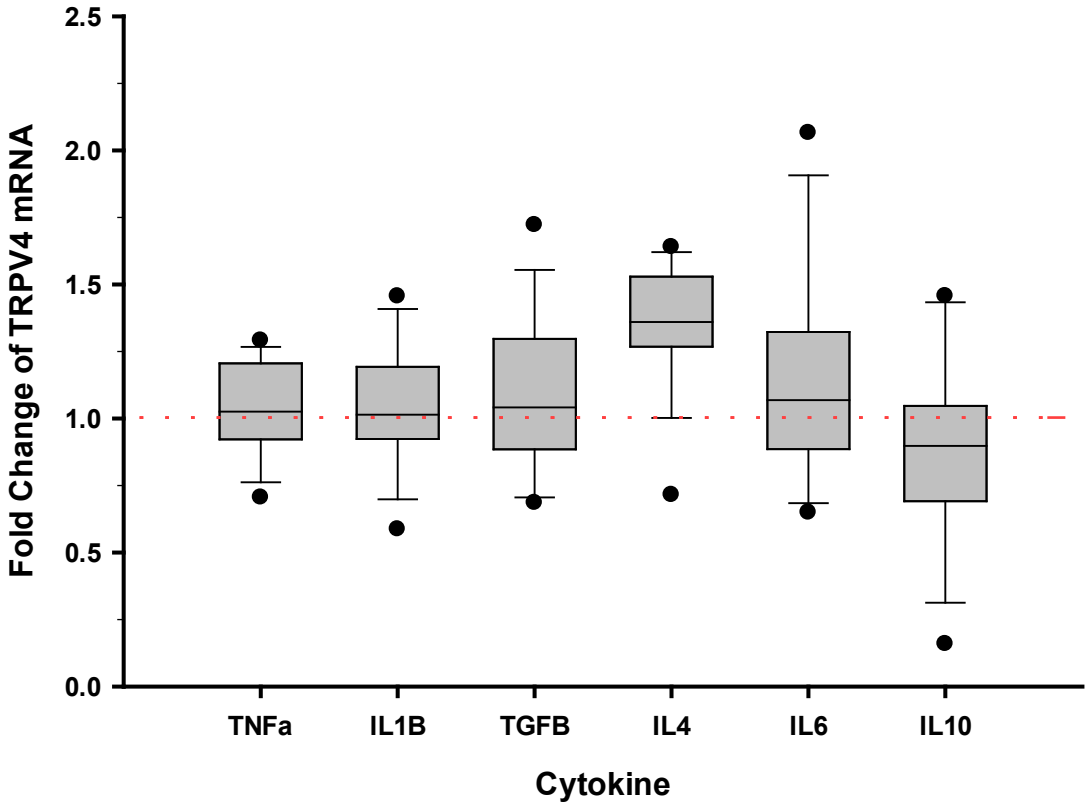

Figure 5.10 Relative Fold Change in TRPV4 24-hrs Post Incubation with Specific Cytokines.

Relative fold change of TRPV4 mRNA in PCP-R cells 24 hours post-incubation with specific cytokines known to be involved in inflammatory responses. TNF-α (0.15 ng/ml), IL-1β (10 ng/ml), TGF-β1 (2 ng/ml), IL-4 (10 ng/ml), IL-6 (20 ng/ml), or IL-10 (5 ng/ml) were added both apically and basolaterally in individual wells (n=5 for each cytokine). The fold change of TRPV4 in treated wells is presented relative to the normalized controls (n=6). GAPDH and RPS18 were used as housekeeping genes to determine the $2^{-\Delta\Delta CT}$ fold change in TRPV4. The minimum and maximum fold-change values are shown as individual points on the graph. Circles signify the maximum and minimum values. Lines within the boxes signify mean values and bars signify ±S.E.M. for number of experiments indicated.

Figure 5.11: Effect of a range of concentrations of arachidonic acid (AA) on TRPV4-mediated transepithelial ion flux and cellular permeability. AA solubilized in 100% EtOH was added to the PCP-R media on both basolateral and apical sides of the membrane at T = -10 minutes. TRPV4 agonist GSK1016790A was added to basolateral side of the membrane only at T = 0 minutes. AA pre-treatment at 10 μM is signified by white circles. AA pre-treatment at 100 μM is signified by gray circles. GSK1016790A control is signified by black circles. Circles signify mean values and bars signify ±S.E.M. for number of experiments indicated. SCC = short circuit current. * = $p < 0.05$ against control. τ = $p < 0.05$ against 10 μM AA pre-treatment.

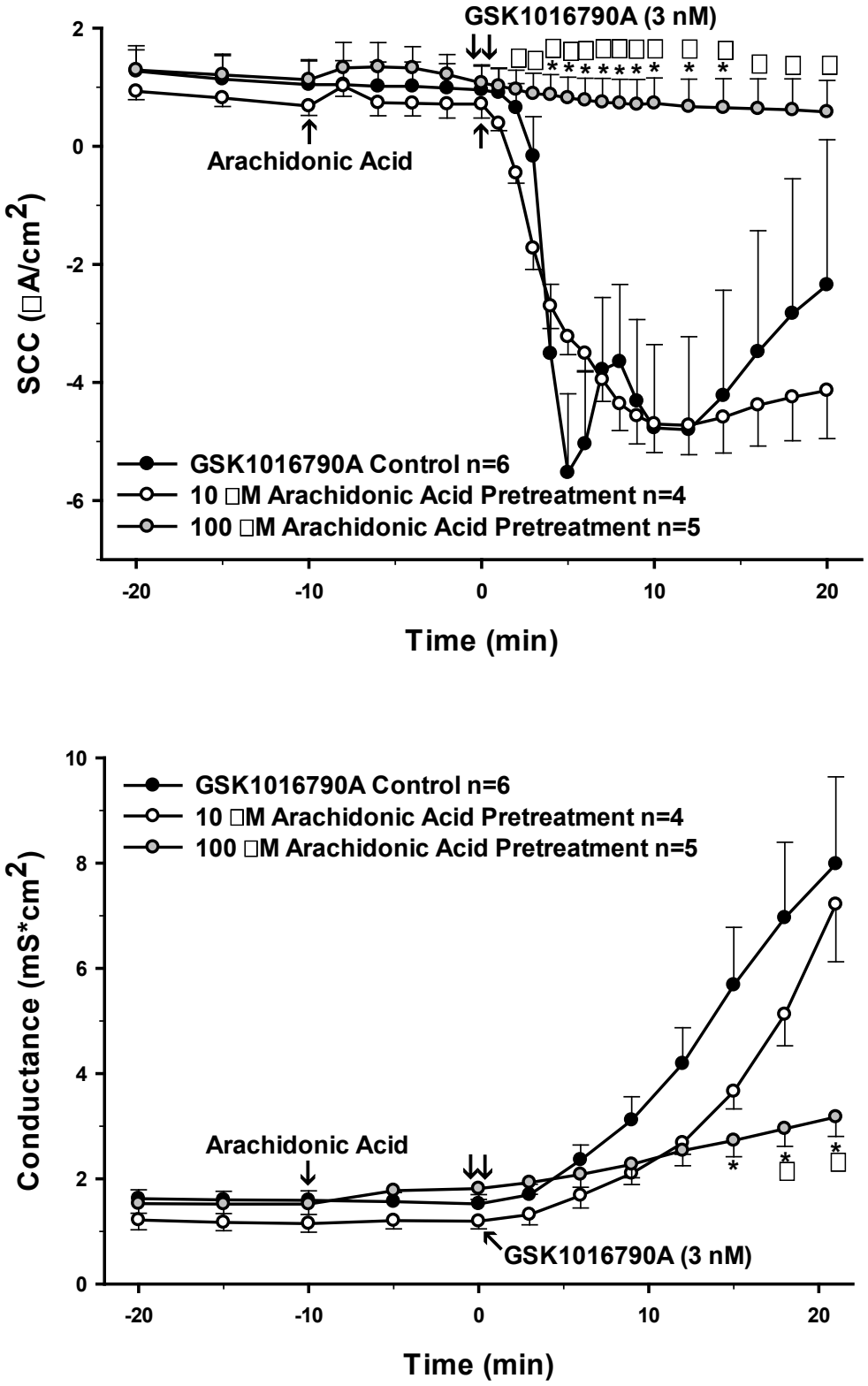

Figure 5.11 Treatment of PCP-R Cells with AA 24-hrs Prior to TRPV4 Agonist Addition.

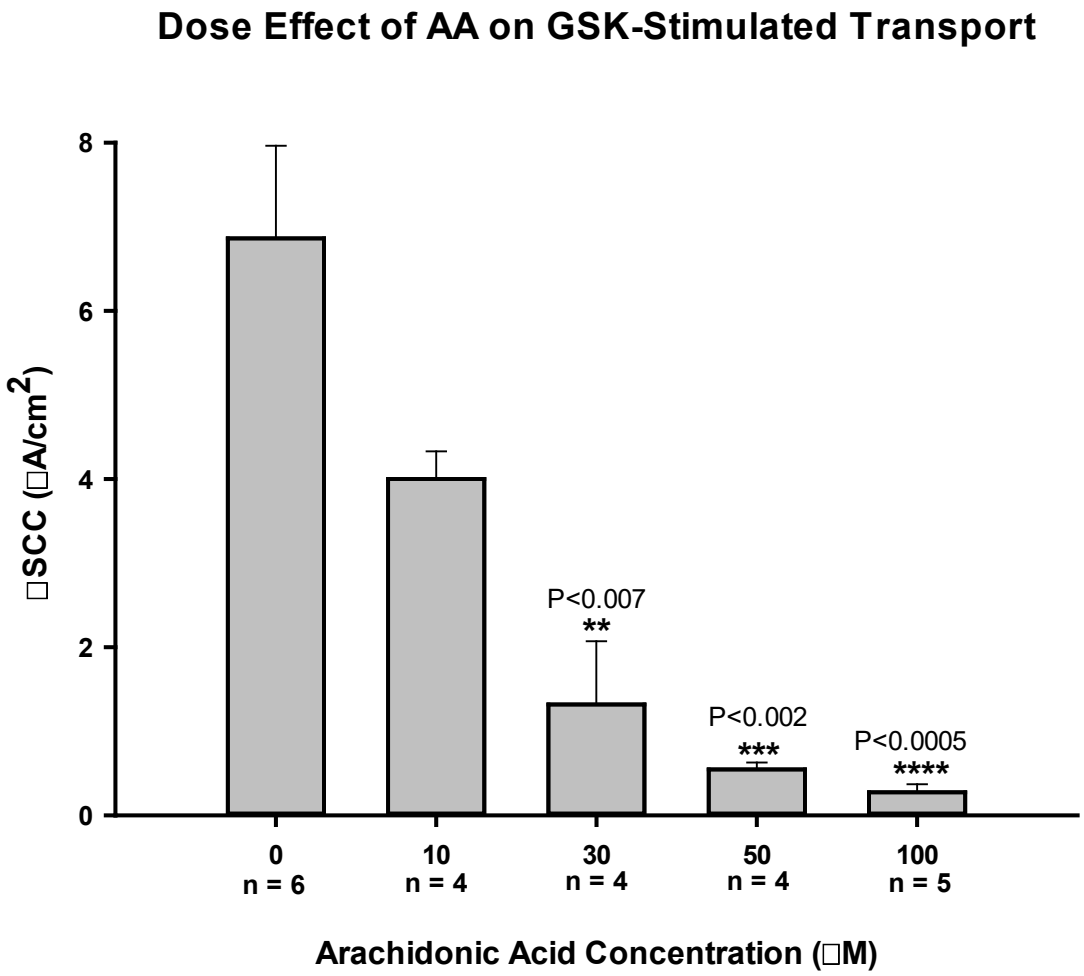

Figure 5.12 Dose Effect of AA on TRPV4-Mediated Transepithelial Ion Flux.

Dose effect of arachidonic acid (AA) on the change in TRPV4-mediated transepithelial ion flux in response to TRPV4-agonist GSK1016790A. PCP-R cells were pre-treated with arachidonic acid (AA) solubilized in 100% EtOH at various concentrations 10 minutes prior to TRPV4 agonist addition. AA was added to the PCP-R media on both basolateral and apical sides of the membrane. The change in transepithelial ion flux was measured 5 minutes after TRPV4 agonist addition (ΔSCC). Error bars signify the S.E.M. for number of experiments indicated. ΔSCC = change in short circuit current. * = significant against 0 μM AA control with p values given.

Figure 5.13: Pre-treatment of PCP-R cells with arachidonic acid (AA) metabolism inhibitors 20-minutes prior to TRPV4 agonist addition. Effect of inhibitor pre-incubation on TRPV4-stimulated transepithelial ion flux and conductance was measured. All inhibitors were solubilized in 100% EtOH. Cyclooxygenase and lipoxygenase inhibitor ETYA was added to the PCP-R media on both basolateral and apical sides of the membrane at T = -20 minutes. Cytochrome P450 inhibitor SKF-525A was added to the PCP-R media on both basolateral and apical sides of the membrane at T = -20 minutes. TRPV4 agonist GSK1016790A was added to basolateral side of the membrane only at T = 0 minutes. ETYA pre-treatment is signified by white circles. SKF-525A pre-treatment is signified by grey circles. GSK1016790A control is signified by black circles. Circles signify mean values and bars signify ±S.E.M. for number of experiments indicated. SCC = short circuit current. * = $p < 0.05$ against control. $\tau = p < 0.05$ against ETYA pre-treatment.

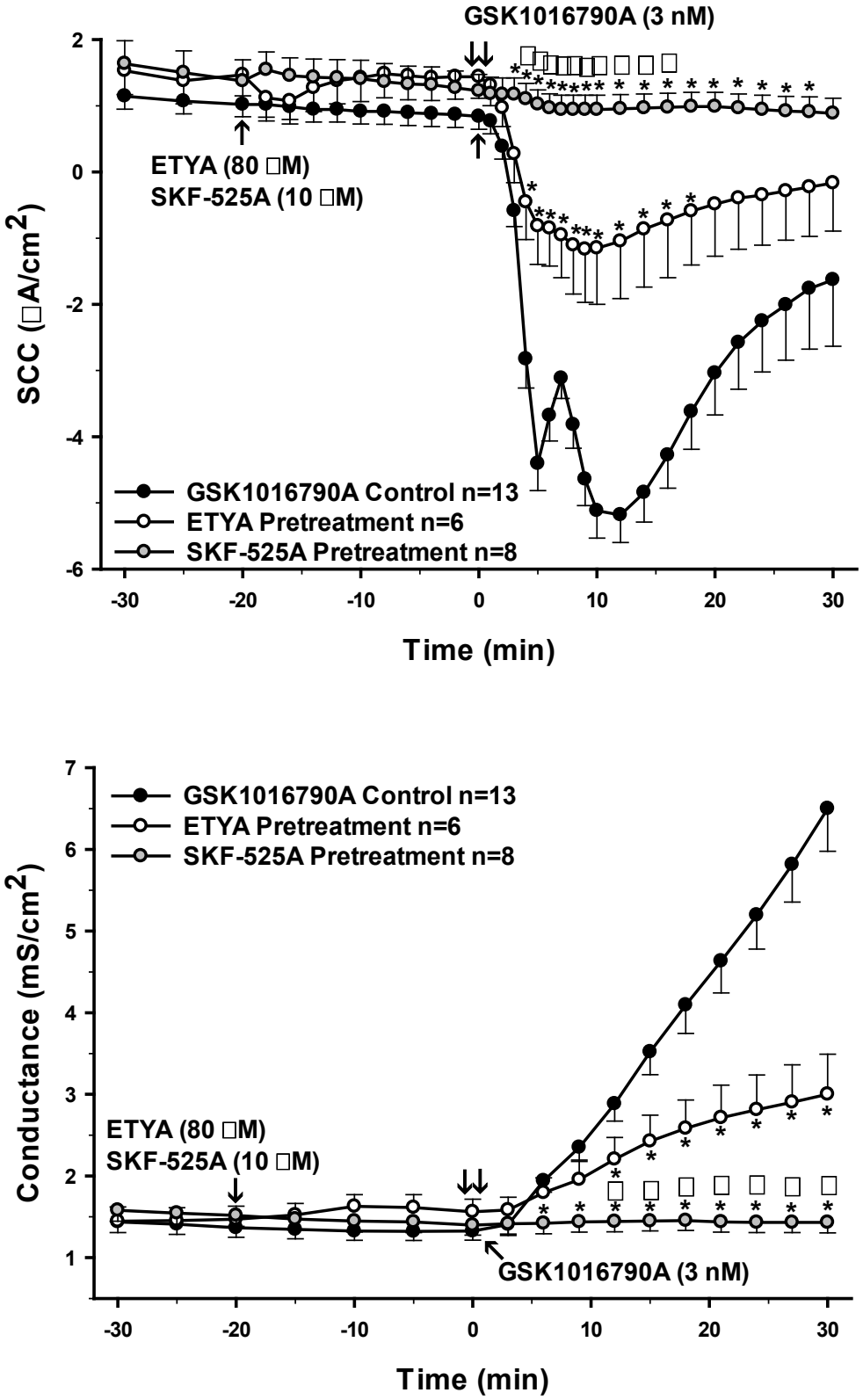

Figure 5.13 AA Metabolite Treatment of PCP-R Cells Prior to TRPV4 Agonist Addition.

Figure 5.14: Pre-treatment of PCP-R cells with arachidonic acid metabolite 5,6-EET at 10-minutes prior to TRPV4 agonist addition. Effect on transepithelial ion flux and conductance was measured. 5,6-EET solubilized in 100% EtOH was added to the PCP-R media on both basolateral and apical sides of the membrane at T = -10 minutes. TRPV4 agonist GSK1016790A was added to basolateral side of the membrane only at T = 0 minutes. 10-minute incubation is signified by white circles. GSK1016790A control is signified by black circles. Circles signify mean values and bars signify ±S.E.M. for number of experiments indicated. SCC = short circuit current.

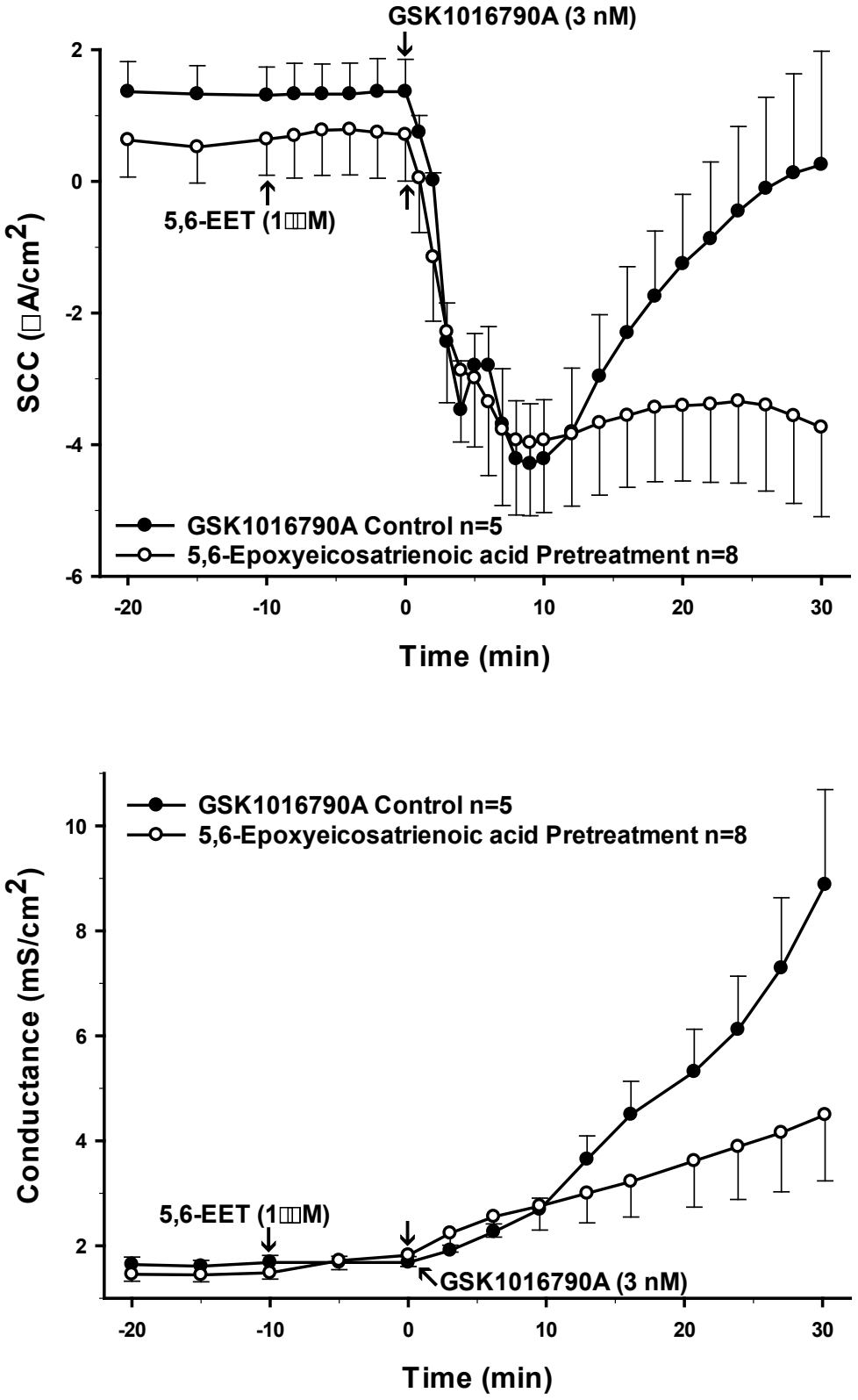

Figure 5.14 Treatment of PCP-R Cells with 5,6-EET Prior to TRPV4 Agonist Addition.

5.11 **References**

1. Akira S, Takeda K. Toll-like receptor signalling. *Nat Rev Immunol* 4: 499-511, 2004.
2. Azizi G, Navabi S, Al-Shukaili A, Seyedzadeh M, Yazdani R, Mirshafiey A. The role of inflammatory mediators in the pathogenesis of Alzheimer's disease. *Sultan Qaboos Univ Med J* 15: e305-316, 2015.
3. Balakrishna S, Song W, Achanta S, Doran S, Liu B, Kaelberer M, Yu Z, Sui A, Cheung M, Leishman E, Eidam H, Ye G, Willette R, Thorneloe K, Bradshaw H, Matalon S, Jordt S. TRPV4 inhibition counteracts edema and inflammation and improves pulmonary function and oxygen saturation in chemically induced acute lung injury. *Am J Physiol Lung Cell Mol Physiol* 307: L158-L172, 2014.
4. Block M, Hong J. Microglia and inflammation-mediated neurodegeneration: Multiple triggers with a common mechanism. *Prog Neurobiol* 76: 77-98, 2005.
5. Cao S, Anishkin A, Zinkevich N, Nishijima Y, Korishettar A, Wang Z, Fang J, Wilcox D, Zhang D. Transient receptor potential vanilloid 4 (TRPV4) activation by arachidonic acid requires protein kinase A–mediated phosphorylation. *J Biol Chem* 293: 5307-5322, 2018.
6. Clop A, Huisman A, van As P, Sharaf A, Derdak S, Sanchez A. Identification of genetic variation in the swine toll-like receptors and development of a porcine TLR genotyping array. *Genet Sel Evol* 48, 2016.
7. Corrigan F, Mander K, Leonard A, Vink R. Neurogenic inflammation after traumatic brain injury and its potentiation of classical inflammation. *J Neuroinflammation* 13, 2016.
8. Csuka E, Morganti-Kossmann MC, Lenzlinger PM, Joller H, Trentz O, Kossmann T. IL-10 levels in cerebrospinal fluid and serum of patients with severe traumatic brain injury: relationship to IL-6, TNF-alpha, TGF-beta1 and blood-brain barrier function. *J. Neuroimmunol* 101: 211–221, 1999.
9. Dalsgaard T, Sonkusare S, Teuscher C, Poynter M, Nelson M. Pharmacological inhibitors of TRPV4 channels reduce cytokine production, restore endothelial function and increase survival in septic mice. *Sci Rep* 6, 2016.
10. Damkier H, Brown P, Praetorius J. Cerebrospinal fluid secretion by the choroid plexus. *Physiol Rev* 93: 1847-1892, 2013.
11. Erickson K, Baron I, Fantie B. Neuropsychological functioning in early hydrocephalus: review from a developmental perspective. *Child Neuropsychol* 7: 199-229, 2001.

12. Filosa J, Yao X, Rath G. TRPV4 and the regulation of vascular tone. *J Cardiovasc Pharmacol* 61: 113-119, 2013.
13. Golomb J. Alzheimer's disease comorbidity in normal pressure hydrocephalus: prevalence and shunt response. *J Neurol Neurosurg Psychiatry* 68: 778-781, 2000.
14. Han G, Li F, Singh TP, Wolf P, Wang XJ. The pro-inflammatory role of TGFβ1: a paradox?. *Int J Biol Sci* 8: 228-235, 2012.
15. Herrero M, Estrada C, Maatouk L, Vyas S. Inflammation in Parkinson's disease: role of glucocorticoids. *Front Neuroanat* 9, 2015.
16. Jankovic J, Newmark M, Peter P. Parkinsonism and acquired hydrocephalus. *Mov Disord* 1: 59-64, 1986.
17. Kant S, Stopa E, Johanson C, Baird A, Silverberg G. Choroid plexus genes for CSF production and brain homeostasis are altered in Alzheimer's disease. *Fluids Barriers CNS* 15, 2018.
18. Karimy J, Zhang J, Kurland D, Theriault B, Duran D, Stokum J, Furey C, Zhou X, Mansuri M, Montejo J, Vera A, DiLuna M, Delpire E, Alper S, Gunel M, Gerzanich V, Medzhitov R, Simard J, Kahle K. Inflammation-dependent cerebrospinal fluid hypersecretion by the choroid plexus epithelium in posthemorrhagic hydrocephalus. *Nat Med* 23: 997-1003, 2017.
19. Kim S, Akindehin S, Kwon H, Son Y, Saha A, Jung Y, Seong J, Lim K, Sung J, Maddipati K, Lee Y. Anti-inflammatory role of 15-lipoxygenase contributes to the maintenance of skin integrity in mice. *Sci Rep* 8, 2018.
20. Krauss J, Regel J, Droste D, Orszagh M, Borremans J, Vach W. Movement disorders in adult hydrocephalus. *Mov Disord* 12: 53-60, 1997.
21. Kushel' YV, Belova YD, Tekoev AR. Intramedullary spinal cord tumors and hydrocephalus: an analysis of the results of surgical treatment in 541 patients. *Zh Vopr Neirokhir Im N N Burdenko* 81: 56, 2017.
22. Langenbach R, Morham S, Tiano H, Loftin C, Ghanayem B, Chulada P, Mahler J, Lee C, Goulding E, Kluckman K, Kim H, Smithies O. Prostaglandin synthase 1 gene disruption in mice reduces arachidonic acid-induced inflammation and indomethacin-induced gastric ulceration. *Cell* 83: 483-492, 1995.
23. Lawrence T. The nuclear factor NF-κB pathway in inflammation. *Cold Spring Harb Perspect Biol* 1: a001651-a001651, 2009.

24. Lee P, Monaco E, Friedlander R. Blocking TGF-β activity and associated inflammation may halt hydrocephalus. *Neurosurgery* 73: N13-N14, 2013.
25. Lehmann J, Lenhard J, Oliver B, Ringold G, Kliewer S. Peroxisome proliferator-activated receptors α and γ are activated by indomethacin and other non-steroidal anti-inflammatory drugs. *J Biol Chem* 272: 3406-3410, 1997.
26. Liedtke W, Choe Y, Martí-Renom M, Bell A, Denis C, Sali A, Hudspeth A, Friedman J, Heller S. Vanilloid receptor–related osmotically activated channel (VR-OAC), a candidate vertebrate osmoreceptor. *Cell* 103: 525-535, 2000.
27. Lin C, Riva-Cambrin J. Management of posterior fossa tumors and hydrocephalus in children: a review. *Childs Nerv Syst* 31: 1781-1789, 2015.
28. Livak K, Schmittgen T. Analysis of relative gene expression data using real-time quantitative PCR and the $2^{-\Delta\Delta CT}$ method. *Methods* 25: 402-408, 2001.
29. Lu K, Huang T, Tsai Y, Yang Y. Transient receptor potential vanilloid type 4 channels mediate Na-K-Cl-co-transporter-induced brain edema after traumatic brain injury. *J Neurochem* 140: 718-727, 2017.
30. Mashima R, Okuyama T. The role of lipoxygenases in pathophysiology; new insights and future perspectives. *Redox Biol* 6: 297-310, 2015.
31. Meves H. Arachidonic acid and ion channels: an update. *Br J Pharmacol* 155: 4-16, 2008.
32. Nilius B, Vriens J, Prenen J, Droogmans G, Voets T. TRPV4 calcium entry channel: a paradigm for gating diversity. *Am J Physiol Cell Physiol* 286: C195-C205, 2004.
33. Node K. Anti-inflammatory properties of cytochrome P450 epoxygenase-derived eicosanoids. *Science* 285: 1276-1279, 1999.
34. Okun E, Griffioen K, Lathia J, Tang S, Mattson M, Arumugam T. Toll-like receptors in neurodegeneration. *Brain Res Rev* 59: 278-292, 2009.
35. Ott B, Jones R, Daiello L, de la Monte S, Stopa E, Johanson C, Denby C, Grammas P. Blood-cerebrospinal fluid barrier gradients in mild cognitive impairment and Alzheimer's disease: relationship to inflammatory cytokines and chemokines. *Front Aging Neurosci* 10, 2018.
36. Palumbo S. Pathogenesis and progression of multiple sclerosis: the role of arachidonic acid–mediated neuroinflammation. *Multiple Sclerosis: Perspectives in Treatment and Pathogenesis* (2017). doi: 10.15586/codon.multiplesclerosis.2017.ch7.

37. Preston D, Simpson S, Halm D, Hochstetler A, Schwerk C, Schroten H, Blazer-Yost B. Activation of TRPV4 stimulates transepithelial ion flux in a porcine choroid plexus cell line. *Am J Physiol Cell Physiol* 315: C357-C366, 2018.
38. Scheller J, Chalaris A, Schmidt-Arras D, Rose-John S. The pro- and anti-inflammatory properties of the cytokine interleukin-6. *Biochim Biophys Acta* 1813: 878-888, 2011.
39. Schroten M, Hanisch F, Quednau N, Stump C, Riebe R, Lenk M, Wolburg H, Tenenbaum T, Schwerk C. A novel porcine in vitro model of the blood-cerebrospinal fluid barrier with strong barrier function. *PLoS ONE* 7: e39835, 2012.
40. Shahabi P, Siest G, Meyer U, Visvikis-Siest S. Human cytochrome P450 epoxygenases: variability in expression and role in inflammation-related disorders. *Pharmacol Ther* 144: 134-161, 2014.
41. Sosvorova L, Mohapl M, Vcelak J, Hill M, Vitku J, Hampl R. The impact of selected cytokines in the follow-up of normal pressure hydrocephalus. *Physiol Res* 64: S283-S290, 2015.
42. Strotmann R, Harteneck C, Nunnenmacher K, Schultz G, Plant T. OTRPC4, a nonselective cation channel that confers sensitivity to extracellular osmolarity. *Nat Cell Biol* 2: 695-702, 2000.
43. Tisoncik J, Korth M, Simmons C, Farrar J, Martin T, Katze M. Into the eye of the cytokine storm. *Microbiol Mol Biol Rev*, 76: 16-32, 2012.
44. Toft-Bertelsen T, Križaj D, MacAulay N. When size matters: transient receptor potential vanilloid 4 channel as a volume-sensor rather than an osmo-sensor. *J Physiol* 595: 3287-3302, 2017.
45. Tully H, Dobyns W. Infantile hydrocephalus: a review of epidemiology, classification and causes. *Eur J Med Genet* 57: 359-368, 2014.
46. Vadivelu S, Rekate H, Esernio-Jenssen D, Mittler M, Schneider S. Hydrocephalus associated with childhood nonaccidental head trauma. *Neurosurg Focus* 41: E8, 2016.
47. Watanabe H, Vriens J, Prenen J, Droogmans G, Voets T, Nilius B. Anandamide and arachidonic acid use epoxyeicosatrienoic acids to activate TRPV4 channels. *Nature* 424: 434-438, 2003.
48. Woodcock T, Morganti-Kossmann M. The role of markers of inflammation in traumatic brain injury. *Front Neurol* 4, 2013.

49. Wu M, Lin T, Chiu Y, Liou H, Yang R, Fu W. Involvement of 15-lipoxygenase in the inflammatory arthritis. *J Cell Biochem* 113: 2279-2289, 2012.
50. Wyss-Coray T, Mucke L. Inflammation in neurodegenerative disease—a double-edged sword. *Neuron* 35: 419-432, 2002.
51. Yamamoto T, Nozaki-Taguchi N. Analysis of the effects of cyclooxygenase (COX)-1 and COX-2 in spinal nociceptive transmission using indomethacin, a non-selective COX inhibitor, and NS-398, a COX-2 selective inhibitor. *Brain Res* 739: 104-110, 1996.
52. Yan Y, Dalmasso G, Thi Thu Nguyen H, Obertone T, Sitaraman S, Merlin D. Ste20-related proline/alanine-rich kinase (SPAK) regulated transcriptionally by hyperosmolarity is involved in intestinal barrier function. *PLoS ONE* 4: e5049, 2009.
53. Zhao L, Cuff C, Moss E, Wille U, Cyrus T, Klein E, Praticò D, Rader D, Hunter C, Puré E, Funk C. Selective interleukin-12 synthesis defect in 12/15-lipoxygenase-deficient macrophages associated with reduced atherosclerosis in a mouse model of familial hypercholesterolemia. *J Biol Chem* 277: 35350-35356, 2002.

CHAPTER 6. SUMMARY

6.1 Summary

The mechanisms of CSF production are still not fully understood. Currently, a large body of research exists implicating various transporters, channels, and aquaporins in playing significant roles in the movement of ions and water, necessary for the production of CSF. Additionally, many kinases have been shown to play key roles in the regulation of these events. However, while various studies have highlighted several possible pathways by which CSF production can be reduced and modulated, no consensus has been reached regarding which proteins establish the net driving forces, and which act as key regulators. In the field of hydrocephalus, there is a large unmet need; that of an effective drug treatment to reduce the production of CSF as an alternative to invasive surgeries. To that end, these studies have contributed to better understanding the mechanisms by which CSF is produced, and regulatory pathways which may be further studied to ultimately modulate how much CSF is being produced in patients with hydrocephalus.

Using the PCP-R cell in vitro model, we have established a method by which we can study the transepithelial movement of ions in CP cells. This allows us to investigate the molecular mechanisms by which CSF is being produced, as well as determine how signals are being integrated, and which proteins interact to regulate the movement of ions across the epithelium. Using the cell line, we have also been able to study the barrier nature of the cells, and determine which effectors play roles in maintaining or compromising the integrity of this barrier. Through use of these effectors, we gain insight in to the roles played by various proteins in barrier maintenance.

The PCP-R cell line is comprised of a high-resistance monolayer epithelium and closely mimics the barrier characteristics observed in the native in vivo tissue. Many of the same junctional proteins, such as Zona Occludens 1 and Claudin-1 are present in both the in vivo tissue and the PCP-R cells. Additionally, similarly to the native tissue, the PCP-R cells polarize, expressing different proteins on each membrane. This polarization allows for net transepithelial ion flux from either the blood (basolateral) to CSF-facing (apical) surfaces, or from CSF to blood. This model

therefore allows us to use drugs targeted to specific proteins to interrogate the role of many of the polarized proteins in moving ions in to, and out of the cell.

In this thesis we have functionally characterized many key transporters and ion channels in the PCP-R cell line which have been previously described in human and rodent choroid plexus. This includes the Ca^{2+}-activated K^+ channels described in chapter 2 (SK2 and IK), the $Na^+/K^+/Cl^-$ and potassium-chloride cotransporters described in chapter 3 (NKCC1, KCC1-4), and the chloride channels described in chapter 4 (TMEM16A, AE2, NCBE, CFTR). In addition, we have identified mRNA for additional proteins previously described in the choroid plexus including carbonic anhydrase II, Na+/K+-ATPase and aquaporin 1 which have been suggested to play key roles in CSF production and cell homeostasis (data not shown).

We have begun to assemble a mechanism by which TRPV4 is capable of stimulating transepithelial ion flux, and ultimately, the production of CSF. First, in chapter 2 we demonstrated that the IK channel, a Ca^{2+}-activated K^+ channel, is necessary for activation of TRPV4. It appears that the influx of Ca^{2+} which occurs in response to TRPV4 activation is responsible for activation of the IK channel, leading to secretion of potassium. In addition to this, in chapter 4 we showed that TMEM16A, a Ca^{2+}-activated Cl^- channel plays a significant role in the TRPV4 mechanism. We demonstrated that TRPV4 and TMEM16A are co-dependent on each other for activation. Inhibition of either TMEM16A or TRPV4 resulted in inhibition of the other, blocking the resulting transepithelial currents. Additionally, we showed that $[Cl^-]$ is tightly regulated within the cells, and is the key ion for cell homeostasis. From this, in chapter 3 we explored a role for NKCC1 in the TRPV4 mechanism. It has been previously shown in the literature that in the choroid plexus, NKCC1 is responsible for regulation of $[Cl^-]$. Here we showed that NKCC1 does in fact play some role in the TRPV4-stimulated pathway, being capable of inhibiting a portion of the TRPV4-induced transepithelial ion flux.

We also wanted to determine whether the regulation of this mechanism was controlled by channel activation via kinases, or whether the mechanism was controlled at the transcriptional level. In chapter 3, we investigated whether the WNK-SPAK/OSR1 pathway could be responsible for activation of TRPV4, and could therefore be used as a regulator of the pathway. Here we

demonstrated that inhibition of SPAK activation via WNK was indeed capable of inhibiting TRPV4, although it appeared to be independent of NKCC1. This demonstrates that SPAK may instead act directly on TRPV4. Finally, to address whether these channels or transporters were regulated at the transcriptional level, we inhibited NKCC1 and SPAK. With respect to NKCC1, inhibition did not appear to affect its own gene regulation or that of any other channel. When inhibiting SPAK, we observed that the expression of NKCC1, WNK3 and SPAK were all decreased approximately 2-fold, while no effect was seen on TRPV4 transcription.

In conclusion, we have identified several ways in which TRPV4 may work to stimulate the production of CSF, as well as identified some potential regulatory pathways by which the CSF production can be reduced. These studies, in conjunction with the many other studies in the field of CSF production may ultimately lead to new insights and innovations which can be used to develop targeted drugs to ameliorate the pathophysiology associated with hydrocephalus.

6.2 Addressing the PCP-R Cell Polarity

Following the writing of this thesis, but prior to final drafting, a concerning discovery was made regarding the polarity of the PCP-R cells. As has been described throughout this thesis, NKCC1 and Na^+/K^+-ATPase have both been identified in the apical membranes of native choroid plexus in several model systems. A recent experiment performed by a collaborator demonstrated that both are localized in the basolateral rather than apical membrane in the PCP-R cells. This suggests that the cells are not correctly polarized and raises concerns about the cells as a model of secretory CP epithelia. It also brings in to question data regarding the role of NKCC1 in TRPV4-mediated transport.

Additional experiments are being conducted by other members of the lab to address these concerns, and future publications will further address the differences in polarity between the PCP-R cells and another choroid plexus cell model, the human choroid plexus papilloma derived (HIBCPP) cell line. These experiments will serve to address the PCP-R cell line as a model of the choroid plexus, and will attempt to further tease out the role of NKCC in the TRPV4 mechanism. Unfortunately, given these findings, the two papers I have prepared for publication, chapters 3 and 4 cannot be submitted in their current form. I will be conducting additional experiments utilizing

a human choroid plexus (HIBCPP) cell line during the remaining time in the laboratory and will work with my co-authors to modify the papers for publication.